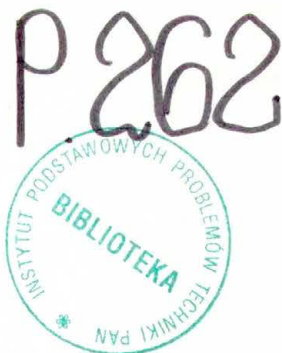


Polish Academy of Sciences  
Institute of Fundamental Technological Research



# Archives of Mechanics

---

Archiwum Mechaniki Stosowanej

---

volume 49

issue 1

---



Polish Scientific Publishers PWN

Warszawa 1997

ARCHIVES OF MECHANICS IS DEVOTED TO  
Theory of elasticity and plasticity • Theory of nonclassical  
continua • Physics of continuous media • Mechanics of  
discrete media • Nonlinear mechanics • Rheology • Fluid  
gas-mechanics • Rarefied gas • Thermodynamics

---

#### FOUNDERS

M.T. HUBER • W. NOWACKI • W. OLSZAK  
W. WIERZBICKI

#### INTERNATIONAL COMMITTEE

J.L. AURIAULT • D.C. DRUCKER • R. DVOŘÁK  
W. FISZDON • D. GROSS • V. KUKUDZHANOV  
G. MAIER • G.A. MAUGIN • Z. MRÓZ  
C.J.S. PETRIE • J. RYCHLEWSKI • W. SZCZEPIŃSKI  
G. SZEFER • V. TAMUŽS • K. TANAKA  
Cz. WOŹNIAK • H. ZORSKI

#### EDITORIAL COMMITTEE

M. SOKOŁOWSKI — editor • L. DIETRICH  
J. HOLNICKI-SZULC • W. KOSIŃSKI  
W.K. NOWACKI • M. NOWAK  
H. PETRYK — associate editor  
J. SOKÓŁ-SUPEL • A. STYCZEK • Z.A. WALENTA  
B. WIERZBICKA — secretary • S. ZAHORSKI

Copyright 1997 by Polska Akademia Nauk, Warszawa, Poland  
Printed in Poland, Editorial Office: Świętokrzyska 21,  
00-049 Warszawa (Poland)

e-mail: publikac@ippt.gov.pl

---

Arkuszy wydawniczych 18,25. Arkuszy drukarskich 15,5  
Papier offset, kl. III 70 g. B1. Oddano do składania w styczniu 1997 r.  
Druk ukończono w lutym 1997 r.  
Skład i łamanie: "MAT-TEX"  
Druk i oprawa: Drukarnia Braci Grodzickich, Zabieniec ul. Przelotowa 7

---

# Subsonic flutter calculation of an aircraft with nonlinear control system based on center-manifold reduction

J. GRZĘDZIŃSKI (WARSZAWA)

THE PAPER PRESENTS a method of calculation of limit cycle subsonic flutter oscillations caused by structural nonlinearities. Numerical examples assume the nonlinearities to be concentrated in the hinges of the aircraft control surfaces. Since nonlinear flutter is essentially the Hopf bifurcation, these oscillations tend asymptotically to a certain two-dimensional attracting subspace called the center manifold. Consequently, an asymptotic motion of the entire aircraft in the neighbourhood of bifurcation point is fully described by only two equations. The method of center-manifold reduction consists in a nonlinear change of coordinates, and transforms the initial multi-dimensional nonlinear integro-differential flutter equation into a system of two nonlinear ordinary differential equations of the first order, having phase-shift symmetry. Under the assumption that the nonlinear term has a formal power series expansion with respect to generalized coordinates (multi-variable Taylor series), the transformation can be also expressed in the form of a power series, and the limit cycle amplitude and frequency can be easily calculated.

## 1. Introduction

DEFORMATIONS of an aircraft structure under aerodynamic loads during flight are responsible for occurrence of self-excited oscillations, called flutter. These often destructive oscillations are driven by the transfer of energy from the airstream to the aircraft structure. The most widely used linear flutter analysis is focused on the particular critical value of flight velocity, above which the steady motion of an aircraft becomes unstable. All velocities below this point are considered to be safe in the sense that any imposed disturbances decay asymptotically in time, regardless of their initial magnitude. This is no more true if either the flow or the structure characteristics are nonlinear. It is known that in a nonlinear case, sufficiently high initial disturbance (e.g. a gust) can trigger self-excited oscillations even below the critical flutter velocity. Since the flutter phenomenon must be completely prevented from occurring within the flight envelope, nonlinear flutter analysis is also of great practical importance.

In the unsteady subsonic motion, the aerodynamic forces depend on the history of motion as a result of shedding of the vortex wake behind an aircraft. Consequently, the aerodynamic operator, relating the unsteady aerodynamic forces to the deflection of an aircraft structure (generalized coordinates), is always of the form of the convolution integral. Thus, in a time domain, the flutter equation is an integro-differential equation (sometimes with infinite delay). This property is the main source of difficulties in nonlinear approach, contrary to other aero-elastic systems described by ordinary differential equations (e.g. supersonic or panel flutter).

It is well known from the theory of dynamical systems [1] that their qualitative behaviour is essentially the same, no matter what physical background they originate from. Therefore, if the steady solution, such as a horizontal flight of an aircraft, bifurcates into the finite amplitude oscillations then the limit cycle attractor appears in the phase space of the system and the Hopf bifurcation takes place. Since the point of interest is an asymptotic motion of an aircraft, it is sufficient to determine only the limit cycle amplitude and frequency for a given velocity in the neighbourhood of the bifurcation point. In the paper, methods of the local bifurcation theory are applied thus restricting the validity of analysis to some finite interval of velocity.

Hopf bifurcation is two-dimensional what means that limit cycle oscillations are described by only two generalized coordinates, no matter how many degrees of freedom are used in order to describe the original aeroelastic system. A two-dimensional subspace containing these asymptotic oscillations is called the center manifold. Thus, as far as an asymptotic analysis is concerned, it is possible to obtain the limit cycle for an entire aircraft from only two differential equations. Calculation procedure for an aeroelastic system of  $N$  degrees of freedom goes through the following steps [2]:

- Replacement of the initial  $N$  flutter equations of the second order by a system of  $2N$  nonlinear integro-differential equations of the first order (all the methods of the bifurcation theory apply to the first order equations).
- Determination of the bifurcation point (critical flutter velocity) by solving the completely linearized flutter equation.
- Unfolding of the aeroelastic system by expanding all functions into power series with respect to velocity  $U$ , and also considering the velocity being temporarily an additional variable – this increases the total number of equations by one, and is done in order to work on an interval in velocity space in the vicinity of a bifurcation point.
- Projection of the aeroelastic system onto the appropriate center manifold by means of nonlinear transformation of variables, which transforms the initial  $(2N+1)$ -dimensional system of integro-differential equations into a two-dimensional system of ordinary differential equations of the first order.
- Normalization of the reduced system by applying the so-called near-identity change of coordinates, resulting in a much simpler system of equations with rotational symmetry.
- Calculation of the limit cycle amplitude and frequency for a given flight velocity – if all nonlinear terms are expanded into multi-variable Taylor series, then the limit cycle parameters are determined by roots of certain polynomials with real coefficients.

It is worth noting here that projection onto the center manifold preserves all information about asymptotic behaviour of the complete initial system and does

not introduce any simplifying assumptions. Numerical algorithm for the above scheme worked out for systems with many degrees of freedom is given in Ref. [3], and Ref. [4] presents the full nonlinear analysis for a single two-dimensional airfoil.

## 2. Flutter equation

Displacements of an aircraft during unsteady motion are described by the  $M$ -dimensional vector of physical coordinates  $\mathbf{u}(t)$  being functions of time  $t$ . In the steady motion with undeflected structure all coordinates are equal to zero,  $\mathbf{u}(t) = 0$ . Usually, for a conventional aircraft structure, the number  $M$  cannot be less than a few hundreds. This is too many even for the classical (linear) flutter analysis. The routine procedure saves much of the computing time by using modal coordinates in order to reduce the total number of equations. Such an approach assumes the vector of physical coordinates  $\mathbf{u}(t)$  as a linear combination of natural vibration modes with coefficients forming new generalized coordinates. It is sufficient for the flutter analysis to set the number of modal coordinates to nearly twenty. Modal coordinates can also be used in nonlinear approach without any changes [5]. It means that no attempt is made to generalize the natural modes for nonlinear structures but the same linear modes are applied.

In the absence of external aerodynamic forces and under the assumption that the problem has been fully linearized, the natural frequencies  $\omega_j$  and modes  $\Phi_j$  ( $j = 1, 2, \dots, N; j \leq M$ ) can be calculated from the eigenvalue problem:

$$(2.1) \quad \omega_j^2 \mathbf{M} \Phi_j = \mathbf{K} \Phi_j,$$

where  $\mathbf{M}$  and  $\mathbf{K}$  are mass and stiffness matrices, respectively. The set of eigenfunctions of Eq. (2.1) is assumed to describe nonlinear limit cycle oscillations with sufficient accuracy. The vector  $\mathbf{q}(t)$  of modal coordinates is defined by the relation

$$(2.2) \quad \mathbf{u}(t) = \Phi \mathbf{q}(t),$$

and in the absence of the structural damping forces, satisfies the equation of motion [6]:

$$(2.3) \quad \ddot{\mathbf{q}}(t) + \mathbf{K}_\omega \mathbf{q}(t) + \mathbf{k}(\mathbf{q}) = \mathbf{F}_A(\mathbf{q}),$$

where  $\mathbf{F}_A(\mathbf{q})$  is the vector of generalized unsteady aerodynamic forces. The matrix  $\Phi$  is built out of eigenvectors of Eq. (2.1). The diagonal generalized stiffness matrix  $\mathbf{K}_\omega$  is composed of squares of the natural frequencies  $\omega_j^2$  ( $j = 1, 2, \dots, N$ ).

Although the source of the nonlinear term  $\mathbf{k}(\mathbf{q})$  can be either aerodynamics or the aircraft structure, it is assumed here that only the structure is nonlinear.

At present, the only general method of describing the center manifold is based on multi-variable Taylor series [7]. In what follows, it is also assumed that the nonlinear term  $\mathbf{k}(\mathbf{q})$  is of the form of a power series of nonlinear coordinates  $\mathbf{q}$ . For structural nonlinearities such an expansion can be easily obtained. Let  $\mathbf{f}_\delta$  be a  $m$ -dimensional vector of nonlinear forces corresponding to the vector of displacements  $\delta$  in a finite number of structure points:

$$(2.4) \quad \mathbf{f}_\delta = \sum_{j \geq 2} \mathbf{K}_j \delta^j,$$

where  $\mathbf{K}_j$  are diagonal matrices of known numbers, and the symbol  $\delta^j$  means that each vector component is raised to the power of  $j$  separately. In practical calculations, the number of terms of Eq. (2.4) remains finite. In particular, the vector  $\mathbf{f}_\delta$  can include nonlinear springs present in the structure and modeling an aircraft control system. On the other hand, Eq. (2.4) can also describe the properly discretized distributed nonlinearities.

For a given structure it is always possible to find a rectangular matrix  $\mathbf{R}$  of order  $m \times M$  relating the  $m$ -dimensional displacement vector  $\delta$  to the  $M$  physical coordinates  $\mathbf{u}$ :

$$(2.5) \quad \delta = \mathbf{R} \mathbf{u}.$$

After using Eqs. (2.4) and (2.5), the vector  $\mathbf{k}(\mathbf{q})$  of nonlinear generalized forces can be written as:

$$(2.6) \quad \mathbf{k}(\mathbf{q}) = (\mathbf{R} \Phi)^T \mathbf{f}_\delta = (\mathbf{R} \Phi)^T \sum_{j \geq 2} \mathbf{K}_j (\mathbf{R} \Phi \mathbf{q})^j.$$

The aim is to find the critical flutter speed for the Eq. (2.3) and also the limit cycle amplitude and frequency in the neighbourhood of the critical point.

Since the aeroelastic system is nonlinear, it is not possible to assume any given form of the motion during the limit cycle oscillations. Therefore, unsteady aerodynamic forces must be written in a general form valid for an arbitrary motion:

$$(2.7) \quad \mathbf{F}_A(\mathbf{q}) = \frac{\rho U^2}{2} \int_{-\infty}^0 \mathbf{g}(-\tau) \mathbf{q} \left( t + \frac{b}{U} \tau \right) d\tau,$$

where  $U$  and  $\rho$  denote the flow velocity and density, respectively, and  $b$  stands for the characteristic length. Elements of the matrix  $\mathbf{g}$  are response functions corresponding to the impulsive changes of generalized coordinates  $\mathbf{q}$ . Finally, the equation of motion (2.3) takes the form of an integro-differential equation containing an integral of convolution type.

The classical linearized flutter analysis assumes oscillatory motion of an aircraft:

$$(2.8) \quad \mathbf{q}(t) = \hat{\mathbf{q}} e^{st},$$

where the complex coefficient

$$(2.9) \quad s = \gamma + i\omega$$

includes circular frequency  $\omega$  and damping factor  $\gamma$ . For such a motion the vector of unsteady aerodynamic forces is given by the simple linear relation

$$(2.10) \quad \mathbf{F}_A(\mathbf{q}) = \mathbf{A}(s; U)\hat{\mathbf{q}}e^{st},$$

where

$$(2.11) \quad \mathbf{A}(s; U) = \frac{\rho U^2}{2} \int_0^{\infty} \mathbf{g}(\tau) e^{-\frac{sb}{U}\tau} d\tau$$

is called the aerodynamic matrix. The only case for which it is possible to calculate the aerodynamic matrix analytically (in terms of Bessel functions) is a thin airfoil in an incompressible flow [8]. More complex aerodynamic models rely entirely on numerical methods. There are many of them in the literature (a list of the most important ones can be found in [9]), all suited for direct calculation of the aerodynamic matrix, mostly for pure harmonic motion ( $\gamma = 0$ ), without evaluating the response matrix  $\mathbf{g}$ . Although the present method does not assume a harmonic motion, it does not require the knowledge of the response matrix either.

Local bifurcation theory of dynamical systems [7] has been developed for the first-order equations. By introducing a  $2N$ -dimensional vector of new coordinates  $\mathbf{y}(t)$ :

$$(2.12) \quad \mathbf{y}(t) = \begin{Bmatrix} \mathbf{q}(t) \\ \dot{\mathbf{q}}(t) \end{Bmatrix},$$

the first-order flutter equation is obtained:

$$(2.13) \quad \dot{\mathbf{y}}(t) = \mathbf{D}_U \mathbf{y}(t) + \int_{-\infty}^0 \mathbf{G}_U(-\Theta; U) \mathbf{y}(t + \Theta) d\Theta + \mathbf{f}_U(\mathbf{y}),$$

where square matrices of order  $2N$ ,  $\mathbf{D}_U$ ,  $\mathbf{G}_U$ , and the nonlinear term  $\mathbf{f}_U(\mathbf{y})$  are given by:

$$\mathbf{D}_U = \begin{bmatrix} \mathbf{0} & \mathbf{I} \\ -\mathbf{K}_\omega & \mathbf{0} \end{bmatrix}, \quad \mathbf{G}_U(-\Theta; U) = \begin{bmatrix} \mathbf{0} & \mathbf{0} \\ \frac{\rho U^3}{2b} \mathbf{g}\left(-\frac{U}{b}\Theta\right) & \mathbf{0} \end{bmatrix}, \quad \mathbf{f}_U(\mathbf{y}) = \begin{Bmatrix} \mathbf{0} \\ -\mathbf{k}(\mathbf{q}) \end{Bmatrix},$$

with  $\mathbf{k}(\mathbf{q})$  given by Eq. (2.6). For oscillatory motion (2.8), the linearized flutter equation reduces to the eigenvalue problem

$$(2.14) \quad (\mathbf{A}(s; U) - \mathbf{K}_\omega) \hat{\mathbf{q}} = s^2 \hat{\mathbf{q}}.$$

Loss of stability occurs when damping drops to zero ( $\gamma = 0$  in Eq. (2.9)) and the flutter boundary is determined by the real negative eigenvalue of Eq. (2.14)

$$(2.15) \quad s^2 = -\omega_0^2,$$

corresponding to the critical flutter velocity  $U = U_0$ .

The critical bifurcation point of the first order equation (2.13) is defined by the eigenvalues of its linear part corresponding to  $\mathbf{f}_U(\mathbf{y}) = 0$ . It can be shown [7, 10] that also in the presence of convolution integral within the linear part, the eigenfunctions have the form

$$\mathbf{y}(t) = \hat{\mathbf{y}}e^{st},$$

where  $s$  is given by (2.9). The resulting eigenvalue problem is:

$$(2.16) \quad \begin{bmatrix} \mathbf{0} & \mathbf{I} \\ \mathbf{A}(s; U) - \mathbf{K}_\omega & \mathbf{0} \end{bmatrix} \hat{\mathbf{y}} = s\hat{\mathbf{y}}.$$

It follows from comparison with (2.14) that at the flutter boundary, the characteristic matrix of linearized first-order flutter equation has a pair of complex-conjugate, pure imaginary eigenvalues  $s = \pm i\omega_0$ .

The eigenvalue problem (2.16) of the linearized flutter analysis can be derived in a more formal way by applying the Laplace transform, which replaces the convolution integral in Eq. (2.13) by the product of two functions. In nonlinear approach there are two possible ways: either the application of Laplace transform in frequency domain or solution of the problem in time domain. The first method is suitable for handling convolution integrals but faces more difficulties due to nonlinear terms. On the other hand, working in time domain shifts the whole problem to proper treatment of the convolution integral. The present paper uses the time-domain method.

The qualitative changes in a behaviour of the nonlinear dynamical system are always indicated by the purely imaginary (or zero) eigenvalues of the linearized operator of the governing equation. For the nonlinear flutter equation (2.13) this operator is of the form:

$$\mathcal{L}\mathbf{y}(t) = \mathbf{D}_U \mathbf{y}(t) + \int_{-\infty}^0 \mathbf{G}_U(-\Theta; U)\mathbf{y}(t + \Theta)d\Theta.$$

Since the operator  $\mathcal{L}$  maps a space of continuous functions onto the Euclidean space, then the eigenvalue problem  $\mathcal{L}\boldsymbol{\varphi} = \lambda\boldsymbol{\varphi}$  cannot be posed directly. Instead, an extension of  $\mathcal{L}$  is made in order to map a space of continuous functions onto

itself. An extended operator is the following [10, 11]:

$$(2.17) \quad \mathcal{L}_U \boldsymbol{\varphi}(\Theta) = \begin{cases} \frac{d\boldsymbol{\varphi}(\Theta)}{d\Theta}, & \text{for } -\infty < \Theta < 0, \\ \mathbf{D}_U \boldsymbol{\varphi}(0) + \int_{-\infty}^0 \mathbf{G}_U(-\tau; U) \boldsymbol{\varphi}(\tau) d\tau, & \text{for } \Theta = 0, \end{cases}$$

and the flutter equation takes the form:

$$(2.18) \quad \frac{d\mathbf{y}_t(\Theta)}{d\Theta} = \mathcal{L}_U \mathbf{y}_t(\Theta) + \begin{cases} 0, & \text{for } -\infty < \Theta < 0, \\ \mathbf{f}(\mathbf{y}_t(0)), & \text{for } \Theta = 0, \end{cases}$$

where the following notation has been introduced:

$$\mathbf{y}_t(\Theta) = \mathbf{y}(t + \Theta).$$

Now, the eigenvalue problem  $\mathcal{L}_U \boldsymbol{\varphi} = \lambda \boldsymbol{\varphi}$  can be formulated. First, the form of the eigenfunction is determined ( $-\infty < \Theta < 0$ ):

$$\frac{d\boldsymbol{\varphi}(\Theta)}{d\Theta} = \lambda \boldsymbol{\varphi}(\Theta) \quad \Rightarrow \quad \boldsymbol{\varphi}(\Theta) = \boldsymbol{\varphi}(0) e^{\lambda t},$$

and next the eigenproblem for the Euclidean vector  $\boldsymbol{\varphi}(0)$  is posed

$$(2.19) \quad \mathbf{D}_U \boldsymbol{\varphi}(0) + \left( \int_{-\infty}^0 \mathbf{G}_U(-\tau; U) e^{\lambda \tau} d\tau \right) \boldsymbol{\varphi}(0) = \lambda \boldsymbol{\varphi}(0).$$

As can be seen, both eigenvalue problems (2.16) and (2.19) are identical. Therefore, since at criticality there is a pair of pure imaginary eigenvalues, flutter instability is the Hopf bifurcation [10].

### 3. Center-manifold reduction

If any bifurcation occurs in a dynamical system, then the phase space splits in general into three manifolds: stable – generated by eigenvalues with  $\text{Re}(\lambda) < 0$ , unstable – generated by eigenvalues with  $\text{Re}(\lambda) > 0$ , and center manifold, corresponding to  $\text{Re}(\lambda) = 0$  [12]. Center manifold is invariant, locally attracting and asymptotically stable. Moreover, it is of finite dimensions – for the Hopf bifurcation it is two-dimensional. It means that in the space of all solutions to Eq. (2.18), bifurcating solution tends asymptotically to a two-dimensional attracting subspace. The asymptotic solution (limit cycle oscillations) satisfies a certain system of two nonlinear ordinary differential equations of the first order,

which can be derived from the integro-differential equation (2.18), written for many degrees of freedom. This procedure of obtaining a low-dimensional system of equations from the initial multi-dimensional system is called center-manifold reduction.

There are two problems associated with the center-manifold reduction. Since the aim is to calculate asymptotic limit cycle oscillations for a general form of the nonlinear term  $\mathbf{f}_U(\mathbf{y})$ , this term is assumed to have a formal power series expansion with respect to generalized coordinates  $\mathbf{y}$ . Consequently, the method of center-manifold reduction is also based on such expansions. The second problem concerns the way the velocity  $U$  should be treated in. The critical flutter conditions correspond to a certain critical value of the velocity  $U = U_0$ , which in turn determines the existence of purely imaginary eigenvalues of Eq. (2.19) and the center manifold, as well. At this critical branch point the amplitude of oscillations tends to zero and, in order to obtain the finite amplitude limit cycle oscillations, the value of velocity must be different from the critical one. Unfortunately, if  $U \neq U_0$ , the characteristic matrix of Eq. (2.19) no longer possesses pure imaginary eigenvalues and the center manifold simply does not exist. On the other hand, the existence of the center manifold has been proven in a certain neighbourhood of equilibrium solution  $\mathbf{y}_0(t)$ , corresponding to  $U = U_0$ , in the space of solutions  $\mathbf{y}(t)$  [10]. For that reason, the center-manifold reduction usually applies to the so-called suspended systems. Suspended aeroelastic system is derived from Eq. (2.13) by introducing the difference

$$(3.1) \quad u = U - U_0$$

as an additional variable satisfying the equation  $\dot{u} = 0$ . The  $2N+1$ -dimensional vector of new generalized coordinates is the following:

$$(3.2) \quad \mathbf{x}(t) = \begin{Bmatrix} \mathbf{q}(t) \\ \dot{\mathbf{q}}(t) \\ u \end{Bmatrix},$$

and satisfies the equation

$$(3.3) \quad \dot{\mathbf{x}}(t) = \mathbf{D} \mathbf{x}(t) + \int_{-\infty}^0 \mathbf{G}(-\Theta; u) \mathbf{x}(t + \Theta) d\Theta + \mathbf{f}(\mathbf{x}),$$

where square matrices of order  $2N + 1$   $\mathbf{D}$ ,  $\mathbf{G}$ , and the nonlinear term  $\mathbf{f}(\mathbf{x})$  are given by

$$\mathbf{D} = \begin{bmatrix} \mathbf{0} & \mathbf{I} & \mathbf{0} \\ -\mathbf{K}_\omega & \mathbf{0} & \mathbf{0} \\ \mathbf{0} & \mathbf{0} & 0 \end{bmatrix}, \quad \mathbf{G}(-\Theta; u) = \begin{bmatrix} \mathbf{0} & \mathbf{0} & \mathbf{0} \\ \frac{\rho(U_0 + u)^3}{2b} \mathbf{g}\left(-\frac{U_0 + u}{b} \Theta\right) & \mathbf{0} & \mathbf{0} \\ \mathbf{0} & \mathbf{0} & 0 \end{bmatrix},$$

$$\mathbf{f}(\mathbf{x}) = \begin{Bmatrix} \mathbf{0} \\ -\mathbf{k}(\mathbf{q}) \\ 0 \end{Bmatrix}.$$

Since the matrix  $\mathbf{G}(-\Theta; u)$  now includes the independent variable  $u$  instead of the bifurcation parameter  $U$ , the integral in Eq. (3.3) is no longer linear with respect to  $\mathbf{x}$ . In what follows, the matrix  $\mathbf{G}$  is replaced by the Taylor series

$$(3.4) \quad \mathbf{G}(-\Theta; u) = \mathbf{G}(-\Theta; 0) + \sum_{j=1}^{\infty} \frac{1}{j!} \frac{d^j \mathbf{G}(-\Theta; 0)}{du^j} u^j.$$

It is also assumed that the multi-variable power series expansion for the non-linear function  $\mathbf{f}(\mathbf{x})$  at the right-hand side of Eq. (3.3) is known:

$$(3.5) \quad \mathbf{f}(\mathbf{x}) = \sum_{\nu \geq 2} \frac{1}{\nu!} \mathbf{f}_{\nu} \mathbf{x}^{\nu},$$

where

$$\mathbf{x}^{\nu} = \{x_1^{\nu_1} \cdot x_2^{\nu_2} \cdots x_{2N+1}^{\nu_{2N+1}}\}, \quad \sum_{j=1}^{2N+1} \nu_j = \nu, \quad \nu_j \geq 0.$$

The number of components of the vector  $\mathbf{x}^{\nu}$  and also the number of columns of each matrix  $\mathbf{f}_{\nu}$  changes from one term to another and equals the number  $c_{\nu, 2N+1}$  of compositions of  $\nu$  into  $2N+1$  parts

$$(3.6) \quad c_{\nu, 2N+1} = \binom{\nu + 2N}{\nu - 1}.$$

The elements of matrices  $\mathbf{f}_{\nu}$  can be easily calculated from Eq. (2.6). Substitution of series (3.4) into Eq. (3.3) yields the integro-differential equation valid in a certain neighbourhood of the critical bifurcation point:

$$(3.7) \quad \dot{\mathbf{x}}(t) = \mathbf{D} \mathbf{x}(t) + \int_{-\infty}^0 \mathbf{G}(-\Theta; 0) \mathbf{x}(t + \Theta) d\Theta + \mathbf{h}(\mathbf{x}),$$

where  $\mathbf{h}(\mathbf{x})$  equals

$$(3.8) \quad \mathbf{h}(\mathbf{x}) = \mathbf{f}(\mathbf{x}) + \sum_{\eta \geq 2} \frac{1}{(\eta - 1)!} \int_{-\infty}^0 \frac{d^{\eta-1} \mathbf{G}(-\Theta; 0)}{du^{\eta-1}} \mathbf{x}^{\eta}(t + \Theta) d\Theta,$$

with  $\mathbf{x}^\eta = \{x_1^{\eta_1} \cdot x_2^{\eta_2} \cdots x_{2N+1}^{\eta_{2N+1}}\}$ , and always  $\eta = \eta_{2N+1} + 1$  ( $x_{2N+1} \equiv u$ ) which implies that  $\sum_{j=1}^{2N} \eta_j = 1$ . Equation (3.7) will be reduced on the center manifold.

The linear spectrum of Eq.(3.7) includes one eigenvalue with zero real part more than the previous spectrum of the non-suspended system (2.13). Hence the center manifold corresponding to Eq.(3.7) is larger than that of Eq.(2.13) and has the dimension of three.

Since the center manifold is tangent to the linear subspace spanned by eigenvectors  $\boldsymbol{\varphi}$ , corresponding to the bifurcating eigenvalues of the extended linear operator  $\mathcal{L}_0$  derived from Eq.(3.7)

$$(3.9) \quad \mathcal{L}_0 \boldsymbol{\varphi}(\Theta) = \begin{cases} \frac{d\boldsymbol{\varphi}(\Theta)}{d\Theta}, & \text{for } -\infty < \Theta < 0, \\ \mathbf{D}\boldsymbol{\varphi}(0) + \int_{-\infty}^0 \mathbf{G}(-\tau; 0)\boldsymbol{\varphi}(\tau) d\tau, & \text{for } \Theta = 0, \end{cases}$$

then it is convenient to introduce the three-dimensional vector  $\mathbf{z}(t)$  of center-manifold coordinates as follows:

$$(3.10) \quad \mathbf{x}_t(\Theta) = \sum_{j=1}^3 z_j(t)\boldsymbol{\varphi}_j(\Theta) + \mathbf{w}(\Theta, t),$$

with the yet unknown function  $\mathbf{w}(\Theta, t)$  satisfying the conditions:

$$(3.11) \quad \mathbf{w}(\Theta, t) = \mathbf{w}(\Theta, \mathbf{z}(t)), \quad \mathbf{w}(\Theta, 0) = 0, \quad \frac{d\mathbf{w}(\Theta, 0)}{d\mathbf{z}} = 0.$$

The above conditions, besides tangency, reflect invariant properties of the center manifold.

In order to restrict the aeroelastic system to the center manifold, the projection operator  $P$  must be determined, satisfying relations

$$(3.12) \quad \begin{aligned} P\mathbf{x}_t(\Theta) &= \mathbf{z}(t), \\ P\mathbf{w}(\Theta, \mathbf{z}(t)) &= 0. \end{aligned}$$

The projection procedure is based on the so-called outer product [10, 11], associated with the extended linear operator  $\mathcal{L}_0$ :

$$(3.13) \quad \langle \mathbf{x}^*, \mathbf{x} \rangle = \bar{\mathbf{x}}^{*T}(0)\mathbf{x}(0) - \int_{-\infty}^0 \int_0^\eta \bar{\mathbf{x}}^{*T}(\xi - \eta)\mathbf{G}(-\eta; u)\mathbf{x}(\xi) d\xi d\eta,$$

with two continuous functions  $\mathbf{x}(\xi)$  and  $\mathbf{x}^*(\eta)$  defined over intervals  $-\infty < \xi < 0$  and  $0 > \eta > \infty$ , respectively. The adjoint operator is defined in a standard way by the relation:

$$\langle \mathbf{x}^*, \mathcal{L}_0 \mathbf{x} \rangle = \langle \mathcal{L}_0^* \mathbf{x}^*, \mathbf{x} \rangle.$$

The eigenvalues and eigenvectors of two eigenproblems  $\mathcal{L}_0 \boldsymbol{\varphi} = \lambda \boldsymbol{\varphi}$  and  $\mathcal{L}_0^* \boldsymbol{\psi} = \lambda^* \boldsymbol{\psi}$  satisfy the equalities  $\lambda^* = \bar{\lambda}$ ,  $\langle \boldsymbol{\psi}_k, \boldsymbol{\varphi}_l \rangle = \delta_{kl}$ . By using Eqs. (3.9)–(3.13), the simple set of three nonlinear first-order ordinary differential equations describing asymptotic motion on the center manifold is obtained [10]:

$$(3.14) \quad \dot{\mathbf{z}} = \mathbf{\Lambda} \mathbf{z} + \overline{\boldsymbol{\Psi}}^T(0) \mathbf{h}_0,$$

where  $\mathbf{\Lambda}$  denotes the diagonal matrix of eigenvalues  $i\omega_0, -i\omega_0, 0$ , and the matrix  $\boldsymbol{\Psi}$  is composed of the corresponding eigenfunctions  $\boldsymbol{\psi}_j$  ( $j = 1, 2, 3$ ). The  $(2N + 1)$ -dimensional vector function  $\mathbf{w}(\Theta, \mathbf{z}(t))$  defines essentially the center manifold and the projection operator as well. It satisfies the integro-differential equation:

$$(3.15) \quad \dot{\mathbf{w}} - \mathcal{L}_0 \mathbf{w} = \begin{cases} -\sum_{j=1}^3 \overline{\boldsymbol{\psi}}_j^T(0) \mathbf{h}_0 \boldsymbol{\varphi}_j(\Theta), & \text{for } -\infty < \Theta < 0, \\ -\sum_{j=1}^3 \overline{\boldsymbol{\psi}}_j^T(0) \mathbf{h}_0 \boldsymbol{\varphi}_j(0) + \mathbf{h}_0, & \text{for } \Theta = 0 \end{cases}$$

and also the orthogonality conditions, which have not yet been implicitly imposed:

$$\langle \boldsymbol{\psi}_j, \mathbf{w} \rangle = 0, \quad j = 1, 2, 3.$$

Both equations (3.14) and (3.15) are coupled by the right-hand side nonlinear term:

$$\mathbf{h}_0 = \mathbf{h}(\mathbf{x}_t(0)) = \mathbf{h} \left( \sum_{j=1}^3 z_j(t) \boldsymbol{\varphi}_j(0) + \mathbf{w}(\mathbf{z}, 0) \right).$$

Although the assumption (3.5) describing the nonlinear term by multi-variable power series has not been used so far, it seems to be rather necessary in order to solve the system of Eqs. (3.14) and (3.15). In what follows, also the function  $\mathbf{w}$  is expanded into such a series

$$(3.16) \quad \mathbf{w}(\mathbf{z}, \Theta) = \sum_{\mu \geq 2} \frac{1}{\mu!} \mathbf{w}_\mu(\Theta) \mathbf{z}^\mu(t).$$

In terms of power series, the Eq. (3.15) takes the form

$$(3.17) \quad \sum_{\mu \geq 2} \frac{1}{\mu!} (\mathbf{w}_\mu(\Theta) \mathbf{\Lambda}_\mu - \mathcal{L}_0 \mathbf{w}_\mu(\Theta)) \mathbf{z}^\mu = \begin{cases} 0, & \text{for } -\infty < \Theta < 0, \\ \sum_{\nu \geq 2} \frac{1}{\nu!} \mathbf{r}_\nu(\Theta) \mathbf{z}^\nu + \left\{ \sum_{\nu \geq 2} \frac{1}{\nu!} \mathbf{h}_{0\nu} \mathbf{z}^\nu, \right. & \text{for } \Theta = 0, \end{cases}$$

where

$$(\Lambda_\mu)_{kk} = \sum_{j=1}^3 \lambda_j \mu_j, \quad k = 1, 2, \dots, c_{\mu, 2N+1},$$

and the first right-hand series of (3.17) is given by

$$\sum_{\nu \geq 2} \frac{1}{\nu!} \mathbf{r}_\nu(\Theta) \mathbf{z}^\nu = - \sum_{j=1}^3 \overline{\boldsymbol{\Psi}}_j^T(0) \mathbf{h}_0 \frac{\partial}{\partial z_j} \sum_{\mu \geq 2} \frac{1}{\mu!} \mathbf{w}_\mu(\Theta) \mathbf{z}^\mu.$$

The method of recursive calculations of coefficients of equations (3.14) and (3.17) is described in details in Ref. [3]. It is worth noting here that calculations can be carried out up to the desired order of approximation.

From a quite formal point of view, the center-manifold reduction is equivalent to the appropriate nonlinear change of coordinates given in the form of a series, linking (3.10) and (3.16):

$$(3.18) \quad \mathbf{x}(t + \Theta) = \sum_{\mu \geq 1} \frac{1}{\mu!} \mathbf{w}_\mu(\Theta) \mathbf{z}^\mu(t),$$

where the vector  $\mathbf{z}(t)$  of new coordinates has only three components. The matrices  $\mathbf{w}_\mu(\Theta)$  of order  $(2N+1) \times c_{\mu,3}$ , where  $c_{\mu,3}$  denotes the number of compositions of  $\mu$  into 3 parts (3.6), are composed of continuous functions defined in the interval  $\Theta \in (-\infty, 0]$ . The algorithm of center-manifold reduction provides the way of calculating these functions and also the method of simultaneous derivation of the first-order ordinary differential equation describing the limit cycle oscillations in terms of new variables  $\mathbf{z}$ :

$$(3.19) \quad \dot{\mathbf{z}}(t) = \Lambda \mathbf{z}(t) + \sum_{\mu \geq 2} \frac{1}{\mu!} \mathbf{d}_\mu \mathbf{z}^\mu,$$

where  $\Lambda$  denotes, as before, the diagonal matrix of eigenvalues  $i\omega_0$ ,  $-i\omega_0$ , 0, and  $\mathbf{d}_\mu$  are rectangular matrices built out of the already known complex numbers. The way in which the suspended system has been introduced implies that  $z_3 \equiv u$  and also  $\dot{z}_3(t) = 0$ , which means that an asymptotic motion is essentially two-dimensional. The third variable  $u$  acts once again as a parameter, while the suspended system serves as a convenient tool for deriving the series expansion with respect to it.

The next important conclusion drawn from the algorithm of center-manifold reduction says that there is no need to know the response functions forming elements of the matrix  $\mathbf{G}(-\Theta; 0)$ . This is because the columns  $\mathbf{w}_{\mu k}(\Theta)$ ,  $k = 1, 2, \dots, c_{\mu, 2N+1}$ ,  $\mu \geq 1$ , of each matrix  $\mathbf{w}_\mu(\Theta)$  of the series (3.16), can be only of the elementary form [3]:

$$\mathbf{w}_{\mu k}(\Theta) = \widehat{\mathbf{w}}_{\mu k} \Theta^j e^{s\Theta},$$

with integer  $j \geq 0$ , and  $s$  being an imaginary number. Consequently, all integrals involving the response functions within the algorithm can be carried out as follows:

$$(3.20) \quad \int_{-\infty}^0 \frac{d^r \mathbf{G}(-\Theta; 0)}{d\Theta^r} \Theta^j e^{s\Theta} d\Theta = \frac{\partial^{r+j} \mathbf{A}(s; U_0)}{\partial U^r \partial s^j},$$

where  $r \geq 0$ , and the only non-zero block of the matrix

$$\mathbf{A}(s; U_0) = \begin{bmatrix} \mathbf{0} & \mathbf{0} & \mathbf{0} \\ \mathbf{A}(s; U_0) & \mathbf{0} & \mathbf{0} \\ \mathbf{0} & \mathbf{0} & 0 \end{bmatrix}$$

is the aerodynamic matrix  $\mathbf{A}(s; U)$  given by Eq. (2.11) and calculated for a pure harmonic motion and the critical velocity  $U_0$ .

Since Eq. (3.19) is an ordinary differential equation, it can be easily transformed to the so-called Poincaré normal form either by the Lie transforms [7] or by recursive change of coordinates [13]. Both methods introduce new variables  $\zeta(t)$  related to  $\mathbf{z}(t)$  by the near-identity transformation

$$(3.21) \quad \mathbf{z}(t) = \zeta(t) + \sum_{\nu \geq 2} \frac{1}{\nu!} \mathbf{b}_\nu \zeta^\nu(t).$$

This transformation retains the form of Eq. (3.19) also with respect to new coordinates  $\zeta(t)$ . The calculation of elements of matrices  $\mathbf{b}_\nu$  requires to make as many coefficients  $\mathbf{d}_\mu$  equal to zero as possible. The simplification achieved lies in the phase-shift symmetry introduced by the transformation (3.21). The normal form of Hopf bifurcation in polar coordinates  $r, \theta$ :

$$(3.22) \quad \zeta_1 = r e^{i\theta}, \quad \zeta_2 = \bar{\zeta}_1$$

may be written as [2]:

$$(3.23) \quad \begin{aligned} \dot{r} &= r \left( \gamma(u) + \sum_{j=1}^{\infty} a_j(u) r^{2j} \right), \\ \dot{\theta} &= \omega(u) + \sum_{j=1}^{\infty} b_j(u) r^{2j}, \end{aligned}$$

where  $\gamma(u) \pm i\omega(u)$  is the pair of complex-conjugate eigenvalues ( $\gamma(0) = 0$ ,  $\omega(0) = \omega_0$ ). All functions  $\gamma(u)$ ,  $\omega(u)$ ,  $a_j(u)$ ,  $b_j(u)$  are real and have the form of power series expansions with respect to  $u$ . In practical calculations, Eqs. (3.23)

are implemented up to some finite order  $n$  ( $j \leq n$ ). Therefore, the amplitude  $r_H$  of the limit cycle oscillations satisfies an algebraic equation obtained from Eq.(3.23)<sub>1</sub> by setting  $\dot{r} = 0$ :

$$(3.24) \quad \gamma(u) + \sum_{j=1}^n a_j(u)r_H^{2j} = 0.$$

For any given  $u$ , the left-hand side of Eq.(3.24) is of the form of a polynomial in  $r_H$ . Hence all possible limit cycle amplitudes are determined by the real positive roots of this polynomial. Since limit cycle oscillations  $\zeta_1 = \zeta_H(t)$  on the center manifold are purely harmonic [10]:

$$(3.25) \quad \zeta_H = r_H e^{i\omega_H t},$$

then for each amplitude  $r_H$  the corresponding frequency  $\omega_H$  is calculated from

$$(3.26) \quad \omega_H = \omega(u) + \sum_{j=1}^n b_j(u)r_H^{2j}.$$

The sequence of transformations of variables given by Eqs.(3.22), (3.21), (3.18), (3.2), (2.12) and (2.2) yields the final limit cycle oscillations of physical variables  $\mathbf{u}(t)$ . Since two of these transformations are nonlinear, the physical variables do not oscillate harmonically in time, contrary to the center-manifold variables  $\zeta(t)$ .

Flutter analysis of an aircraft imposes a number of requirements not satisfied by solutions of the Hopf bifurcation for functional differential equations, available in the literature. First of all, it is not sufficient to take into account only the highest order term of (3.24), which gives the characteristic square-root growth of the limit cycle amplitude

$$r_H = \sqrt{\beta u},$$

where

$$(3.27) \quad \beta = -\frac{1}{a_1(0)} \frac{d\gamma(0)}{du},$$

because the region of validity of this approximation is too close to the bifurcation point to be of practical importance. An example of such a limited analysis is included in [10] and has given a good starting point for the present method. A two-term approximation, however not using the center-manifold reduction, is given in [14], but because of the very special method of solution of the problem, it cannot be directly extended to the arbitrary number of terms and to systems with many degrees of freedom.

#### 4. Numerical examples

All numerical examples presented in this section assume that the nonlinearities are concentrated in the points of connection between the lifting and control surfaces of an aircraft, producing nonlinear restoring moments when the control surfaces perform rotation about the hinge lines. It is also assumed that each hinge moment  $M_\delta$  is a cubic function of the local angle of rotation  $\delta$

$$(4.1) \quad M_\delta = K_\delta(\delta + c\delta^3),$$

where  $K_\delta$  is a standard linear spring constant, and the coefficient  $c$  describes the strength of nonlinearity. The last assumption means that there is only one non-zero matrix  $\mathbf{K}_2$  in Eq. (2.4).

Since each nonlinear analysis is essentially an extension of the corresponding linearized problem, it is impossible to calculate the limit cycle parameters for an aircraft without having a suitable computer program for the linear flutter analysis. The standard output of such program includes critical flutter velocity  $U_0$ , the corresponding frequency  $\omega_0$  and the flutter mode in the form of a right eigenvector  $\hat{\mathbf{q}}$  of Eq. (2.14). For a nonlinear flutter analysis the following additional data should be supplied:

- elements of the aerodynamic matrix (2.11) corresponding to the flutter point,
- a set of derivatives (3.20) of the aerodynamic matrix corresponding to the flutter velocity and calculated for  $s = \pm i\omega_0, \pm 2i\omega_0, \pm 3i\omega_0 \dots$  up to the desired order of approximation,
- elements of the matrix  $\mathbf{R}$  (2.5) defining locations of nonlinear springs within the aircraft structure.

Since the aerodynamic matrix is essentially a function of nondimensional variable  $p = \omega b/U$ , the derivatives of the aerodynamic matrix with respect to variables  $s$  and  $U$  can be easily evaluated if the corresponding derivatives with respect to  $p$  are known. For the  $n$ -th order of approximation of the Eqs. (3.23), the highest derivatives are of order  $2n - 1$ . Although some simpler unsteady aerodynamic models allow for an analytical calculation of derivatives (e.g. strip theory), it seems that in general, the only efficient way is numerical differentiation. This is because in most cases the aerodynamic matrix is known only numerically (i.e. as a set of numbers). It has been found that satisfactory results, especially for higher-order derivatives, gives a simple integration scheme based on the Cauchy integral in the complex  $p$ -plane:

$$\frac{d^j a_{kl}(p)}{dp^j} = \frac{j!}{2\pi i} \oint_C \frac{a_{kl}(z)}{(z-p)^{j+1}} dz \approx \frac{j!}{2\pi i} \sum_{r=1}^m \frac{a_{kl}(z_r)}{(z_r-p)^{j+1}} \Delta z_r,$$

where  $a_{kl}(p)$  denotes an element of the aerodynamic matrix. Integration nodes  $z_r$  are placed on a small circle  $C$  with an origin in the point  $p$ . All values of

argument  $p$  of the derivatives appearing in center-manifold reduction are purely imaginary numbers, hence the standard numerical methods for calculation of the aerodynamic matrix can be applied.

The number of degrees of freedom of an aircraft may cause some computational problems since the amount of numerical work required grows very fast. For an aircraft with only six degrees of freedom (modal coordinates) and four-term center-manifold approximation ( $n = 4$  in Eqs. (3.24) and (3.26)), the number of components of the last, 9-th vector  $\mathbf{x}^n$  in Eq. (3.8) equals 293930. Therefore, it is very important to select only the most significant natural modes out of all the modes included in the flutter mode, in order to save both the computer time and memory. Since the center manifold is tangent to the linear subspace spanned by two complex-conjugate eigenvectors of the linear operator (2.17), such a selection is done in the same way as in the conventional linear flutter analysis.

Sample calculations of the limit cycle amplitude and frequency were made for the aileron and flap flutter of two gliders. All hinge springs of the control surfaces were assumed to produce hardening cubic nonlinearities. The number of physical degrees of freedom used to calculate the natural modes was equal to nearly 200. Six modal coordinates were taken into account, including two or three rigid modes. The first glider revealed symmetric and also antisymmetric flap-aileron flutter at velocities 187 km/h and 178 km/h, respectively. Similar antisymmetric flutter at 225 km/h occurred for the second glider.

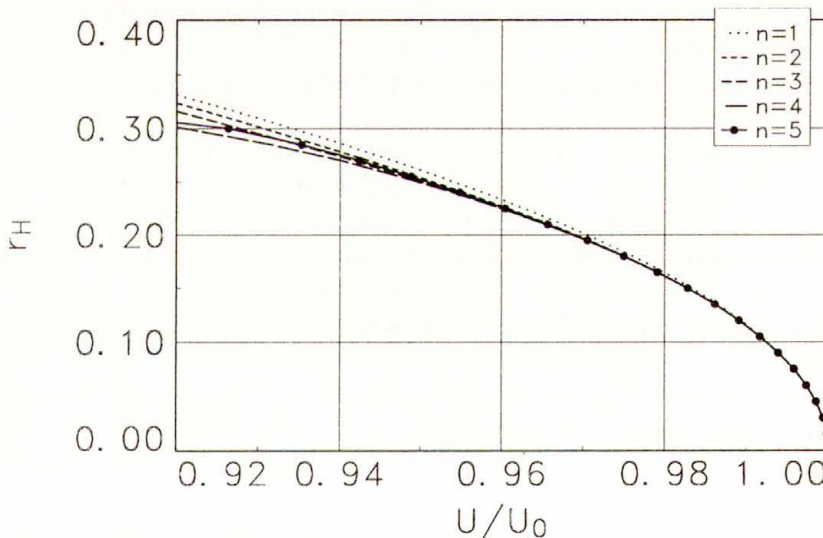


FIG. 1. Amplitude of center-manifold Hopf limit cycle (symmetric flutter).

Both gliders had one nonlinear aileron hinge spring with  $c = 50$  (4.1). Results of calculations for the first glider are presented in Figs. 1–8. Figures 9–12 concern the second glider. Symbol  $n$  in all figures denotes the number of terms of the

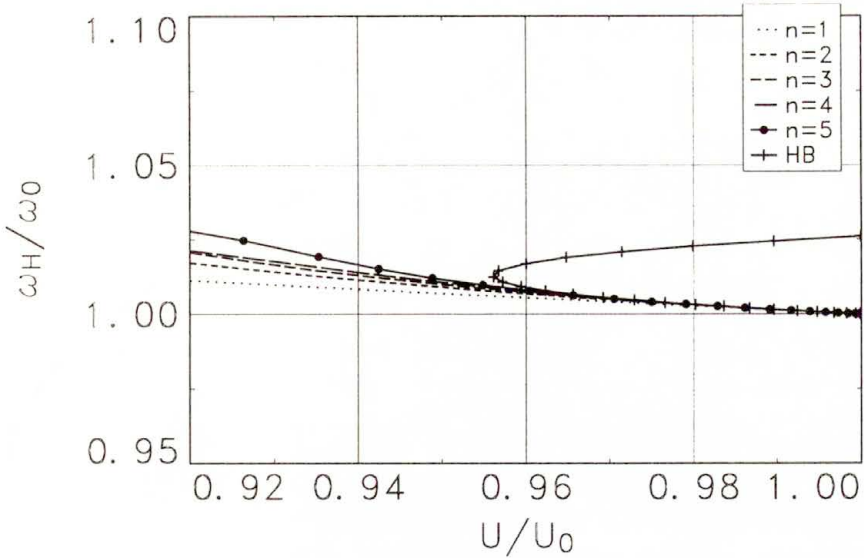


FIG. 2. Frequency of center-manifold Hopf limit cycle (symmetric flutter).

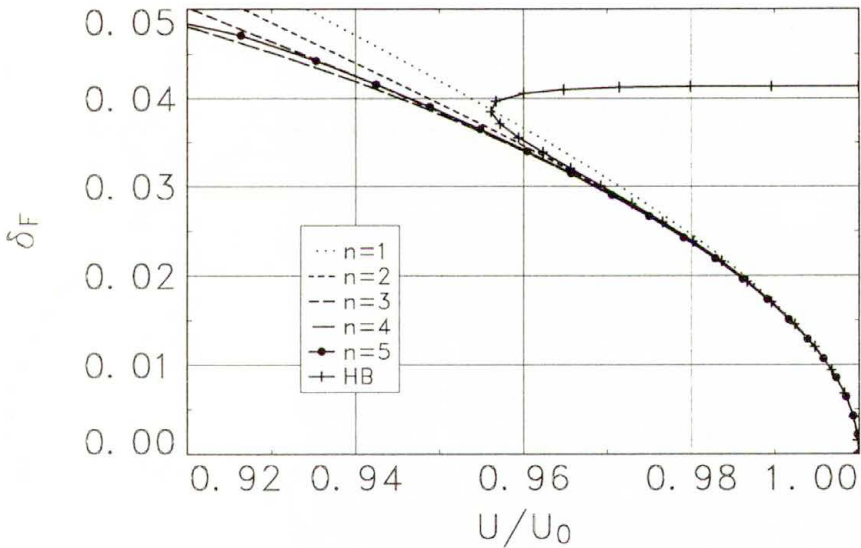


FIG. 3. Flap limit cycle amplitude (symmetric flutter).

series (3.24) and (3.26). As the final results of calculations, the Hopf limit cycle amplitude  $r_H$  (3.24), normalized with respect to  $\sqrt{\beta}$  (3.27), and frequency  $\omega_H/\omega_0$  (3.26) are plotted against the nondimensional velocity  $U/U_0$ . There is a sequence of five approximations in each chart, corresponding to  $n = 1, 2, 3, 4, 5$ . Note that

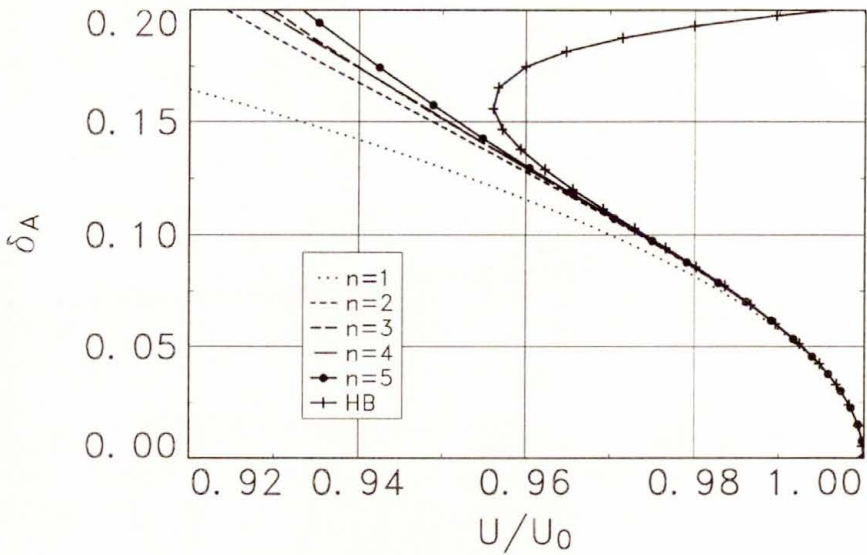


FIG. 4. Aileron limit cycle amplitude (symmetric flutter).

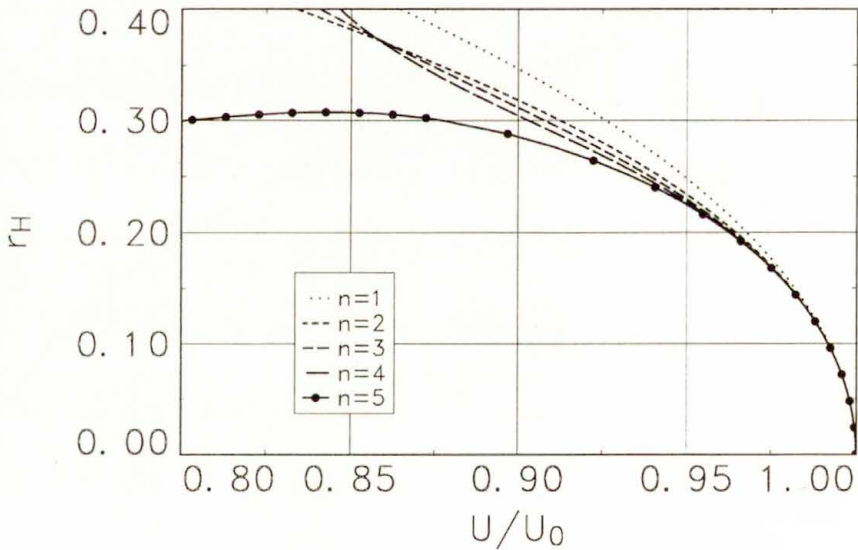


FIG. 5. Amplitude of center-manifold Hopf limit cycle (antisymmetric flutter).

$n$ -th order approximation of a center-manifold limit cycle requires  $2n + 1$  terms in the power series expansion (3.18).

Once the center manifold limit cycle parameters are known, it is possible to calculate the physical deflections of a glider during oscillations. Only two of them

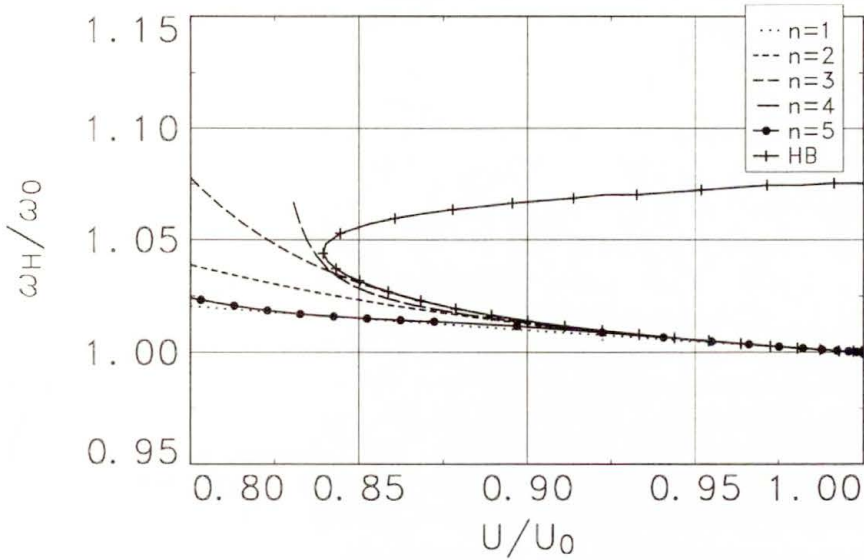


FIG. 6. Frequency of center-manifold Hopf limit cycle (antisymmetric flutter).

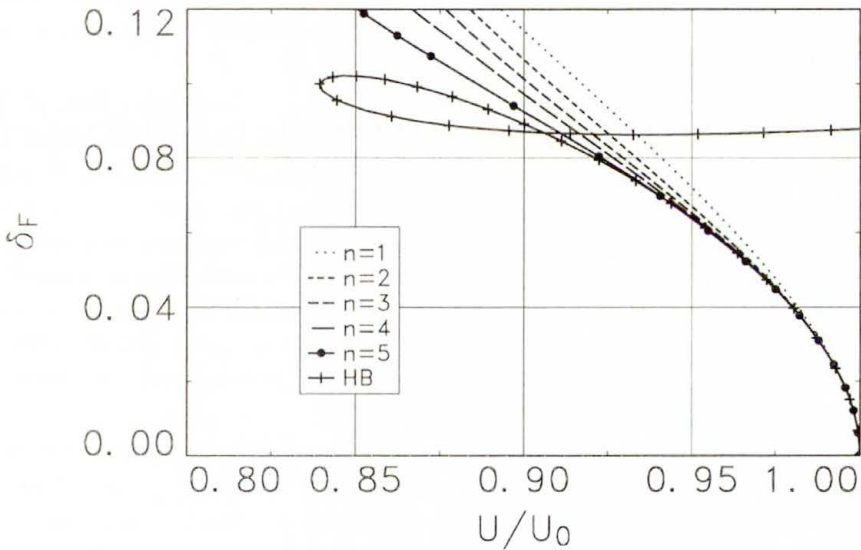


FIG. 7. Flap limit cycle amplitude (antisymmetric flutter).

are plotted: local hinge-line rotation of flap  $\delta_F$  and aileron  $\delta_A$ . Both correspond to the location of nonlinear springs and are measured in radians. Because physical coordinates do not oscillate harmonically in time (though in a very similar manner), the amplitude of oscillations is not well-defined. Therefore,  $\delta_F$  and  $\delta_A$

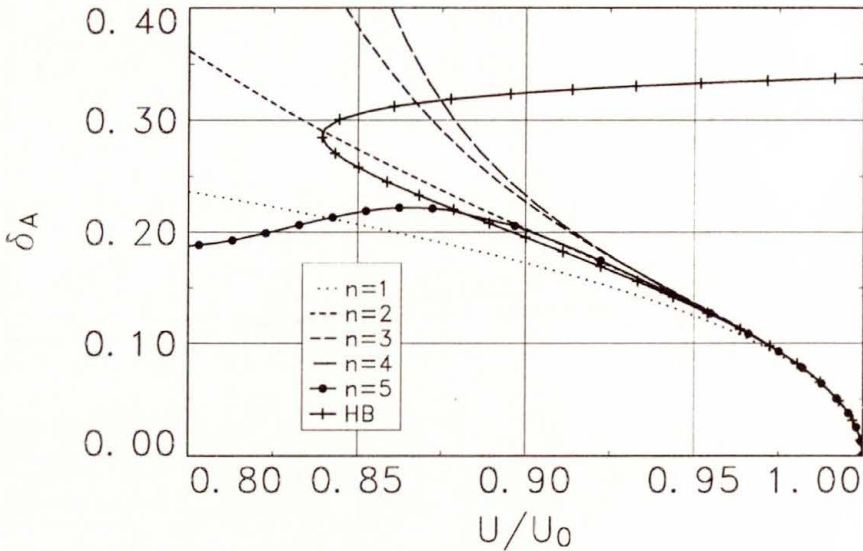


FIG. 8. Aileron limit cycle amplitude (antisymmetric flutter).

denote maximum values of the rotation angle reached during a single period. In all figures the unstable limit cycles appear in the vicinity of the corresponding bifurcation points.

In almost every chart there is an additional line taken from Ref. [17], and denoted HB, describing the amplitude of limit cycle oscillations calculated by the harmonic balance method [15], by using the continuation subroutines package [16]. Harmonic balance method replaces each nonlinear restoring force by the first term of its Fourier transform. If there is only one nonlinear force present in a system, then for any given limit cycle amplitude the linearized flutter equation can be solved for the corresponding flight velocity. Multiple nonlinearities result in greater complexity of calculations, because the amplitudes of aircraft deflections at concentration points are not known prior to the calculations, but their ratios are determined by the resulting flutter mode.

There is a very good agreement between the results of the present method and the harmonic balance method, in a range of a few percent below the linear flutter velocity  $U_0$ . However, beyond this interval a qualitative discrepancy of the results of both methods are observed, and also the power series derived by the present method are not convergent anymore.

It was impossible to establish the real behaviour of limit cycle oscillations of the gliders because neither the flight tests nor direct numerical integration of the nonlinear flutter equation were performed. Nevertheless, it is important that the limit cycle oscillations are detected below the linear flutter velocity despite the fact that their amplitude is uncertain. These oscillations can be initiated by a

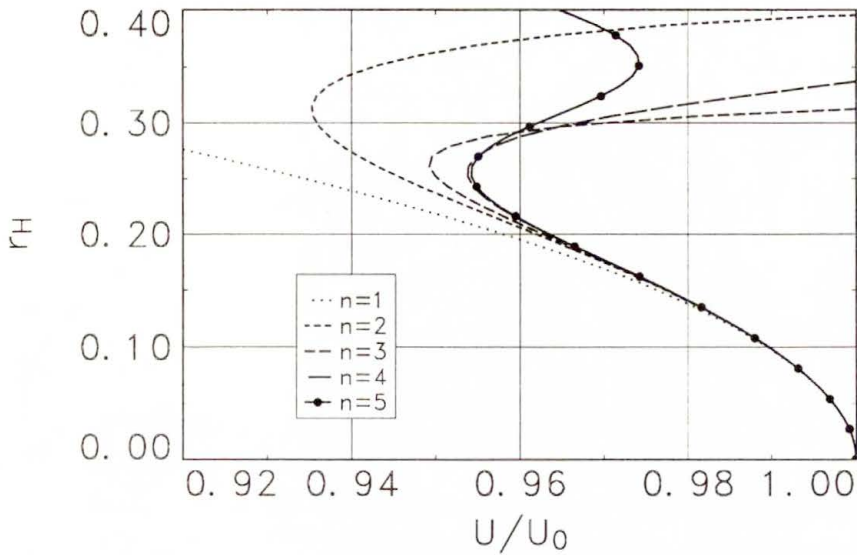


FIG. 9. Amplitude of center-manifold Hopf limit cycle (antisymmetric flutter).

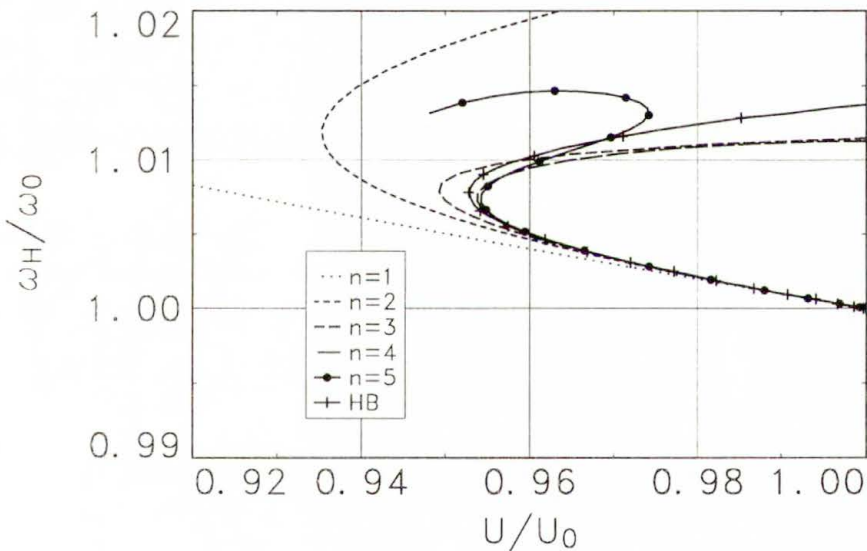


FIG. 10. Frequency of center-manifold Hopf limit cycle (antisymmetric flutter).

sufficiently high disturbance, the magnitude of which is known from the presented results of calculations and which is given by the unstable branch of amplitude curves (the part of plots between the bifurcation point and the turning point in Figs. 11 and 12).

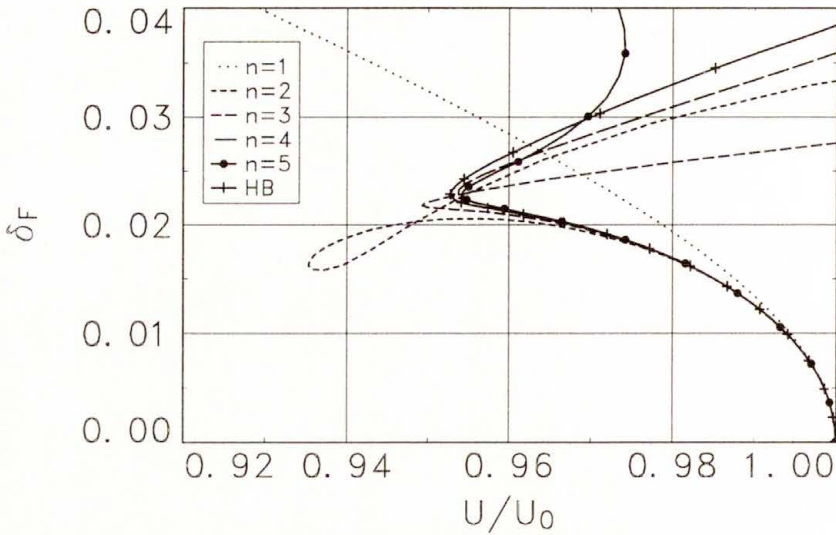


FIG. 11. Flap limit cycle amplitude (antisymmetric flutter).

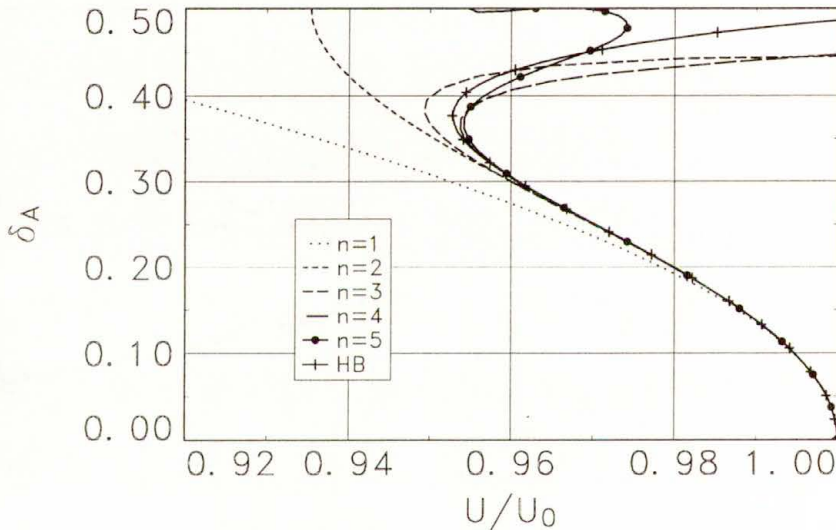


FIG. 12. Aileron limit cycle amplitude (antisymmetric flutter).

## 5. Concluding remarks

The discrepancy between the present method and the harmonic balance method in a region located not very close to the bifurcation point is not an unexpected result. The harmonic balance method assumes pure harmonic oscillations of a structure, that may not be satisfied, and also treats nonlinear springs in a simplified manner. The method of center-manifold reduction is a method

of local validity and, afterwards, is based on asymptotic series expansions, the usefulness of which cannot be expected in a wide range of velocity. Nevertheless, there is a good agreement between these two methods locally. Hence, the main advantage of the center-manifold reduction lies in a possibility of extension of this method to such aeroelastic systems for which harmonic balance method cannot be handled easily (e.g. multiple concentrated nonlinearities), and to systems for which the direct numerical integration method cannot be used in a sufficiently effective way.

The method of center-manifold reduction does not limit the number of degrees of freedom. The problem of treatment of higher degree of freedom systems affects only the efficiency of calculations. The method itself (and the corresponding computer code as well) can be applied to any number of degrees of freedom "as it is". However, the hardware used may bound this number significantly if there is not enough RAM available. It has been found that the computer direct access memory is the bottle-neck of the calculations. The reason is that the main series (3.18) is not a series of numbers but rather a series of functions. These functions are described by a rapidly growing number of parameters, when the number of terms increases, and moreover, all of them must be stored in memory during the entire computation process. On the other hand, not very high number of terms is sufficient to determine the behaviour of the aeroelastic system under considerations in the neighbourhood of a bifurcation point.

The method of center manifold reduction is an asymptotic and local method (i.e. looking near a single point) and, therefore, is not suited for treatment of more complex global bifurcations or transition to chaotic oscillations. Such oscillations appear also in aeroelastic systems.

## Acknowledgments

This work has been supported by the State Committee for Scientific Research, Poland, under Grant 3P404 001 04.

## References

1. M.W. HIRSCH and S. SMALE, *Differential equations, dynamical systems, and linear algebra*, Academic Press, New York and London 1974.
2. J.D. CRAWFORD, *Introduction to bifurcation theory*, Reviews of Modern Physics, **63**, 4, October 1991.
3. J. GRZĘDZIŃSKI, *Calculation of coefficients of a power series approximation of a center manifold for nonlinear integro-differential equations*, Arch. Mech., **45**, 2, pp. 235–250, 1993.
4. J. GRZĘDZIŃSKI, *Flutter analysis of a two-dimensional airfoil with nonlinear springs based on center manifold reduction*, Arch. Mech., **46**, 5, pp. 735–755, 1994.
5. F. POIRION, *Effects of structural nonlinearities on flutter analysis*, Proc. International Forum on Aeroelasticity and Structural Dynamics, Strasbourg, May 24-26, 1993.
6. V.J.E. STARK, *General equations of motion for an elastic wing and method of solution*, AIAA J., **22**, 8, pp. 1146–1153, August 1984.

7. S.-N. CHOW and J.K. HALE, *Methods of bifurcation theory*, Grundlehren der mathematischen Wissenschaften 251, Springer-Verlag, 1982.
8. T. THEODORSEN, *General theory of aerodynamic instability and the mechanism of flutter*, NACA Rept. No. 496, 1935.
9. D.D. LIU, P.C. CHEN, Z.X. YAO and D. SARHADDI, *Recent advances in lifting surface methods*, Proc. The International Forum on Aeroelasticity and Structural Dynamics 1995, Manchester, 26-28 June 1995, Published by The Royal Aeronautical Society, London 1995.
10. B.D. HASSARD, N.D. KAZARINOFF and Y.-H. WAN, *Theory and applications of Hopf bifurcation*, Cambridge University Press, 1981.
11. N. CHAFEE, *A bifurcation problem for a functional differential equation of finitely retarded type*, J. Math. Anal. and Appl., **35**, pp. 312–348, 1971.
12. A. KELLEY, *The stable, center-stable, center, center-unstable, unstable manifolds*, J. Differential Equations, **3**, 546–570, 1967.
13. L. HSU and L. FAVRETTO, *Recursive formulae for normal form and center manifold theory*, J. Math. Anal. and Appl., **101**, 2, pp. 562–574, July 1984.
14. H.W. STECH, *Hopf bifurcation calculations for functional differential equations*, J. Math. Anal. and Appl., **109**, 2, 472–491, August 1985.
15. S.F. SHEN, *An approximate analysis of nonlinear flutter problems*, J. Aerospace Sciences, **28**, pp. 25–32, January 1959.
16. W.C. RHEINBOLDT, *A locally parametrized continuation process*, ACM Trans. Math. Software, **9**, 2, pp. 215–235, 1983.
17. W. POTKAŃSKI, *Nonlinear flutter analysis by a continuation method*, Proc. Euromech-Kolloquium 349 “Simulation of Structure Fluid Interaction in Aeronautics”, Goettingen, 16-18 September 1996.

POLISH ACADEMY OF SCIENCES  
INSTITUTE OF FUNDAMENTAL TECHNOLOGICAL RESEARCH  
e-mail: jgrzedz@ippt.gov.pl

Received February 29, 1996.

# Lagrange's equations for holonomic systems with rigid bodies

A. MORRO (GENOVA)

A HOLONOMIC SYSTEM is considered which consists of rigid bodies and material points. Any rigid body is regarded as a continuous system and its position is described by the so-called angular vectors. Starting from the characterization of the constraints and using some identities for the angular vectors, the motion of the holonomic system is shown to be governed by the usual Lagrange's equations. The essential role of the angular vectors is emphasized through comparison with a previous approach.

## 1. Introduction

A RIGID BODY is a system with a number of degrees of freedom not greater than 6. Nevertheless, treatments of analytical mechanics deal only with material points and hence rigid bodies are modelled as a set of material points though such points are not characterized operatively. The results are then deemed to apply for continuous bodies by merely replacing the summation over the particles by a volume integration, with the point mass becoming a mass density (cf. [1–5]).

Quite naturally, instead, a rigid body might be viewed as a continuous body whose mechanical state in space is characterized by the position of a point and the orientation of a rigidly attached triple of non-coplanar axes. This view is customary in connection with the kinematics of rigid body motion and Euler's equations of motion where angular vectors are used to describe the position of the body (cf. [6–8]).

The standard approach of analytical mechanics can be modified so that both the material points and the rigid bodies are incorporated and, moreover, rigid bodies are considered systematically as continuous bodies with the corresponding number of degrees of freedom. It is the purpose of this note to derive the equations of motion from the characterization of the constraints. The system  $S$  under consideration is holonomic and consists of  $N$  material points and  $B$  rigid bodies. The approach is based on the use of angular vectors [9]. As a result, the motion of the system is shown to be governed by the usual form of Lagrange's equations.

To the author's knowledge, the literature shows one previous approach to Lagrange's equations, where the rigid body was viewed as a continuum [10]. An immediate comparison emphasizes the conceptual difficulty that arises if the angular vectors are not involved.

## 2. Angular vectors and characterization of the constraints

Let  $P$  be any point of a rigid body,  $G$  the center of gravity, and  $\boldsymbol{\omega}$  the angular velocity. The velocities  $\mathbf{v}_P$  and  $\mathbf{v}_G$  of  $P$  and  $G$  are related by

$$\mathbf{v}_P = \mathbf{v}_G + \boldsymbol{\omega} \times (P - G).$$

The time-dependent velocity field  $\mathbf{v}_P(t) = \mathbf{v}(P, t)$  is then characterized by the two time-dependent vectors  $\mathbf{v}_G(t)$  and  $\boldsymbol{\omega}(t)$ . Two pairs  $\mathbf{v}_G^{(1)}, \boldsymbol{\omega}^{(1)}$  and  $\mathbf{v}_G^{(2)}, \boldsymbol{\omega}^{(2)}$  determine the corresponding fields

$$\mathbf{v}_P^{(1)} = \mathbf{v}_G^{(1)} + \boldsymbol{\omega}^{(1)} \times (P - G), \quad \mathbf{v}_P^{(2)} = \mathbf{v}_G^{(2)} + \boldsymbol{\omega}^{(2)} \times (P - G).$$

A field of virtual velocity  $\boldsymbol{\nu}$  is defined to be the difference of any pair of velocity fields. Analogously, a virtual angular velocity  $\boldsymbol{\varpi}$  is defined to be the difference of any pair of angular velocities. Hence, letting  $\boldsymbol{\nu} = \mathbf{v}^{(1)} - \mathbf{v}^{(2)}$ ,  $\boldsymbol{\varpi} = \boldsymbol{\omega}^{(1)} - \boldsymbol{\omega}^{(2)}$  we have

$$(2.1) \quad \boldsymbol{\nu}_P = \boldsymbol{\nu}_G + \boldsymbol{\varpi} \times (P - G).$$

The vectors  $\boldsymbol{\omega}$  and  $\boldsymbol{\varpi}$  are now related to the generalized coordinates.

Let  $\{\mathbf{e}_h\}$  be the unit vectors of a Cartesian set of axes fixed in the rigid body,  $h = 1, 2, 3$ . For greater generality we let

$$\mathbf{e}_h = \mathbf{e}_h(q, t),$$

where  $q = q(t)$  is a set of generalized (or Lagrangian) coordinates for the body. By definition, the angular velocity is given by

$$\boldsymbol{\omega} = \frac{1}{2} \sum_h \mathbf{e}_h \times \dot{\mathbf{e}}_h = \frac{1}{2} \sum_h \mathbf{e}_h \times \frac{\partial \mathbf{e}_h}{\partial q_j} \dot{q}_j + \frac{1}{2} \sum_h \mathbf{e}_h \times \frac{\partial \mathbf{e}_h}{\partial t},$$

where a superposed dot denotes the (total) time derivative  $d/dt$ ; the sum over repeated indices is understood. Define the *angular vectors*  $\boldsymbol{\Omega}_j, \boldsymbol{\Omega}_t$  as

$$\boldsymbol{\Omega}_j = \frac{1}{2} \sum_h \mathbf{e}_h \times \frac{\partial \mathbf{e}_h}{\partial q_j}, \quad \boldsymbol{\Omega}_t = \frac{1}{2} \sum_h \mathbf{e}_h \times \frac{\partial \mathbf{e}_h}{\partial t}.$$

We have

$$\boldsymbol{\omega} = \boldsymbol{\Omega}_j \dot{q}_j + \boldsymbol{\Omega}_t$$

whence

$$(2.2) \quad \boldsymbol{\Omega}_j = \frac{\partial \boldsymbol{\omega}}{\partial \dot{q}_j}.$$

Let  $\{\dot{q}_j^{(1)}\}, \{\dot{q}_j^{(2)}\}$  be the sets of generalized velocities associated with  $\mathbf{v}_P^{(1)}, \mathbf{v}_P^{(2)}$ . Letting  $\eta_j = \dot{q}_j^{(1)} - \dot{q}_j^{(2)}$  we have

$$(2.3) \quad \mathbf{v}_\alpha = \frac{\partial P_\alpha}{\partial q_j} \eta_j, \quad \boldsymbol{\omega} = \boldsymbol{\Omega}_j \eta_j.$$

For later use we need the expression of the time derivative  $\dot{\boldsymbol{\Omega}}_j$ . Letting

$$\Omega_{jp} = \boldsymbol{\Omega}_j \cdot \mathbf{e}_p$$

and

$$\mathbf{e}_{h,j} = \partial \mathbf{e}_h / \partial q_j, \quad \mathbf{e}_{h,t} = \partial \mathbf{e}_h / \partial t,$$

we obtain

$$\Omega_{jp} = \frac{1}{2} \sum_h (\mathbf{e}_h \times \mathbf{e}_{h,j}) \cdot \mathbf{e}_p = \frac{1}{2} \sum_h (\mathbf{e}_p \times \mathbf{e}_h) \cdot \mathbf{e}_{h,j} = \frac{1}{2} \sum_{h,l} \varepsilon_{phl} \mathbf{e}_{h,j} \cdot \mathbf{e}_l$$

and

$$\mathbf{e}_{h,k} \dot{q}_k + \mathbf{e}_{h,t} = \boldsymbol{\Omega}_k \times \mathbf{e}_h \dot{q}_k + \boldsymbol{\Omega}_t \times \mathbf{e}_h = \boldsymbol{\omega} \times \mathbf{e}_h.$$

Substitution and some rearrangement yield

$$\begin{aligned} \dot{\Omega}_{jp} &= \frac{1}{2} \varepsilon_{phl} (\mathbf{e}_{h,jk} \dot{q}_k + \mathbf{e}_{h,jt}) \cdot \mathbf{e}_l + \frac{1}{2} \varepsilon_{phl} \mathbf{e}_{h,j} \cdot \boldsymbol{\omega} \times \mathbf{e}_l \\ &= \frac{\partial}{\partial q_j} \frac{1}{2} \varepsilon_{phl} \boldsymbol{\omega} \times \mathbf{e}_h \cdot \mathbf{e}_l - \frac{1}{2} \varepsilon_{phl} \boldsymbol{\omega} \times \mathbf{e}_h \cdot \mathbf{e}_{l,j} + \frac{1}{2} \varepsilon_{phl} \mathbf{e}_{h,j} \cdot \boldsymbol{\omega} \times \mathbf{e}_l \\ &= \frac{\partial \omega_p}{\partial q_j} - \frac{1}{2} (\mathbf{e}_p \times \mathbf{e}_h) \cdot \mathbf{e}_l (\boldsymbol{\omega} \times \mathbf{e}_h) \cdot (\boldsymbol{\Omega}_j \times \mathbf{e}_l) + \frac{1}{2} (\mathbf{e}_p \times \mathbf{e}_h) \cdot \mathbf{e}_l (\boldsymbol{\Omega}_j \times \mathbf{e}_h) \cdot (\boldsymbol{\omega} \times \mathbf{e}_l) \\ &= \frac{\partial \omega_p}{\partial q_j} - \frac{1}{2} (\boldsymbol{\omega} \times \mathbf{e}_h) \cdot [\boldsymbol{\Omega}_j \times (\mathbf{e}_p \times \mathbf{e}_h)] + \frac{1}{2} (\boldsymbol{\Omega}_j \times \mathbf{e}_h) \cdot [\boldsymbol{\omega} \times (\mathbf{e}_p \times \mathbf{e}_h)] \\ &= \frac{\partial \omega_p}{\partial q_j} - \frac{1}{2} (\boldsymbol{\omega} \times \mathbf{e}_h) \cdot \Omega_{jh} \mathbf{e}_p + \frac{1}{2} (\boldsymbol{\Omega}_j \times \mathbf{e}_h) \cdot \boldsymbol{\omega}_h \mathbf{e}_p. \end{aligned}$$

Accordingly we have

$$\dot{\Omega}_{jp} = \frac{\partial \omega_p}{\partial q_j} + \boldsymbol{\Omega}_j \times \boldsymbol{\omega} \cdot \mathbf{e}_p.$$

Hence the time differentiation of  $\boldsymbol{\Omega}_j = \Omega_{jp} \mathbf{e}_p$  yields

$$(2.4) \quad \dot{\boldsymbol{\Omega}}_j = \frac{\partial \omega_p}{\partial q_j} \mathbf{e}_p.$$

Let  $\Phi_i$  be the force of constraint at any point  $i$  of  $S$ , namely, at any material point or at any point of the rigid bodies. Denote by  $\mathbf{v}_i$  the virtual velocity of

the point  $i$  and let  $A$  be the set of labels for the constrained points. Hence we characterize the constraints by assuming that

$$(2.5) \quad \sum_{i \in A} \phi_i \cdot \boldsymbol{\nu}_i = 0$$

for every set of virtual velocities  $\{\boldsymbol{\nu}_i\}$  compatible with the constraints.

For formal convenience we separate the values of  $i$  pertaining to the material points from those pertaining to rigid bodies; we label by  $\alpha = 1, \dots, N$  the material points, and by the pair  $b \beta_b$ ,  $b = 1, \dots, B$ ,  $\beta_b = 1, \dots, N_b$ , we denote the constrained points of the  $B$  rigid bodies. Denote by  $\mathbf{R}_b^r$  and  $\mathbf{M}_{G_b}^r$  the total constraint force and the total constraint torque acting on the body  $b$ , i.e.

$$\mathbf{R}_b^r = \sum_{b, \beta_b} \phi_{b\beta_b}, \quad \mathbf{M}_{G_b}^r = \sum_{b, \beta_b} (P_{b\beta_b} - G_b) \times \phi_{b\beta_b}.$$

The total applied force  $\mathbf{R}_b^a$  and the total applied torque  $\mathbf{M}_{G_b}^a$  are defined analogously by replacing the constraint forces with the applied forces. By means of (2.1) we have

$$\sum_{b, \beta_b} \phi_{b\beta_b} \cdot \boldsymbol{\nu}_{b\beta_b} = \sum_{b, \beta_b} \phi_{b\beta_b} \cdot \boldsymbol{\nu}_{G_b} + \sum_{b, \beta_b} \phi_{b\beta_b} \cdot \boldsymbol{\omega}_b \times (P_{b\beta_b} - G_b) = \mathbf{R}_b^r \cdot \boldsymbol{\nu}_{G_b} + \mathbf{M}_{G_b}^r \cdot \boldsymbol{\omega}_b.$$

For any body  $b$ , the balance of linear momentum,  $\mathbf{P}_b$ , and of angular momentum,  $\mathbf{L}_b$ , is written as

$$\dot{\mathbf{P}}_b = \mathbf{R}_b^a + \mathbf{R}_b^r, \quad \dot{\mathbf{L}}_b = \mathbf{M}_b^a + \mathbf{M}_b^r.$$

The equation of motion for any material point  $\alpha$  is given in the form

$$\mu_\alpha \mathbf{a}_\alpha = \mathbf{F}_\alpha + \phi_\alpha,$$

where  $\mu_\alpha$  is the mass,  $\mathbf{a}_\alpha$  – the acceleration,  $\mathbf{F}_\alpha$  – the applied force. Substitution enables us to write the condition (2.5) in the form

$$(2.6) \quad \sum_{\alpha} (\mu_\alpha \mathbf{a}_\alpha - \mathbf{F}_\alpha) \cdot \boldsymbol{\nu}_\alpha + \sum_b (\dot{\mathbf{P}}_b - \mathbf{R}_b^a) \cdot \boldsymbol{\nu}_{G_b} + \sum_b (\dot{\mathbf{L}}_b - \mathbf{M}_{G_b}^a) \cdot \boldsymbol{\omega}_b = 0.$$

### 3. Lagrange's equations

Let now  $q = (q_1, \dots, q_n)$  be the set of generalized coordinates for the whole holonomic system. Substitution of (2.3) into (2.6) yields

$$\sum_{\alpha} (\mu_\alpha \mathbf{a}_\alpha - \mathbf{F}_\alpha) \cdot \frac{\partial P_\alpha}{\partial q_j} \eta_j + \sum_b (\dot{\mathbf{P}}_b - \mathbf{R}_b^a) \cdot \frac{\partial G_b}{\partial q_j} \eta_j + \sum_b (\dot{\mathbf{L}}_b - \mathbf{M}_{G_b}^a) \cdot \boldsymbol{\Omega}_j^b \eta_j = 0.$$

The arbitrariness of the  $n$ -tuple  $\eta_1, \dots, \eta_n$  implies that

$$(3.1) \quad \tau_j - Q_j = 0, \quad j = 1, \dots, n,$$

where

$$(3.2) \quad \tau_j = \sum_{\alpha} \mu_{\alpha} \mathbf{a}_{\alpha} \cdot \frac{\partial P_{\alpha}}{\partial q_j} + \sum_b \dot{\mathbf{P}}_b \cdot \frac{\partial G_b}{\partial q_j} + \sum_b \dot{\mathbf{L}}_b \cdot \boldsymbol{\Omega}_j^b,$$

$$(3.3) \quad Q_j = \sum_{\alpha} \mathbf{F}_{\alpha} \cdot \frac{\partial P_{\alpha}}{\partial q_j} + \sum_b \mathbf{R}_b \cdot \frac{\partial G_b}{\partial q_j} + \sum_b \mathbf{M}_b \cdot \boldsymbol{\Omega}_j^b.$$

It is natural to view  $\tau_j$  ( $Q_j$ ) as the  $j$ -th component of the generalized inertia force (generalized force).

To find a convenient form of  $\tau_j$  we observe that, for any material point  $P$  of mass  $\mu$ , by means of the known identities, we have

$$\mu \mathbf{a} \cdot \frac{\partial P}{\partial q_h} = \mu \frac{d\mathbf{v}}{dt} \cdot \frac{\partial P}{\partial q_h} = \frac{d}{dt} \left( \mu \mathbf{v} \cdot \frac{\partial \mathbf{v}}{\partial q_h} \right) - \mu \mathbf{v} \cdot \frac{\partial \mathbf{v}}{\partial q_h} = \frac{d}{dt} \frac{\partial}{\partial \dot{q}_h} \frac{1}{2} \mu \mathbf{v}^2 - \frac{\partial}{\partial q_h} \frac{1}{2} \mu \mathbf{v}^2.$$

In the same manner, since  $\mathbf{P} = m\mathbf{v}_G$ , we have

$$\dot{\mathbf{P}} \cdot \frac{\partial G}{\partial q_h} = m \mathbf{a}_G \cdot \frac{\partial G}{\partial q_h} = \frac{d}{dt} \frac{\partial}{\partial \dot{q}_h} \frac{1}{2} m \mathbf{v}_G^2 - \frac{\partial}{\partial q_h} \frac{1}{2} m \mathbf{v}_G^2.$$

Let  $\mathbf{I}$  be the inertia tensor of a body, relative to the corresponding center of gravity. Hence  $\mathbf{L} = \mathbf{I}\boldsymbol{\omega}$ . We now use (2.2) and (2.4) to obtain

$$\begin{aligned} \dot{\mathbf{L}} \cdot \boldsymbol{\Omega}_h &= \frac{d(\mathbf{I}\boldsymbol{\omega})}{dt} \cdot \frac{\partial \boldsymbol{\omega}}{\partial \dot{q}_h} = \frac{d}{dt} \left[ (\mathbf{I}\boldsymbol{\omega}) \cdot \frac{\partial \boldsymbol{\omega}}{\partial \dot{q}_h} \right] - (\mathbf{I}\boldsymbol{\omega}) \cdot \frac{d}{dt} \frac{\partial \boldsymbol{\omega}}{\partial \dot{q}_h} \\ &= \frac{d}{dt} \left[ \frac{1}{2} \boldsymbol{\omega} \cdot \mathbf{I} \boldsymbol{\omega} \right] - (\mathbf{I}\boldsymbol{\omega}) \cdot \frac{d\boldsymbol{\Omega}_h}{dt} = \frac{d}{dt} \left[ \frac{1}{2} \boldsymbol{\omega} \cdot \mathbf{I} \boldsymbol{\omega} \right] - \frac{\partial}{\partial q_h} \left[ \frac{1}{2} \boldsymbol{\omega} \cdot \mathbf{I} \boldsymbol{\omega} \right]. \end{aligned}$$

The expression of the kinetic energy of the system, viz.

$$T = \sum_{\alpha} \frac{1}{2} \mu_{\alpha} \mathbf{v}_{\alpha}^2 + \sum_b \frac{1}{2} m_b \mathbf{v}_{G_b}^2 + \sum_b \frac{1}{2} \boldsymbol{\omega}_b \cdot \mathbf{I}_b \boldsymbol{\omega}_b$$

allows  $\tau_j$  to be written as

$$(3.4) \quad \tau_j = \frac{d}{dt} \frac{\partial T}{\partial \dot{q}_j} - \frac{\partial T}{\partial q_j}.$$

Accordingly, the conditions (3.1) become

$$(3.5) \quad \frac{d}{dt} \frac{\partial T}{\partial \dot{q}_j} - \frac{\partial T}{\partial q_j} = Q_j, \quad j = 1, \dots, n,$$

namely Lagrange's equations of the second kind.

#### 4. Comparison with a previous approach

The view that the rigid body is a continuum rather than a set of material points, is expressed in [10]. A comparison is then necessary to assess the conceptual improvement in the present approach.

The approach in [10] starts from the D'Alembert principle for a single body which, in the notation of this note, may be written in the form

$$(4.1) \quad \mathbf{R}^a \cdot \boldsymbol{\nu}_G + \mathbf{M}_G^a \cdot \boldsymbol{\varpi} - \int_{\mathcal{R}} \varrho \boldsymbol{\nu} \cdot \mathbf{a} \, dv = 0,$$

where  $\varrho$  is the mass density; the integral over the region  $\mathcal{R}$ , occupied by the body, is regarded as the power of inertia forces. The assumption (2.5) seems to be more convincing. Yet it follows easily that Eqs. (2.6) and (4.1) are equivalent when a single body is involved, since the observation that

$$\frac{\partial P}{\partial q_j} \cdot \mathbf{a} = \frac{d}{dt} \frac{\partial}{\partial \dot{q}_j} \frac{1}{2} \mathbf{v}^2 - \frac{\partial}{\partial q_j} \frac{1}{2} \mathbf{v}^2$$

and substitution of  $\boldsymbol{\nu} = (\partial P / \partial q_j) \boldsymbol{\eta}_j$  yields

$$\int_{\mathcal{R}} \varrho \boldsymbol{\nu} \cdot \mathbf{a} \, dv = \tau_j \eta_j,$$

where  $\tau_j$  has the form (3.4) in terms of the kinetic energy. Here, the expression (3.2) also leads to (3.4).

The crucial point consists in expressing the power  $\mathbf{R}^a \cdot \boldsymbol{\nu}_G + \mathbf{M}_G^a \cdot \boldsymbol{\varpi}$  in terms of the generalized coordinates. First, the "primitive" coordinates  $\lambda_s$  are considered and the power  $\mathbf{R}^a \cdot \boldsymbol{\nu}_G + \mathbf{M}_G^a \cdot \boldsymbol{\varpi}$  is written as a linear form in the virtual time derivatives of  $\lambda_s$ ; the corresponding coefficients are denoted by  $A_s$ . Hence, for holonomic systems  $\lambda_s = \lambda_s(q, t)$  and it follows that

$$\mathbf{R}^a \cdot \boldsymbol{\nu}_G + \mathbf{M}_G^a \cdot \boldsymbol{\varpi} = \sum_j Q_j \eta_j,$$

where

$$Q_j = \sum_s A_s \frac{\partial \lambda_s}{\partial q_j}.$$

Accordingly, the arbitrariness of the set  $\{\eta_j\}$  implies that Lagrange's equations (3.5) hold. Unfortunately, without the angular vectors, the quantities  $Q_j$  are not defined per se. Indeed,  $Q_j$  can be viewed as the coefficient of  $\eta_j$  in the expression of the virtual power. The use of the angular vectors, instead, allows us to write  $Q_j$  in the form (3.3). The occurrence of the angular vectors  $\boldsymbol{\Omega}_j$  makes it apparent why we are unable to write the expression for  $Q_j$  if the angular vectors are not considered.

## References

1. H. GOLDSTEIN, *Classical mechanics*, Addison Wesley, Reading, Mass. 1964.
2. L. LANDAU and E. LIFCHITZ, *Mécanique*, Mir, Moscow 1966.
3. C.W. KILMISTER and J.E. REEVE, *Rational mechanics*, Longmans, London 1966.
4. A.I. LUR'E, *Mécanique analytique*, Librairie Universitaire, Louvain 1968.
5. L. MEIROVITCH, *Methods of analytical mechanics*, McGraw-Hill, New York 1970.
6. M. CAZIN, *Cours de mécanique générale et industrielle*, Gauthier-Villars, Paris 1972.
7. P. MAISSER, *Analytische dynamik von Mehrkörpersysteme*, ZAMM, **68**, 463–481, 1988.
8. J.G. PAPASTAVRIDIS, *On the transitivity equations of rigid-body dynamics*, ASME J. Appl. Mech., **59**, 955–962, 1992.
9. M. BENATI and A. MORRO, *Angular vectors and kinetic energy of rigid bodies*, European J. Mech. A/ Solids, **13**, 819–832, 1994.
10. A. SIGNORINI, *Meccanica razionale con elementi di statica grafica*, Ch. 16, Perrella, Roma 1954.

UNIVERSITÀ, DIBE, GENOVA, ITALY

e-mail: morro@dibe.unige.it

Received May 20, 1996.

# Asymptotic expansion of solution of the torsion problem for an elastic rod with a cavity and a thin bonded multilayer

G. S. MISHURIS (RZESZÓW)

THE FIRST TERM of the asymptotic expansion of the solution of the torsion problem for an elastic rod is derived using the method of a matched asymptotic expansion. The prismatic rod is weakened by an internal cavity with angular points, one of which is situated on the exterior boundary. The exterior boundary of the rod is reinforced by a thin elastic multilayer. Difference between the exact and approximate solution of the problem are estimated by the norm of the Sobolev spaces. Relations for stress intensity factors in the angular points are found and verified.

## 1. Introduction

STRUCTURAL ELEMENTS reinforced by thin surface layers have found wide application in modern technology. Such elements can seriously change the elastic and strength properties of the structures. The corresponding boundary value problems have been investigated in [2, 3, 4, 20]. In those problems it is assumed that curvature of the thin layers is small. In this way, note paper [9], in which “averaged” boundary conditions are obtained for a thin surface layer with arbitrary curvature by the operator method. All the mentioned problems are related to the so-called boundary value problems with regular perturbations of the boundaries [7, 8].

However, in the cases when stress concentrators are situated near the thin layer, singular perturbations of the boundaries appear. The methods of solution of such problems have been proposed in [6, 12, 19]. One of them is the method of matched asymptotic expansion. It consists in the solution of the limiting (internal and external) problems, and later – in their coordination in some intermediate region [6, 12].

In paper [15] the method of solving the boundary value problems in infinite domains represented by wedges and layers is proposed. For some values of the parameters, homogeneous problems discussed in [15] have nontrivial solutions, which are of some class of solutions of the internal limiting boundary value problems. These solutions can be calculated by functions belonging to the kernel of special singular integral operators [14, 15]. In [13] the numerical method of deriving the functions from the kernel of the operators has been introduced.

In the paper, a singular perturbed boundary value problem is considered, which corresponds to the torsion problem of a prismatic rod with a cavity and a thin multilayer. A similar problem for a homogeneous rod with a linear crack was investigated in [1].

## 2. Formulation of the problem

Let us consider a domain  $\Omega_h$  with compact closure  $\overline{\Omega}_h \subset \mathbb{R}^2$ , smooth exterior boundary  $\Gamma_e$  (for example,  $\Gamma_e \in C^1$ ), and piecewise smooth interior boundary  $\Gamma_0$  ( $\partial\Omega_h = \Gamma_e \cup \Gamma_0$ ). By  $\Gamma_1$  we denote the closed curve:  $\Gamma_1 = \{P \in \Omega_h : \text{dist}(P, \partial\Omega_h) = h\}$ , (see Fig. 1).

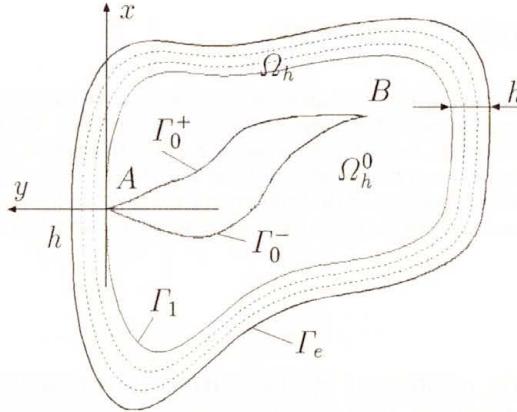


FIG. 1.

Assume that  $A, B \in \Gamma_0$  are corner points which divide the closed curve  $\Gamma_0 = \Gamma_0^+ \cup \Gamma_0^-$ , and

$$(2.1) \quad \begin{aligned} & \text{(i)} \quad \text{dist}(A, \Gamma_e) = h \ll 1, \quad r_{\Omega_e} \geq 1, \quad \text{dist}(B, \Gamma_e) \sim 1, \\ & \text{(ii)} \quad \angle(\Gamma_1, \Gamma_0^\pm)|_A = \pi/2 \mp \phi_A, \quad \angle(\Gamma_0^+, \Gamma_0^-)|_B = 2\phi_B, \\ & \text{(iii)} \quad k_{\Gamma_1}(A) = k_{\Gamma_0^\pm}(A) = k_{\Gamma_0^\pm}(B) = 0, \end{aligned}$$

where  $\phi_A, \phi_B \in (0, \pi/2)$ ,  $k_{\Gamma_1}(A)$ ,  $k_{\Gamma_0^\pm}(A)$  are curvatures of the curves  $\Gamma_1$ , and  $\Gamma_0^\pm$  in point  $A$ , but  $r_{\Omega_e} = \sup\{r : B_r \subset \Omega_e\}$  is the Chebyshev radius of the domain  $\Omega_e$  (here  $\partial\Omega_e = \Gamma_e$ , and  $B_r$  is open disk of a radius  $r$ ).

Let  $(s, n)$  be a local coordinate system connected with the curve  $\Gamma_1$ . Its origin is at the point  $A \in \Gamma_1$ , and  $n > 0$  along the outer normal. A Cartesian coordinate system  $(x, y)$  coincides with the local system  $(s, n)$  at point  $A$  ( $A = (0, 0)$ ).

If  $m \in \mathbb{N}$ ,  $\mu_0, \mu_j \in \mathbb{R}_+$  ( $j = 1, 2, \dots, m$ ) are some positive constants, and  $0 = h_0 < h_1 < \dots < h_j < \dots < h_{m-1} < h_m = h$ , then we consider the step function:

$$(2.2) \quad \mu(s, n) = \begin{cases} \mu_{j+1}, & (s, n) \in \Omega_h \wedge h_j < n < h_{j+1}, \\ \mu_0, & (s, n) \in \Omega_h \wedge -\infty < n < 0, \end{cases}$$

and from the assumption it follows

$$(2.3) \quad 0 < \min_{0 \leq j \leq m} \{\mu_j\} = \underline{\mu} \leq \mu(x, y) \leq \bar{\mu} = \max_{0 \leq j \leq m} \{\mu_j\} < \infty.$$

We shall use also the symbols ( $j = 0, 1, \dots, m$ ):

$$(2.4) \quad \begin{aligned} \Omega_h^j &= \Omega_h \cap \{(x, y) : \mu(x, y) = \mu_j\}, \\ \Gamma_{j+1} &= \{(s, n) : (s, n) \in \Omega_h \wedge n = h_j\}. \end{aligned}$$

We shall seek a harmonic function  $u(x, y)$  in each domain  $\Omega_h^j$  (the torsion function [18]), satisfying along the interior boundaries  $\Gamma_j$  ( $j = 1, 2, \dots, m$ ) between different materials the conditions:

$$(2.5) \quad (u_j - u_{j-1})|_{\Gamma_j} = 0, \quad \frac{\partial}{\partial n}(\mu_j u_j - \mu_{j-1} u_{j-1})|_{\Gamma_j} = f_j(x, y).$$

But along  $\partial\Omega_h$  we have

$$(2.6) \quad \mu_m \frac{\partial}{\partial n} u_m|_{\Gamma_e} = f_m(x, y), \quad \mu_0 \frac{\partial}{\partial n} u_0|_{\Gamma_0^\pm} = -f_0^\pm(x, y),$$

with some functions  $f_j, f_0^\pm \in C^\infty(\Gamma_j)$  (see [18]), so that the following conditions are satisfied:

$$(2.7) \quad f_j(0, h_j), f_0^\pm(0, 0) = 0, \quad \frac{\partial}{\partial s} f_j(0, h_j), \frac{\partial}{\partial s} f_0(0, 0) \sim 1.$$

For solvability of the problem we should assume, in addition [18], that

$$(2.8) \quad \sum_{j=0}^{m+1} \int_{\Gamma_j} f_j(s) ds = 0,$$

where  $\Gamma_{m+1} = \Gamma_e$ , but to secure the uniqueness of the solution we normalize it by the condition:

$$(2.9) \quad u(B) = 0.$$

Using the results from [10], one can show that the linear problem (2.4)–(2.8) has the unique solution  $u_h$  in the space  $W_2^1(\Omega_h, B) \equiv \{u \in W_2^1(\Omega_h) \wedge u(B) = 0\}$ . It can be easily seen on the basis of the results of [5], that the solution belongs to  $C^\infty(\Omega_h^j)$ . Besides, we can prove that  $u_h \in C(\overline{\Omega_h})$ , however,  $u_h \notin W_2^2(\Omega_h)$ . To verify the first fact, it is sufficient to investigate the asymptotic behaviour of the solution near any point situated on the interior boundary  $\Gamma_j$  ( $j = 1, \dots, m$ ); but to check the second conclusion, we should know the behaviour of the solution in the neighbourhood of points  $A$  or  $B$ . We shall consider in detail only the second proposition. Namely, let us represent the solution near these points in the form:  $u_h = \chi(r/\varepsilon)u_h + (1 - \chi(r/\varepsilon))u_h$  with some small  $\varepsilon > 0$  ( $\varepsilon < h_1$ ). Here and further on, by  $\chi \in C^\infty(\mathbb{R}_+)$ , we shall understand a cut-off function defined by

$$(2.10) \quad \chi(t) = \begin{cases} 1, & 0 \leq t \leq 1/3, \\ 0, & 2/3 \leq t < \infty. \end{cases}$$

Let us note that the function  $u_{\varepsilon}|_l = \chi(r/\varepsilon)u_h|_l \in L_1(\mathbb{R}_+)$ , where  $l$  is an arbitrary radius with origin at point  $A$  ( $B$ ) so that  $l \cap \Omega_h \neq \emptyset$ . Then applying the Mellin transform technique to the corresponding problem for the function  $u_{\varepsilon} = \chi(r/\varepsilon)u_h$ , and taking into account the assumptions on curvatures (2.1), we obtain

$$(2.11) \quad \begin{aligned} u_h(h, r, \phi) &= d_A + c_A \nu_A^{-1} r^{\nu_A} F(\phi) + O(r^{\delta_A}), \quad r \rightarrow 0, \\ u_h(h, r, \phi) &= d_B + c_B \nu_B^{-1} r^{\nu_B} F(\phi) + O(r^{\delta_B}), \quad r \rightarrow 0, \end{aligned}$$

where  $(r, \phi)$  are local coordinates connected with point  $A$  (or  $B$ ), and the angle  $\phi$  calculated with respect to the bisector of the corresponding corner angles, are situated in the domains  $\Omega_h^1$  ( $\Omega_h^0$ , respectively), but

$$(2.12) \quad F(\phi) = \begin{cases} \frac{\sin \phi \nu}{\sin(\pi \nu / 2)}, & |\phi| \leq \pi / 2, \\ \text{sign} \phi \frac{\cos(\pi - \phi_0 - |\phi|) \nu}{\cos(\pi / 2 - \phi_0) \nu}, & \pi / 2 < |\phi| < \pi - \phi_0, \end{cases}$$

where  $\phi_0 = \phi_A(\phi_B)$ ,  $d_B = 0$  ( $u_h \in W_2^1(\Omega_h, B)$ ), but constants  $\nu_A, \nu_B \in (0, 1)$  are the first zeros of the function:

$$\Delta_c(s) = \kappa \cos \phi_0 s - \cos(\pi - \phi_0) s, \quad \kappa_A = \frac{\mu_0 - \mu_1}{\mu_0 + \mu_1}, \quad \kappa_B = 0,$$

which are the nearest to the imaginary axis. Since  $\kappa_B = 0$ , the relation for the function  $F(\phi)$  at point  $B$  has a similar form for  $|\phi| \leq \pi/2$  as well as for  $|\phi| > \pi/2$ . Here the values of the parameters  $\delta_A, \delta_B \in (1, 2)$  in (2.11) are calculated as follows:

$$\delta_A = \min\{\nu_A^{(2)}, \tau_A\}, \quad \delta_B = \min\{\nu_B^{(2)}, \tau_B\},$$

where  $\nu_A^{(2)}, \nu_B^{(2)}$  are the second zeros of the function  $\Delta_c(s)$ , but  $\tau_A, \tau_B$  are the first zeros ( $\tau_A, \tau_B > 0$ ) of the function:  $\Delta_s(s) = s^{-1}[\kappa \sin \phi_0 s + \sin(\pi - \phi_0) s]$ , with the respective value of the parameter  $\kappa$  ( $\kappa_A, \kappa_B$ ).

The constants  $c_A, c_B$  in (2.11) play an important role in fracture mechanics [17] (stress intensity factors). The next mechanical parameter which can be calculated from the solution  $u_h$  of the problem (2.5)–(2.9) is the stiffness [18]:

$$(2.13) \quad C = \iint_{\Omega_h} \mu(x, y) \left( x^2 + y^2 + \left( x \frac{\partial}{\partial y} - y \frac{\partial}{\partial x} \right) u_h(h, x, y) \right) d\Omega.$$

However, the numerical process used for solving the problem (2.5)–(2.9) is difficult in view of the existence of the small parameter  $h$ , and of the singularity of the solution in the neighbourhood of point  $A$  situated near the exterior boundary of the domain. Further on, we find the first term of the asymptotic expansion of the solution  $\tilde{u}_h$ , which is close to  $u_h$  in the norm  $W_2^1(\Omega_h)$ , and makes it possible to obtain the values of coefficients  $c_A, c_B, C$  from (2.11), (2.13).

### 3. Limiting boundary value problems

#### 3.1. External problem

Now we consider similar problem but the domain will be somewhat different. Namely, by  $\Omega_0$  we denote the simply connected domain with boundary  $\partial\Omega_0 = \partial\Omega_h \cup M_0^+ \cup M_0^-$ , where  $M_0^\pm = \{(x, y) : 0 < y < h \wedge x = 0^\pm\}$ . Along the curves  $M_0^\pm$  we define functions  $f_M^\pm(s) \equiv 0$ , hence, the condition (2.9) holds true and the function along the boundary  $\partial\Omega_0$  is continuous. Problem (2.5)–(2.9) in the domain  $\Omega_0$  also has a unique solution  $u_0$ , belonging to  $W_2^1(\Omega_0, B)$ . Besides,  $u_0 \in C^\infty(\Omega_0^j)$ ,  $u_0 \in C(\Omega_0)$ , but  $u_0 \notin C(\overline{\Omega_0})$ . This is because the domain  $\Omega_0$  has not the “segment” property (see [10]), and  $u_0 \in W_2^1(\Omega_0, B)$  is a multifunction near the parts  $M_0^\pm$  of the boundary  $\partial\Omega_0$  (as  $(x, y)$  tends to a point  $(0, y_*)$  on the boundaries  $M_0^\pm$  from different sides of the domain  $\Omega_0$ , the function  $u_0$  has different limiting values).

The solution  $u_0$  exhibits the asymptotic behaviour (2.11)<sub>2</sub> near point  $B$  with a constant  $c_B^0$ , but in the neighbourhood of the point  $A$

$$(3.1) \quad u_0(h, x, y) = \pm d_0^\pm + O(r^{\tau_A}), \quad r \rightarrow 0, \quad 0 < \pm\phi < \pi - \phi_A.$$

Hence,  $u_0$  cannot be considered as an approximation of  $u_h$  near the zero point.

#### 3.2. Green's function

We shall also need the Green function  $\mathcal{G}_A(x, y)$  for this problem in the domain  $\Omega_0$ , with delta-functions concentrated near point  $A$ . It will be normalized by the relation (2.9). Asymptotic behaviour of the Green function near point  $B$  is of the form (2.11) (similar to  $u_h$  and  $u_0$ ) with  $d_B = 0$  and the constant  $c = g_B$ , but near the zero point

$$(3.2) \quad \mathcal{G}_A(h, x, y) = \pm \ln r \pm g_0^\pm + O(r^{\tau_A}), \quad r \rightarrow 0, \quad 0 < \pm\phi < \pi - \phi_A,$$

where  $g_0^\pm$  are some constants.

Let us note that the Green function  $\mathcal{G}_A$  is uniquely determined, and can be calculated using the representation

$$\mathcal{G}_A = \chi(r/h) \cdot \text{sign}\phi \cdot \ln r + v_0,$$

where the function  $v_0 \in W_2^1(\Omega_0, B)$  satisfies Poisson equation with the right-hand side:  $\text{sign}\phi \cdot (\ln r \Delta \chi(r/h) + 2(rh)^{-1} \chi'(r/h))$  and the boundary conditions (2.5), (2.6) with functions  $\hat{f}_j(s) = \frac{\partial}{\partial n} [\chi(r/h) \ln r]$  along the curves  $\Gamma_j$ . All these functions are smooth, and  $\hat{f}_M^\pm(y) \equiv 0$ ,  $\hat{f}_0^\pm(A)$ ,  $\hat{f}_1(A) = 0$ , in view of the assumption (2.1) for curvatures of the curves near point  $A$ . Hence, the problem for the function  $v_0 \in W_2^1(\Omega_0, B)$  and the problem of the Subs. 3.1 for the function  $u_0 \in W_2^1(\Omega_0, B)$  are similar from the point of view of their numerical realization.

3.3. Internal problem

Now let us consider the infinite domain  $G = G_0^\pm \cup G_j$  represented in Fig. 2, and try to find nontrivial harmonic function  $w(x', y')$  satisfying the homogeneous internal boundary conditions (2.6) along the boundaries  $\zeta_{j+1} = \{(x', y') : y' = y_j = h_j/h, x' \in \mathbb{R}\}$  between the domains  $G_{j-1}, G_j$  ( $j = 1, \dots, m$ ), and homogeneous conditions (2.8) along the boundaries  $\zeta_{m+1}, \zeta_0^\pm$ .

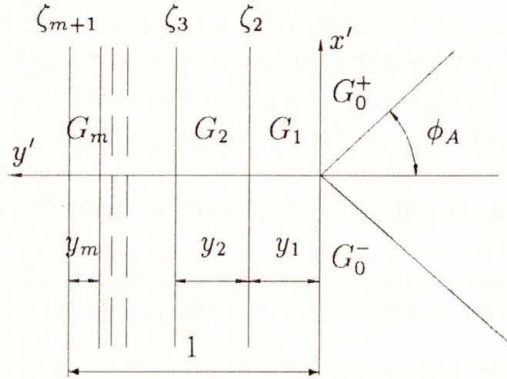


FIG. 2.

At infinity we assume, in addition, that  $w = O(\ln r)$ ,  $r \rightarrow \infty$ . There are two linearly independent harmonic functions satisfying such conditions:  $w_1(x', y') = \text{const}$  – even function with respect to argument  $x'$ , and odd function  $w_2(x', y')$ . The function  $w_2(x', y')$  can be calculated, using the inverse Fourier transform, by the nontrivial solution  $z(\xi)$  of the singular integral equation obtained in [15] (the corresponding equation (3.16)). From theorem B.4 [15], it follows that  $z \in W_{(l)}^{p,\alpha,\beta}(\mathbb{R}_+)$  for any  $l \in \mathbb{N}$ ,  $p \in [1, \infty)$ ,  $\alpha > 0$ ,  $\beta < \nu_A$ , and

$$(3.3) \quad \begin{aligned} z(\xi) &= \ln \xi + z_0 + O(\xi^2), & \xi \rightarrow 0, \\ z(\xi) &= z_\infty \xi^{-\nu_A} + O(\xi^{-\nu_A(2)}), & \xi \rightarrow \infty. \end{aligned}$$

Here,  $W_{(l)}^{p,\alpha,\beta}(\mathbb{R}_+)$  is the space of functions, which are summable (together with their  $l$ -derivatives) with a special weight (see [14]). The space  $W_{(l)}^{p,\alpha,\beta}(\mathbb{R}_+)$  does not coincide with usual Sobolev spaces  $W_p^l(\mathbb{R}_+)$ . In turn, the method of numerical calculation of this nontrivial solution has been proposed in [13]. Finally,  $w_2(x', y')$  can be determined (with accuracy to a multiplier) from the relation:

$$(3.4) \quad w_2(x', y') = 2 \int_0^\infty [\text{ch } y' \xi + [\xi \mu_1 M_p(\xi)]^{-1} \text{sh } y' \xi] z(\xi) \sin(x' \xi) d\xi, \quad (x', y') \in G_1,$$

$$(3.4) \quad w_2(x', y') = \frac{1}{\pi i} \int_{-i\infty-\delta}^{i\infty-\delta} \Gamma(s) \sin(\pi s/2) \frac{\cos(\pi - \phi_A - \phi)s}{\cos(\pi/2 - \phi_0)s} \\ \cdot \int_0^\infty z(\xi)(r\xi)^{-s} d\xi ds, \quad (x', y') \in G_0^+,$$

where  $0 < \delta < \nu_A$ , the function  $M_p(\xi)$  can be calculated by recurrence formulae from [15], and besides,  $M_p(\xi) = O(\xi^{-2})$ ,  $\xi \rightarrow 0$ ,  $M_p(\xi) = -(\mu_1 \xi)^{-1} + O(e^{-2\xi x_1})$ ,  $\xi \rightarrow \infty$ .

Using this information, we can show that the asymptotic behaviour of the function  $w_2(x', y')$  near the zero point is of the form (2.11), with the constant  $c_w = 2\pi^{-1} z_\infty \Gamma(1 - \nu_A) \sin(\pi \nu_A/2)$ ,  $d_w = 0$ , and  $\nu_A^{(2)}$  instead of the parameter  $\delta$ ; but at infinity we obtain

$$(3.5) \quad w_2(x', y') = \pm \begin{cases} \ln r + \gamma + z_0, & (x', y') \in G_0, \\ \ln |x'| + \gamma + z_0, & (x', y') \in G_j, \end{cases} + O(r^{-2}), \\ r \rightarrow \infty, \quad \pm x' > 0,$$

where  $\gamma = \Gamma'(1)$  is the Euler constant.

#### 4. Main result

Using the method of matched asymptotic expansion (see [6, 19]), we shall consider function  $w_2(s/h, n/h) + \text{const}$  as an approximation of the solution  $u_h$  in the neighbourhood of point  $A$ , but a linear combination of the functions  $u_0(h, x, y)$ ,  $\mathcal{G}_A(h, x, y)$  in the remaining part of domain  $\Omega_h$ . Let  $\alpha \in (0, 1)$  be some constant, and

$$(4.1) \quad \tilde{u}_h^{(1)}(h, x, y) = (1 - \chi(r/h^\alpha)) [u_0(h, x, y) + D\mathcal{G}_A(h, x, y)] \\ + \chi(r/h^\alpha) [Dw_2(s/h, n/h) + E].$$

Unknown constants  $D, E$  should be calculated in such a way that both parts (internal and external) of the solution (4.1) will coincide on the distance  $r = h^\alpha/2$ :

$$(4.2) \quad u_0(h, x, y) + D\mathcal{G}_A(h, x, y) - Dw_2(s/h, n/h) - E = O\left(h^{\min\{\tau_A\alpha, 2-2\alpha\}}\right), \\ \nabla[u_0(h, x, y) + D\mathcal{G}_A(h, x, y) - Dw_2(s/h, n/h) - E] \\ = O\left(h^{\min\{\tau_A\alpha, 2-2\alpha\}-\alpha}\right),$$

for  $h^\alpha/3 < r < 2h^\alpha/3$  uniformly with respect to the angular coordinate  $\theta$ ; then

$$(4.3) \quad D = \frac{d_0^+ + d_0^-}{2(z_0 + \gamma - \ln h) - g_0^+ - g_0^-}, \quad E = \frac{1}{2}[d_0^+ - d_0^- + D(g_0^+ - g_0^-)].$$

Let us note, that the function  $\tilde{u}_h^{(1)}$  from (4.1) belongs to the space  $W_2^1(\Omega_h, B)$ , and the constants in the main terms of asymptotics (2.11) near points  $A, B$  are:

$$(4.4) \quad \tilde{c}_A = \frac{2}{\pi} z_\infty D h^{-\nu_A} \Gamma(1 - \nu_A) \sin(\pi \nu_A / 2), \quad \tilde{c}_B = c_B^0 + D g_B.$$

**THEOREM 1.** *Let  $\alpha \in (0, 1)$  and  $h \ll 1$ , then for the function  $\tilde{u}_h^{(1)} \in W_2^1(\Omega_h, B)$ , the following estimates hold true:*

$$\begin{aligned} \|u_h - \tilde{u}_h^{(1)}\|_{W_2^1} &= O\left(h^{\min\{\alpha(\tau_A-1), 2-3\alpha\}}\right), \\ C - \tilde{C} &= O\left(h^{\min\{\alpha(\tau_A-1), 2-3\alpha\}}\right), \\ c_A - \tilde{c}_A &= O\left(h^{\min\{\alpha(\tau_A-\nu_A), 2-\alpha(2+\nu_A)\}}\right), \\ c_B - \tilde{c}_B &= O\left(h^{\min\{\alpha(\tau_A+\nu_A), 2-\alpha(2-\nu_A)\}}\right). \end{aligned}$$

**P r o o f.** First of all note, that the difference between  $u_h$  and  $\tilde{u}_h^{(1)}$  in each domain  $\Omega_h^j$  satisfies the Poisson equation with the right-hand side  $\mathcal{R}^{(1)}(h, x, y)$ :

$$\begin{aligned} \mathcal{R}^{(1)}(h, x, y) &= \mathcal{R}_1^{(1)}(h, x, y) - \mathcal{R}_2^{(1)}(h, x, y), \\ \mathcal{R}_1^{(1)}(h, x, y) &= [u_0(h, x, y) + D\mathcal{G}_A(h, x, y) - Dw_2(s/h, n/h) - E]\Delta\chi(r/h^\alpha) \\ &\quad + 2\nabla[u_0(h, x, y) + D\mathcal{G}_A(h, x, y) - Dw_2(s/h, n/h) - E]\nabla\chi(r/h^\alpha), \\ \mathcal{R}_2^{(1)}(h, x, y) &= D\chi(r/h^\alpha)\Delta_{x,y}w_2(s/h, n/h), \end{aligned}$$

and fulfills the boundary conditions (2.5), (2.6) with the functions

$$\begin{aligned} \tilde{f}_j^{(1)} &= \chi(r/h^\alpha)f_j + (\mu_{j-1} - \mu_j)\left[u_0 + D\mathcal{G}_A - Dw_2(s/h, n/h) \right. \\ &\quad \left. - E\right]\frac{\partial}{\partial n}\chi(r/h^\alpha), \\ \tilde{f}_0^{(1)} &= \chi(r/h^\alpha)f_0 - \mu_0\left[u_0(x, y) + D\mathcal{G}_A(x, y) - Dw_2(s/h, n/h) \right. \\ &\quad \left. - E\right]\frac{\partial}{\partial n}\chi(r/h^\alpha), \\ \tilde{f}_m^{(1)} &= \chi(r/h^\alpha)f_m + \mu_m\left[u_0(x, y) + D\mathcal{G}_A(x, y) - Dw_2(s/h, n/h) \right. \\ &\quad \left. - E\right]\frac{\partial}{\partial n}\chi(r/h^\alpha), \end{aligned}$$

instead of  $f_j$ . Such a problem (for the function  $u_h - \tilde{u}_h^{(1)}$ ) has also a unique solution in the space  $W_2^1(\Omega_h, B)$ .

Taking into account (4.2), we can obtain for  $h \rightarrow 0$

$$\begin{aligned}\mathcal{R}_1^{(1)}(h, x, y) &= O(h^{\min\{\alpha(\tau_A-2), 2-4\alpha\}}), \\ \text{supp}\mathcal{R}_1^{(1)} &= \{(x, y) \in \Omega_h : h^\alpha/3 < r < 2h^\alpha/3\},\end{aligned}$$

but to estimate the function  $\mathcal{R}_2^{(1)}(h, x, y)$  ( $\text{supp}\mathcal{R}_2^{(1)} = \{(x, y) \in \Omega_h : 0 < r < h^\alpha/3\}$ ), the Laplace operator should be considered in the curvilinear coordinate system  $(s, n)$ :

$$\begin{aligned}\Delta_{x,y}w_2(s/h, n/h) &= \frac{1}{1-nk(s)} \left[ \frac{\partial}{\partial n} \left( (1-nk(s)) \frac{\partial w_2}{\partial n} \right) \right. \\ &\quad \left. + \frac{\partial}{\partial s} \left( \frac{1}{1-nk(s)} \frac{\partial w_2}{\partial s} \right) \right].\end{aligned}$$

Denoting  $\xi = s/h, \eta = n/h$ , we can conclude, in view of assumption (2.1) on the curves  $\Gamma_1$ , and taking into account the asymptotic formula (3.5) for the function  $w_2$ , that  $\mathcal{R}_2^{(1)}(h, x, y) = \mathcal{R}_3^{(1)}(\xi, \eta) + O(h)$ , where

$$\mathcal{R}_3^{(1)}(\xi, \eta) = O(\rho^{\nu_A}), \quad \rho \rightarrow 0, \quad \mathcal{R}_3^{(1)}(\xi, \eta) = O(1), \quad \rho \rightarrow \infty.$$

The functions  $\tilde{f}_j^{(1)}$  in the boundary conditions (2.5), (2.6) can be represented as a sum  $\tilde{f}_j^{(1)} = \tilde{f}_{j1} + \tilde{f}_{j2}$ , which at  $h \rightarrow 0$  have the properties:

$$\begin{aligned}\tilde{f}_{j1} &= O(h^\alpha), & \text{supp}\tilde{f}_{j1} &= \{(x, y) \in \Omega_h : 0 < r < 2h^\alpha/3\}, \\ \tilde{f}_{j2} &= O(h^{\min\{2-3\alpha, \alpha(\tau_A-1)\}}), & \text{supp}\tilde{f}_{j2} &= \{(x, y) \in \Omega_h : h^\alpha/3 < r < 2h^\alpha/3\}.\end{aligned}$$

We can then conclude that

$$\begin{aligned}\|\mathcal{R}_1^{(1)}\|_{L_2(\Omega_h)} &= O(h^{\min\{\alpha(\tau_A-1), 2-3\alpha\}}), & \|\mathcal{R}_2^{(1)}\|_{L_2(\Omega_h)} &= O(h^\alpha), \\ \|\tilde{f}_{j1}^{(1)}\|_{L_2(\Gamma_j)} &= O(h^{\min\{\alpha(\tau_A-1/2), 2-5\alpha/2\}}), & \|\tilde{f}_{j2}^{(1)}\|_{L_2(\Gamma_j)} &= O(h^{3\alpha/2}).\end{aligned}$$

Now, the first conclusion of Theorem 1 follows from the results [10]. However, the constant in the estimate ( $\|u_h - \tilde{u}_h^{(1)}\| \leq \text{Const } h^{\min\{\alpha(\tau_A-1), 2-3\alpha\}}$ ) cannot be effectively obtained. It depends on the norm of the inverse operator of problem (2.5)–(2.9). The second relation follows immediately from the Hölder inequality.

For estimation of the constants  $c_A, c_B$  in the main terms of the asymptotics (2.11), we shall use the MAZ'YA, PLAMENEVSKY method [11]. Following [11] (see also [17]), we can define “non-energetic” harmonic function  $\Psi_A^- \in L_2(\Omega_h)$  satisfying the homogeneous problem (2.5)–(2.9) with asymptotic behaviour (2.11) near point  $B$ , but in the neighbourhood of point  $A$  satisfying the condition

$$(4.5) \quad \Psi_A^-(x, y) = r^{-\nu_A} F(\phi) + O(r^{\nu_A}), \quad r \rightarrow 0,$$

where function  $F(\phi)$  is defined in (2.11). The function  $\Psi_A^-(x, y)$  can be calculated from the representation ( $\varepsilon < h_1$ ):

$$\Psi_A^-(x, y) = \chi(r/\varepsilon)r^{-\nu_A}F(\phi) + \Psi_\varepsilon^-(x, y), \quad \Psi_\varepsilon^- \in W_2^1(\Omega_h, B),$$

because the corresponding problem for function  $\Psi_\varepsilon^-$  has a unique solution in the space  $W_2^1(\Omega_h, B)$ . Further on we define  $\omega_\varepsilon = \{(x, y) : r < \varepsilon\}$  and write the Green formulae for the functions as  $\hat{u}_h = u_h - \tilde{u}_h^{(1)}$  and  $\Psi_A^-$  in the domains of  $\Omega_h^0 \setminus \omega_\varepsilon, \Omega_h^1 \setminus \omega_\varepsilon, \Omega_h^j$  ( $j = 2, \dots, m$ ). The sum of the corresponding relations is in the form of:

$$\begin{aligned} \iint_{\Omega_h \setminus \omega_\varepsilon} \mu(x, y) \left[ \Psi_A^- \Delta \hat{u}_h - \hat{u}_h \Delta \Psi_A^- \right] d\Omega &= \int_{\Gamma_{m+1}} \mu_m \left[ \Psi_A^- \frac{\partial \hat{u}_h}{\partial n} - \hat{u}_h \frac{\partial \Psi_A^-}{\partial n} \right] d\sigma \\ &+ \sum_{j=1}^m \int_{\Gamma_j \cap (\Omega_h \setminus \omega_\varepsilon)} \left\{ \mu_j \left[ \Psi_A^- \frac{\partial \hat{u}_h}{\partial n} - \hat{u}_h \frac{\partial \Psi_A^-}{\partial n} \right] - \mu_{j-1} \left[ \Psi_A^- \frac{\partial \hat{u}_h}{\partial n} - \hat{u}_h \frac{\partial \Psi_A^-}{\partial n} \right] \right\} d\sigma \\ &- \int_{\Gamma_0 \cap (\Omega_h \setminus \omega_\varepsilon)} \mu_0 \left[ \Psi_A^- \frac{\partial \hat{u}_h}{\partial n} - \hat{u}_h \frac{\partial \Psi_A^-}{\partial n} \right] d\sigma - \int_{\partial \omega_\varepsilon} \mu(x, y) \left[ \Psi_A^- \frac{\partial \hat{u}_h}{\partial n} - \hat{u}_h \frac{\partial \Psi_A^-}{\partial n} \right] d\sigma, \end{aligned}$$

or taking into account the equations and the boundary conditions for functions  $\hat{u}_h$  and  $\Psi_A^-$ , this relation can be rewritten as follows ( $\varepsilon < h_1$ ):

$$\begin{aligned} (4.6) \quad &\int_{\partial \omega_\varepsilon} \mu(x, y) \left[ \Psi_A^- \frac{\partial \hat{u}_h}{\partial n} - \hat{u}_h \frac{\partial \Psi_A^-}{\partial n} \right] d\sigma \\ &= \sum_{j=2}^{m+1} \int_{\Gamma_j} \Psi_A^- \tilde{f}_j^{(1)} d\sigma + \int_{\Gamma_1 \cap (\Omega_h \setminus \omega_\varepsilon)} \Psi_A^- \tilde{f}_1^{(1)} d\sigma + \int_{\Gamma_0 \cap (\Omega_h \setminus \omega_\varepsilon)} \Psi_A^- \tilde{f}_0^{(1)} d\sigma \\ &\quad - \iint_{\Omega_h \setminus \omega_\varepsilon} \mu(x, y) \Psi_A^- \left[ \mathcal{R}_1^{(1)}(h, x, y) - \mathcal{R}_2^{(1)}(h, x, y) \right] d\Omega. \end{aligned}$$

The net result will be obtained by passing to the limit  $\varepsilon \rightarrow 0$ :

$$\begin{aligned} (4.7) \quad &\Phi(\mu_0, \mu_1, \phi_A)(c_A - \tilde{c}_A) \\ &= \sum_{j=0}^{m+1} \int_{\Gamma_j} \Psi_A^- \left[ \tilde{f}_{j1}^{(1)} + \tilde{f}_{j2}^{(1)} \right] d\sigma - \iint_{\Omega_h} \mu \Psi_A^- \left[ \mathcal{R}_1^{(1)} - \mathcal{R}_2^{(1)} \right] d\Omega. \end{aligned}$$

Here we use information (2.11) and (4.5) about the asymptotic behaviour of the functions  $\hat{u}_h, \Psi_A^-$  near point  $A$  for calculating the integral on the left-hand side

of (4.6):

$$(4.8) \quad \Phi(\mu_0, \mu_1, \phi_A) = 2 \left\{ \mu_1 \frac{\pi \nu_A - \sin \pi \nu_A}{1 - \cos \pi \nu_A} + \mu_0 \frac{(\pi - 2\phi_A)\nu_A + \sin(\pi - 2\phi_A)\nu_A}{1 + \cos(\pi - 2\phi_A)\nu_A} \right\}.$$

The first and the fourth terms on the right-hand side of (4.7) are estimated as  $O(h^{\alpha(2-\nu_A)})$ , but the remaining two terms are  $O(h^{\min\{\alpha(\tau_A-\nu_A), 2-\alpha(2+\nu_A)\}})$ . Consequently, the third conclusion of Theorem 1 is proved. The remaining estimation of Theorem 1 is performed in a similar manner. For this purpose, we should take the “non-energetic” function  $\Psi_B^-$  (instead of  $\Psi_A^-$ ), which exhibits the asymptotic behaviour (2.11) near the point  $A$ , but in the neighbourhood of point  $B$  in the form of (4.5) with  $\nu_B$ . Then, repeating the same reasoning, we obtain the fourth conclusion of Theorem 1. Let us note that the constants in the last two estimates have been obtained effectively.

**COROLLARY 1.** The optimal value of the parameter  $\alpha$  is  $\alpha_* = 2/(2 + \tau_A)$ , then the estimates are:

$$\|u_h - \tilde{u}_h^{(1)}\|_{W_2^1}, |C - \tilde{C}| = O(h^{2-3\alpha_*}),$$

$$c_A - \tilde{c}_A = O(h^{2-\alpha_*(\tau_A+\nu_A)}), \quad c_B - \tilde{c}_B = O(h^{2-\alpha_*(\tau_A-\nu_A)}).$$

**REMARK 1.** As it follows from the proof of Theorem 1, the results would be improved, if we could more precisely estimate the terms of solution  $u_0$  and the Green function  $\mathcal{G}_A$  of the asymptotic behaviour:  $O(r^{\tau_A})$ ,  $r \rightarrow 0$ . For this purpose, note that the corresponding problem for function  $u_0$  is the perturbation boundary value problem with the regular boundary layer near  $\Gamma_{m+1} = \Gamma_e$ . The main terms of such problems have been constructed in [4]. Basing on the results from [4], one can show that the term  $O(r^{\tau_A})$  in (3.1) can be estimated as:  $\text{const}(h)F_*(\phi)r^{\tau_A}$ , where  $\text{const}(h) = O(h^\beta)$  with some  $0 < \beta \leq \tau_A^0 - \tau_A$ . Here,  $\tau_A^0$  is the corresponding parameter in (3.1) for the solution  $u_0^0(x, y)$  of the nonperturbed problem ( $\mu(x, y) = \mu_0, h = 0$ ). In a similar manner, the estimation of the corresponding term of the Green function (3.2) can be obtained. Then we can formulate

**THEOREM 2.** Let  $\alpha \in (0, 1)$  and  $h \ll 1$ , then for function  $\tilde{u}_h^{(1)} \in W_2^1(\Omega_h, B)$  estimates hold true:

$$\begin{aligned} \|u_h - \tilde{u}_h^{(1)}\|_{W_2^1} &= O(h^{\min\{\alpha, \beta + \alpha(\tau_A - 1), 2 - 3\alpha\}}), \\ C - \tilde{C} &= O(h^{\min\{\alpha, \beta + \alpha(\tau_A - 1), 2 - 3\alpha\}}), \\ c_A - \tilde{c}_A &= O(h^{\min\{\alpha(2 - \nu_A), \beta + \alpha(\tau_A - \nu_A), 2 - \alpha(2 + \nu_A)\}}), \\ c_B - \tilde{c}_B &= O(h^{\min\{\alpha(2 + \nu_A), \beta + \alpha(\tau_A + \nu_A), 2 - \alpha(2 - \nu_A)\}}). \end{aligned}$$

COROLLARY 2. Then the optimal value of the parameter  $\alpha$  in Corollary 1 is

$$\alpha_* = \max \{1/2, (2 - \beta)/(2 + \tau_A)\}.$$

## 5. Remarks and conclusions

In this section we propose some generalizations under which the mentioned results of the theorems will hold true.

First of all note that from [18] it follows that  $f_j = (\mu_{j-1} - \mu_j)[y \cos(n, x) - x \cos(n, y)]$ ,  $f_{m+1} = \mu_m[y \cos(n, x) - x \cos(n, y)]$ ,  $f_0 = \mu_0[y \cos(n, x) - x \cos(n, y)]$ . Consequently, these functions satisfy the conditions (2.7). Nevertheless, the results still remain valid, if the functions are "little affected" in the neighbourhood of point  $A$ . For this purpose, it is sufficient to find the solution in the form:  $u_h = \bar{u}_h + \chi(r/h)v_1(s, n)$ , where the function is  $v_1 = a_j + b_j s + c_j n$  in each region  $\Omega_h^j$ . The constants  $a_j, b_j, c_j$  should be calculated so that  $v_1$  is continuous along  $\Gamma_j$ , but for function  $\bar{u}_h$  the conditions (2.7) have been satisfied.

Further on, note that the conditions (iii) in (2.1) can be weakened like this:  $k_{\Gamma_1}(A), k_{\Gamma_0^\pm}(A), k_{\Gamma_0^\pm}(B) \sim 1$ . The angle of corner  $A$  can be nonsymmetric with respect to the normal to the boundary  $\Gamma_0$  at this point, in contrast to (ii). Then the functions  $F(\phi)$  in (2.11) and the transcendental functions  $\Delta_{s(c)}(s)$  (necessary to determine the parameters  $\tau, \nu$ ) should be corrected; but the corresponding internal boundary value problems can be calculated by solving of the systems of singular integral equations [15], instead of the singular integral equations as it is in the symmetric cases.

The step function  $\mu(x, y)$  allows for the following generalization:

1. The boundaries of discontinuity  $\Gamma_j$  of function  $\mu(x, y)$  can be defined as in (2.2) with functions  $h_j(s)$  instead of parameters  $h_j$ . We should assume only that:  $h_j(s) > h_{j-1}(s)$ ,  $h_m(s) = O(h)$ ,  $h'_j(0) = 0$ ,  $h''_j(0) \sim 1$ .

2. In each domain  $\Omega_h^j$  the conditions are true:  $\mu \in C^2(\Omega_h^j)$ , and  $\frac{\partial}{\partial x}\mu(0, y) = 0$ ,  $\frac{\partial^2}{\partial x^2}\mu(0, y) \sim 1$ ,  $(0, y) \in \Omega_h^j$  ( $j > 0$ ),  $\frac{\partial}{\partial r}\mu(0, \theta) = 0$ ,  $\frac{\partial^2}{\partial r^2}\mu(0, \theta) \sim 1$ ,  $(0, \theta) \in \Omega_h^0$ . The function  $\mu(x, y)$  depends weakly on the argument  $x$  in the multilayer near the angle vertex. Then we shall find solution  $u_h$  of equation  $\nabla(\mu(x, y)\nabla u_h) = 0$  instead of the Laplace equation  $\Delta u_h = 0$  used in the paper. Such a problem corresponds to the general case of a nonhomogeneous elastic rod. Note in this connection that the internal boundary value problems (Sec. (3.2)) can be also solved in this case by the method [15] (see Appendix in [16]).

The boundary conditions can be also generalized. Namely, the first of the conditions (2.5) can be represented in the form:  $[u_h] - a(s)\frac{\partial}{\partial n}u_h = \bar{f}_j$ ,  $a'(0) = 0$ ,  $a''(0) \sim 1$ , instead of  $[u_h] = 0$ . The corresponding internal boundary value problems can be solved by the same method [15, 16].

Let us note in conclusion, that the first two conditions (i) cannot be modified, of course (these conditions make it possible to use the asymptotic methods). If the third condition is not true and  $\text{dist}(B, \Gamma_e) = O(h)$ , then the asymptotic expansion of the solution can also be constructed. However, the corresponding external boundary value problems are different from those shown in the paper (Sec. (3.1)), and the representation of the solution (4.1) should be changed. In [19], such a problem in a homogeneous domain with the linear crack has been considered.

## Acknowledgment

The author is grateful to Professor Z.S. OLESIAK for a helpful discussion.

## References

1. O.B. AGALARYAN and S.A. NAZAROV, *On change of stress intensity factors in soldering of crack in prismatic rod*, Dokl. Akad. Nauk Arm. SSR, **72**, 1, 18–21, 1981.
2. V.M. ALEKSANDROV and S.M. MHTIARYAN, *Contact problems for bodies with thin covers and layers* [in Russian], Nauka, Moscow 1983.
3. V.M. ALEKSANDROV, B.I. SMETANIN and B.V. SOBOL, *Thin stress concentrators in elastic bodies* [in Russian], Nauka, Moscow 1993.
4. H.N. ARUTYUNYAN and B.L. ABRAMYAN, *Torsion of elastic bodies* [in Russian], Nauka, Moscow 1968.
5. D. GILBARG and N.S. TRUDINGER, *Elliptic partial differential equations of second order*, Springer-Verlag, Berlin – New-York – Tokyo 1983.
6. A.M. ILIN, *On the method of matched asymptotic expansions of boundary value problems* [in Russian], Nauka, Moscow 1989.
7. L.A. IVANOV, L.A. KOTKO and S.G. KREIN, *Boundary value problems in varying domains* [in Russian], [in:] *Differential Equations and Their Applications*, **19**, 6–161, 1977.
8. T. KATO, *Theory of perturbed linear operators* [in Russian], Mir, Moscow 1972.
9. YU.M. KOLYANO and M.E. CHOMIAKIEWICZ, *Generalized heat conduction in solids with thin surface layer of an arbitrary curvature* [in Russian], *J. Engng. Physics and Thermophysics*, Minsk, **65**, 6, 745–749, 1993.
10. O.A. LADYZHENSKAYA, *The boundary-value problems of mathematical physics*, *Applied Mathematical Science*, Vol. **49**, Springer-Verlag, 1985.
11. V.G. MAZ'YA and B.A. PLAMENEVSKY, *On coefficients in asymptotics of elliptic boundary value problems in domains with conical points* [in Russian], *Mathematische Nachrichten*, **76**, 29–60, 1977.
12. V.G. MAZ'YA, S.A. NAZAROV and B.A. PLAMENEVSKY, *Asymptotics of solutions of singular perturbed elliptic boundary value problems* [in Russian], Tbilisi 1981.
13. G. MISHURIS, *On nontrivial solution of one singular integral equation*, *Folia Sci. Univ. Tech. Resoviensis, Math.*, **16**, 113–130, 1994.
14. G.S. MISHURIS and Z.S. OLESIAK, *On boundary value problems in fracture of elastic composites*, *Euro. J. Appl. Math.*, **6**, 591–610, 1995.
15. G. MISHURIS, *Boundary value problems for Poisson's equations in multi-wedge – multi-layered region*, *Arch. Mech.*, **47**, 2, 295–335, 1995.
16. G. MISHURIS, *Boundary value problems for Poisson's equations in multi-wedge – multi-layered region. Part II. General type of interfacial conditions*, *Arch. Mech.*, **48**, 4, 711–745, 1996.
17. N.F. MOROZOV, *Mathematical problems of the crack theory* [in Russian], Nauka, Moscow 1984.

18. N.I. MUSCHELISHVILI, *Mathematical problems of theory of elasticity* [in Russian], Nauka, Moscow 1966.
19. S.A. NAZAROV, *Introduction to asymptotic methods of the theory of elasticity* [in Russian], Edition of Leningrad State University, 1983.
20. G.Ya. POPOV, *Stress concentration near stamps, cracks, thin inclusions and covers* [in Russian], Nauka, Moscow 1982.

DEPARTMENT OF MATHEMATICS,  
RZESZÓW UNIVERSITY OF TECHNOLOGY  
e-mail: [miszuris@prz.rzeszow.pl](mailto:miszuris@prz.rzeszow.pl)

*Received May 20, 1996.*

---

# A formulation of continuum mechanics as a dimensional reduction of a finite-dimensional dynamical system

J. KACZMAREK (GDAŃSK)

IN THE PAPER a generalized formulation of the continuum mechanics is suggested. The generalization consists in the assumption that the energy balance equation is not satisfied for all subbodies of a body but only for their chosen family. This formulation leads to fields in the continuum which create a finite-dimensional space. With the help of the chosen family of subbodies, a volume of averaging related to the continuum model is defined. This volume is connected with a more elementary dynamical system which takes part in determination of the form of constitutive equations. In general, the mechanical model of the continuum is seen as a dimensional reduction of the more elementary dynamical system related to another continuum or to a discrete set of material points.

## 1. Introduction

PHYSICAL PHENOMENA related to a microstructure are frequently taken into considerations in mechanical modelling of material behaviour [1, 2, 3].

The evolution of the microstructure can be quite complicated. In such cases it is difficult to postulate the form of the equations, and particularly the form of the constitutive equations for highly averaged models of the continuum.

A good illustration of such a situation is the martensitic transformation related to the shape memory alloys. In small scale we observe different martensite variants, different kinds of moving interfaces, shuffles, internal rotations, stabilization of the martensite etc. These phenomena make a mechanical description in the small scale quite complicated. On the other hand, simpler descriptions can be carried out for a more averaged continuum. However, it is then difficult to determine the form of constitutive equations. This suggests a multiscale approach, where the equations related to a small scale should form the theoretical and numerical base for those related to the larger scale. Such an approach was proposed and discussed in [12, 13, 14].

Considerations related to the model with a small scale create, in turn, new difficulties. The determination of all constants and functions related to material properties of the model in small scale often require complex discrete calculations. Then, a discrete model can form a foundation for the continuous one.

At the moment we have the following problem. All discrete models are finite-dimensional ones. During reformulating them into a continuum model, the description itself undergoes a simplification but all the fields obtained in the continuous body become infinite-dimensional ones. It is expected that continuous model should be dimensionally reduced as compared with a discrete one, and therefore the continuum theory should be finite-dimensional as well.

The next problem is related to the degree of averaging. The notion of the volume of averaging is intuitively intelligible. On the other hand, it is related to physical foundations of the mechanical model. Therefore, the notion of volume of averaging should be introduced and elucidated in detail.

The above mentioned remarks suggest that in considering complicated microstructure, it is difficult to avoid discrete calculations.

There are many efforts to provide discrete foundations for continuum mechanics [7–11] as well as simplifications in the description of complex discrete systems. The statistical mechanics reduces enormous number of degrees of freedom by the statistical averaging [4, 5]. In analytical mechanics, the well known method of constraints reduces the number of degrees of freedom [26]. There is an averaging method known in nonlinear dynamical systems [6] which leads to replacement of the complicated evolution by a simpler one. Thus, simplifications in mathematical description of complicated systems were frequently studied in literature.

The aim of this paper is to give a generalized formulation of the continuum mechanics. This formulation is in a position to adopt the point of view that the continuum appears as a dimensionally reduced discrete system, or another more complicated continuum system. Furthermore, in the frame of this formulation, the notion of volume of averaging is elucidated sufficiently.

## 2. An idea of a dimensional reduction

The discussion carried out in the introduction suggests that the continuum models should appear as a dimensional reduction of discrete systems. Behaviour of a system of atoms in many cases can be well approximated by a classical system of material particles. It can be obtained with the help of the Born–Oppenheimer approximation [27].

Therefore, at the beginning of our considerations an idea of a dimensional reduction of a dynamical system described by the Hamilton equations will be discussed.

Let us consider a system of  $N$  material points with masses  $m_i$ ,  $i \in I_N = \{1, \dots, N\}$ . The position of the  $i$ -th mass is given by  $\mathbf{q}_i = \{q_1, q_2, q_3\}$ , the velocity by  $\mathbf{v}_i = \dot{\mathbf{q}}_i$ , and the linear momentum by  $\mathbf{p}_i = m_i \mathbf{v}_i$ . Let  $H$  stand for the Hamiltonian of the system under consideration, and let  $\mathbf{f}_i$  be the force related to the  $i$ -th point.

Equations of motion for this system of points are discussed in analytical mechanics and are given in the well known form [26]

$$(2.1) \quad \frac{d\mathbf{q}_i}{dt} = \frac{\partial H}{\partial \mathbf{p}_i}, \quad \frac{d\mathbf{p}_i}{dt} = -\frac{\partial H}{\partial \mathbf{q}_i} + \mathbf{f}_i.$$

Let us introduce the concise notations  $\mathbf{d}_i = \{\mathbf{q}_i, \mathbf{v}_i\}$ ,  $\mathbf{d} = \{\mathbf{d}_i\}$ ,  $\mathbf{f} = \{\mathbf{f}_i\}$ ,  $L(\mathbf{d}, \mathbf{f}) = \left\{ \frac{\partial H}{\partial \mathbf{p}_i}, \frac{1}{m_i} \left( -\frac{\partial H}{\partial \mathbf{q}_i} + \mathbf{f}_i \right) \right\}$ ,  $i \in I_N$ . Then, Eqs. (2.1) can be rewritten concisely as  $\dot{\mathbf{d}} = L(\mathbf{d}, \mathbf{f})$ .

The evolution function for the dynamical system defined by (2.1) can be expressed as a generalization of linearized solutions of these equations (see for instance [28]) in the form

$$(2.2) \quad \chi(\mathbf{d}_0, \mathbf{f})(t) = e^{\int_{t_0}^t \frac{\partial L}{\partial \mathbf{d}}(\mathbf{d}, \mathbf{f}) dt} \mathbf{d}_0,$$

where the existence of  $\partial L / \partial \mathbf{d}$  is assumed.

We would like to introduce a dynamical system which would have a considerably lower dimension than the original one. Let  $\mathcal{M}$  be a manifold consisting of all admissible  $\mathbf{d}$ . A dimensional reduction relies on introducing a smaller number of variables and on deriving a new appropriate evolution equation. Let  $\bar{\mathbf{d}}$  be a variable of such a new kind of a system, and let, by analogy  $\bar{\mathcal{M}} = \{\bar{\mathbf{d}}\}$ . The connection between these variables can be given with the help of a map  $\pi : \mathcal{M} \rightarrow \bar{\mathcal{M}}$ .

External forces undergo a dimensional reduction as well. Indeed, the reduced dynamical system should be insensitive to some fine features of forces  $\{\mathbf{f}_i\}$  related to a more complicated system. Therefore, by analogy, we define  $\mathcal{F} = \{\mathbf{f}\}$ ,  $\bar{\mathcal{F}} = \{\bar{\mathbf{f}}\}$  and  $\pi_f : \mathcal{F} \rightarrow \bar{\mathcal{F}}$ .

The map  $\pi$  formally reduces the dimension of the system. However, such a reduction can be accompanied by a simplification of behaviour of the system in some time interval  $T = [t_0, t_0 + T]$ .

Let  $(\mathcal{M} \times T)_f = \{\chi(\mathbf{d}_0, \mathbf{f})(t) : t \in T, \mathbf{d}_0 \in \mathcal{M}\}$ . This set consists of elements which are possible solutions of the equation (2.1) with the initial condition  $\mathbf{d}(t_0) = \mathbf{d}_0$  and the given function  $\mathbf{f}(t) \in \mathcal{F}_T$ , where  $\mathcal{F}_T = \{\mathbf{f}(t) : t \in T\}$ . In a similar way we define the sets  $(\bar{\mathcal{M}} \times T)_{\bar{f}} = \{\bar{\chi}(\bar{\mathbf{d}}_0, \bar{\mathbf{f}}) : t \in T, \bar{\mathbf{d}}_0 \in \bar{\mathcal{M}}\}$  and  $\bar{\mathcal{F}}_T = \{\bar{\mathbf{f}}(t) : t \in T\}$ . With the help of these sets we can introduce new maps  $\pi_T : (\mathcal{M} \times T)_f \rightarrow (\bar{\mathcal{M}} \times T)_{\bar{f}}$  and  $\pi_{fT} : \mathcal{F}_T \rightarrow \bar{\mathcal{F}}_T$ .

For convenience, let us introduce a more general set of all continuous functions with sufficiently high time derivative  $C(\bar{\mathbf{d}}_0) = \{\varphi(t) : \varphi : T \rightarrow \bar{\mathcal{M}}, \varphi(t_0) = \bar{\mathbf{d}}_0\}$ .

The relation between  $\pi$  and  $\pi_T$  lies in the fact that for each  $t = \bar{t}$ ,  $\pi_T(\bar{t})$  has the same domain and range as  $\pi$ . Thus,  $\pi_T$  does not introduce new variables.

The evolution function  $\bar{\chi} : T \rightarrow \bar{\mathcal{M}}$  for the dimensionally reduced dynamical system is unknown. Let us assume that the form of  $\bar{\chi}$  can be expressed as

$$(2.3) \quad \bar{\chi}(\mathbf{C}, \bar{\mathbf{d}}_0, \bar{\mathbf{f}})(t) = e^{\int_{t_0}^t \frac{\partial \bar{L}}{\partial \bar{\mathbf{d}}}(\mathbf{C}, \bar{\mathbf{d}}, \bar{\mathbf{f}}) dt} \bar{\mathbf{d}}_0,$$

where  $\mathbf{C} \in \mathcal{C}$ , with  $\mathcal{C}$  being a set of all admissible constants  $\mathbf{C}$ . Thus, the expression  $(\partial \bar{L} / \partial \bar{\mathbf{d}})(\mathbf{C}, \bar{\mathbf{d}}, \bar{\mathbf{f}})$  is postulated to be dependent on  $\mathbf{C}$  and operation  $\partial / \partial \bar{\mathbf{d}}$  is assumed to be realizable. Consequently, the determination of a dimensionally

reduced dynamical system rests on finding  $\pi, \pi_T, \pi_f, \pi_{fT}$  and the best  $\mathbf{C}^* \in \mathcal{C}$ . To this end appropriate criteria should be formulated.

We can consider two kinds of dimensionally reduced time processes. The first one is induced by the Hamiltonian system. We have  $\chi(\mathbf{d}_0, \mathbf{f})(t) \in (\mathcal{M} \times T)_f$ . With the help of the introduced mappings  $\{\pi_T, \pi_{fT}\}$ , we obtain induced process  $\pi_T(\chi(\mathbf{d}_0, \mathbf{f})(t))$  which belongs to a new set  $(\pi\mathcal{M} \times T)_{\bar{f}}$ . The second time process is related to the evolution function  $\bar{\chi}(\mathbf{C}, \bar{\mathbf{d}}_0, \bar{\mathbf{f}})(t)$  which is parametrized by  $\mathbf{C}$ . Let us assume that for each  $\mathbf{C}$  the evolution function  $\bar{\chi}$  is determined. Then we are able to define a new set  $(\bar{\mathcal{M}}_C \times T)_{\bar{f}} = \{\bar{\chi}(\mathbf{C}, \bar{\mathbf{d}}_0, \bar{\mathbf{f}})(t) : t \in T, \bar{\mathbf{d}}_0 \in \bar{\mathcal{M}}\}$  and two injections  $i : (\pi\mathcal{M} \times T)_{\bar{f}} \rightarrow C$  and  $i_c : (\bar{\mathcal{M}}_c \times T)_{\bar{f}} \rightarrow C$ .

Now we have a possibility to compare two processes introduced previously. To this end, a metric on  $C$  has to be introduced. Thus, let  $\rho : C \times C \rightarrow R^+ \cup \{0\}$  be a metric on  $C$ .

With the help of the assumption (2.3) we can generate a family of processes dependent on  $\mathbf{C}$  in the form  $\bar{\chi}(\mathbf{C}, \bar{\mathbf{d}}_0, \bar{\mathbf{f}})(t)$ ,  $\mathbf{C} \in \mathcal{C}$ ,  $\bar{\mathbf{d}}_0 = \pi(\mathbf{d}_0)$ ,  $\bar{\mathbf{f}} = \pi_{fT}(\mathbf{f})$ , where  $\mathbf{d}_0$  and  $\mathbf{f}$  are applied to determine the Hamiltonian process  $\chi(\mathbf{d}_0, \mathbf{f})(t)$ .

Let us define a function

$$(2.4) \quad h(\bar{\mathbf{d}}_0, \bar{\mathbf{f}}) = \inf_{\mathbf{C} \in \mathcal{C}} \rho(i_c(\bar{\chi}(\mathbf{C}, \bar{\mathbf{d}}_0, \bar{\mathbf{f}})(t)), i(\pi_T(\chi(\mathbf{d}_0, \mathbf{f})(t)))).$$

By  $\mathbf{C}^*$  we denote the constant  $\mathbf{C} \in \mathcal{C}$  which minimizes the function  $h$ . Accordingly,  $\mathbf{C}^* = \mathbf{C}^*(\bar{\mathbf{d}}_0, \bar{\mathbf{f}})$ . A satisfactory approximation should have the property that  $\mathbf{C}^*$  displays a weak dependence on  $\bar{\mathbf{d}}_0$  and  $\bar{\mathbf{f}}$ . It depends, in turn, on an assumed function  $\pi_T$  for the dimensional reduction. Finally,

$$(2.5) \quad \bar{\mathbf{C}} = \text{Av}\{\mathbf{C}^* : \mathbf{C}^* = \mathbf{C}^*(\bar{\mathbf{d}}_0, \bar{\mathbf{f}}), \bar{\mathbf{d}}_0 \in \bar{\mathcal{M}}, \bar{\mathbf{f}} \in \bar{\mathcal{F}}_T\},$$

where  $\text{Av}$  means an averaging operation. Thus,  $\bar{\mathbf{C}}$  determines the evolution function of the reduced system  $\bar{\chi}(\bar{\mathbf{C}})(t)$ .

Thus, as a result of the dimensional reduction, we have obtained a new dynamical system. Let us characterize the main elements of the dimensional reduction. First, we have to choose new variables represented by  $\bar{\mathbf{d}}$ . Similarly, the forces are also dimensionally reduced to the  $\bar{\mathbf{f}}$ . Next, we have to assume or to infer the form of expression  $(\partial\bar{L}/\partial\bar{\mathbf{d}})(\mathbf{C}, \bar{\mathbf{d}}, \bar{\mathbf{f}})$ . This equation creates a skeleton of a new dynamical system  $SDS$  which can be characterized by  $SDS(\mathbf{C}) = \{\bar{\mathbf{d}}, \bar{\mathbf{f}}, (\partial\bar{L}/\partial\bar{\mathbf{d}})(\mathbf{C}, \bar{\mathbf{d}}, \bar{\mathbf{f}})\}$ . We should also determine the family of maps  $\{\pi\} = \{\pi, \pi_T, \pi_f, \pi_{fT}\}$ . Dimensionally reduced dynamical system  $RDS(\bar{\mathbf{C}})$  is obtained with the help of an approximation method  $app$  given by (2.4), (2.5). Consequently, the dimensional reduction operation can be characterized by  $DR = \{SDS, \{\pi\}, app\}$ . Finally, the pair  $\{EDS, DR\}$  leads to  $RDS(\bar{\mathbf{C}})$ , where  $EDS$  is the elementary dynamical system determined in (2.1).

Continuum models should be such dynamical systems which describe a material behaviour. Thus, they should appear as dimensionally reduced dynamical

systems describing a behaviour of a set of atoms which constitute the material of the body. Therefore, in the paper, just such a formulation of continuum mechanics is discussed.

### 3. A generalized formulation of continuum mechanics

The continuum mechanics has been developed by creating its precise mathematical foundations. These problems were widely discussed in the literature, for instance in [15, 16, 17, 18, 19].

In this paper we propose a generalization of the formulation of the continuum theory. This generalization is based on weakening of an assumption that the energy balance equation is satisfied for each subbody of the body  $B$ . It is assumed here that this is the case only for a distinguished family of subbodies of  $B$ . Such a theory comprises the traditional formulation as well, since the distinguished family of subbodies can, in particular, consist of all subbodies of  $B$ .

Let us note that for discrete system, energy depends on a finite number of variables which are related to positions and velocities of particles of the discrete system. During a dimensional reduction the number of variables decreases. Such a new variable represents usually a group of particles from its discrete set. This leads to justification of the theorem that the balance of energy can be introduced for the finite subbodies of the whole body only.

Let us consider a set  $B$  and a family of its subsets which create a countable additive field  $S$ .

**DEFINITION 1.** *The body  $B$  is a space with a positive measure  $M : S \rightarrow R^+ \cup \emptyset$ . The measure  $M$  is called the mass.*

**DEFINITION 2.** *The body  $B$  is the continuous body if it is endowed with a structure defined by a non-empty class  $C$  of maps which satisfy the following axioms:*

a. *The members of  $C$  are invertible maps from  $B$  onto open subsets of the Euclidean space.*

b. *If  $\kappa, \gamma \in C$ , then  $\kappa \circ \gamma^{-1}$  is a homeomorphism in  $E^3$ .*

c. *If  $\kappa \in C$ ,  $\lambda$  is a homeomorphism in  $E^3$  and  $\text{Range } \kappa = \text{Dom } \lambda$ , then  $\lambda \circ \kappa \in C$ .*

The members of  $C$  are called the placements of  $B$ . The range  $\kappa(B)$ ,  $\kappa \in C$ , is called the region occupied by  $B$  in the placement  $\kappa$ .

The function  $\lambda = \gamma \circ \kappa^{-1}$  is called the displacement function between placement  $\kappa$  and  $\gamma$ . The last definition follows from [19].

**DEFINITION 3.** *The continuous map of the time interval  $[0, T]$  onto the set  $C$  is called the motion of the body  $B$ .*

Let  $\chi(\mathbf{X}, t)$  be a motion of the body  $B$ , where  $\mathbf{X} \in B$ . The velocity  $\mathbf{v}$  is defined as  $\mathbf{v} = \frac{\partial}{\partial t} \chi(\mathbf{X}, t)$ .

Let  $\mathcal{K} = \{K_i : K_i \in \mathcal{S}, i \in I\}$ ,  $I = \{1, 2, \dots, N\}$ ,  $K_i \cap K_j = \emptyset$  for each  $i, j \in I$  and  $\bigcup_{i \in I} K_i = B$ . Thus,  $\mathcal{K} \subset \mathcal{S}$  is a subfamily of subsets of  $B$  which represents a decomposition of the body into subsets  $K_i$ ,  $i \in I$ .

Let us consider a function  $\bar{\chi} : \mathcal{K} \rightarrow R^3$ ,  $\bar{\chi}(K_h) = \chi_h \in R^3$ . Let  $I_h^a \subset I$ ,  $h \in I$  and  $\{\chi_m\}$  be a set of values of the function  $\bar{\chi}$  for  $m \in I_h^a$ . We can define the set  $\Phi_a = \{a_h : a_h : \{\chi_m\} \rightarrow R^p, m \in I_h^a, p \in N\}$ . Then, we introduce a function  $a : \mathcal{K} \rightarrow \Phi_a$ ,  $a(K_h) = a_h$ .

The function  $\bar{\chi}$  assigns a set of discrete values of the field  $\chi_h$ ,  $h \in I$  to the body  $B$  with the help of the family  $\mathcal{K}$ . Similarly, the function  $a$  assigns a set of discrete values of the field  $a_h$ ,  $h \in I$ . However,  $a_h$  depends on the finite set of values  $\chi_m$ ,  $m \in I_h^a$ . The definition of the finite set is introduced with the help of a set of indices  $I_h^a$ . This set in turn, contains numbers of elements of  $\mathcal{K}$  which have influence on the value of  $a_h$ . Usually, it will be some neighbourhood sets  $K_i$  for  $K_h$ . Thus, the functions  $\bar{\chi}$  and  $a$  together can express nonlocal properties of  $\chi_h$ .

Let  $\bar{V}_D = \{\{\bar{\chi}, a\} : \{\chi_h, a_h\}, h \in I\}$ . Let us define the space  $V_\kappa$  of displacement functions  $\chi_\kappa$  of the body  $B$  with respect to a configuration  $\kappa$  as  $V_\kappa = \{\chi_\kappa : \chi_\kappa = \lambda \circ \kappa^{-1}, \lambda, \kappa \in \mathcal{C}\}$ . Let furthermore,  $\alpha : \bar{V}_D \rightarrow V_\kappa$  be a linear function and  $\chi_\kappa^K = \alpha(\{\chi_h, a_h\})$ .

Let us consider a Cartesian coordinate system. Then,  $\mathbf{X} = (X_1, X_2, X_3)$ . We define a function  $C_\kappa : \mathcal{K} \rightarrow R^3$ ,  $C_\kappa(K_h) = \mathbf{X}_h$ . We assume that in particular cases the function  $a_h$  can be expressed as  $a_h = \{a_{1h}, \dots, a_{Lh}\}$ . In this case we assume that the function  $\alpha$  satisfies also the following conditions

$$\chi_\kappa^K(\mathbf{X}_h) = \chi_h, \quad (a_{ih})_{kl_1 \dots l_m} = \frac{\partial^i (\chi_\kappa^K)_k}{\partial^{i_1} X_{l_1} \dots \partial^{i_m} X_{l_m}}(\mathbf{X}_h),$$

$$i_1 + \dots + i_m = i, \quad i \in \{1, 2, \dots, L\}, \quad k, l_1, \dots, l_m \in I_3 = \{1, 2, 3\}.$$

Then,  $(a_{1h})_{kl} = \frac{\partial (\chi_\kappa^K)_k}{\partial X_l}$  can be interpreted as an approximation of the gradient of deformation and we can consider  $((a_{1h})^{-1})_{kl}$  as well.

**DEFINITION 4.** *The displacement function associated with the family of sets  $\mathcal{K}$  is a function  $\chi_\kappa^K$  of the form  $\chi_\kappa^K = \alpha(\{\chi_h, a_h\})$ .*

The function  $\alpha$  assigns a displacement function field  $\chi_\kappa^K$  to the set of discrete values. The aim of this function is to introduce a continuous field  $\chi$  on the body  $B$ . Thus, the space of such fields  $\text{Im } \alpha \subset V_\kappa$  is finite-dimensional, where  $\text{Im } \phi$  means the image of a function  $\phi$ .

**DEFINITION 5.** *The motion of the body  $B$  associated with the family of sets  $\mathcal{K}$  is a continuous map  $\chi_t : [0, T] \rightarrow \{\chi_\kappa^K\}$ .*

We also introduce a function  $\bar{T}$  on  $\mathcal{K}$ , which will represent temperature, as  $\bar{T} : \mathcal{K} \rightarrow R, \bar{T}(K_h) = T_h$ . Let  $I_h^b \subset I$  and  $\{T_n\}$  be a set of values of the function  $\bar{T}$  for  $n \in I_h^b$ . We define a set  $\Phi_b = \{b_h : \{T_n\} \rightarrow R^q, n \in I_h^b, q \in N\}$ . Similarly as for the function  $a$ , we introduce a function  $b : \mathcal{K} \rightarrow \Phi_b, b(K_h) = b_h$ . Let  $\bar{V}_T = \{\{\bar{T}, b\} : \{\bar{T}, b\} = \{T_h, b_h\}, h \in I\}, V_T = \{T(\mathbf{X}) : \mathbf{X} \in B\}$ . Let us consider a function  $\beta : \bar{V}_T \rightarrow V_T$  which is linear by definition and  $T^\mathcal{K} = \beta(\{T_h, b_h\})$ . We assume also that  $T^\mathcal{K}(\mathbf{X}_h) = T_h$  and  $\frac{\partial T^\mathcal{K}}{\partial X_l}(\mathbf{X}_h) = b_h$ .

**DEFINITION 6.** *The temperature field  $T^\mathcal{K}$  associated with the family  $\mathcal{K}$  is the field obtained with the help of function  $\beta$  as  $T^\mathcal{K} = \beta(\{T_h, b_h\})$ .*

Thus, we have obtained a finite-dimensional space of temperature fields  $\text{Im } \beta \subset V_T$  in the body  $B$ .

Let us consider the functions: the internal energy  $E_t$ , the entropy  $S_t$ , the energy flux  $W_t$ , the power of inertia forces  $P_t$ , the entropy flux  $H_t$ , the energy source  $R_t$ , and the entropy source  $N_t$ . Here  $E_t : \mathcal{K} \rightarrow R, S_t : \mathcal{K} \rightarrow R, W_t : \partial\mathcal{K} \rightarrow R, P_t : \mathcal{K} \rightarrow R, H_t : \partial\mathcal{K} \rightarrow R, R_t : \mathcal{K} \rightarrow R, N_t : \mathcal{K} \rightarrow R$ , where  $\partial\mathcal{K}$  is the family of sets  $K_i \cap \partial B$ . These functions are determined for any time instant, thus they represent some processes. It is also assumed that they are differentiable enough with respect to time.

Neglecting at the moment the detailed representations of these functions, we assume the energy balance equation in the form

$$(3.1) \quad \dot{E}_t(B) - \dot{P}_t(B) + W_t(\partial B) - R_t(B) = 0,$$

where

$$B = \bigcup_i K_i, \quad K_i \in \mathcal{K}, \quad \partial B = \bigcup_j K_j \cap \partial B.$$

The second law of thermodynamics is expressed with the help of the entropy balance equation and takes the form

$$(3.2) \quad \dot{S}_t(B) + H_t(\partial B) - N_t(B) \geq 0.$$

We introduce also the function  $\Psi_t : \mathcal{K} \rightarrow R$  which is interpreted as the free energy.

#### 4. An example of a continuum with finite-dimensional fields

An example of a finite-dimensional continuum presented here is connected with a special choice of the family  $\mathcal{K}$ , functions which appear in (3.1), (3.2), the variables and the form of constitutive equations.

Let  $\mathcal{K} = \{K_i\}, i \in I$  be a division of the body  $B$  into a sum of geometrical complexes  $K_i$  which have a cubicoïd form. Let the coordinate axes  $\{X_1, X_2, X_3\}$

be perpendicular to the faces of cuboids in the undeformed state. We can introduce a discrete field on the set of complexes  $K_i$ . Then, we assign a value of a field to the center of gravity of each  $K_i$ ,  $i \in I$ .

We have introduced discrete fields related to the family  $\mathcal{K}$ . Thus, the following expressions will be helpful in what follows:

$$(4.1) \quad \begin{aligned} D_2(y_m) &= \frac{1}{2\Delta}(y_{m+1} - y_{m-1}), \\ A(y_m) &= \frac{1}{2}(y_{m+1} + y_{m-1}), \\ D_2(y_m z_m) &= D_2(y_m)A(z_m) + D_2(z_m)A(y_m), \end{aligned}$$

where  $\Delta$  is a distance between centers of neighbourhood complexes  $K_m$ . It is assumed that, for simplicity,  $\Delta$  is the same for the whole body. Let  $D_{2i}(y_h) = (1/2\Delta)(y_{h_{i2}} - y_{h_{i1}})$ ,  $i = 1, 2, 3$ , where  $h_{i2}$ ,  $h_{i1}$  stand, respectively, for indices of two neighbourhood complexes for  $K_h$  in the direction  $X_i$ . By analogy, we introduce also  $A_i(y_h) = (1/2)(y_{h_{i2}} + y_{h_{i1}})$ .

Let  $p_h = \{p_{hi}, i \in I_3\}$  be a discrete field assigned to the center of  $K_h$ . By means of the above formulas we can introduce a discrete version of the Gauss theorem which is convenient for our purposes

$$(4.2) \quad \sum_{h \in I} D_{2i}(p_{hi}) \approx \sum_{h \in I} \sum_{s_h \in I_h} p_{s_h i} N_{s_h i},$$

where  $p_{s_h i}$  is the same field  $p_h$  which has been assigned to the center of face  $S_{s_h}$  of the complex  $K_h$ ,  $N_{s_h}$  are components of the unit vector normal to the face  $S_{s_h}$ . Furthermore,  $p_{hi} = J(a_{1h}^{-1})_{ik} \bar{p}_{hk}$  is a connection between vectors dependent on space and material variables.

In general we assume that  $p_{s_h i} = \lambda(p_{hi}, p_{li})$ , where  $h, l$  are indices related to complexes which have common face  $S_{s_h}$ .  $\lambda$  is a function chosen in such a way that the formula (4.2) would be satisfactorily satisfied.

Let us introduce a function  $a_h$  of the form  $a_h = \{D_{21}(\chi_h), D_{22}(\chi_h), D_{23}(\chi_h)\}$ ,  $\chi_h = \{\chi_{hn}\}$ ,  $n \in I_3 = \{1, 2, 3\}$ ,  $h \in I$ . Thus,  $a_h = \{a_{hni}\}$ ,  $n, i \in I_3$ .

We assume the following representations for functions related to the energy balance equation and the second law of thermodynamics:

$$(4.3) \quad E(K_h) = E_h, \quad \dot{E}(K_h) = \dot{\Psi}_h + S_h \dot{T}_h,$$

$$(4.4) \quad \dot{E}(K_h) = \dot{E}_h, \quad \ddot{E}(K_h) = \dot{\Psi}_h + \dot{S}_h \dot{T}_h + S_h \ddot{T}_h,$$

$$(4.5) \quad W(\partial K_h) = \sum_{s_h} q_{s_h i} N_{s_h i} - \sum_{s_h} p_{s_h i} \dot{\chi}_{s_h i},$$

$$(4.6) \quad P(K_h) = -m_h \ddot{\chi}_{hi} \dot{\chi}_{hi} + D_{2m}(i_{hmn} \ddot{a}_{hkn}) \dot{\chi}_{hk},$$

$$(4.7) \quad R(K_h) = R_{eh} + f_{hi} \dot{\chi}_{hi},$$

$$(4.8) \quad S(K_h) = S_h, \quad \dot{S}(K_h) = \dot{S}_h,$$

$$(4.9) \quad H(\partial K_h) = \sum_{s_h} \frac{1}{T_{s_h}} q_{s_h i} N_{s_h i},$$

$$(4.10) \quad N(K_h) = \frac{1}{T_h} R_{eh},$$

where  $m_h$  is a mass assigned to the complex  $K_h$ ,  $i_{hnm}$  is an inertia tensor related to  $K_h$ .  $f_h = \{f_{hi}\}$  and  $R_{eh}$  are a force and a heat source related to  $K_h$ .  $q_{s_h} = \{q_{s_h i}\}$  and  $p_{s_h} = \{p_{s_h i}\}$  are a heat flux and a surface force related to the surface  $S_{s_h}$ . Let us note that the expression (4.6) is obtained with the help of definition of the kinetic energy  $E_k = \int \rho \dot{x}_i \dot{x}_i dV$ .

We assume that the energy balance equation is fulfilled for each  $K_h \in \mathcal{K}$  separately. Then, the energy balance equation takes the form

$$(4.11) \quad \dot{\Psi}_h + \dot{S}_h T_h + S_h \dot{T}_h + m_h \ddot{\chi}_{hi} \dot{\chi}_{hi} - D_{2m}(i_{hnmn} \ddot{a}_{hkn}) \dot{\chi}_{hk} - R_{eh} + \sum_{s_h} q_{s_h i} N_{s_h i} - f_{hi} \dot{\chi}_{hi} - \sum_{s_h} p_{s_h i} \dot{\chi}_{s_h i} = 0.$$

The term  $\dot{\Psi}_h$  can be expressed as

$$(4.12) \quad \begin{aligned} \dot{\Psi}_h &= \frac{\partial \Psi_h}{\partial a_{hni}} \dot{a}_{hni} + \frac{\partial \Psi_h}{\partial T_h} \dot{T}_h = \frac{\partial \Psi_h}{\partial a_{hni}} D_{2i}(\dot{\chi}_{hn}) + \frac{\partial \Psi_h}{\partial T_h} \dot{T}_h \\ &= D_{2i} \left( \frac{\partial \Psi_h}{\partial a_{hni}} \dot{\chi}_{hn} \right) - D_{2i} \left( \frac{\partial \Psi_h}{\partial a_{hni}} \right) A_i(\dot{\chi}_{hn}) + \frac{\partial \Psi_h}{\partial T_h} \dot{T}_h, \end{aligned}$$

where the properties given by the formula (4.1) have been used. The summation convention does not concern the index  $i$  in  $A_i$ . Furthermore, we assume that  $A_i(\dot{\chi}_{hn}) \approx \dot{\chi}_{hn}$ .

With the help of (4.12) and the discrete Gauss theorem (4.2), we can transform (4.11) into the form

$$(4.13) \quad \begin{aligned} \left[ -D_{2i} \left( \frac{\partial \Psi_h}{\partial a_{hni}} \right) - f_{hn} + m_h \ddot{\chi}_{hn} - D_{2m}(i_{hmp} \ddot{a}_{hnp}) \right] \dot{\chi}_{hn} \\ + \left( \frac{\partial \Psi_h}{\partial T_h} + S_h \right) \dot{T}_h + \dot{S}_h T_h \\ + D_{2i}(q_{hi}) - R_{eh} + \sum_{s_h} \left( \frac{\partial \Psi_{s_h}}{\partial a_{s_h ni}} N_{s_h i} - p_{s_h n} \right) \dot{\chi}_{s_h n} = 0. \end{aligned}$$

Then assuming that an arbitrary time process  $\dot{\chi}_h$  is admissible, we obtain from (4.13) the following system of equations:

$$(4.14) \quad -D_{2i} \left( \frac{\partial \Psi_h}{\partial a_{hni}} \right) - f_{hn} + m_h \ddot{\chi}_{hn} - D_{2m}(i_{hmp} \ddot{a}_{hnp}) = 0,$$

$$(4.15) \quad S_h = -\frac{\partial \Psi_h}{\partial T_h},$$

$$(4.16) \quad \dot{S}_h T_h + D_{2i}(q_{hi}) - R_{eh} = 0$$

and

$$(4.17) \quad \frac{\partial \Psi_{s_h}}{\partial a_{s_h ni}} N_{s_h i} - p_{s_h n} = 0.$$

The Clausius – Duhem inequality can be expressed with the help of (3.2), (4.8)–(4.10) as

$$(4.18) \quad \dot{S}_h - R_{eh} \frac{1}{T_h} + D_{2i} \left( q_{hi} \frac{1}{T_h} \right) \geq 0.$$

Taking into account dissipative processes and introducing internal state variables  $\xi_h$  we can generalize Eqs. (4.14)–(4.16) to the form

$$(4.19) \quad -D_{2i} \left( \frac{\partial \Psi_h}{\partial a_{hni}} + t_{hni}^d \right) - f_{hn} + m_h \ddot{\chi}_{hn} - D_{2m}(i_{hmp} \ddot{a}_{hnp}) = 0,$$

$$(4.20) \quad S_h = -\frac{\partial \Psi_h}{\partial T_h} + S_h^d,$$

$$(4.21) \quad \dot{S}_h T_h + D_{2i}(\bar{q}_{hi}) - R_{eh} + S_h^d \dot{T}_h - t_{hni}^d \dot{a}_{hni} + \frac{\partial \Psi_h}{\partial \xi_h} \dot{\xi}_h = 0.$$

The constitutive equations should be assumed for the functions  $r_h = \{\Psi_h, S_h, \mathbf{t}_h, \mathbf{q}_h\}$  and  $\mathbf{t}_h = (\partial \Psi_h / \partial a_h) + \mathbf{t}_h^d$ . The constitutive equations will then depend on the variables  $\mathbf{h}_h = \{\chi_h, a_h, T_h, b_h\}$  and  $\xi_h$ . We assume that the equations take the form

$$(4.22) \quad \Psi_h = \Psi_h(\mathbf{C}_\psi, \mathbf{h}_h, \xi_h),$$

$$(4.23) \quad S_h = S_h(\mathbf{C}_s, \mathbf{h}_h, \xi_h),$$

$$(4.24) \quad \mathbf{t}_h = \mathbf{t}_h(\mathbf{C}_t, \mathbf{h}_h, \xi_h),$$

$$(4.25) \quad \mathbf{q}_h = \mathbf{q}_h(\mathbf{C}_q, \mathbf{h}_h, \xi_h),$$

$$(4.26) \quad \dot{\xi}_h = A_h(\mathbf{C}_A, \mathbf{h}_h, \xi_h),$$

where  $\mathcal{C} = \{\mathbf{C} : \mathbf{C} = \{\mathbf{C}_\psi, \mathbf{C}_s, \mathbf{C}_t, \mathbf{C}_q, \mathbf{C}_A\}\}$  are constants which define these constitutive equations.

The generalization in our formulation rests on the fact that our theory is formulated for a given subfamily  $\mathcal{K}$ . In the particular case when  $\mathcal{K} = \mathcal{S}$  we obtain the classical continuum theory.

It is possible to carry out two different procedures for obtaining a continuous field from the discrete one given on the family  $\mathcal{K}$ .

The first procedure, called further the A-procedure, consists in the interpolation of the sets of the discrete values. It can be performed with the help of maps  $\alpha, \beta$  introduced above, which replace the discrete fields  $\{\chi_h, a_h, T_h, b_h\}$  by some continuous ones.

We should also introduce some additional maps which will be useful for interpolation of the remaining variables which appear in our description. Thus, let us introduce the following spaces

$$\begin{aligned}\bar{V}_\varrho &= \{m : m = \{m_h\}, h \in I\}, & V_\varrho &= \{\varrho(\mathbf{X}) : \mathbf{X} \in B\}, \\ \bar{V}_r &= \{r : r = \{\Psi_h, S_h, \mathbf{t}_h, \mathbf{q}_h\}, h \in I\}, \\ V_r &= \{r(\mathbf{X}) : r(\mathbf{X}) = \{\psi(\mathbf{X}), s(\mathbf{X}), \mathbf{t}(\mathbf{X}), \mathbf{q}(\mathbf{X})\}, \mathbf{X} \in B\}, \\ \bar{V}_\xi &= \{\xi : \xi = \{\xi_h\}, h \in I\}, & V_\xi &= \{\xi(\mathbf{X}) : \mathbf{X} \in B\}, \\ \bar{V}_f &= \{\{\mathbf{f}, R_e, \mathbf{p}\} : \{\mathbf{f}_h, R_{eh}, \mathbf{p}_h\}, h \in I\}, \\ V_f &= \{\{\mathbf{f}(\mathbf{X}), r_e(\mathbf{X}), \mathbf{p}(\mathbf{X})\} : \mathbf{X} \in B\}.\end{aligned}$$

Let us consider the following maps which act on the introduced spaces  $\rho : \bar{V}_\varrho \rightarrow V_\varrho, \mu : \bar{V}_r \rightarrow V_r, \mu_\xi : \bar{V}_\xi \rightarrow V_\xi, \nu : \bar{V}_f \rightarrow V_f$ . The introduced maps are linear by assumption and with the help of these maps, discrete fields are replaced by continuous ones. However, in order to obtain satisfactory approximation, the continuous fields obtained above should satisfactorily fulfill the following conditions

$$\begin{aligned}m_h &= \int_{K_h} \varrho dV, & \Psi_h &= \int_{K_h} \varrho \psi dV, & S_h &= \int_{K_h} \varrho s dV, \\ D_{2i}(t_{hni}) &= \int_{K_h} t_{ij,i} dV = \int_{\partial K_h} t_{nk} N_k dA, \\ (4.27) \quad D_{2i}(q_{hi}) &= \int_{K_h} q_{i,i} dV = \int_{\partial K_h} q_k N_k dA, \\ f_h &= \int_{K_h} f dV, & R_{eh} &= \int_{K_h} r_e dV, & p_{s_{hi}} &= \int_{\partial K_h} p_i dA,\end{aligned}$$

where  $q_{hk} = J(a_h^{-1})_{kl} \bar{q}_{hl}$ ,  $t_{hni} = J(a_h^{-1})_{il} \bar{t}_{hnl}$  are quantities determined with respect to the reference configuration. Finally, we obtain continuous finite-dimensional fields on the continuum with the help of the A-procedure.

The second procedure, called further the L-procedure, is connected with a limit transition. Let  $B = \bigcup_{i \in I} K_i$ ,  $K_i \in \mathcal{K}$  be a division of the body  $B$ . Let us consider a sequence of  $\{\mathcal{K}_m\}$ ,  $m = 1, 2, 3, \dots$  of such divisions and  $\mathcal{K}_1 = \mathcal{K}$ . Thus, for each  $m$ ,  $B = \bigcup_{i \in I_m} K_{mi}$ ,  $K_{mi} \in \mathcal{K}_m$ . Let us assume that constants  $\mathcal{C}$  are already determined for the family  $\mathcal{K}$ .

For each  $\mathcal{K}_m$  we introduce the sets of indices  $I_{mh}^a, I_{mh}^b$ . Consequently, we have sequences  $\{I_m\}, \{\mathcal{K}_m\}, \{I_{mh}^a\}, \{I_{mh}^b\}$ ,  $h \in I_m$ ,  $m = 1, 2, 3, \dots$ . With the help of these sequences we can carry out a limit L for the equations (4.18)–(4.21) and the constitutive equations (4.22)–(4.26). However, in order to make this operation realizable, let us assume that variables which appear in (4.18)–(4.21) have representations in the form given by (4.27). We assume also that during this operation  $\lim_{m \rightarrow \infty} \delta(K_{mi}) = 0$ , where  $\delta$  is a diameter of the set  $K_{mi}$ . It is assumed that the constants related to the constitutive equations do not undergo any change.

During this limit transition  $\mathbf{h}_h \rightarrow \mathbf{h}$  appears, where  $\mathbf{h} = \{\chi_i, (\partial\chi_i/\partial X_n), T, (\partial T/\partial X_n)\}$  in the considered case. The final form of this limit depends on the previously assumed functions  $a_h, b_h$ . In particular, limits connected with these functions can lead also to higher gradients of  $\chi$  and  $T$ .

The limit form of Eqs. (4.18)–(4.21) can be obtained by dividing them first by volume of  $K_h$  marked by  $V_h$ . Next, during the limit transition we obtain  $i_{hmn} \rightarrow 0$ ,  $(m_h/V_h) \rightarrow \rho$ ,  $D_{2i}(q_{hi}) \rightarrow \text{Div } \mathbf{q}$ ,  $D_{2i}(t_{hni}) \rightarrow \text{Div } \mathbf{t}$ . Finally, we obtain the well known expressions for the local forms of balance equations and the Clausius–Duhem inequality [16].

Let us note that the L procedure leads to the infinite-dimensional fields on the continuum. However, the starting point of this procedure has decisive meaning. Namely, the first element  $\mathcal{K}_1$  of the sequence  $\{\mathcal{K}_m\}$  is assumed. This element influences the final form of the constitutive equations.

The first element of the sequence  $\{\mathcal{K}_m\}$  will be related to the volume of averaging. This problem will be discussed in the next section. The volume of averaging is especially connected with the form of the constitutive equations.

## 5. Volume of averaging related to the continuum model

The primary motivation for discussing the continuum theory suggested in the paper is to create a possibility of determining the equations of the continuum (for instance (4.18)–(4.26)) from a more elementary level. This elementary level can be connected with a discrete system of material points or with a continuum which is much more complicated.

Let us assume that on the more elementary level, the behaviour of a body is described by a dynamical system. Let  $\mathbf{d}$  be a variable of this system,  $V = \{\mathbf{d}\}$  is a set of admissible values of this variable, and let  $\varphi : [0, T] \rightarrow V$  be an evolution function of the dynamical system.

On the other hand, let  $\bar{\mathbf{d}} = \{\{\chi_h, a_h, \dot{\chi}_h, \dot{a}_h, T_h, b_h, \xi_h\} : h \in I\}$ ,  $\bar{V} = \{\bar{\mathbf{d}}\}$ ,  $\bar{\mathbf{f}} = \{\mathbf{f}_h, R_{eh}, \mathbf{p}_h\}$  and let  $\bar{\varphi} : [0, T] \rightarrow \bar{V}$  be an evolution function which is determined by equations (4.18)–(4.26).

At this moment we can return to notations from the Sec. 2 where we have defined two dynamical systems and a dimensional reduction method. The *SDS* introduced in Sec. 2 can be now identified with  $SDS(\mathbf{C}) = \{\mathcal{K}, \bar{\mathbf{d}}, \bar{\mathbf{f}}, \{BE, r(\mathbf{C})\}\}$ , where  $\mathcal{K}$  is the previously discussed family of subsets of the body and influences the option of variables  $\bar{\mathbf{d}}$  and forces  $\bar{\mathbf{f}}$ . *BE* means the set of balance equations (4.18)–(4.21) and  $r(\mathbf{C})$  represents the parametrized family of constitutive equations (4.22)–(4.26). The pair  $\{BE, r(\mathbf{C})\}$  corresponds to  $\frac{\partial \bar{\mathbf{L}}}{\partial \bar{\mathbf{d}}}(\mathbf{C})$  which describes evolution of *SDS*. The dimensional reduction method has the same form as previously  $DR = \{SDS, \{\pi\}, app\}$ .

In this section we discuss the continuum dynamical system *CDS* which should be obtained as a result of the dimensional reduction. This system can be characterized by  $CDS(\mathbf{C}) = SDS(\mathbf{C})$ . Thus, we can choose an elementary dynamical system *EDS* which can be a discrete or a continuous one but more complicated than  $SDS(\mathbf{C})$ . Then,  $\{EDS, DR\}$  creates an  $RDS(\bar{\mathbf{C}}) = CDS(\bar{\mathbf{C}})$ .

Now, we are able to define a volume of averaging related to the continuum model. Let  $\mathcal{K}$  be a family of sets  $K_i$  and  $B = \bigcup_i K_i$ ,  $K_i \cap K_j = \emptyset$ . Let  $\varphi$  be a dynamical system whereby the discrete field related to  $\mathcal{K}$  is determined. Next, let the L-procedure or the A-procedure be applied in order to attain the continuum model. Then, the average of values  $\mu(K_i)$  represents a volume of averaging for the continuum model obtained, where  $\mu$  is the volume measure.

In a natural way, we can generalize this approach to a multiscale description. Then,  $(CDS)_n = \{(CDS)_{n-1}, (DR)_{n-1}\}$ , where  $(CDS)_{n-1}$  represents the more elementary dynamical system and  $(DR)_{n-1}$  means a dimensional reduction which is then applied.

## 6. Volume of averaging connected with the martensitic transformation

The martensitic transformation, especially the one related to the shape memory alloys, exhibits a complicated structure and moving interfaces. As it has been discussed previously, different scales should be taken into account in a mechanical modelling of this transformation. Let us try to discuss what these scales should mean.

In a small scale, we can observe the single martensite variants. They can create fine twins or selfaccomodating groups. In a larger scale, such structures usually create a complicated composition. However, in a large scale a coalescence of martensite variants can appear, and only one martensite variant is also possible.

Let us consider, for instance, the CuAl alloy. We observe twenty four martensite variants which create six selfaccomodating groups [22]. In Fig. 1, the struc-

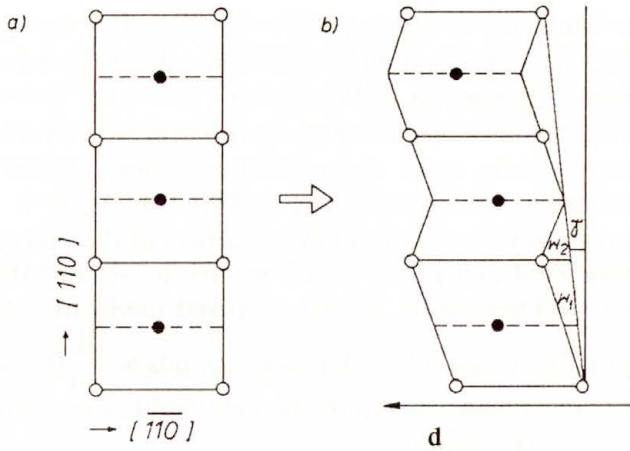


FIG. 1. Structure of austenite and martensite in CuAl alloy.

ture of austenite and martensite unit for CuAl alloy is shown. They have nine atomic layers which characterize this unit and define fully this martensite variant. The austenite structure and stress-induced martensite variants for CuAlNi alloy is shown in Fig. 2, where eighteen atom layers define the martensite unit [23]. Consequently, a linear dimension which characterizes the small volume of averaging in the considered cases should exceed the dimension of the martensite unit and should be between  $10^{-9}$  m and  $10^{-8}$  m. On this level of description, single martensite variants and single interfaces will be distinguished.

In Fig. 3 the selfaccomodating group is shown for CuAl alloy. In this structure different kinds of single martensite variants are composed. Another structure related to the fine twinning of martensite for CuAlNi alloy is shown in Fig. 4. Compositions of this kind of structures bring a considerable nonhomogeneity. Therefore, the scale of averaging for theories which do not distinguish different martensite variants should be connected with such a volume in which the composition of martensities can be approximated by a homogeneous structure. Taking into account observable structures [24, 25], one should assume that the linear dimension related to the volume of averaging is between  $10^{-6}$  m and  $10^{-4}$  m for models with the larger scale.

In papers [12, 13] a continuum model related to the small volume of averaging is introduced. As a consequence of this kind of averaging shuffles are taken into considerations. They are introduced with the help of the relative displacement vectors  $\mathbf{w}_\lambda$  which are shown in Fig. 1. The role of shuffles is valid on this level of description. They take place in determining the martensite variants. They have also some influence on the kind of internal rotation of the martensite variant towards the habit plane. Thus, the dynamical system related to this model has variable  $\mathbf{d} = \{\mathbf{x}, \dot{\mathbf{x}}, \mathbf{w}_\lambda, \dot{\mathbf{w}}_\lambda, T, \alpha, \beta, \delta\}$ , where  $\alpha, \beta, \delta$  are internal variables related to dissipation connected with shuffles, related to jumps of the creating

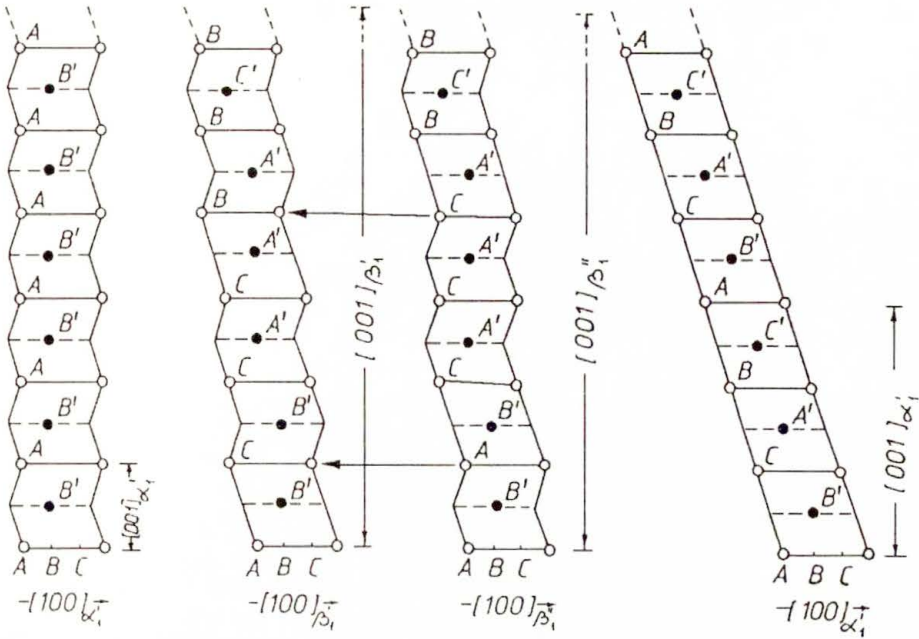


FIG. 2. Structure of stress-induced martensite in CuAlNi alloy.

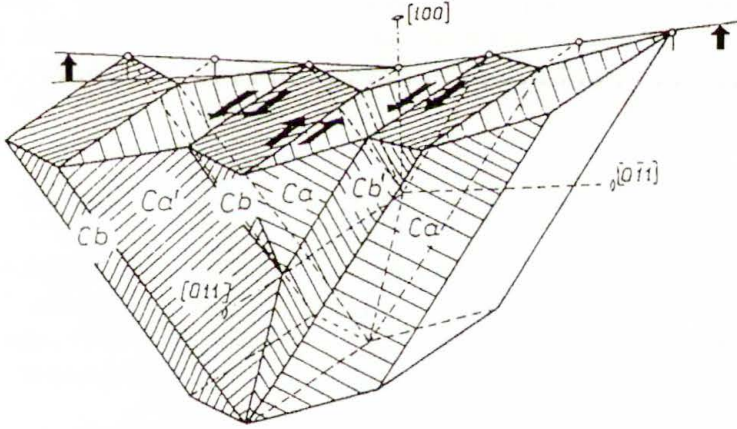


FIG. 3. The selfaccomodating group of martensite variants in CuAl alloy.

martensitic structure over an anenergetic barrier and stabilization of the martensite, respectively.

On the other hand, we can introduce variable  $\bar{d}$  given in previous section, where  $\xi$  can be in particular connected with the mass of martensite in the whole structure. Then, the model of larger scale of averaging is considered. Such models have been discussed in literature [20, 21].

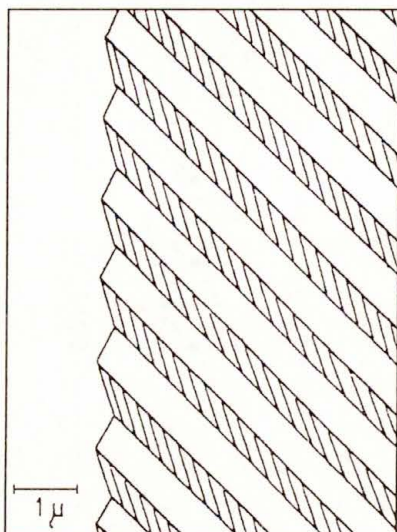


FIG. 4. The fine twinning which appears in CuAlNi alloy.

With the help of the procedure given in Sec.4, a connection between these two models could be determined. However, such procedure will certainly be not simple. It requires, first, precise identification of the constants and functions related to material properties for the model with the small scale. Then, another difficult problem appears. This is connected with a satisfactory form of approximation given by (2.4), a form of dependence of functions in (4.22)–(4.26) on  $\mathbf{C}$  and choosing an appropriate kind of internal variables  $\xi$ .

## 7. Final remarks

The suggested formulation of continuum mechanics makes it possible to obtain a continuum model as a dimensional reduction of a discrete system. It seems to be convenient to consider a discrete dynamical system as a physical basis for continuum model. Furthermore, multiscale approach for continuum description can also be introduced in this way.

The main stress has been laid on the description of dynamics. It is displayed by the introduced method of dynamical reduction by means of maps  $\pi_T$ ,  $\pi_{fT}$ , and by introduction of internal state variables in dimensionally reduced systems. Such an approach is suggested by the example of a moving microstructure in case of the martensitic transformation. Then, it is difficult to use, for instance, the homogenization method since we do not know the dynamical laws of microstructure evolution.

Furthermore, it is hoped that the suggested procedure will be convenient in determination of the constants and functions connected with the material consid-

ered. It is valid especially for small scale of the averaging models. Then, we have not too many possibilities to obtain such constants and functions experimentally.

## References

1. P. PERZYNA, *Thermodynamics of inelastic materials*, PWN, Warszawa 1978.
2. T. MURA, *Micromechanics of defects in solids*, Martinus Nijhoff Publishers, 1982.
3. S. YIP, *Atomistic simulations in material science*, [in:] *Molecular Dynamics Simulations of Statistical-Mechanical Systems*, G. CICCOTTI, W.G. HOOVER [Eds.], 1986.
4. O. PENROSE, *Foundations of statistical mechanics*, Rep. Prog. Phys., **42**, 1937, 1979.
5. R. BALESCU, *Equilibrium and nonequilibrium statistical mechanics*, John Wiley & Sons, 1975.
6. J.A. SANDERS and F. VERHULST, *Averaging methods in nonlinear dynamical systems*, Springer Verlag, New York 1985.
7. A.I. MURDOCH, *On the relationship between balance relations for generalised continua and molecular behaviour*, Int. J. Engng. Sci., **25**, 883–914, 1987.
8. R.S. RIVLIN, *The passage from a particle system to a continuum model*, Arch. Mech., **28**, 549–561, 1976.
9. W. LUDWIG, *Invariance conditions in the transmission from discrete lattice models to the continuum limit*, Arch. Mech., **28**, 501–515, 1976.
10. J.A. KRUMHANSL, *Generalized continuum field representation for lattice vibrations*, p. 627 [in:] *Lattice Dynamics*, R.F. WALLIS [Ed.], Pergamon Press, 1965.
11. D. ROGULA, *Quasicontinuum theory of crystals*, Arch. Mech., **28**, 563–569, 1976.
12. J. KACZMAREK, *A thermodynamical model of solids undergoing martensitic phase transformations with shuffles*, Arch. Mech., **45**, 167–181, 1993.
13. J. KACZMAREK, *A model of the free energy for materials which undergo martensitic phase transformations with shuffles*, Int. J. Engng. Sci., **32**, 369–384, 1994.
14. J. KACZMAREK, *Multiscale treatment of the martensitic transformation in a single crystal*, [in:] Proc. of IUTAM Symposium on Micromechanics of Plasticity and Damage of Multiphase Materials, Sevres, France 1995.
15. C. TRUESDELL, *A first course in rational mechanics*, Baltimore, Maryland 1972.
16. C. TRUESDELL and W. NOLL, *The nonlinear field theories of mechanics*, [in:] *Handbuch der Physik*, S. FLÜGGE [Ed.], III/3, 1–602, Springer, Berlin 1965.
17. M.E. GURTIN and W.O. WILLIAMS, *An axiomatic foundations for continuum thermodynamics*, Arch. Rat. Mech. Anal., **26**, 83–117, 1967.
18. W.O. WILLIAMS, *Axioms for work and energy in general continua*, I, II, **42**, 2, 93–114, 1971; **49**, 225–240, 1972.
19. W. NOLL, *Lectures on the foundations of continuum mechanics and thermodynamics*, Arch. Rat. Mech. Anal., **52**, 1, 62–69, 1973.
20. B. RANIECKI and C. LEXCELLENT,  *$R_L$ -model for pseudoelasticity and their specification for some shape memory solids*, Eur. J. Mech. A/Solids, **13**, 1, 21–50, 1994.
21. T. INOUE and ZHIGANG WANG, *Coupling between stress, temperature, and metallic structures during processes involving phase transformations*, Mat. Sci. Techn., **1**, 845–850, 1985.
22. Z. NISHIJAMA and S. KAJIWARA, *Electron microscope study of the crystal structure of the martensite in a copper-aluminium alloy*, Jap. J. App. Phys., **8**, 2, 1963.
23. K. OTSUKA, H. SAKAMOTO and K. SHIMIZU, *Successive stress-induced martensitic transformation and associated transformation pseudoelasticity in CuAlNi alloys*, Acta Metall., **27**, 585, 1979.
24. K. SHIMIZU and K. OTSUKA, *Optical and electron microscope observation of transformation and deformation characteristics in CuAlNi memory alloys*, [in:] *Shape Memory Effects in Alloys*, J. PERKINS [Ed.], 1975.

25. P.R. SWANN and H. WARLIMONT, *The electron-metallography and crystallography of copper-aluminium martensities*, *Acta Met.*, **11**, 511, 1963.
26. D.ter HAAR, *Elements of Hamiltonian mechanics*, Oxford 1971.
27. A. GOŁĘBIEWSKI, *Elements of mechanics and quantum chemistry*, PWN, Warszawa 1982.
28. M.W. HIRSCH and S. SMALE, *Differential equations, dynamical systems and linear algebra*, Academic Press, New York, London 1974.

POLISH ACADEMY OF SCIENCES  
INSTITUTE OF FLUID-FLOW MACHINERY  
ul. J. Fiszera 14, 80-952 Gdańsk, Poland.

*Received May 22, 1996.*

# Uniqueness in nonlinear theory of porous elastic materials

R. QUINTANILLA (BARCELONA)

THIS NOTE is concerned with static deformations in a nonlinear theory of elastic materials with voids. First we extend some conservation laws to the nonlinear theory. A uniqueness result is presented under a condition related to the quasi-convexity assumptions.

## 1. Introduction

IN [1], KNOPS AND STUART proved the uniqueness of the solutions to certain displacement boundary-value problems in the context of the nonlinear theory of homogeneous hyperelasticity for a body occupying a star-shaped bounded region. Recently, this result has been extended to the theory of interacting continua [22]. In this paper we extend some of these results to the theory of nonlinear elastic materials with voids.

The theory of elastic materials with voids is a recent extension of the classical theory of elasticity. The nonlinear theory has been established by NUNZIATO and COWIN [2]. In this theory the bulk density is the product of two scalar fields, the matrix material density and the volume fraction field. An intensive work on this kind of materials is developing currently [3–9]. An extensive review on elastic materials with voids has been presented in [10].

Existence and uniqueness results in the statical linear theory of an elastic material with voids have been presented [10, 11]; meanwhile many other theorems have been presented for the dynamic case [12–14], and in [15] for the dynamical nonlinear problem. We remark that in [10] CIARLETTA and IEŞAN have obtained a uniqueness and existence theorem for the static equations of porous elastic materials, but the authors noted that their results apply the one-dimensional case only.

We consider the homogeneous deformation  $(\mathbf{x}, \nu) : \mathbf{X} \rightarrow (\mathbf{M}\mathbf{X} + \mathbf{b}, \nu_0)$ , where  $\mathbf{M}$  is a fixed regular square matrix such that  $\det(\mathbf{M}) > 0$ ,  $\mathbf{b}$  is a fixed vector,  $0 < \nu_0 \leq 1$  is a constant number and  $\mathbf{X}$  represents the material point. We suppose that this deformation is a solution to the equilibrium problem with boundary conditions  $(\mathbf{x}, \nu) : \mathbf{X} \rightarrow (\mathbf{M}\mathbf{X} + \mathbf{b}, \nu_0)$ . For star-shaped elastic materials we will prove, under suitable assumptions concerning the energy function  $\Sigma$ , that there is no other solution satisfying these boundary conditions.

The method follows the ideas of [1]. We first extend a conservation law established by GREEN [16] in the case of hyperelasticity.

Following the method used in [1], we impose start with a basic assumption on the energy to obtain our result. We suppose that the energy satisfies a condition

related with the quasi-convexity, an assumption introduced by MORREY [17] and employed in the classical works of BALL [18–20]. Nevertheless, in this paper we are not concerned with the problem of existence of solutions.

In Sec. 2 we state the basic equations and the assumptions. We also extend some conservation laws to the nonlinear theory of elastic materials with voids. The uniqueness result is presented in Sec. 3.

## 2. Preliminaries

We consider a body which occupies a bounded regular region  $B$  of the Euclidean  $n$ -dimensional space with the boundary surface  $\partial B$ . We assume that  $B$  is star-shaped and that  $\partial B$  is sufficiently regular to ensure the validity of the usual laws of transformation of surface integrals.

Throughout this paper we employ the usual summation and differentiation conventions: subscripts preceded by a comma denote partial differentiation with respect to the corresponding Cartesian coordinate;  $\nabla$  is the gradient operator with respect to the position  $\mathbf{X}$ . We let  $N_A$  be the components of the outward unit normal to  $\partial B$  and denote the scalar product of two tensors by an interposed dot. By  $\mathbf{a} \otimes \mathbf{b}$  we denote the tensor product of the vectors  $\mathbf{a}$  and  $\mathbf{b}$ .

We assume that  $B$  is occupied by an elastic material with voids. A deformation in  $B$  is described by the spatial position field  $\mathbf{x}$  and the volume fraction field  $\nu$ . The deformations determine the deformation gradient  $\mathbf{F} = \nabla \mathbf{x}$ , and the gradient of the volume fraction  $\mathbf{G} = \nabla \nu$ . By  $\mathcal{M}^+$  we denote the set of all real square matrices  $\mathbf{F}$  of order  $n$  such that  $\det(\mathbf{F}) > 0$ . As usual, we suppose that  $\mathbf{F} \in \mathcal{M}^+$  and  $0 < \nu \leq 1$  for all deformations.

We also assume that the material possesses internal energy  $\Sigma$  per unit initial volume. We denote by  $\mathbf{T}$  the first Piola–Kirchhoff stress tensor,  $\mathbf{S}$  the equilibrated stress and by  $g$  the equilibrated body force per unit volume. In what follows, occasionally it will be convenient to write various expressions in component form and to represent the vector and tensor fields by their components referred to the considered system of Cartesian axes. Thus, the components of the deformation  $(\mathbf{x}, \nu)$  will be denoted by  $(x_i, \nu)$ , while the components of the deformation gradient fields  $\mathbf{F}$  and  $\mathbf{G}$  will be denoted by  $F_{iA}$  and  $G_A$ , respectively.

A deformation  $(\mathbf{x}, \nu)$  in  $B$ , defined for all  $\mathbf{X}$  in  $B$ , is a smooth equilibrium solution provided  $x_i, \nu \in C^2(B, \mathbb{R}^n) \cap C^1(\bar{B}, \mathbb{R}^n)$  and the equilibrium equations (see, e.g. [10])

$$(1) \quad \begin{aligned} T_{Ai,A} &= 0, \\ S_{A,A} + g &= 0, \end{aligned}$$

are satisfied.

The material at the point  $\mathbf{X}$  is characterized by the constitutive relations

$$(2) \quad \begin{aligned} \Sigma &= \Sigma^*(\mathbf{F}, \mathbf{G}, \nu), & \mathbf{T} &= \mathbf{T}^*(\mathbf{F}, \mathbf{G}, \nu), \\ \mathbf{S} &= \mathbf{S}^*(\mathbf{F}, \mathbf{G}, \nu), & g &= g^*(\mathbf{F}, \mathbf{G}, \nu), \end{aligned}$$

where  $\Sigma^*$ ,  $\mathbf{T}^*$ ,  $\mathbf{S}^*$ ,  $g^*$  are smooth functions.

We suppose that the Piola - Kirchhoff stress tensor, the equilibrated stress and equilibrated body force are related to the energy in the following manner:

$$(3) \quad \mathbf{T} = \left( \frac{\partial \Sigma}{\partial \mathbf{F}} \right)^\top, \quad \mathbf{S} = \left( \frac{\partial \Sigma}{\partial \mathbf{G}} \right)^\top, \quad g = - \frac{\partial \Sigma}{\partial \nu}.$$

We recall that equalities (3) are used in the analysis of elastic materials with voids in the absence of dissipation (see [10]).

Let us assume that  $\mathbf{M}$  is a fixed regular square matrix in  $\mathcal{M}^+$ ,  $\mathbf{b}$  is a fixed vector and  $0 < \nu_0 \leq 1$  is a constant number. In this paper we suppose that the motion

$$(4) \quad \mathbf{x} = \mathbf{M}\mathbf{X} + \mathbf{b}, \quad \nu = \nu_0 \quad \text{in } B,$$

is a solution of the problem determined by the equilibrium equations (1) and the boundary conditions

$$(5) \quad \mathbf{x} = \mathbf{M}\mathbf{X} + \mathbf{b}, \quad \nu = \nu_0 \quad \text{in } \partial B.$$

It is clear that the equality

$$(6) \quad \frac{\partial \Sigma}{\partial \nu}(\mathbf{M}, 0, \nu_0) = 0,$$

is the necessary and sufficient condition for the energy function  $\Sigma$  to ensure that the deformation (4) is a solution to the problem determined by the equilibrium equations (1) and the boundary conditions (5).

Let us also note for later use that the divergence theorem applied to the equilibrium equations gives

$$(7) \quad \int_{\partial B} \mathbf{T} \cdot \mathbf{N} ds = 0, \quad \text{and} \quad \int_{\partial B} \mathbf{S} \cdot \mathbf{N} ds + \int_B g dv = 0.$$

In order to obtain the uniqueness result, we will introduce some assumptions on the energy function. We suppose that

(i)  $\Sigma$  is rank-one convex at  $(\mathbf{M}, 0, \nu_0)$ , i.e. the following inequality holds

$$(8) \quad \Sigma(\mathbf{M} + \mathbf{a} \otimes \mathbf{d}, \tilde{\mathbf{a}}, \nu_0) \geq \Sigma(\mathbf{M}, 0, \nu_0) + \frac{\partial \Sigma}{\partial \mathbf{F}}(\mathbf{M}, 0, \nu_0) \mathbf{a} \otimes \mathbf{d} + \frac{\partial \Sigma}{\partial \mathbf{G}}(\mathbf{M}, 0, \nu_0) \tilde{\mathbf{a}},$$

for all  $\mathbf{a}$ ,  $\mathbf{d}$ ,  $\tilde{\mathbf{a}}$  in an  $n$ -dimensional Euclidean space, and

(ii)  $\Sigma$  satisfies the inequality

$$(9) \quad \int_D \left[ \Sigma(\mathbf{M} + \nabla\phi(\mathbf{X}), \nabla\psi(\mathbf{X}), \nu_0 + \eta(\mathbf{X})) - \frac{1}{n} \frac{\partial\Sigma}{\partial\nu}(\mathbf{M} + \nabla\phi(\mathbf{X}), \nabla\psi(\mathbf{X}), \nu_0 + \eta(\mathbf{X})) \cdot \eta(\mathbf{X}) \right] dv \geq \Sigma(\mathbf{M}, 0, \nu_0) \text{ volume } (D).$$

for all non-empty bounded subsets  $D$  and for all Lipschitz-continuous vectorial fields  $\eta$ ,  $\phi$  and  $\psi$  which vanish on the boundary of  $D$ , such that  $\mathbf{M} + \nabla\phi(\mathbf{X}) \in \mathcal{M}^+$  for all  $\mathbf{X} \in B$  and  $\nabla\eta = \nabla\psi$ . Furthermore we suppose that equality holds only when  $\eta = \psi = 0$  and  $\phi = 0$ .

We remark that the last condition is related to a quasi-convexity assumption. The rank-one convexity and quasi-convexity assumptions are usual in the studies of nonlinear elasticity [1, 18–21]. One expects that the energetic condition:

(ii')  $\Sigma$  satisfies the inequality

$$\int_D [\Sigma(\mathbf{M} + \nabla\phi(\mathbf{X}), \nabla\psi(\mathbf{X}), \nu_0 + \eta(\mathbf{X}))] dv \geq \Sigma(\mathbf{M}, 0, \nu_0) \text{ volume } (D)$$

and (i) could be sufficient to allow our uniqueness result, but our analysis does not guarantee it.

We can obtain a family of functions satisfying (i) and (ii). Let  $W(\mathbf{F}, \mathbf{G}, \nu)$  be a function satisfying (i) and (ii') and  $\partial W / \partial \nu(\mathbf{M}, 0, \nu_0) = 0$ , and let  $\Sigma(\mathbf{F}, \mathbf{G}, \nu)$  be the solution of the equation

$$n\Sigma + (\nu_0 - \nu)\partial\Sigma/\partial\nu = W.$$

Then  $\Sigma$  satisfies conditions (i) and (ii). An easy quadrature shows that

$$\Sigma(\mathbf{F}, \mathbf{G}, \nu) = (\nu - \nu_0)^n \int_{\nu_0}^{\nu} W(\mathbf{F}, \mathbf{G}, \xi)(\xi - \nu_0)^{-(n+1)} d\xi.$$

We finish this section by stating a Lemma on equalities of the conservation type.

LEMMA 1. Let  $(\mathbf{x}, \nu)$  be a solution to the equations of equilibrium (1). Then the following equalities are satisfied:

- (i)  $(T_{Ai}x_i + S_A\nu)_{,A} = T_{Ai}x_{i,A} + S_A\nu_{,A} - g\nu$ ,
- (ii)  $\Sigma_{,K} = (T_{Ai}x_{i,K} + S_A\nu_{,K})_{,A}$ ,
- (iii)  $n\Sigma - g\nu + (X_K(T_{Ai}x_{i,K} + S_A\nu_{,K}))_{,A} = (X_K\Sigma)_{,K} + (T_{Ai}x_i + S_A\nu)_{,A}$ .

**P r o o f.** The first equality follows from multiplying the first equation (1) by  $x_i$  and the second by  $\nu$ . After addition we have

$$0 = T_{Ai,A}x_i + (S_{A,A} + g)\nu = (T_{Ai}x_i + S_A\nu)_{,A} - \{T_{Ai}x_{i,A} + S_A\nu_{,A} - g\nu\}.$$

Thus, the first equality is proved.

To obtain the second equality we proceed in a similar way, but multiply by  $x_{i,K}$  and  $\mu_{,K}$ , respectively, to obtain

$$\begin{aligned} 0 &= T_{Ai,A}x_{i,K} + (S_{A,A} + g)\nu_{,K} \\ &= (T_{Ai}x_{i,K} + S_A\nu_{,K})_{,A} - (T_{Ai}x_{i,AK} + S_A\nu_{,KA} - g\nu_{,K}), \end{aligned}$$

which on using (3), becomes

$$0 = (T_{Ai}x_{i,K} + S_{Ai}y_{i,K})_{,A} - \Sigma_{,K},$$

and the second equality is proved.

The third equality is obtained from the second one by multiplying by  $X_K$ . We have

$$\begin{aligned} 0 &= X_K \{(T_{Ai}x_{i,K} + S_A\nu_{,K})_{,A} - \Sigma_{,K}\} \\ &= (X_K(T_{Ai}x_{i,K} + S_A\nu_{,K}))_{,A} + n\Sigma - (T_{Ai}x_{i,A} + S_A\nu_{,A}) - (X_K\Sigma)_{,K}. \end{aligned}$$

From the equality (i), we finally obtain

$$0 = (n\Sigma - g\nu) + (X_K(T_{Ai}x_{i,K} + S_A\nu_{,K}))_{,A} - (X_K\Sigma)_{,K} - (T_{Ai}x_i + S_A\nu)_{,A},$$

which implies (iii).

### 3. The uniqueness result

In this section we obtain a uniqueness theorem to the problem determined by the equilibrium equations (1) and the boundary conditions (5). To this end, it will be useful to introduce the function

$$(10) \quad \mathcal{J}(\mathbf{x}, \nu) = \int_B \Sigma \, dv - \frac{1}{n} \int_B g\nu \, dv.$$

Throughout this section, we suppose that  $B$  is an open bounded domain of the three-dimensional Euclidean space and that  $B$  is star-shaped with respect the origin which is located in  $B$ . It is clear that

$$(11) \quad \mathbf{X} \cdot \mathbf{N} \geq 0, \quad \text{for all } \mathbf{X} \in \partial B.$$

We have the following result:

LEMMA 2. Let  $B$  be defined as above. Let  $(\mathbf{x}, \nu)$  be a smooth equilibrium solution to the system (1). Then

$$(12) \quad n\mathcal{J}(\mathbf{x}, \nu) = \int_{\partial B} \left\{ (\mathbf{N} \cdot \mathbf{X})\Sigma + \mathbf{T}^\top \cdot \left[ \mathbf{N} \otimes \left( \mathbf{x} - r \frac{\partial \mathbf{x}}{\partial r} \right) \right] + \mathbf{S}^\top \cdot \left[ \mathbf{N} \otimes \left( \nu - r \frac{\partial \nu}{\partial r} \right) \right] \right\} ds,$$

where  $r = (\mathbf{X} \cdot \mathbf{X})^{1/2}$ .

**P r o o f.** The proof follows by application of the divergence theorem to equality (iii) and use of the identities  $r(\partial \mathbf{x} / \partial r) = \mathbf{X} \cdot \nabla \mathbf{x}$  and  $r(\partial \nu / \partial r) = \mathbf{X} \cdot \nabla \nu$ .

Our uniqueness theorem follows by considering the difference between two solutions and using the function  $\mathcal{J}$ .

Let  $(\mathbf{x}, \nu)$  and  $(\bar{\mathbf{x}}, \bar{\nu})$  be two solutions to the equilibrium equations (1) satisfying the same boundary conditions (5). Then we have

$$\begin{aligned} n(\mathcal{J}(\mathbf{x}, \nu) - \mathcal{J}(\bar{\mathbf{x}}, \bar{\nu})) &= \int_{\partial B} (\mathbf{N} \cdot \mathbf{X}) \{ \Sigma(\nabla \mathbf{x}, \nabla \nu, \nu) - \Sigma(\nabla \bar{\mathbf{x}}, \nabla \bar{\nu}, \bar{\nu}) \} ds \\ &\quad + \int_{\partial B} \left( \mathbf{T}^\top(\nabla \mathbf{x}, \nabla \nu, \nu) \cdot \left[ \mathbf{N} \otimes \left( \mathbf{x} - r \frac{\partial \mathbf{x}}{\partial r} \right) \right] \right. \\ &\quad \left. - \mathbf{T}^\top(\nabla \bar{\mathbf{x}}, \nabla \bar{\nu}, \bar{\nu}) \cdot \left[ \mathbf{N} \otimes \left( \bar{\mathbf{x}} - r \frac{\partial \bar{\mathbf{x}}}{\partial r} \right) \right] \right) ds \\ &\quad + \int_{\partial B} \left( \mathbf{S}^\top(\nabla \mathbf{x}, \nabla \nu, \nu) \cdot \left[ \mathbf{N} \otimes \left( \nu - r \frac{\partial \nu}{\partial r} \right) \right] \right. \\ &\quad \left. - \mathbf{S}^\top(\nabla \bar{\mathbf{x}}, \nabla \bar{\nu}, \bar{\nu}) \cdot \left[ \mathbf{N} \otimes \left( \bar{\nu} - r \frac{\partial \bar{\nu}}{\partial r} \right) \right] \right) ds. \end{aligned}$$

Now, on  $\partial B$  the two solutions  $(\mathbf{x}, \nu)$  and  $(\bar{\mathbf{x}}, \bar{\nu})$  coincide, so that

$$\mathbf{x} = \bar{\mathbf{x}} = \mathbf{M}\mathbf{X} + \mathbf{b} \quad \text{and} \quad \nu = \bar{\nu} = \nu_0, \quad \text{on } \partial B$$

and we deduce

$$\begin{aligned} &\mathbf{T}^\top(\nabla \mathbf{x}, \nabla \nu, \nu) \cdot \left[ \mathbf{N} \otimes \left( \mathbf{x} - r \frac{\partial \mathbf{x}}{\partial r} \right) \right] - \mathbf{T}^\top(\nabla \bar{\mathbf{x}}, \nabla \bar{\nu}, \nu) \cdot \left[ \mathbf{N} \otimes \left( \bar{\mathbf{x}} - r \frac{\partial \bar{\mathbf{x}}}{\partial r} \right) \right] \\ &\quad = \mathbf{T}^\top(\nabla \mathbf{x}, \nabla \nu, \nu) \cdot \left[ \mathbf{N} \otimes \left( r \frac{\partial \bar{\mathbf{x}} - \partial \mathbf{x}}{\partial r} \right) \right] \\ &\quad + \left[ \mathbf{T}^\top(\nabla \mathbf{x}, \nabla \nu, \nu) - \mathbf{T}^\top(\nabla \bar{\mathbf{x}}, \nabla \bar{\nu}, \nu) \right] \cdot \left[ \mathbf{N} \otimes \left( \bar{\mathbf{x}} - r \frac{\partial \bar{\mathbf{x}}}{\partial r} \right) \right] \end{aligned}$$

and

$$\begin{aligned} \mathbf{S}^\top(\nabla \mathbf{x}, \nabla \nu, \nu) \cdot \left[ \mathbf{N} \otimes \left( \nu - r \frac{\partial \nu}{\partial r} \right) \right] - \mathbf{S}^\top(\nabla \bar{\mathbf{x}}, \nabla \bar{\nu}, \nu) \cdot \left[ \mathbf{N} \otimes \left( \bar{\nu} - r \frac{\partial \bar{\nu}}{\partial r} \right) \right] \\ = \mathbf{S}^\top(\nabla \mathbf{x}, \nabla \nu, \nu) \cdot \left[ \mathbf{N} \otimes \left( r \frac{\partial \bar{\nu} - \partial \nu}{\partial r} \right) \right] \\ + \left[ \mathbf{S}^\top(\nabla \mathbf{x}, \nabla \nu, \nu) - \mathbf{S}^\top(\nabla \bar{\mathbf{x}}, \nabla \bar{\nu}, \nu) \right] \cdot \left[ \mathbf{N} \otimes \left( \bar{\nu} - r \frac{\partial \bar{\nu}}{\partial r} \right) \right]. \end{aligned}$$

We also recall the following identities on  $\partial B$  (see [1])

$$r \frac{\partial(\bar{\mathbf{x}} - \mathbf{x})}{\partial r} = (\mathbf{N} \cdot \mathbf{X}) \frac{\partial(\bar{\mathbf{x}} - \mathbf{x})}{\partial \mathbf{N}}, \quad r \frac{\partial(\bar{\nu} - \nu)}{\partial r} = (\mathbf{N} \cdot \mathbf{X}) \frac{\partial(\bar{\nu} - \nu)}{\partial \mathbf{N}}$$

and

$$\begin{aligned} \nabla \bar{\mathbf{x}} &= \nabla \mathbf{x} + \nabla \bar{\mathbf{x}} - \nabla \mathbf{x} = \nabla \mathbf{x} + \frac{\partial(\bar{\mathbf{x}} - \mathbf{x})}{\partial \mathbf{N}} \otimes \mathbf{N}, \\ \nabla \bar{\nu} &= \nabla \nu + \nabla \bar{\nu} - \nabla \nu = \nabla \nu + \frac{\partial(\bar{\nu} - \nu)}{\partial \mathbf{N}} \otimes \mathbf{N}. \end{aligned}$$

From the previous equalities we deduce

$$\begin{aligned} (13) \quad n(\mathcal{J}(\mathbf{x}, \nu) - \mathcal{J}(\bar{\mathbf{x}}, \bar{\nu})) &= \int_{\partial B} (\mathbf{N} \cdot \mathbf{X}) \left\{ \Sigma(\nabla \mathbf{x}, \nabla \nu, \nu) \right. \\ &\quad \left. - \Sigma \left( \nabla \mathbf{x} + \frac{\partial \bar{\mathbf{x}} - \partial \mathbf{x}}{\partial \mathbf{N}} \otimes \mathbf{N}, \nabla \nu + \frac{\partial \bar{\nu} - \partial \nu}{\partial \mathbf{N}} \otimes \mathbf{N}, \nu \right) \right. \\ &\quad \left. + \mathbf{T}(\nabla \bar{\mathbf{x}}, \nabla \bar{\nu}, \nu) \cdot \left[ \frac{\partial \bar{\mathbf{x}} - \partial \mathbf{x}}{\partial \mathbf{N}} \otimes \mathbf{N} \right] + \mathbf{S}(\nabla \bar{\mathbf{x}}, \nabla \bar{\nu}, \nu) \cdot \left[ \frac{\partial \bar{\nu} - \partial \nu}{\partial \mathbf{N}} \otimes \mathbf{N} \right] \right\} ds \\ &\quad + \int_{\partial B} \left\{ [\mathbf{T}(\nabla \mathbf{x}, \nabla \nu, \nu) - \mathbf{T}(\nabla \bar{\mathbf{x}}, \nabla \bar{\nu}, \nu)] \cdot \left[ \left( \bar{\mathbf{x}} - r \frac{\partial \bar{\mathbf{x}}}{\partial r} \right) \otimes \mathbf{N} \right] \right. \\ &\quad \left. + [\mathbf{S}(\nabla \mathbf{x}, \nabla \nu, \nu) \mathbf{X} - \mathbf{S}(\nabla \bar{\mathbf{x}}, \nabla \bar{\nu}, \nu)] \cdot \left[ \left( \bar{\nu} - r \frac{\partial \bar{\nu}}{\partial r} \right) \otimes \mathbf{N} \right] \right\} ds. \end{aligned}$$

Now, we may state:

LEMMA 3. Let  $B$  be defined as above and let  $(\mathbf{x}, \nu)$  be a smooth solution to the equilibrium system (1) such that boundary conditions (5) are satisfied. Let us suppose that  $\Sigma$  satisfies the condition (8). Then

$$(14) \quad \mathcal{J}(\mathbf{x}, \nu) + \frac{\bar{\nu}}{n} \int_B g \, dv \leq \mathcal{J}(\bar{\mathbf{x}}, \bar{\nu}),$$

where  $(\bar{\mathbf{x}}, \bar{\nu})$  is a solution defined by (4).

**P r o o f.** We apply the inequalities (8) and (11) to the first integrand on the right-hand side of equality (13) to conclude that

$$(15) \quad n(\mathcal{J}(\mathbf{x}, \nu) - \mathcal{J}(\bar{\mathbf{x}}, \bar{\nu})) \leq \int_{\partial B} \left\{ [\mathbf{T}(\nabla \mathbf{x}, \nabla \nu, \nu) - \mathbf{T}(\nabla \bar{\mathbf{x}}, \nabla \bar{\nu}, \nu)] \cdot \left[ \left( \bar{\mathbf{x}} - r \frac{\partial \bar{\mathbf{x}}}{\partial r} \right) \otimes \mathbf{N} \right] + [\mathbf{S}(\nabla \mathbf{x}, \nabla \nu, \nu) - \mathbf{S}(\nabla \bar{\mathbf{x}}, \nabla \bar{\nu}, \nu)] \cdot \left[ \left( \bar{\nu} - r \frac{\partial \bar{\nu}}{\partial r} \right) \otimes \mathbf{N} \right] \right\} ds.$$

On the other hand, from (4), we have  $\nabla \bar{\mathbf{x}} = \mathbf{M}$  for all  $\mathbf{X} \in B$ . Then it follows that

$$\bar{\mathbf{x}} - r \frac{\partial \bar{\mathbf{x}}}{\partial r} = \mathbf{b} \quad \text{and} \quad \bar{\nu} - r \frac{\partial \bar{\nu}}{\partial r} = \nu_0,$$

and inequality (15) therefore yields

$$n(\mathcal{J}(\mathbf{x}, \nu) - \mathcal{J}(\bar{\mathbf{x}}, \bar{\nu})) \leq \int_{\partial B} [\mathbf{T}(\nabla \mathbf{x}, \nabla \nu, \nu) - \mathbf{T}(\nabla \bar{\mathbf{x}}, \nabla \bar{\nu}, \bar{\nu})] \cdot [\mathbf{b} \otimes \mathbf{N}] ds + [\mathbf{S}(\nabla \mathbf{x}, \nabla \nu, \nu_0) - \mathbf{S}(\nabla \bar{\mathbf{x}}, \nabla \bar{\nu}, \nu_0)] \cdot [\nu_0 \otimes \mathbf{N}] ds.$$

Inequality (14) follows from (7) on recalling that  $\mathbf{b}$  and  $\nu_0$  are constants.

Now, we may state the uniqueness result:

**THEOREM 1.** *Let  $B$ ,  $(\mathbf{x}, \nu)$ ,  $(\bar{\mathbf{x}}, \bar{\nu})$ ,  $\mathbf{M}$  and  $\nu_0$  be as in the previous Lemma, and let the energy  $\Sigma$  satisfy the condition (9). Then  $(\mathbf{x}, \nu)$  is a solution defined by (4).*

**P r o o f.** Let us suppose that  $(\mathbf{x}, \nu) \neq (\bar{\mathbf{x}}, \bar{\nu}) = (\mathbf{M}\mathbf{X} + \mathbf{b}, \nu_0)$ . Then assumption (9) implies

$$\bar{\mathcal{J}}(\bar{\mathbf{x}}, \bar{\nu}) < \mathcal{J}(\mathbf{x}, \nu) + \frac{\bar{\nu}}{n} \int_B g \, dv,$$

which contradicts Lemma 3. Hence  $(\mathbf{x}, \nu) = (\bar{\mathbf{x}}, \bar{\nu})$  for all  $\mathbf{X} \in B$ .

## References

1. R.J. KNOPS and C.A. STUART, *Quasiconvexity and uniqueness of equilibrium solutions in nonlinear elasticity*, Arch. Rational Mech. Anal., **86**, 133–149, 1984.
2. J.W. NUNZIATO and S.C. COWIN, *A nonlinear theory of elastic materials with voids*, Arch. Rational Mech. Anal., **72**, 175–201, 1979.
3. S.C. COWIN and J.W. NUNZIATO, *Linear elastic materials with voids*, J. Elasticity, **13**, 125–147, 1983.
4. S.C. COWIN and P. PURI, *The classical pressure vessel problems for linear elastic materials with voids*, J. Elasticity, **13**, 157–163, 1983.
5. G. CAPRIZ and P. PODIO-GUIDUGLI, *Materials with spherical structure*, Arch. Rational Mech. Anal., **75**, 269–279, 1981.
6. M. CIARLETTA, *Reciprocal and variational theorems for viscoelastic materials with voids*, Atti Accad. Sci., Torino, Cl. Sci. Fis. Mat. Nat., **123**, 243–252, 1989.

7. M. CIARLETTA and A. SCALIA, *On some theorems in the linear theory of viscoelastic materials with voids*, J. Elasticity, **25**, 149–158, 1991.
8. D. IESAN and R. QUINTANILLA, *Decay estimates and energy bounds for porous elastic cylinders*, J. Appl. Math. Phys. (ZAMP), **46**, 268–281, 1995.
9. F. MARTINEZ and R. QUINTANILLA, *Existence and uniqueness of solutions to the equations of the incremental thermoelasticity with voids*, Proc. STAMM94, Interactions of Mechanics and Mathematics [to appear].
10. M. CIARLETTA and D. İEŞAN, *Non-classical elastic solids*, vol. 293, Pitman Research Notes in Mathematics Series, New York 1993.
11. G. RUSU, *Existence theorems in elastostatics of materials with voids*, An. St. Univ. Iași, Matematica, **30**, 193–204, 1985.
12. D.S. CHANDRASEKHARALAH and S.C. COWIN, *Unified complete solutions for the theories of thermoelasticity and poroelasticity*, J. Elasticity, **21**, 121–126, 1989.
13. D.S. CHANDRASEKHARALAH, *Complete solutions in the theory of elastic materials with voids*, Q. J. Mech. Appl. Math., **42**, 41–54, 1989.
14. G. RUSU, *On existence and uniqueness in thermoelasticity of materials with voids*, An. St. Univ. Iași, Matematica, **30**, 193–204, 1985.
15. E. SCARPETTA, *A uniqueness theorem in the non-linear dynamics of elastic materials with voids*, An. St. Univ. Iași, Matematica, **50**, **35**, 289–295, 1989.
16. A.E. GREEN, *On some general formulae in finite elastostatics*, Arch. Rational Mech. Anal., **50**, 73–80, 1973.
17. C.B. MORREY, Jr., *Quasi-convexity and the lower semicontinuity of multiple integrals*, Pacific J. Math., **2**, 25–53, 1952.
18. J.M. BALL, *Convexity conditions and existence theorems in nonlinear elasticity*, Arch. Rational Mech. Anal., **63**, 337–403, 1977.
19. J.M. BALL, *Constitutive inequalities and existence theorems in nonlinear elastostatics*, [in:] Nonlinear Analysis and Mechanics: Heriot-Watt Symposium, R.J. KNOPS [Ed.], vol. I, Pitman, London 1977, pp. 187–238.
20. J.M. BALL, *Strict convexity, strong ellipticity and regularity in the calculus of variations*, Math. Proc. Cam. Phil. Soc., **87**, 501–513, 1980.
21. P.G. CIARLET, *Mathematical elasticity*, vol. I. *Three-dimensional elasticity*, North-Holland, Amsterdam 1988.
22. R. QUINTANILLA, *Uniqueness of equilibrium solutions in nonlinear theory of elastic mixtures*, J. Appl. Math. Mech. (ZAMM), **75**, 947–950, 1995.

DEPARTAMENTO MATEMÁTICA APLICADA II  
UNIVERSIDAD POLITÉCNICA DE CATALUNYA, BARCELONA, SPAIN.  
e-mail: ramon@ma2.upc.es

Received June 24, 1996.

# An idea of thin-plate thermal mirror

## I. Mirror created by a heat pulse

Z. PŁOCHOCKI (WARSZAWA)

and A. MIOUCHOWSKI (EDMONTON)

AN IDEA AND THE THEORY of thermal mirrors created on the surfaces of a simply supported thin plane circular plate of an isotropic thermoelastic solid material by a uniform heat pulse, which is applied to one of the plate surfaces, is presented. Such a thermal mirror is – within the approximations applied for obtaining the solutions of the heat conduction and thermoelasticity equations – an ideal (aberration-free) optical mirror. The optical properties of the thermal mirror and their time evolution are derived and discussed in two asymptotical time regimes: the short-time and the long-time ones. Observability conditions for optical characteristics of the thermal mirror are estimated. Theoretical possibilities of an application of the thermal mirror to experimental determination of the temperature conductivity of a material are discussed. The theory presented can be also used for estimations of distortions of optical properties of pulse high power optical systems, originated by absorption of light by optical mirrors in such systems.

### 1. Introduction

IN THE PREVIOUS PAPER by the Authors [5] the idea of thermal mirror was presented following an example of the thermal mirror created by a focused heat pulse on the surface of an isotropic thermoelastic solid material half-space. In the present paper an opposite (in some sense) case is examined, namely – the thermal mirror created on the surfaces of a simply supported thin plane circular plate of a material of the same kind by a heat pulse, which is applied to one of the plate surfaces and is homogeneous across the surface. The aim is to calculate the fundamental optical properties of the mirror (i.e. – its aberration characteristic, optical power, and focal length), and their time evolution.

All the fundamental assumptions adopted here are the same as in the previous paper [5]; these are: thermal stresses theory approximation (rigid heat conductor approximation), quasi-static treatment of all the mechanical phenomena, and linearization of: the thermoelasticity and the heat conduction equations, and suitable boundary conditions (which are formulated at the undeformed surfaces of the plate); the plate is also assumed to be adiabatically insulated on its surfaces. Criteria of applicability of the thermal stresses theory approximation and the quasi-static displacement field one will be discussed in a separate paper by the Authors; here we note only that the former approximation depends on neglecting the influence of deformation rate on heat conduction processes, and the latter one denotes, that all the phenomena are observed in the time scale specific for heat conduction processes (the time scale specific for dynamic mechanical processes is much shorter). Some comments on the quasi-static displacement

field approximation and on the adiabatic insulation are given in Secs. 7 and 8, respectively.

### Main symbols

- $c_p$  specific heat (the value of  $c_p$  for the numerical estimations is assumed together with  $\varrho_0$ ),  
 $D = 1/f$  optical power,  
 $E$  Young's modulus,  
 $f$  focal length,  
 $h$  half-thickness of the (unperturbed) plate (the numerical estimations are performed for  $2h \doteq 10^{-3}$  m, and  $10^{-2}$  m),  
 $\text{ierfc}(x)$  integral complementary error function:  
 $\text{ierfc}(x) = \int_x^\infty \text{erfc}(t) dt$ ,  $\text{erfc}(t) = 1 - \text{erf}(t) = \frac{2}{\sqrt{\pi}} \int_t^\infty \exp[-y^2] dy$ ,  
 $l$  (subscript) refers to the lower surface of the plate,  
 $M_T$  see suitable equation at the beginning of Sec. 4 and Eq. (4.1)<sub>2</sub>,  
 $N_T$  see suitable equation at the beginning of Sec. 4 and Eq. (4.1)<sub>1</sub>,  
 $O^*$  assumed small number ( $\ll 1$ ), determining the accuracy of a given approximation (the value of the order of 0.01 is assumed for the numerical estimations),  
 $Q_{\text{tot}}$  total energy of the heat pulse,  
 $r, \varphi, z$  cylindrical coordinates,  
 $r_0$  radius of the (unperturbed) plate (for the numerical estimations  $r_0$  is assumed to be of the order of  $10 \cdot (2h)$ ),  
 $t$  time,  
 $T$  temperature, measured from an initial (constant) value,  
 $T_\infty$  final temperature, defined by Eq. (3.1),  
 $u$  (superscript) refers to the upper surface of the plate,  
 $u_\alpha$   $\alpha$ -th coordinate of the displacement vector,  
 $U$  vertical displacement (shift) of the surface with respect to its initial (unperturbed) level (Fig. 1),  
 $z$  see  $r, \varphi, z$ ,  
 $\alpha$  linear heat expansion coefficient (the value of the order of  $10^{-5}$  1/K is assumed for the numerical estimations),  
 $\delta(x - x_0)$  Dirac's delta distribution,  
 $\delta^u, \delta_l$  small terms (Eqs. (4.4)),  
 $\Delta U(r) := U(0) - U(r)$ ,  
 $\varepsilon$  deflection angle (Fig. 2),  
 $\zeta := z/(2h)$  - dimensionless  $z$ -coordinate,  
 $\Theta = T/T_\infty$  - dimensionless temperature,  
 $\kappa := \lambda/(\varrho_0 c_p)$  - temperature conductivity (heat diffusivity), ( $\lambda$  - heat conductivity), (the values of the order of  $(10^{-7} - 10^{-4})$  m<sup>2</sup>/s are assumed for the numerical estimations, where the first value refers to the worst temperature conductors, and the second to the best ones),  
 $\nu$  Poisson's coefficient,  
 $\varrho_0$  mass density of the (unperturbed) material (the value of  $\varrho_0 c_p$ , as being of the order of  $5 \cdot 10^6$  J/(m<sup>3</sup>K), is assumed for the numerical estimations),  
 $\tau := t \kappa / (2h)^2$  - dimensionless time,  
 $\varphi$  see  $r, \varphi, z$ ,  
 $\doteq$  reads: is of the order of.

**2. Statement of the problem**

Let us consider a plane circular plate of an isotropic thermoelastic solid material of thickness  $2h$  and of radius  $r_0$  (Fig. 1). The plate is described using the cylindrical coordinate system with the origin located in the center of the plate and with  $z$ -axis perpendicular to the main surfaces of the plate (before deformation). The plate is perturbed thermally by a heat pulse (in Fig. 1 the pulse is applied to the upper surface), which is homogeneous across the surface.

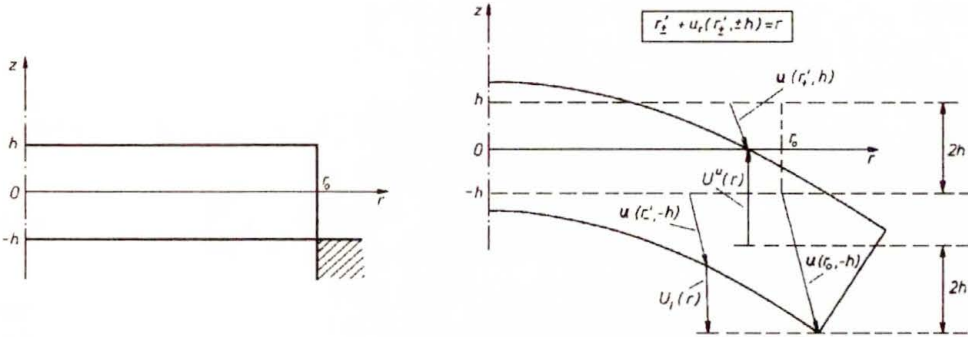


FIG. 1. Geometry of displacements.

The aim is to calculate the fundamental optical properties of the thermal mirror, i.e. – its aberration characteristic and optical power (focal length).

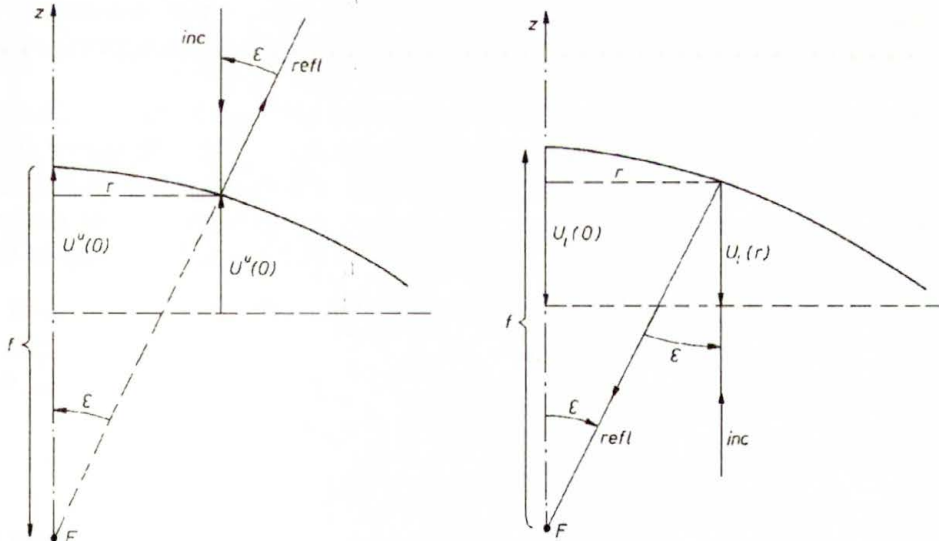


FIG. 2. Geometry of light rays.

The aberration characteristic is understood as a dependence:  $\epsilon = \epsilon(r)$ , where  $\epsilon$  is an angle between incident testing light ray parallel to the symmetry axis and this ray after reflection from the mirror (Fig.2). The deflection angle  $\epsilon$  is

understood to be negative in the case of defocusing mirror (the upper surface in our case), and positive in the case of focusing mirror (the lower surface in our case).

The relationship between the deflection angle  $\varepsilon$  and the function  $U$ , which describes the vertical displacement of the surface with respect to its initial (unperturbed) level (Figs. 1 and 2), is (for both the upper and lower surfaces):

$$\tan \frac{\varepsilon}{2} = \frac{\partial U}{\partial r} \quad \text{or} \quad \tan \varepsilon = \frac{2 \frac{\partial U}{\partial r}}{1 - \left(\frac{\partial U}{\partial r}\right)^2},$$

therefore the aberration characteristic of the mirror is given by the formula:

$$(2.1) \quad \varepsilon = 2 \arctan \frac{\partial U}{\partial r} = \arctan \frac{2 \frac{\partial U}{\partial r}}{1 - \left(\frac{\partial U}{\partial r}\right)^2} \cong 2 \frac{\partial U}{\partial r},$$

where the approximation is valid if:

$$(2.2) \quad \left(\frac{\partial U}{\partial r}\right)^2 \leq \frac{3O^*}{1 + O^*} \cong 3O^*,$$

where, in turn,  $O^*$  stands for an assumed small number, which determines an approximation accuracy in the sense, that a relative error of an approximation does not exceed  $O^*$ .

The classical definition of the focal length is used [2], namely: the focal length  $f$  of the mirror is defined as a distance of the focal point  $F$  from the mirror along the mirror symmetry axis (Fig. 2); the focal length is understood to be negative in the case of defocusing mirror (the upper surface in our case), and positive in the case of focusing mirror (the lower surface in our case). According to this definition we have (Fig. 2):

$$\tan \varepsilon = \frac{r}{f + \Delta U(r)},$$

where

$$(2.3) \quad \Delta U(r) := U(0) - U(r);$$

therefore the optical power  $D$  and the focal length  $f$  of the mirrors are given by the formula:

$$(2.4) \quad D = \frac{1}{f} = \frac{\tan \varepsilon}{r} \frac{1}{1 - \Delta U \frac{\tan \varepsilon}{r}} = \frac{2}{r} \frac{\partial U}{\partial r} \frac{1}{1 - \left(\frac{\partial U}{\partial r}\right)^2 - \frac{2}{r} \frac{\partial U}{\partial r} \Delta U} \cong \frac{2}{r} \frac{\partial U}{\partial r},$$

where the approximation holds, if

$$(2.5) \quad \left| \left( \frac{\partial U}{\partial r} \right)^2 + \frac{2}{r} \frac{\partial U}{\partial r} \Delta U \right| \leq O^*.$$

In an ideal case both  $D$  and  $f$  do not depend on  $r$ , i.e. – each of these two functions has the same value for each testing ray, or – the focal point  $F$  is the same for all the testing rays, independently of  $r$ . Such a situation takes place when  $U$  is simply proportional to  $r^2$  (parabolic mirror) <sup>(1)</sup>.

Thus, in order to find the fundamental optical characteristics of the mirror and their time evolution, it is sufficient to find the function  $U(r, t)$ .

The function  $U(r, t)$  is determined by both coordinates  $u_z$  and  $u_r$  of the displacement field in the material at a given surface (at  $z = \pm h$ , Fig. 1):

$$(2.6) \quad \begin{aligned} U^u(r) &= u_z(r'_+, h) - u_z(r_0, -h), \\ U_l(r) &= u_z(r_0, -h) - u_z(r'_-, -h), \end{aligned}$$

where  $r'_+(r)$  and  $r'_-(r)$  are solutions of the equations:  $r'_\pm + u_r(r'_\pm, \pm h) = r$  with respect to  $r'_\pm$ , respectively (criteria of linearization of these formulae, which depend on the approximation:  $r'_\pm \cong r$ , are given in Sec. 6).

Thus, in order to find the fundamental optical characteristics of the mirror, it is sufficient to find the displacement field (the vertical displacement  $u_z$  only, if linearized Eqs. (2.6) are applied) at a given surface. This information will be deduced from the solution of the Lamé thermoelasticity equation, for which we need the solution of the heat conduction equation first. Thus, we will examine, first, the thermal part of the problem, and next – the thermoelastic part. Having suitable information we will come back to the analysis of the optical properties of the mirror.

### 3. Thermal problem

Following the specification of the thermal perturbation, the temperature field in the material is assumed to be dependent on  $z$  and  $t$  only:  $T = T(z, t)$ . Therefore, according to the general assumptions adopted, the heat conduction equation is:

$$\frac{\partial \Theta}{\partial \tau} = \frac{\partial^2 \Theta}{\partial \zeta^2} + \delta(\tau - 0) \delta \left( \zeta - \frac{1}{2} \right),$$

<sup>(1)</sup> Both criteria expressed by Ineqs. (2.2) and (2.5) determine the so-called paraxial optics approximation:

$$D = \frac{1}{f} = \frac{\varepsilon}{r} = \frac{2}{r} \frac{\partial U}{\partial r}.$$

An ideal case in this approximation is characterized by simple proportionality of  $\varepsilon$  to  $r$ .

It will be proved later that this approximation is not necessary for the mirrors examined, because for such mirrors the left-hand side of Ineq. (2.5) is identically equal to zero (and only the approximation  $\arctan x \cong x$  may be applied).

where

$$\tau := \frac{\kappa}{(2h)^2} t, \quad \zeta := \frac{z}{2h}$$

stand for dimensionless time and  $z$ -coordinate, respectively,  $\kappa = \lambda/(\rho_0 c_p)$  is the temperature conductivity (heat diffusivity) of a given material,  $\lambda$ ,  $\rho_0$  and  $c_p$  stand for heat conductivity, density and specific heat of a given material, respectively,  $\delta(x - x_0)$  stands for the Dirac's delta distribution, and

$$\Theta(\zeta, \tau) = \frac{T[z = z(\zeta), t = t(\tau)]}{T_\infty}$$

stands for dimensionless temperature (as a function of dimensionless variables), where, in turn,

$$(3.1) \quad T_\infty := T(t = \infty) = \frac{Q_{\text{tot}}}{\pi r_0^2} \frac{1}{2h\rho_0 c_p},$$

and  $Q_{\text{tot}}$  stands for the total energy of the heat pulse. The boundary and initial conditions are:

$$\frac{\partial \Theta}{\partial \zeta} \left( \zeta = \pm \frac{1}{2} \right) = 0 = \Theta(\tau = 0).$$

The Green function for the thermal problem in the whole space is known [3]. Applying therefore the method of sources and sinks one may write the solution of our problem in the form:

$$(3.2) \quad \Theta = \frac{1}{\sqrt{\pi\tau}} \sum_{m=0}^{\infty} \left\{ \exp \left[ -\frac{\left(2m + \frac{1}{2} - \zeta\right)^2}{4\tau} \right] + \exp \left[ -\frac{\left(2m + \frac{3}{2} + \zeta\right)^2}{4\tau} \right] \right\} \\ = 1 + 2 \sum_{k=1}^{\infty} (-1)^k \exp[-k^2\pi^2\tau] \cos k\pi \left( \zeta + \frac{1}{2} \right),$$

where the first line represents the original solution obtained using the method mentioned<sup>(2)</sup>, and the second one – that solution after expansion into Fourier cosine series<sup>(3)</sup> (the function  $\Theta(\zeta, \tau)$  is symmetric with respect to  $\zeta + 1/2$ , and it satisfies the Dirichlet conditions).

<sup>(2)</sup> The same result is obtainable by applying the Laplace transformation method to solve the following equivalent problem:

$$\frac{\partial \Theta}{\partial \tau} = \frac{\partial^2 \Theta}{\partial \zeta^2}, \quad \frac{\partial \Theta}{\partial \zeta} \left( \zeta = -\frac{1}{2} \right) = 0, \quad \frac{\partial \Theta}{\partial \zeta} \left( \zeta = \frac{1}{2} \right) = \delta(\tau - 0), \quad \Theta(\tau = 0) = 0.$$

<sup>(3)</sup> The same result is obtainable by applying the Fourier method of separation of independent variables to

#### 4. The thermoelastic problem

The solution of the Lamé thermoelasticity equation for a simply supported plane finite thin plate<sup>(4)</sup> with  $T = T(z)$  and with no external forces is known [1] (in the approximation, which depends on replacing the local boundary conditions for the stress tensor coordinates at the side surface of the plate by suitable integral ones); in the case of circular plate we have:

$$u_r(r, z) = \frac{r}{E} \left[ \frac{N_T}{2h} + \frac{3z}{2h^3} M_T \right],$$

$$u_z(r, z) = -\frac{3M_T}{4h^3 E} r^2 + \frac{1}{1-\nu} \left[ (1+\nu)\alpha \int_0^z T dz - \frac{\nu z}{hE} N_T - \frac{3\nu z^2}{2h^3 E} M_T \right],$$

where  $\alpha$  stands for the (linear) heat expansion coefficient,  $E$  – for the Young's modulus,  $\nu$  – for the Poisson's coefficient, and

$$N_T := \alpha E \int_{-h}^h T dz, \quad M_T := \alpha E \int_{-h}^h T z dz.$$

Using the formulae representing the solution of the thermal problem (Eq.(3.2)) we have:

$$(4.1) \quad \begin{aligned} N_T &= 2hE\alpha T_\infty, \\ M_T &= 2h^2 E\alpha T_\infty \left[ 1 - \frac{4}{\sqrt{\pi}} \sqrt{\tau} - 8\sqrt{\tau} \sum_{m=1}^{\infty} (-1)^m \operatorname{ierfc} \frac{m}{2\sqrt{\tau}} \right] \\ &= 2h^2 E\alpha T_\infty \sum_{k=1}^{\infty} \frac{8}{\pi^2} \frac{1}{(2k-1)^2} \exp[-(2k-1)^2 \pi^2 \tau], \end{aligned}$$

where  $\operatorname{ierfc}(x)$  stands for the integral complementary error function:

$$\operatorname{ierfc}(x) = \int_x^{\infty} \operatorname{erfc}(t) dt, \quad \operatorname{erfc}(t) = 1 - \operatorname{erf}(t) = \frac{2}{\sqrt{\pi}} \int_t^{\infty} \exp[-y^2] dy.$$

solve the following equivalent problem:

$$\frac{\partial \Theta}{\partial \tau} = \frac{\partial^2 \Theta}{\partial \zeta^2}, \quad \frac{\partial \Theta}{\partial \zeta} \left( \zeta = \pm \frac{1}{2} \right) = 0, \quad \Theta(\tau = 0) = \delta \left( \zeta - \frac{1}{2} \right).$$

It may be useful to note that, if the initial condition is not specified, then the solution of the heat conduction equation has the same form with coefficients  $2(-1)^k$  replaced by unknown coefficients  $a_k$  (which are determinable from the initial condition after it will be specified), i.e. the structure of time-dependence of the solution (in the Fourier cosine representation) does not depend on the initial condition.

<sup>(4)</sup> The plate is understood to be thin in the sense that the following approximate conditions for the stress tensor coordinates are valid:  $\sigma_{rz} = \sigma_{\varphi z} = \sigma_{zz} = 0$ .

Using these formulae one may rewrite Eqs.(2.6) in the form:

$$(4.2) \quad \begin{aligned} U^u &= \frac{N_T}{E} + U_{\max} \left[ 1 - \left( \frac{r}{r_0} \right)^2 \frac{1}{(1 + \delta^u)^2} \right] \cong \frac{N_T}{E} + U_{\max} \left[ 1 - \left( \frac{r}{r_0} \right)^2 \right], \\ U_l &= -U_{\max} \left[ 1 - \left( \frac{r}{r_0} \right)^2 \frac{1}{(1 - \delta_l)^2} \right] \cong -U_{\max} \left[ 1 - \left( \frac{r}{r_0} \right)^2 \right], \end{aligned}$$

where

$$(4.3) \quad U_{\max} = \frac{3M_T}{4h^3E} r_0^2,$$

$$(4.4) \quad \delta_l^u = \pm \frac{1}{r} u_r(r, \pm h) = \frac{1}{2hE} \left[ \pm N_T + \frac{3}{h} M_T \right],$$

where, in turn: the superscript  $u$  and the upper sign refer to the upper surface of the plate; the subscript  $l$  and the lower sign refer to the lower surface;  $N_T$  is given by Eq.(4.1)<sub>1</sub> and  $M_T$  – by Eq.(4.1)<sub>2</sub> or Eq.(4.1)<sub>3</sub>; and the approximations in Eqs.(4.2) (which correspond to the linearization of Eqs.(2.6)) are valid if the functions  $\delta$  can be neglected (see Sec.6).

## 5. The optical problem

After substitution of Eqs.(4.2) into Eq.(2.1), the aberration characteristic of the thermal mirrors examined is obtained:

$$(5.1) \quad \begin{aligned} \varepsilon_l^u &= \mp 2 \arctan \left[ \frac{2U_{\max}}{r_0} \frac{r}{r_0} \frac{1}{(1 \pm \delta_l^u)^2} \right] \\ &\cong \mp 2 \arctan \left[ \frac{2U_{\max}}{r_0} \frac{r}{r_0} \right] \cong \mp \frac{4U_{\max}}{r_0} \frac{r}{r_0}, \end{aligned}$$

where (as previously): the superscript  $u$  and the upper sign refer to the upper surface of the plate; the subscript  $l$  and the lower sign refer to the lower surface;  $U_{\max}$  is given by Eq.(4.3) with Eqs.(4.1)<sub>2,3</sub>;  $\delta$  are given by Eq.(4.4) with Eqs.(4.1); the first approximation (which corresponds to the linearization of Eqs.(2.6)) is valid, if the functions  $\delta$  can be neglected (see Sec.6), and the second one (the paraxial optics approximation) – if (in addition)

$$(5.2) \quad \left( \frac{2U_{\max}}{r_0} \right)^2 \frac{r^2}{r_0^2} \leq \frac{3 O^*}{1 + O^*} \cong 3 O^*,$$

where  $O^*$  is an assumed small number.

It may be useful to comment at this place on the condition of applicability of the paraxial optics approximation, as given by Ineq.(5.2). The functions  $\delta$  are

assumed to be negligible. As it follows from Eqs.(4.1)<sub>2,3</sub>, the function  $M_T$  is a monotonically decreasing one from  $2h^2 E \alpha T_\infty$  to 0, as time varies from 0 to  $\infty$ , respectively. Therefore, according to Eq.(4.3) we have:

$$0 \leq \frac{U_{\max}}{r_0} \leq 3 \frac{r_0}{2h} \alpha T_\infty ,$$

where the right-hand side of this inequality represents the value of  $U_{\max}$  at  $\tau = 0$ , and the left-hand one – at  $\tau = \infty$ . The criterion of applicability of the paraxial optics approximation can be therefore written in the form:

$$\left(\frac{r}{r_0}\right)^2 \leq \frac{1}{12} \frac{O^*}{1 + O^*} \left(\frac{2h}{r_0}\right)^2 \frac{1}{(\alpha T_\infty)^2} .$$

Assuming

- $O^* \doteq 10^{-2}$  ,
- $r_0 \doteq 10 \cdot (2h)$ ,
- $\alpha \doteq 10^{-5}$  1/K ,
- $T_\infty \doteq (1 - 10)$  K ,

(the sign  $\doteq$  reads: is of the order of) and taking into account that the maximum value of  $r$  is very close to  $r_0$ , one can see, that the right-hand side of the inequality given above is of the order of  $10^5 - 10^3$ , so the criterion examined is well satisfied (it can be violated only in a case of very strong requirements; if for instance:  $O^* \doteq 10^{-4}$ ,  $r_0 \doteq 10^2 \cdot (2h)$ , and  $\alpha T_\infty \doteq 10^{-4}$ , then the right-hand side of the inequality given above may be even of the order of  $10^{-1}$  in the worst case).

The aberration characteristic obtained represents an ideal case, therefore both the upper and lower surfaces of the plate considered represent an ideal (parabolic) mirror (the upper – defocusing mirror, and the lower – focusing one). In fact, substituting Eqs.(4.2) into Eq.(2.4) we obtain the optical power  $D$  and the focal length  $f$  of the mirror as independent of distance  $r$ :

$$(5.3) \quad D_l^u = \frac{1}{f_l^u} = \mp \frac{4}{r_0^2} U_{\max} \frac{1}{(1 \pm \delta_l^u)^2} \cong \mp \frac{4}{r_0^2} U_{\max} ,$$

where  $U_{\max}$  is given by Eq.(4.3) with Eq.(4.1)<sub>2,3</sub>, and  $\delta$  are given by Eqs.(4.4) with Eqs.(4.1); and the approximation holds, if the functions  $\delta$  can be neglected (see Sec.6).

The results expressed by Eqs.(5.3) denote, that the mirrors considered are aberration-free, and no paraxial optics approximation is needed to idealize them (although this approximation may be applied for simplifying the formulae for the functions  $\varepsilon$ , if it is allowable (see comment given above)). It should be noted, that our results are not valid for an arbitrary plate, because they were obtained under defined assumptions.

As it is seen from the formulae given above, the time evolution of the displacement function  $U$  and the optical properties of the thermal mirror is governed by the dependence of the function  $U_{\max}$  (Eqs. (4.3) and (4.1)) and, in addition, by that of the functions  $\delta$  – on time. This dependence is complicated and difficult for a simple interpretation. It can be simplified in two steps: first, by neglecting the functions  $\delta$  in the suitable expressions (see Sec. 6); then, second, significant simplification can be obtained for sufficiently short or long time (see Secs. 7 or 8, respectively).

## 6. Criterion for neglecting the functions $\delta$

Because the quantity  $N_T$  (Eqs. (4.1)<sub>1</sub>) is independent of time, and the quantity  $M_T$  (Eqs. (4.1)<sub>2,3</sub>) is a monotonically decreasing function of time, which varies from  $2h^2 E \alpha T_\infty$  at  $\tau = 0$  to 0 at  $\tau = \infty$ , therefore the functions  $\delta$  vary within the limits:

$$\begin{aligned} \alpha T_\infty &\leq \delta^u \leq 4\alpha T_\infty, \\ -\alpha T_\infty &\leq \delta_l \leq 2\alpha T_\infty, \end{aligned}$$

where the right-hand side limits correspond to  $\tau = 0$ , and the left-hand side ones – to  $\tau = \infty$ . Adopting the previously assumed values for  $\alpha$  and  $T_\infty$  one has:

$$\begin{aligned} \delta^u &\leq 4 \cdot (10^{-5} - 10^{-4}), \\ |\delta_l| &\leq 2 \cdot (10^{-5} - 10^{-4}), \end{aligned}$$

where the first value in the brackets corresponds to  $T_\infty = 1 \text{ K}$ , and the second one – to  $T_\infty = 10 \text{ K}$ .

Thus, in practical cases the functions  $\delta$  are in fact small quantities in comparison with unity. Criteria for neglecting these functions in each of the formulae for  $U^u$ ,  $U_l$ ,  $\varepsilon^u$ ,  $\varepsilon_l$  and  $D = 1/f$  are examined in details in the Appendix. This discussion suggests the following assumption as the common criterion for neglecting the functions  $\delta$  in all the formulae mentioned (in the sense, that a relative error of an approximation in any case does not exceed  $O^*$ , if this criterion is satisfied)<sup>(5)</sup>:

$$(6.1) \quad |\delta_i^u| \leq 4 \alpha T_\infty \leq \frac{1}{2} O^*$$

(which is approximated in some cases, with a reasonable accuracy however, as it is pointed out in the Appendix). This assumption implies no limitation for the distance  $r$  in the case of the functions  $\varepsilon$  and  $D = 1/f$ , whereas in the case of

<sup>(5)</sup> If this criterion would be formulated for the upper and the lower surfaces separately, then for the upper surface it would have the form as given by Ineq. (6.1), and for the lower one – by the same inequality with only number 4 replaced by number 2.

the functions  $U$  it is (approximately) equivalent to the following condition for  $r$  (see Appendix):

$$r \leq \frac{1}{\sqrt{2}} r_0 \cong 0.7071 r_0.$$

It may be useful to note here, that using Eq. (3.1) one can rewrite Ineq. (6.1) as a criterion for the maximum pulse energy  $Q_{\text{tot}}$ , for which Ineq. (6.1) is satisfied. Assuming (in addition to the assumptions of this kind adopted previously):

- $\varrho_0 c_p \doteq 5 \cdot 10^6 \text{ J}/(\text{m}^3 \text{K})$

we obtain in this way

$$(6.2) \quad \begin{aligned} Q_{\text{tot}} &\leq \begin{cases} 2 \cdot 10^2 \text{ J}, & \text{for } 2h \doteq 10^{-3} \text{ m}, \\ 2 \cdot 10^5 \text{ J}, & \text{for } 2h \doteq 10^{-2} \text{ m}; \end{cases} \\ \frac{Q_{\text{tot}}}{\pi r_0^2} &\leq \begin{cases} 6 \cdot 10^5 \text{ J}/\text{m}^2, & \text{for } 2h \doteq 10^{-3} \text{ m}, \\ 6 \cdot 10^6 \text{ J}/\text{m}^2, & \text{for } 2h \doteq 10^{-2} \text{ m}. \end{cases} \end{aligned}$$

## 7. Short-time regime

For sufficiently short time the sum in the brackets in Eq. (4.1)<sub>2</sub> can be truncated after the second term. Let us note, that because  $\text{ierfc}(x)$  is a monotonically decreasing function, therefore  $\text{ierfc}(m/2\sqrt{\tau}) > \text{ierfc}[(m+1)/2\sqrt{\tau}]$ . In addition, if  $\tau < \pi/16 \cong 0.196$ , then  $\text{ierfc}(1/2\sqrt{\tau}) < 1/2\sqrt{\pi}$ . The whole sum in the brackets in Eq. (4.1)<sub>2</sub> can be therefore treated as a Leibniz-type series<sup>(6)</sup>. Then, the sum considered can be approximated by the first two terms only with an accuracy to  $O^*$ , if

$$8\sqrt{\tau} \text{ierfc} \frac{1}{2\sqrt{\tau}} \leq O^* \left( 1 - \frac{4\sqrt{\tau}}{\sqrt{\pi}} \right).$$

This inequality is satisfied, if

$$\tau \leq \tau_2 := \frac{1}{4x_0^2},$$

<sup>(6)</sup> The Leibniz-type series ( $LS$ ) is understood to be a convergent series of the type:

$$LS := \sum_{m=0}^{\infty} (-1)^m a_m, \quad a_m > a_{m+1} > 0.$$

Such a series can be precisely estimated as follows (Leibniz's theorem):

$$\sum_{m=0}^{2k} (-1)^m a_m > LS > \sum_{m=0}^{2k-1} (-1)^m a_m.$$

In particular case one may obtain

$$a_0 - a_1 + a_2 > LS > a_0 - a_1,$$

therefore  $LS \cong a_0 - a_1$  with an accuracy to  $O^*$ , if  $a_2 \leq O^*(a_0 - a_1)$ .

where  $x_0$  stands for a solution of the equation:  $\text{ierfc } x = O^* \left( \frac{x}{4} - \frac{1}{2\sqrt{\pi}} \right)$  with respect to  $x$ .

Assuming (as previously)  $O^* = 0.01$ , one may find  $x_0 \cong 1.87$ , and

$$(7.1) \quad \tau \leq \tau_{\text{short}} = \tau_2 \cong 7 \cdot 10^{-2}.$$

Assuming, in addition

- $\kappa \doteq (10^{-7} - 10^{-4}) \text{ m}^2/\text{s}$ ,

where the first value in the brackets refers to the worst temperature conductors and the second one – to the best temperature conductors, one may rewrite the criterion expressed by Ineq. (7.1) in dimensional form<sup>(7)</sup>

$$(7.2) \quad t \leq t_{\text{short}} = t_2 \doteq \begin{cases} 7 \cdot (10^{-1} - 10^{-4}) \text{ s}, & \text{for } 2h \doteq 10^{-3} \text{ m}, \\ 7 \cdot (10 - 10^{-2}) \text{ s}, & \text{for } 2h \doteq 10^{-2} \text{ m}. \end{cases}$$

By the way let us note here that all the mechanical phenomena are treated in the quasi-static approximation, i.e. observation time  $\tau$  should be sufficiently large. The following criterion is assumed:

$$(7.3) \quad \tau \geq \tau_{\text{min}} = \frac{1}{O^*} \frac{r_0}{c} \frac{\kappa}{4h^2}, \quad t \geq t_{\text{min}} = \frac{1}{O^*} \frac{r_0}{c},$$

where the first condition is written in the dimensionless form (in the time scale applied in the paper), the second condition is written in the usual dimensional form, and  $c$  stands for velocity of sound in a given material. Assuming (in addition to the assumptions of this kind adopted previously):

- $c \doteq 2 \cdot 10^3 \text{ m/s}$ ,

we have (in dimensionless and in dimensional forms):

$$(7.4) \quad \begin{aligned} \tau \geq \tau_{\text{min}} &\doteq \begin{cases} 5 \cdot (10^{-5} - 10^{-2}), & \text{for } 2h \doteq 10^{-3} \text{ m}, \\ 5 \cdot (10^{-6} - 10^{-3}), & \text{for } 2h \doteq 10^{-2} \text{ m}, \end{cases} \\ t \geq t_{\text{min}} &\doteq \begin{cases} 5 \cdot 10^{-4} \text{ s}, & \text{for } 2h \doteq 10^{-3} \text{ m}, \\ 5 \cdot 10^{-3} \text{ s}, & \text{for } 2h \doteq 10^{-2} \text{ m}. \end{cases} \end{aligned}$$

Comparing Ineqs. (7.4) and (7.1) [(7.2)] one can see, that within the quasi-static displacement fields approximation, there exists a relatively large field for the short-time regime approximation<sup>(8)</sup>.

<sup>(7)</sup> For  $O^* = 10^{-3}$  or  $10^{-4}$  one may find  $x_0 \cong 2.25$  or  $2.61$ , respectively, and the number 7 in Ineqs. (7.1) and (7.2) is replaced by the number 5 or 4, respectively.

<sup>(8)</sup> Let us note in addition, that the perturbing heat pulse is assumed to be instantaneous, therefore the observation time has to be much longer than the time of duration of the real physical pulse.

If the criterion expressed by Ineq. (7.1) (or (7.2)) is satisfied, then the sum in the brackets in Eq. (4.1)<sub>2</sub> can be approximated by its first two terms only, which is decreasing from 1 to about 0.4 as  $\tau$  is increasing from 0 to  $\tau_{\text{short}} = 7 \cdot 10^{-2}$ .

Thus, if the criteria expressed by Ineqs. (7.1) (or (7.2)) and (6.1) are satisfied, then the sum in the brackets in Eq. (4.1)<sub>2</sub> can be truncated after the second term, and the functions  $\delta$  can be ignored (the total relative error of this double approximation does not exceed  $(1 + O^*)^2 - 1 \cong 2O^*$ ). In this approximation, the function  $U_{\text{max}}$ , and therefore also  $U$ ,  $D$ , and  $f$  are linear functions of  $\sqrt{\tau}$ :

$$(7.5) \quad \begin{aligned} U_{\text{max}} &= U_{\text{max}}(0) \left( 1 - \frac{4}{\sqrt{\pi}} \sqrt{\tau} \right), \\ U^u &= U_{\text{max}}(0) \left\{ \frac{1}{3} \left( \frac{2h}{r_0} \right)^2 + \left[ 1 - \left( \frac{r}{r_0} \right)^2 \right] \left( 1 - \frac{4}{\sqrt{\pi}} \sqrt{\tau} \right) \right\}, \\ U_l &= -U_{\text{max}}(0) \left[ 1 - \left( \frac{r}{r_0} \right)^2 \right] \left( 1 - \frac{4}{\sqrt{\pi}} \sqrt{\tau} \right), \\ D_l^u &= \frac{1}{f_l^u} = \mp \frac{4}{r_0^2} U_{\text{max}}(0) \left( 1 - \frac{4}{\sqrt{\pi}} \sqrt{\tau} \right), \end{aligned}$$

where the superscript  $u$  and the upper sign refer to the upper surface of the plate, and the subscript  $l$  and the lower sign  $-$  to the lower surface,

$$U_{\text{max}}(0) := 3\alpha \frac{r_0^2}{(2h)^2} \frac{Q_{\text{tot}}}{\pi r_0^2 \varrho_0 c_p}.$$

The deflection angle

$$(7.6) \quad \begin{aligned} \varepsilon_l^u &= \mp 2 \arctan \left[ 2 \frac{U_{\text{max}}(0)}{r_0} \frac{r}{r_0} \left( 1 - \frac{4}{\sqrt{\pi}} \sqrt{\tau} \right) \right] \\ &\cong \mp 4 \frac{U_{\text{max}}(0)}{r_0} \frac{r}{r_0} \left( 1 - \frac{4}{\sqrt{\pi}} \sqrt{\tau} \right) \end{aligned}$$

is a linear function of  $\sqrt{\tau}$  only in the paraxial optics approximation (the approximated part of Eq. (7.6)), which holds (with an accuracy to  $O^*$ ), if (cf. Ineq. (2.2))

$$\frac{4}{r_0^2} U_{\text{max}}^2(0) \left( \frac{r}{r_0} \right)^2 \left( 1 - \frac{4}{\sqrt{\pi}} \sqrt{\tau} \right)^2 \leq \frac{3O^*}{1 + O^*} \cong 3O^*$$

(the total relative error of this triple approximation does not exceed  $(1 + O^*)^3 - 1 \cong 3O^*$ ).

Thus, the short-time approximation seems to be realistic (except for very thin plates with the best temperature conductors) and offering simple interpretation of the time evolution of the optical properties of the mirror considered.

## 8. Long-time regime

Although the short-time regime, discussed in the previous section, seems to be sufficient for use and interpretation of the results obtained earlier, we will discuss shortly the opposite regime – the long-time one for the completeness of the picture. For this purpose it is more convenient to use the second version of the solution of the thermal problem (Eq. (3.2)<sub>2</sub>), and therefore – also the second version of the function  $M_T$  (Eq. (4.1)<sub>3</sub>).

The idea of the long-time approximation is similar to that used previously in the case of the short-time approximation. We have to find criteria, which allow us to simplify the expression for the function  $M_T$  as far as possible (the assumption, that the functions  $\delta$  can be ignored, will also be used).

For sufficiently long time, the series in Eq. (4.1)<sub>3</sub> can be approximated by its first term only with an accuracy to an assumed small number  $O^*$ . For this purpose it is sufficient to require:

- the second term of the series to be much smaller than the first one in the following sense:

$$\frac{1}{9} \exp[-8\pi^2\tau] \leq 0.9 O^*,$$

- and the  $(k+1)$ -th term,  $k \geq 2$ , to be not larger than 0.1 of the  $k$ -th term:

$$\exp[-8k\pi^2\tau] \leq 0.1 \left( \frac{2k+1}{2k-1} \right)^2.$$

These inequalities are satisfied if, respectively:

$$\begin{aligned} \tau &\geq \frac{1}{8\pi^2} [-\ln 8.1 O^*], \\ \tau &\geq \frac{1}{8\pi^2 k} \ln \left[ 10 \left( \frac{2k-1}{2k+1} \right)^2 \right]. \end{aligned}$$

The latter inequality is the strongest one for  $k = 2$ , therefore we have:

$$\begin{aligned} \tau &\geq \tau_{2/1} := \frac{1}{8\pi^2} [-\ln 8.1 O^*], \\ \tau &\geq \tau_{3/2} := \frac{1}{16\pi^2} \ln 3.6 \cong 8.1 \cdot 10^{-3}. \end{aligned}$$

Because  $\tau_{2/1} \cong \tau_{3/2}$  for  $O^* \cong 6.5 \cdot 10^{-2}$ , therefore for  $O^* < 6.5 \cdot 10^{-2}$  the first of these two conditions is stronger than the second one, and inversely for  $O^* > 6.5 \cdot 10^{-2}$ .

Assuming (as previously)  $O^* = 0.01$  we have<sup>(9)</sup>:

$$(8.1) \quad \tau \geq \tau_{\text{long}} = \tau_{2/1} \cong 3.2 \cdot 10^{-2};$$

<sup>(9)</sup> For  $O^* = 10^{-3}$  or  $10^{-4}$  the number 3.2 in Ineqs. (8.1) and (8.2) is replaced by the number 6.1 or 9.0, respectively.

assuming also (as previously)  $\kappa \doteq (10^{-7} - 10^{-4}) \text{ m}^2/\text{s}$ , we rewrite criterion expressed by Ineq. (8.1) in the dimensional form:

$$(8.2) \quad t \geq t_{\text{long}} = t_{2/1} \doteq \begin{cases} 3.2 \cdot (10^{-1} - 10^{-4}) \text{ s}, & \text{for } 2h \doteq 10^{-3} \text{ m}, \\ 3.2 \cdot (10 - 10^{-2}) \text{ s}, & \text{for } 2h \doteq 10^{-2} \text{ m}. \end{cases}$$

Let us note by the way, comparing Ineqs. (8.1) [(8.2)] and (7.4), that the latter one is always fulfilled in the long-time regime.

If the criterion expressed by Ineq. (8.1) (or (8.2)) is satisfied, then the series in Eq. (4.1)<sub>3</sub> can be approximated by its first term only, which for  $\tau = \tau_{2/1} \cong 3.2 \cdot 10^{-2}$  is equal to about 0.59, whereas the whole series for  $\tau = 0$  is equal to unity (see [4]).

Thus, if the criteria expressed by Ineqs. (8.1) (or (8.2)) and (6.1) are satisfied, then the series in Eq. (4.1)<sub>3</sub> reduces to the first term, and the functions  $\delta$  in Eqs. (5.1) and (5.3) are neglected (the total relative error of this double approximation does not exceed  $(1 + O^*)^2 - 1 \cong 2O^*$ ). Then the quantity  $U_{\text{max}}$ , and therefore also the functions  $U^u - U^u(r = 0)$ ,  $U_l$ ,  $D$  and  $f$  - depend on time exponentially:

$$(8.3) \quad \begin{aligned} U_{\text{max}} &= U_{\text{max}}(0) \frac{8}{\pi^2} \exp[-\pi^2 \tau], \\ U^u &= U_{\text{max}}(0) \left\{ \frac{1}{3} \left( \frac{2h}{r_0} \right)^2 + \left[ 1 - \left( \frac{r}{r_0} \right)^2 \right] \frac{8}{\pi^2} \exp[-\pi^2 \tau] \right\}, \\ U_l &= -U_{\text{max}}(0) \left[ 1 - \left( \frac{r}{r_0} \right)^2 \right] \frac{8}{\pi^2} \exp[-\pi^2 \tau], \\ D_l^u &= \frac{1}{f_l^u} = \mp \frac{4}{r_0^2} U_{\text{max}}(0) \frac{8}{\pi^2} \exp[-\pi^2 \tau], \end{aligned}$$

where the superscript  $u$  and the upper sign refer to the upper surface of the plate, and the subscript  $l$  and the lower sign  $-$  to the lower surface, and  $U_{\text{max}}(0)$  is defined by the equation following Eqs. (7.5). The deflection angle

$$(8.4) \quad \begin{aligned} \varepsilon_l^u &= \mp 2 \arctan \left[ \frac{16}{\pi^2} \frac{U_{\text{max}}(0)}{r_0} \frac{r}{r_0} \exp[-\pi^2 \tau] \right] \\ &\cong \mp \frac{32}{\pi^2} \frac{U_{\text{max}}(0)}{r_0} \frac{r}{r_0} \exp[-\pi^2 \tau] \end{aligned}$$

depends exponentially on time only in the paraxial optics approximation (the approximated part of Eq. (8.4)), which holds (with an accuracy to  $O^*$ ), if (cf. Ineq. (2.2))

$$\frac{256}{\pi^4} \frac{U_{\text{max}}^2(0)}{r_0^2} \left( \frac{r}{r_0} \right)^2 \exp[-2\pi^2 \tau] \leq \frac{3O^*}{1 + O^*} \cong 3O^*$$

(the total relative error of this triple approximation does not exceed  $(1 + O^*)^3 - 1 \cong 3O^*$ ).

Let us note by the way, that  $\tau$  can not be too large. The plate is assumed to be adiabatically insulated on all its surfaces. This assumption can be violated, after sufficiently long time, at least by the radiation heat exchange between the plate and its surroundings. The (dimensionless) relaxation time for the latter process  $\tau_{\text{rad}}$  (in the time scale applied in the paper) may be estimated as follows. We start from the heat conduction equation with no heat sources, assuming the boundary conditions in the form (see Footnote 3):

$$\frac{\partial \Theta}{\partial \zeta} \left( \zeta = \frac{1}{2} \right) = -\beta_1 \Theta \left( \zeta = \frac{1}{2} \right), \quad \frac{\partial \Theta}{\partial \zeta} \left( \zeta = -\frac{1}{2} \right) = \beta_2 \Theta \left( \zeta = -\frac{1}{2} \right),$$

where  $\beta_1, \beta_2$  stand for (dimensionless) coefficients of surface losses (assumed to be constants). The solution of the heat conduction equation with these boundary conditions (as obtained using the Fourier method of separating the independent variables) has the form:

$$\Theta = \sum_{k=1}^{\infty} \exp[-\mu_k^2 \tau] \left[ A_k \cos \mu_k \left( \zeta + \frac{1}{2} \right) + B_k \sin \mu_k \left( \zeta + \frac{1}{2} \right) \right],$$

where  $\beta_2 A_k = \mu_k B_k$ , coefficients  $A_k$  (or  $B_k$ ) are (in principle) determinable from an initial condition, and  $\mu_k$  stands for positive solutions of the following characteristic equation:

$$\tan \mu = \frac{\mu(\beta_1 + \beta_2)}{\mu^2 - \beta_1 \beta_2}.$$

For small surface losses ( $\beta_1, \beta_2 \ll 1$ ) one may obtain (in the linear approximation):

$$\mu_k \cong k\pi + \frac{1}{k\pi} (\beta_1 + \beta_2),$$

therefore:

$$\exp[-\mu_k^2 \tau] \cong \exp[-k^2 \pi^2 \tau] \exp[-2(\beta_1 + \beta_2) \tau].$$

Thus, the (dimensionless) relaxation time connected with the surface losses is

$$\tau_{\text{rel}} \cong \frac{1}{2(\beta_1 + \beta_2)}.$$

If the plate loses its energy through its surfaces by thermal radiation only, then using the linearized Stefan-Boltzmann law one may write:

$$\beta_1 = \beta_2 = \frac{2h}{\kappa} \frac{4b \sigma_{SB} T_0^3}{\rho_0 c_p},$$

where  $\sigma_{SB}$  stands for the Stefan – Boltzmann constant,  $b$  – for a correction factor for a real body as compared with the perfectly black one, and  $T_0$  – for the initial temperature (before the perturbation); thus,

$$\tau_{\text{rad}} = \frac{\kappa}{2h} \frac{\varrho_0 c_p}{8b \sigma_{SB} T_0^3}.$$

The thermal radiation losses can be therefore neglected, if the observation time  $\tau$  is much shorter than  $\tau_{\text{rad}}$ :

$$\tau \leq \tau_{\text{max}} := O^* \tau_{\text{rad}} = O^* \frac{\kappa}{2h} \frac{\varrho_0 c_p}{8b \sigma_{SB} T_0^3},$$

where  $O^*$  stands for an assumed small number.

Assuming (in addition to the assumptions of this kind adopted previously):

- $b \doteq 0.1$ ,
- $\sigma_{SB} \cong 5.67 \cdot 10^{-8} \text{ J}/(\text{m}^2 \text{ s K}^4)$ ,
- $T_0 \doteq 3 \cdot 10^2 \text{ K}$ ,

we have (in dimensionless and in dimensional forms):

$$(8.5) \quad \begin{aligned} \tau \leq \tau_{\text{max}} &\doteq \begin{cases} 4 \cdot (1 - 10^3), & \text{for } 2h \doteq 10^{-3} \text{ m,} \\ 4 \cdot (10^{-1} - 10^2), & \text{for } 2h \doteq 10^{-2} \text{ m,} \end{cases} \\ t \leq t_{\text{max}} &\doteq \begin{cases} 40 \text{ s,} & \text{for } 2h \doteq 10^{-3} \text{ m,} \\ 4 \cdot 10^2 \text{ s,} & \text{for } 2h \doteq 10^{-2} \text{ m.} \end{cases} \end{aligned}$$

This criterion restricts the applicability of the theory presented, however there still remains a relatively large field for application of the long-time regime (as it is seen by comparison of Ineqs. (8.5) with (8.1) [(8.2)]). Thus, the long-time regime seems to be a realistic and useful supplement to the short-time regime<sup>(10)</sup>. It starts relatively quickly. The values of  $U_{\text{max}}$  at the beginning of this regime are only a dozen percent lower than the initial value of  $U_{\text{max}}$ . By comparing Ineqs. (8.1) and (7.1) one may see, that for  $O^* = 0.01$  both regimes – the short- and the long-time ones – cover the full time range from  $\tau_{\text{min}}$  to  $\tau_{\text{max}}$  (for smaller  $O^*$  the situation is not so comfortable – see Footnotes 7 and 9).

## 9. Estimations for possible experiments

### 9.1. Introductory remarks

In principle, the thermal mirror considered may be experimentally studied by investigating the functions:  $U$ ,  $\varepsilon$  and  $f$ . Each of these quantities can be experimentally investigated and interpreted using the theoretical scheme presented, if some conditions are fulfilled.

<sup>(10)</sup> Supplement only, because of the restriction mentioned in Subsec.9.2 (see also estimations given in Subsecs.9.3, 9.4, 9.5, and cf. Ineq. (9.1) and Ineqs. (9.3), (9.4), (9.5)).

## 9.2. General conditions

Some general conditions, which should be taken into account in any experiment, were discussed earlier. Here the last such a condition will be mentioned. It follows from the requirement that the heat perturbation can not significantly change the properties of the material. Assuming the perturbation region to be a layer of thickness  $\Delta h$ , and the temperature not to exceed some critical value  $T^*$ , we can write this requirement in the form:

$$Q_{\text{tot}} \leq Q_{\text{max}} := \rho_0 c_p T^* \Delta h \pi r_0^2.$$

Assuming (in addition to the assumptions of this kind adopted previously):

- $T^* \doteq 2 \cdot 10^2 \text{ K}$ ,
- $\Delta h \doteq 0.05 \cdot (2h)$ ,

we have:

$$(9.1) \quad \begin{aligned} Q_{\text{tot}} \leq Q_{\text{max}} &\doteq \begin{cases} 15 \text{ J}, & \text{for } 2h \doteq 10^{-3} \text{ m}, \\ 1.5 \cdot 10^4 \text{ J}, & \text{for } 2h \doteq 10^{-2} \text{ m}, \end{cases} \\ \frac{Q_{\text{tot}}}{\pi r_0^2} \leq \frac{Q_{\text{max}}}{\pi r_0^2} &\doteq \begin{cases} 5 \cdot 10^4 \text{ J/m}^2, & \text{for } 2h \doteq 10^{-3} \text{ m}, \\ 5 \cdot 10^5 \text{ J/m}^2, & \text{for } 2h \doteq 10^{-2} \text{ m}. \end{cases} \end{aligned}$$

Comparing the conditions expressed by Ineqs. (9.1) and (6.2) one may see, that the latter is weaker than the former one, i.e. if Ineq. (9.1) is satisfied, then the functions  $\delta$  can be neglected in all the previous formulae.

## 9.3. Observability conditions for $U$

According to Eqs. (7.5) and (8.3) (for the short- and the long-time regimes, respectively), the condition for the minimum pulse energy  $Q_{\text{tot}}$  allowing  $U$  to be observable on the level at least of  $U^*$  can be written in the form:

$$Q_{\text{tot}} \geq Q_{\text{min}}^U := U^* \frac{\rho_0 c_p}{\alpha} (2h)^2 \frac{\pi}{3} \frac{1}{1 - \left(\frac{r}{r_0}\right)^2} \psi(\tau),$$

where

$$(9.2) \quad \psi(\tau) \cong \begin{cases} \left[1 - \frac{4}{\sqrt{\pi}} \sqrt{\tau}\right]^{-1} & \text{in the short-time regime,} \\ \frac{\pi^2}{8} \exp[\pi^2 \tau] & \text{in the long-time regime,} \end{cases}$$

and the contribution of  $N_T$  to  $U^u$  was neglected.

Assuming (in addition to the assumptions of this kind adopted previously):

- $U^* \doteq 10^{-6}$  m,
- $r \ll r_0$ ,
- $\tau \doteq 7 \cdot 10^{-2}$  (see Ineqs. (7.1) and (8.1))

we have:

$$(9.3) \quad Q_{\text{tot}} \geq Q_{\text{min}}^U \doteq \begin{cases} 1 \text{ J}, & \text{for } 2h \doteq 10^{-3} \text{ m}, \\ 10^2 \text{ J}, & \text{for } 2h \doteq 10^{-2} \text{ m}, \end{cases}$$

$$\frac{Q_{\text{tot}}}{\pi r_0^2} \geq \frac{Q_{\text{min}}^U}{\pi r_0^2} \doteq 4 \cdot 10^3 \text{ J/m}^2$$

(cf. Ineqs. (9.1), (9.4) and (9.5)).

#### 9.4. Observability conditions for $\varepsilon$

According to Eqs. (7.6) and (8.4) (for the short- and the long-time regimes, respectively) the condition for the minimum pulse energy  $Q_{\text{tot}}$  allowing  $\varepsilon$  to be observable on the level at least of  $\varepsilon^*$  can be written in the form:

$$Q_{\text{tot}} \geq Q_{\text{min}}^\varepsilon := \varepsilon^* \frac{\varrho_0 c_p}{\alpha} (2h)^2 \frac{1}{12} \frac{\pi r_0^2}{r} \psi(\tau),$$

where  $\psi(\tau)$  is given by Eq. (9.2).

Assuming (in addition to the assumptions of this kind adopted previously):

- $\varepsilon^* \doteq 10^{-4}$  rad,
- $r \cong r_0$

we have:

$$(9.4) \quad Q_{\text{tot}} \geq Q_{\text{min}}^\varepsilon \doteq \begin{cases} 3 \cdot 10^{-1} \text{ J}, & \text{for } 2h \doteq 10^{-3} \text{ m}, \\ 3 \cdot 10^2 \text{ J}, & \text{for } 2h \doteq 10^{-2} \text{ m}, \end{cases}$$

$$\frac{Q_{\text{tot}}}{\pi r_0^2} \geq \frac{Q_{\text{min}}^\varepsilon}{\pi r_0^2} \doteq \begin{cases} 10^3 \text{ J/m}^2, & \text{for } 2h \doteq 10^{-3} \text{ m}, \\ 10^4 \text{ J/m}^2, & \text{for } 2h \doteq 10^{-2} \text{ m} \end{cases}$$

(cf. Ineqs. (9.1), (9.3) and (9.5)).

#### 9.5. Observability conditions for $f$

According to Eqs. (7.5) and (8.3) (for the short- and the long-time regimes, respectively), the minimum pulse energy  $Q_{\text{tot}}$  allowing  $f$  to be observable on the level not higher than  $f^*$  can be written in the form:

$$Q_{\text{tot}} \geq Q_{\text{min}}^f := \frac{1}{f^*} \frac{\varrho_0 c_p}{\alpha} (2h)^2 \frac{1}{12} \pi r_0^2 \psi(\tau),$$

where the function  $\psi(\tau)$  is given by Eq. (9.2).

Assuming (in addition to the assumptions of this kind adopted previously)

- $f^* \doteq 40$  m

we have:

$$(9.5) \quad Q_{\text{tot}} \geq Q_{\text{min}}^f \doteq \begin{cases} 0.8 \text{ J}, & \text{for } 2h \doteq 10^{-3} \text{ m}, \\ 8 \cdot 10^3 \text{ J}, & \text{for } 2h \doteq 10^{-2} \text{ m}, \end{cases}$$

$$\frac{Q_{\text{tot}}}{\pi r_0^2} \geq \frac{Q_{\text{min}}^f}{\pi r_0^2} \doteq \begin{cases} 3 \cdot 10^3 \text{ J/m}^2, & \text{for } 2h \doteq 10^{-3} \text{ m}, \\ 3 \cdot 10^5 \text{ J/m}^2, & \text{for } 2h \doteq 10^{-2} \text{ m} \end{cases}$$

(cf. Ineqs. (9.1), (9.3) and (9.4)).

### 10. Possible applications for determining the temperature conductivity (and the surface losses coefficients)

As it is seen from the suitable formulae given above (after coming back to dimensional time  $t = \tau (2h)^2 / \kappa$ ), the time evolution of the thermal mirror depends, among others, on temperature conductivity  $\kappa$  of the material. Measuring suitable properties of the mirror it is therefore possible to determine  $\kappa$ . However, as it is seen from the formulae mentioned, such a procedure performed in arbitrary conditions may require some additional information (which should be known or measured), and may prove to be complicated for interpretation.

The problem simplifies in the short-time and the long-time regimes. In fact, as it follows from Eqs. (7.5) and (7.6), in the short-time regime the quantities:  $U$ ,  $\tan(\varepsilon/2)$ , and  $f$  are linear functions of  $\sqrt{t}$  with coefficient (at  $\sqrt{t}$ ) equal to  $4\sqrt{\kappa}/(2h\sqrt{\pi})$ . Measuring the evolution of these quantities one may therefore determine this coefficient and, knowing it and the plate thickness  $2h$  of the plate – find  $\kappa$  of a given material.

Analogously, as it follows from Eqs. (8.3) and (8.4), logarithms of the following quantities:  $U^u(r=0) - U^u(r)$ ,  $|U_l|$ ,  $|\tan(\varepsilon/2)|$  and  $|f|$  in the long-time regime are linear functions of time  $t$  with the coefficient (at  $t$ ) equal to  $\pi^2 \kappa / (2h)^2$ . Measuring the evolution of these quantities one may therefore determine this coefficient, and knowing it and the plate thickness  $2h$  – determine  $\kappa$  of a given material.

By the way let us note shortly, that one may think also on applying the thermal mirrors considered for experimental determining the surface losses coefficients  $\beta_1$ , or  $\beta_2$  (see the end of Sec.8), if the temperature conductivity  $\kappa$  of a given material is known. Using equations given at the end of Sec.8 for  $\Theta$  and suitable equations for the optical characteristics of the mirror, and applying the same argumentation as it was used for specification the long-time regime, one may conclude that for sufficiently long time the suitable optical characteristics  $F$  of the mirror are simply proportional to  $\exp[-\mu_1^2 \tau]$ . From measurements of the time evolution of  $\ln|F|$  one may therefore determine the quantity  $\mu_1$ . Then from the

characteristic equation for  $\mu$  one may determine:  $\beta_2 = \mu_1 \tan \mu_1$ , if  $\beta_1 = 0$  (an ideal thermal insulation on the perturbed surface);  $\beta_1 = \mu_1 \tan \mu_1$ , if  $\beta_2 = 0$  (an ideal thermal insulation on the opposite surface);  $\beta_1 = -\mu_1 / \tan \mu_1$ , if  $\beta_2 = \infty$  (ideal losses on the opposite surface, realized for instance by a thermostat).

## 11. Remark on distortion of properties of optical mirrors

Absorption of light by mirrors in high power optical systems causes thermal deformation of the mirrors, and therefore changes their optical properties. The theory presented may be useful for estimations of such effects in light-pulse optical systems. In particular, the criteria given in Subsecs. 9.3, 9.4 and 9.5 may be useful (in reversed form) for estimation of the maximum allowable energy of light pulse, which do not distort optical properties of the mirrors over an assumed level.

## 12. Conclusions

The thermal mirrors created on the surfaces of a thin plate of an isotropic thermoelastic solid material by a heat pulse, which is applied to one of the plate surface and is homogeneous across this surface, is – within the approximations applied in the paper – an ideal (aberration-free) optical mirror. These mirror effects are relatively very small, however they may be studied experimentally using high precision optics. The variations of the optical properties of the mirror considered are comparable with those of the half-space thermal mirror [5], however, because the thin-plate thermal mirror is free of aberrations, therefore it seems to be easier for experimental research.

In general, the time dependence of the thin-plate thermal mirror is complicated. However, there exist two regimes: the short-time and the long-time ones, in which this dependence becomes much simpler and easy for interpretation. In these conditions the thermal mirror considered may be, in principle, used for experimental determination of the temperature conductivity of a material.

## Appendix. Detailed criteria for neglecting the functions $\delta$

### A.1. Criterion for neglecting $\delta^u$ in the formula for $U^u$

The relative error of neglecting the function  $\delta^u$  in Eq.(4.2)<sub>1</sub> does not exceed  $O^*$ , if the following criterion is satisfied:

$$\left[ \left( \frac{r}{r_0} \right)^2 - O^* \left( 1 + \frac{N_T}{E U_{\max}} \right) \right] \delta^u (2 + \delta^u) \leq O^* \left[ \left( 1 + \frac{N_T}{E U_{\max}} \right) - \left( \frac{r}{r_0} \right)^2 \right]$$

or

$$\left( \frac{r}{r_0} \right)^2 [O^* + \delta^u (2 + \delta^u)] \leq O^* (1 + \delta^u)^2 \left( 1 + \frac{N_T}{E U_{\max}} \right).$$

Three cases should be considered to analyze this criterion. If

$$\left(\frac{r}{r_0}\right)^2 \leq O^* \left(1 + \frac{N_T}{E U_{\max}}\right),$$

then the criterion considered is always satisfied for an arbitrary  $\delta^u$ , i.e. – for sufficiently small  $r$  the function  $\delta^u$  can be always neglected in Eq.(4.2)<sub>1</sub>.

If

$$O^* \left(1 + \frac{N_T}{E U_{\max}}\right) < \left(\frac{r}{r_0}\right)^2 < \left(1 + \frac{N_T}{E U_{\max}}\right),$$

then the criterion considered is satisfied for

$$\delta^u < \left(\frac{r}{r_0}\right) \frac{\sqrt{1 - O^*}}{\sqrt{\left(\frac{r}{r_0}\right)^2 - O^* \left(1 + \frac{N_T}{E U_{\max}}\right)}} - 1$$

or

$$\left(\frac{r}{r_0}\right)^2 < \frac{O^* (1 + \delta^u)^2 \left(1 + \frac{N_T}{E U_{\max}}\right)}{O^* + \delta^u (2 + \delta^u)}.$$

If, in particular,

$$\delta^u < \frac{1}{2} O^*,$$

then the latter inequality is satisfied for

$$\left(\frac{r}{r_0}\right)^2 \leq \frac{1}{2}.$$

If

$$\left(\frac{r}{r_0}\right)^2 \geq \left(1 + \frac{N_T}{E U_{\max}}\right),$$

then there exists no function  $\delta^u$  satisfying the criterion considered, i.e. – for sufficiently large  $r$  the function  $\delta^u$  can not be neglected in Eq.(4.2)<sub>1</sub> (however, this case may have only symbolical meaning, because of the approximation applied for solving the thermoelasticity equation, as it was mentioned at the beginning of Sec. 4).

#### A.2. Criterion for neglecting $\delta_l$ in the formula for $U_l$

Because the function  $\delta_l$  decreases from  $2\alpha T_\infty$  to  $-\alpha T_\infty$  as  $\tau$  varies from 0 to  $\infty$  (see Sec. 6), therefore the criterion for neglecting the function  $\delta_l$  in the formula for  $U_l$  should be examined separately for  $\delta_l \geq 0$  and  $\delta_l \leq 0$ .

**A.2.1. The case of  $\delta_l \geq 0$ .** The relative error of neglecting the function  $\delta_l \geq 0$  in Eq. (4.2)<sub>2</sub> does not exceed  $O^*$ , if the following criterion is satisfied.

$$\left[ \left( \frac{r}{r_0} \right)^2 + O^* \right] \delta_l (2 - \delta_l) \leq O^* \left[ 1 - \left( \frac{r}{r_0} \right)^2 \right]$$

or

$$\left( \frac{r}{r_0} \right)^2 [O^* + \delta_l (2 - \delta_l)] \leq O^* (1 - \delta_l)^2.$$

If  $r = 0$ , then this criterion is satisfied for an arbitrary  $\delta_l$ .

If  $r \neq 0$ , then the criterion considered is satisfied for<sup>(11)</sup>

$$\delta_l \leq 1 - \frac{r}{r_0} \frac{\sqrt{1 + O^*}}{\sqrt{\left( \frac{r}{r_0} \right)^2 + O^*}}$$

or

$$\left( \frac{r}{r_0} \right)^2 \leq \frac{O^* (1 - \delta_l)^2}{O^* + \delta_l (2 - \delta_l)}.$$

If, in particular,

$$\delta_l \leq \frac{1}{2} O^*,$$

then the latter inequality is satisfied for

$$\left( \frac{r}{r_0} \right)^2 \leq \frac{1}{2} \frac{\left( 1 - \frac{1}{2} O^* \right)^2}{1 - \frac{1}{8} O^*} \cong \frac{1}{2},$$

(exactly: for  $O^* = 0.01, 0.001, 0.0001$  the double right-hand side of this inequality is equal to 0.99126, 0.999125, 0.9999125, respectively).

**A.2.2. The case of  $\delta_l \leq 0$ .** The discussion and the conclusion in this case are exactly the same as in the case examined in Subsec. A.1 with  $N_T = 0$  and  $\delta^u$  replaced by  $|\delta_l|$ .

**A.3. Criterion for neglecting  $\delta^u$  in the formula for  $\varepsilon^u$**

The relative error of neglecting the function  $\delta^u$  in Eq. (5.1) for  $\varepsilon^u$  does not exceed  $O^*$ , if the following criterion is satisfied:

$$\arctan \left[ \frac{2U_{\max}}{r_0} \frac{r}{r_0} \right] \leq (1 + O^*) \arctan \left[ \frac{2U_{\max}}{r_0} \frac{r}{r_0} \frac{1}{(1 + \delta^u)^2} \right].$$

<sup>(11)</sup> This is a very fair condition in case of small  $r$ . If, for instance,  $r = 0.1r_0$  and  $O^* = 0.01$ , then this inequality reads:  $\delta \leq 0.2893$  (see Sec. 6 and cf. Sec.A.1).

Because  $x \arctan y \leq \arctan xy$  for  $x \leq 1$ ,  $y \ll 1$ , therefore this criterion may be replaced by the following stronger one:

$$(\delta^u)^2 + 2\delta^u - O^* \leq 0,$$

which is satisfied for

$$\delta^u \leq \sqrt{1 + O^*} - 1 \cong \frac{1}{2} O^*$$

(exactly: for  $O^* = 0.01$ ,  $0.001$ ,  $0.00001$  the double right-hand side of this inequality divided by  $O^*$  is  $0.9975$ ,  $0.99975$ ,  $0.99997$ , respectively).

#### A.4. Criterion for neglecting $\delta_l$ in the formula for $\varepsilon_l$

The relative error of neglecting the function  $\delta_l \geq 0$  in Eq. (5.1) for  $\varepsilon_l$  does not exceed  $O^*$ , if the following criterion is satisfied:

$$\arctan \left[ \frac{2U_{\max}}{r_0} \frac{r}{r_0} \right] \geq (1 - O^*) \arctan \left[ \frac{2U_{\max}}{r_0} \frac{r}{r_0} \frac{1}{(1 - \delta_l)^2} \right].$$

Because  $x \arctan y \geq \arctan xy$  for  $x \geq 1$ ,  $y \ll 1$ , therefore this criterion may be replaced by the following stronger one:

$$(\delta^u)^2 - 2\delta^u + O^* \geq 0,$$

which is satisfied for

$$\delta^u \leq \frac{1}{2} O^* \leq 1 - \sqrt{1 - O^*}.$$

The discussion and the conclusion in the case of  $\delta_l < 0$  are exactly the same as in the case examined in Subsec. A.3 with only  $\delta^u$  replaced by  $|\delta_l|$ .

#### A.5. Criteria for neglecting $\delta$ in the formulae for $D = 1/f$

The relative error of neglecting the functions  $\delta$  in Eqs. (5.3) does not exceed  $O^*$ , if the following criteria are satisfied:

$$\begin{aligned} \delta^2 + 2\delta - O^* &\leq 0, & \delta &= \delta^u, & -\delta_l &> 0, \\ \delta_l^2 - 2\delta_l + O^* &\geq 0, & \delta_l &> 0, & & \end{aligned}$$

for the upper surface and the lower one, respectively. These inequalities are satisfied for

$$\begin{aligned} \delta &\leq \sqrt{1 + O^*} - 1 \cong \frac{1}{2} O^*, & \delta &= \delta^u, & -\delta_l &> 0, \\ \delta_l &\leq \frac{1}{2} O^* \leq 1 - \sqrt{1 - O^*}, & \delta_l &> 0 & & \end{aligned}$$

(see and cf. Subsecs. A.3, A.4).

## A.6. Conclusion

The criteria for neglecting the functions  $\delta$  in the suitable formulae are different in various cases. In order to discuss this problem in a uniform way for all the cases, one needs a common criterion, which will be satisfied in all the cases. Such a criterion is proposed in Sec. 6 (see Ineq. (6.1)).

## Acknowledgment

The Authors would like to express thanks to Prof. Dr. M. SOKOŁOWSKI and his coworkers, Institute of Fundamental Technological Research, Warszawa, for fruitful and helpful discussions.

## References

1. B.A. BOLEY and J.H. WEINER, *Theory of thermal stresses*, J. Wiley, New York-London 1960.
2. M. BORN and E. WOLF, *Principles of optics*, Pergamon Press, Oxford-London 1968.
3. H.S. CARSLAW and J.C. JAEGER, *Conduction of heat in solids*, 2nd ed., Clarendon Press, Oxford, 1989; see also: A.V. LUIKOV, *Analytical heat diffusion theory* [transl. from Russian], Academic Press, New York-London 1968.
4. I.S. GRADSHTEYN and I.M. RYZHIK, *Tables of integrals, series and products* [transl. from Russian], Academic Press, New York-San Francisco-London 1965.
5. Z. PŁOCHOCKI, A. MIOUCHOWSKI and J.F. MAĆZYŃSKI, *An idea of half-space thermal mirror*, ZAMP, **46**, 339–354, 1995.

POLISH ACADEMY OF SCIENCES  
INSTITUTE OF FUNDAMENTAL TECHNOLOGICAL RESEARCH  
ul. Świętokrzyska 21, 00-049 WARSZAWA, POLSKA

and

UNIVERSITY OF ALBERTA  
DEPARTMENT OF MECHANICAL ENGINEERING, EDMONTON, CANADA  
e-mail: mioducho@sneezy.mece.ualberta.ca

Received July 5, 1996.

## Can the system of discrete vortices imitate a boundary layer ?

T. LIPNIACKI (WARSZAWA)

THE PROBLEM of dissipative flow of superfluid due to the vortex interaction with the boundary is considered within the hydrodynamics approximation. The numerical simulations were applied to show that, when the boundary starts moving, the vortices pinned to microscopic surface irregularities can stretch. The array of the growing vortices give rise to the specific boundary layer, which in some aspects is similar to the boundary layer in viscous fluids.

SUPERFLUID  $^4\text{He}$  behaves as an ideal fluid with rotation restricted to quantized vortex filaments. The experiments of AWSCHALOM and SCHWARZ [1] suggest that some remnant vortices are always expected to occur. The essentially hydrodynamics description of its dynamics is valid down to a scale comparable to the core radius of the vortex  $a_0$  which is of order  $1\text{\AA}$ . In the zero temperature limit, when the interaction between the vortex and the thermal excitation gas (the normal fluid) may be neglected, the motion of an individual quantized vortex  $S(\xi, t)$  (in local induction approximation – LIA) is accurately described by [2]

$$(1) \quad \dot{S} = \beta S' \times S'' + V_s,$$

where  $V_s$  is the local average superfluid velocity, and  $\beta = (\kappa/4\pi) * \ln(c_1/S'' a_0)$ , with  $c_1$  constant of order 1 and  $\kappa = h/m_{\text{He}}$  quantum of circulation. The primes denote differentiation with respect to arc length. The equation must be supplemented by a nonlocal interaction term when the vortex approaches another vortex or a boundary.

The aim of present paper is to consider the dynamics of vortices terminating on the flat infinite boundary. The problem of vortex dissipative line dynamics in relatively narrow channels has been already studied by SCHWARZ [3, 4] who pointed earlier [4] that the moving vortex may be pinned to the microscopic surface irregularities. We recall [5] that a vortex filament terminating on a perfectly smooth surface will move without hindrance. When the end of the vortex encounters a bump, however, it will remain pinned there until it bows over up to some critical angle with the surface. Next it jumps off and resumes its motion. Quantized vortices may pin on bumps of only a few Angströms, so that in practice this process is always expected to occur. Moreover Schwarz, while considering the static case, concluded that the depinning angle (angle between the vortex end and the normal to the surface) depends logarithmically on the size of the pinning site. It means that the leading role may be played by small protrusions which are more abundant. SCHWARZ [3, 4] found that the pinning and release process

makes the vortex line elongate across the channel. In such a process the energy is dissipated by being fed into the growing vortex lines which then annihilate at the opposite wall. The vortices also transfer the momentum between the boundary and the superfluid; the vortex exerts the stream-wise force on the boundary via its interaction with the pinning site. Respectively, the boundary must be exerting a retarding force on the superfluid via its interaction with the vortex.

In some important aspects, the vortex dynamics in the vicinity of a single surface is different from the dynamics described by Schwarz in narrow channels. First of all, vortices can not be spanned between perpendicular or opposite walls, and second, there is no opposite wall to annihilate the growing vortices.

Consider at the beginning the simple example of a vortex pinned to  $z = 0$  plane and subjected to the applied velocity  $v_s$  in the  $\hat{x}$  direction. Assume that initially the vortex filament having the shape of a half circle of radius  $R$  lies in plane  $x = 0$  (i.e. plane perpendicular to the applied velocity and the boundary plane). If the driving velocity is equal in the value but opposite in direction to the self-induced velocity

$$(2) \quad v_i = \frac{\beta}{R} := v_{\text{cr}},$$

the configuration is stationary. The higher applied velocity bends the vortex stream-wise and stretches it out. At some critical angle of declination (i.e. depinning angle dependent on the size of pinning site) the ends of the vortex depin. If the driving velocity is smaller than the critical one, the vortex bows against the flow and decreases. The vortex oriented in another direction, so that the driving velocity adds to the self-induced one, will bow with the flow, but then the self-induced velocity directs it to the boundary, where it annihilates. The numerical simulations done by the author confirm the above considerations.

Statistically, when the driving velocity is applied (or the boundary starts moving), roughly a half of the pinned vortices has a chance to grow, other will annihilate. It means that the motion of the boundary introduces some order, and it is easy to check that the orientation of the remaining vortices is such, that close to the boundary the superfluid is moving in the same direction as the wall.

As it was stated above, the end of vortex depins at some critical angle, dependent on the size of the pinning site, and then moves freely till the next bump. The two end points of a filament may encounter various irregularities and consequently must depin simultaneously. Hence, one can conclude, from the preceding analysis that a “well oriented” big enough vortex loop will grow any time, when pinned, while other loops will decrease. The situation simplifies when the small protrusions occur so densely, that the pinning and release events are so frequent, that the intermittent motion of vortex end points may be approximated by a continuous motion with friction. When the friction is present, the moving end of vortex is bowed to the boundary at such angle that tangent component of tension

force equals the friction force  $f_s$ . Namely

$$(3) \quad \sin \Theta = \frac{f_s}{f_t},$$

where  $\Theta$  is the angle between the vortex at its end points and the normal to the boundary, and  $f_t$  is the value of tension force. The angle  $\Theta$ , corresponding to the average angle of declination, may be considered as the material constant depending on the density and the size of boundary irregularities. It means that for normally “smooth” surface  $\sin \theta$  is small when compared to unity.

Consider then the following example:

Let the boundary plane  $z = 0$  be moving with constant velocity  $V_d = (V_d, 0, 0)$  with respect to the fluid. Consider the dynamics of a vortex which at the initial time has the shape of a half circle symmetrically placed with respect to plane  $y = 0$ , and the driving velocity. Assume that the self-induced velocity  $V_i$  is smaller than the driving velocity  $V_d$ , and that the vortex loop is moving so that the angle between the vortex at its end points and the normal to the boundary is  $\Theta$ . The self-induced velocity (in LIA), at the given point of the vortex, is binormal to the vortex line at that point. Hence, at the ends of the vortex, the angle between the self-induced velocity and the wall is  $\theta$ , but for one (*positive*) orientation of the vortex the self-induced velocity is directed out from the wall, and for another (*negative*) orientation it is directed to the boundary. For the positive orientation the vortex loop will be growing. The rate of growth may be calculated as follows: let  $a$  be a point moving with the vortex and  $p$  be a vortex end point (Fig. 1).

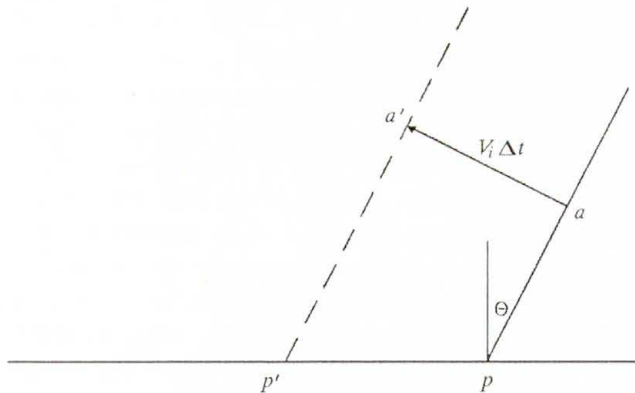


FIG. 1. Fragment of the vortex close to the boundary. The vortex moves so that point  $a$  goes to  $a'$  while end point  $p$  goes to  $p'$ . Vector  $\overline{ap}$  is parallel to the vector  $\overline{a'p'}$ .

In a short time  $\Delta t$  the point  $a$  moves to  $a' = a + \Delta t V_i$ . In the same time the end point moves to such a point  $p'$  that  $\overline{a'p'}$  is parallel to  $\overline{ap}$ . If so, the initial fragment of vortex line grows up by  $\Delta t V_i \sin \Theta$ . Because there are two ends, the

vortex growing rate  $\partial l/\partial t$  satisfies the condition

$$(4) \quad \frac{\partial l^+}{\partial t} = 2V_i(t) \sin \Theta,$$

where + means the growing vortex. The oppositely oriented vortex is decreasing at the rate

$$(5) \quad \frac{\partial l^-}{\partial t} = -2V_i(t) \sin \Theta,$$

where sign – means a shrinking vortex.

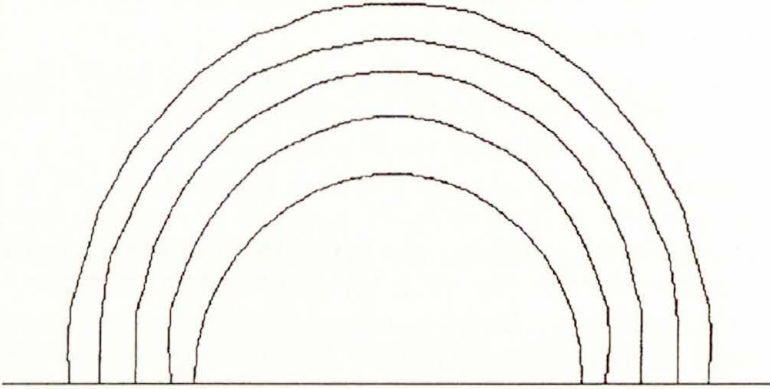


FIG. 2. Motion of a vortex when friction is present. The figure shows the projection of vortex filament on the plane perpendicular to the boundary and the driving velocity.

It may look curious that the driving velocity does not appear in Eqs. (4), (5). However it plays an important role: only these vortex loops for which the self-induced velocity is smaller than the imposed one, can grow. So for bigger driving velocity another smaller loops can grow, and as one can see from the last equation, smaller loops grow faster. It should be said also, that Eqs. (4), (5) are not valid for the driving velocities only slightly bigger than the critical one. When there is no friction (i.e. for  $\Theta = 0$ ), the vortex maintains its shape of a half circle. Also for small declination angles ( $\sin \Theta < 0.3$ ), numerical simulations (Fig. 2) show that the vortex grows maintaining approximately the shape of a half circle. For bigger declination angles, however, the vortex becomes elongated. The instant radius of uniformly growing loop is  $R = l/\pi$ , while its self-induced velocity is  $v_i = \beta/R$ . Those relations put into Eqs. (4), (5) give the equation for  $R(t)$ :

$$(6) \quad \frac{\partial R^\pm}{\partial t} = \pm \frac{2\beta \sin \Theta}{\pi R}$$

leading to

$$(7) \quad R^\pm = \left( \pm \frac{4\beta t \sin \Theta}{\pi} + R_0^2 \right)^{1/2}.$$

Consider now the array of vortices with end points on the boundary. If at time  $t = 0$  the boundary wall starts moving with some constant velocity  $V_b$ , some vortices will grow and some will decrease. As a result, a layer of superfluid close to the boundary starts moving in the same direction as the wall.

To consider this mechanism in more detail, assume that, at the time  $t = 0$ :

- all vortices have the shape of the half circle of the same radius  $R_0$ ;
- the vortex loops form a regular pattern where half of the loops have positive orientation (positive vortices) and another half has the negative orientation (negative vortices);
- the driving velocity  $V_b$  is bigger than the initial critical one so the positive vortices can grow (i.e.  $V_b > \beta/R_0$ );
- the declination  $\Theta$  is small, so as was stated above, the vortex loops maintain their shape of a half circle;
- there are  $n$  growing vortices and  $n$  decreasing.

Then Eq. (7) allows to calculate the average velocity at a given distance from the wall  $z$ . The velocities  $V^+$  and  $V^-$  generated by positive and negative vortices, respectively, will be calculated separately. The resultant velocity is  $V = V^+ - V^-$ .

The average velocity  $V^+$  (at a given distance  $z$ ) may be calculated from the Ampere principle. Let  $F$  be the surface  $z = z_0$ . For  $z_0 < R^+ \cos \Theta$  that surface is pierced twice by every vortex loop. The distance between the piercing points, (or the diameter of "the cut-off" loop segment) is:

$$(8) \quad s^+ = 2 \left( (R^+)^2 - z^2 / \cos^2 \Theta \right)^{1/2} \quad \text{for } z < R^+ \cos \Theta.$$

Above the large square lying on the surface  $F$  there are  $N_s = nA^2$  positive loops (where  $A$  is the side of the square). It means that in average, above a line with length  $A$  lying on  $F$  along the  $\hat{x}$  axis, there are  $N_a = s^+ An$  vortex segments. Then from the Ampere principle, which states that the circulation of the velocity field around a closed path is equal to the flux of the vorticity linked through this path, the average induced velocity is

$$(9) \quad V^+ = s^+ \kappa n.$$

The  $V^-$  velocity may be calculated similarly. In the explicit form both velocities read:

$$(10) \quad V^\pm(z, t) = \kappa n \left( \pm \frac{4\beta t \sin \Theta}{\pi} + R_0^2 - \frac{z^2}{\cos^2 \Theta} \right)^{1/2}.$$

At the time  $T_c = \pi R_0 / (4\beta \sin \Theta)$  the decreasing loops vanish, and so, the velocity  $V^-$  becomes zero everywhere.

For times  $t < T_s$  the induced velocity  $V$  is:

$$(11) \quad V = \begin{cases} 0 & \text{for } z > R^+ \cos \theta, \\ V^+ & \text{for } z \in (R^- \cos \Theta, R^+ \cos \theta), \\ V^+ - V^- & \text{for } z \in (0, R^- \cos \Theta). \end{cases}$$

For times  $t > T_s$ ,  $V$  is:

$$(12) \quad V = \begin{cases} 0 & \text{for } z > R^+ \cos \theta, \\ V^+ & \text{for } z \in (0, R^+ \cos \theta), \end{cases}$$

since  $V^- \equiv 0$ .

One can see from Eq. (12) that the thickness of the boundary layer (i.e. that layer where the velocity  $V > 0$ ) grows as  $R_+ \cos \theta$  proportionally to  $\sqrt{\beta t \sin \Theta}$ . The induced velocity has the same direction as the velocity of the boundary, so it reduces the relative velocity between the superfluid and the boundary.

Recall that velocity of a viscous fluid in the boundary layer appearing when the wall starts moving with some constant velocity  $v_b$ , is described by the diffusion equation:

$$(13) \quad \frac{\partial v}{\partial t} - \nu \frac{\partial^2 v}{\partial z^2} = 0.$$

The usual assumption that there is no slip, leads to the boundary condition  $v(0, t) = v_b$ . Then with the initial condition  $v(z, 0) = v_b$  the equation leads to

$$(14) \quad v(z, t) = v_b \Phi \left( \frac{z}{2\sqrt{\nu t}} \right),$$

where

$$(15) \quad \Phi(x) = \frac{2}{\sqrt{\pi}} \int_0^x e^{-\alpha^2} d\alpha.$$

One can see that in a viscous fluid, the characteristic thickness of the boundary layer is  $\sqrt{\nu t}$ .

In the considered "vortex boundary layer", if there are few vortices at the beginning, there is a slip i.e. the fluid velocity at the boundary is different from the velocity of the wall. The role of the viscosity is played here by the parameter  $\beta \sin \Theta$  – proportional to the quantum of circulation and surface roughness. The fact that the "nonsmooth" velocity profiles were obtained is due to the assumption, that at the beginning all vortex loops were identical.

In conclusion, a consideration of vortex friction on microscopic boundary roughness leads to the mechanisms of the origin of specific vortex boundary layer in some aspects similar to the boundary layer in viscous fluids. It is still interesting, however, to consider that problem under more general assumptions, namely when there are different vortices and they interact with each other.

## Acknowledgments

The author is grateful to prof. Z. PERADZYŃSKI for helpful discussion and support.

## References

1. D.D. AWSCHALOM and K.W. SCHWARZ, Phys. Rev. Lett., **52**, 49, 1984.
2. H.E. HALL and H.E. VINEN, Proc. R. Soc. London, Ser. A **238**, 204, 1956.
3. K.W. SCHWARZ, Phys. Rev. Lett., **57**, 1448, 1986.
4. K.W. SCHWARZ, Phys. Rev. Lett., **69**, 3342, 1992.
5. K.W. SCHWARZ, Phys. Rev., **B 31**, 5782, 1985.

POLISH ACADEMY OF SCIENCES  
INSTITUTE OF FUNDAMENTAL TECHNOLOGICAL RESEARCH  
ul. Świętokrzyska 21, 00-049 Warszawa, Polska.

*Received July 24, 1996.*

---

# Unsteady compressible boundary layer flow at the stagnation point of a rotating sphere with an applied magnetic field

A. SAU and G. NATH (BANGALORE)

THE PAPER is concerned with the unsteady compressible boundary layer flow near the forward stagnation point of a rotating sphere in a uniform axial stream of conducting fluid, with magnetic field normal to the surface. The unsteadiness in the flow is created by (i) giving a sudden change in the wall temperature (enthalpy) as the impulsive motion has started, (ii) impulsive change of the rotation of the sphere, and (iii) sudden changing of the free stream velocity. The motion is governed by a coupled set of three nonlinear time-dependent partial differential equations which are solved accurately by Newton's linearization technique and an implicit finite difference scheme. Attention is given to the transient phenomenon from the initial flow to the final steady state solution. The numerical results show changes in the flow pattern with time, rotation and strength of the magnetic field, and are in good agreement with earlier theoretical results. The calculated skin friction, heat transfer, displacement thickness and enthalpy thickness show interesting dependence on time and the physical parameters, which are quite similar to the earlier investigations, and the mechanism of dependence is closely examined.

## 1. Introduction

CURRENT USE of blunt bodies of revolution for the solution of hypersonic flight problems has placed special emphasis on accurate prediction of aerodynamic heating. Design of hypersonic re-entry vehicles such as a re-entering satellite requires reasonably accurate predictions of the stagnation point heat transfer to obtain optimum configurations. The high stagnation temperature accompanying flight at high Mach numbers renders the air sufficiently ionized behind the bow shock so that it may be considered as an electrically conducting fluid. Under these circumstances, the presence of a magnetic field will tend to modify both the flow field and the heat transfer.

An axisymmetric boundary layer flow over a rotational symmetric body set into impulsive axial motion was first studied by BOLTZE [1], who expanded the stream function and vorticity in series of powers of time ( $t$ ) after the impulsive start and obtained numerical solution for terms up to  $t^3$ . DENNIS and WALKER [2] improved the accuracy of Boltze solution by numerically computing the solution for terms up to  $t^7$ . The unsteady flow past an impulsively started sphere has also been discussed by DENNIS and WALKER [3] and the results were extended to larger values of time. The boundary layer growth near the equator of an impulsively started sphere was considered by BANKS and ZATUSKA [4]. The evolution of unsteady boundary layers close to the stagnation region of a slender prolate spheroid in uniform motion at constant angle of attack after an impulsive start have been discussed by CEBECI *et al.* [5]. DENNIS and DUCK [6] have presented

the Navier–Stokes solutions for an impulsively started rotating sphere. In a recent study DUCK [7] investigated the effect of small amplitude, time-periodic, free stream disturbances on the axisymmetric boundary layers. The unsteady boundary layer flow past an impulsively started translating and spinning, rotationally symmetric body has been studied by ECE [8], and he obtained initial stages of flow by expanding the stream function and swirl velocity in series of power of time. All the above studies deal with incompressible flows. KUMARI and NATH [9] have studied the unsteady compressible stagnation point boundary layer flow over a rotating body of revolution (sphere) when the free stream velocity, rotation, the surface mass transfer and the wall temperature varied arbitrarily with time. VIMALA and NATH [10] have solved the two-dimensional stagnation point flow for accelerating and oscillating free streams.

In this paper we evaluate the characteristics of unsteady compressible boundary layer flow of an electrically conducting fluid near the forward stagnation point of a rotating sphere, immersed in a uniform flow and having a normal magnetic field applied at the surface. Three separate situations have been considered in which there is an initial steady state that is perturbed by either (i) a step change in the wall enthalpy, (ii) a sudden change in the rotational velocity, and (iii) a sudden change in mainstream speed. The time-dependent development of the boundary layer is computed until a new steady state is reached. Extensive numerical results are presented showing the temporal development of various boundary layer properties.

## 2. Basic equations and boundary conditions

To fix the problem mathematically, we consider an orthogonal curvilinear coordinate system (Fig. 1) in which  $x$  measures the distance along a meridian from the forward stagnation point,  $y$  represents the distance in the direction of rotation, and  $z$  its distance normal to the body. We assume the flow to be axisymmetric and the external flow is homentropic, the dissipation terms and effect of surface curvature being negligible near the stagnation point;  $r(x)$ , the normal distance of a point on the body from the axis of rotation is equal to  $x$  in the neighbourhood of the pole (or stagnation point in this case). A uniform magnetic field of strength  $B_0$  is applied to the boundary layer in the  $z$ -direction. The magnetic Reynolds number is considered to be small, hence the magnetic field becomes independent of fluid motion. At time  $t \leq 0$ , the total enthalpy at the wall is  $H_w$ , and at  $t > 0$  it is impulsively changed to  $H_w^*$ . Alternatively, at time  $t \leq 0$ , the angular velocity of rotation is  $\Omega$ , and at  $t > 0$  it is impulsively changed to  $\Omega^*$ . Similarly at  $t \leq 0$ , the meridional component of free-stream velocity is  $u_e$ , and at time  $t > 0$  it is suddenly changed to  $u_e^*$ . These sudden changes cause unsteadiness in the flow field. Under the foregoing assumptions, the boundary layer equations for the unsteady

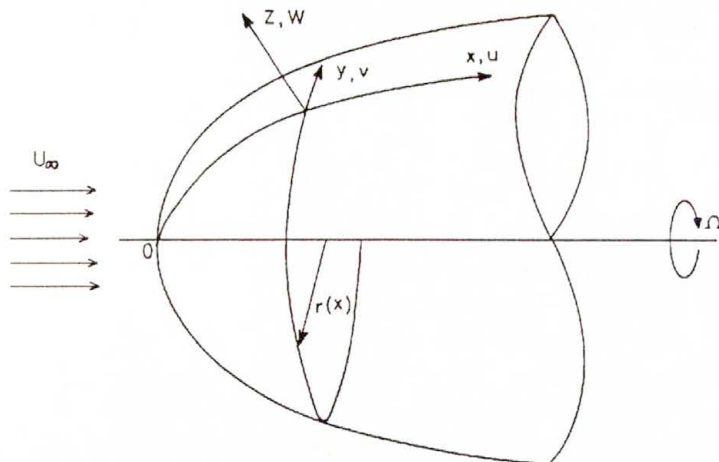


FIG. 1. Flow model and coordinate system for a rotating body of revolution.

compressible flow are given by [11, 12]

$$(2.1) \quad (\rho x)_t + (\rho x u)_x + (\rho x w)_z = 0,$$

$$(2.2) \quad \begin{aligned} \rho(u_t + uu_x + wu_z - v^2/x) &= \rho_e [(u_e)_t + u_e(u_e)_x] + (\mu u_z)_z - B_0^2(\sigma u - \sigma_e u_e), \\ \rho(v_t + vv_x + wv_z + uv/x) &= (\mu v_z)_z - \sigma B_0^2 v, \\ \rho(H_t + uH_x + wH_z) &= \left(\frac{\mu}{\text{Pr}} H_z\right)_z, \end{aligned}$$

where  $u$ ,  $v$ ,  $w$  are the velocity components along the  $x$ ,  $y$ ,  $z$  axes, respectively.  $\rho$ ,  $\mu$ ,  $\sigma$  and  $\text{Pr}$  are, respectively, the density, viscosity, electrical conductivity and the Prandtl number;  $H$  is the total enthalpy and  $u_e$  is the  $x$ -component of the flow velocity at the edge of the boundary layer. The subscripts denote the partial derivatives with respect to the corresponding variables.

The initial and boundary conditions are:

$$(2.3) \quad \begin{aligned} \text{at } t = 0: & \quad u(x, 0, z) = u_i(x, z), & \quad v(x, 0, z) = v_i(x, z), \\ & \quad w(x, 0, z) = w_i(x, z), & \quad H(x, 0, z) = H_i(x, z), \\ \text{and for } t > 0: & \quad u(x, t, 0) = 0, & \quad v(x, t, 0) = \Omega^* x, \\ & \quad w(x, t, 0) = w_w, & \quad H(x, t, 0) = H_w^*, \\ & \quad u(x, t, \infty) = u_e^*(x, t), & \quad v(x, t, \infty) = 0, \\ & & \quad H(x, t, \infty) = H_e. \end{aligned}$$

The subscripts  $i$ ,  $w$ ,  $e$  denote initial conditions, conditions at the wall and at the edge of the boundary layer, respectively.

### 3. Boundary layer transformations

Now we introduce the transformations

$$\eta = \left( \frac{2a\rho_e}{\mu_e} \right)^{1/2} \int_0^z \frac{\rho}{\rho_e} dz, \quad t^* = at,$$

$a$  is a constant having dimension (time)<sup>-1</sup>,

$$u = u_e F(\eta, t^*), \quad F = f', \quad u_e = ax,$$

$$v = v_w s(\eta, t^*), \quad v_w = \Omega x, \quad H = H_e g(\eta, t^*).$$

We assume that the fluid has variable properties  $\rho \propto T^{-1}$ ,  $\mu \propto T^\omega$ ,  $\sigma \propto T^n$ , where  $T$  is the temperature,  $0 < \omega \leq 1$  is the index in the power-law variation of viscosity and  $n$  is the exponent in the power-law variation of electrical conductivity of the fluid. The set of Eqs. (2.2), with the help of continuity Eq. (2.1) and the above transformations, reduce, respectively, to

$$(3.1) \quad \begin{aligned} (NF')' + fF' + (g - F^2)/2 + \lambda^2 s^2/2 - Mg(Fg^n - 1)/2 - Ft^*/2 &= 0, \\ (Ns')' + fs' - Fs - Msg^{n+1}/2 - st^*/2 &= 0, \\ (Ng')' + Prfg' - Prgt^*/2 &= 0, \end{aligned}$$

where  $F$ ,  $s$  and  $g$  are non-dimensional meridional and azimuthal velocity and non-dimensional total enthalpy, respectively. The prime and the subscript  $t^*$  denote the partial differentiation with respect to the variables  $\eta$  and  $t^*$ , respectively.

Use is made of the following relations:

$$\rho_e/\rho = T/T_e = h/h_e = H/H_e = g$$

(since  $h/h_e \rightarrow H/H_e$  at the stagnation region,  $h$  being the specific enthalpy),

$$N = \rho\mu/\rho_e\mu_e = (T/T_e)^{\omega-1} = g^{\omega-1}, \quad \sigma = \sigma_e(T/T_e)^n = \sigma_e g^n,$$

$\lambda = \Omega/a$  is the rotation parameter,

$$M = \frac{\text{ponderomotive force}}{\text{inertia force}} = \frac{\sigma_e B_0^2 x}{\rho_e u_e}.$$

The initial conditions are governed by the solution of the corresponding steady state equations obtained from Eqs. (3.1) by putting  $F_{t^*} = s_{t^*} = g_{t^*} = 0$  in them. As stated earlier, there will be three different cases under the present study and the relevant boundary conditions corresponding to each case are:

CASE 1. At time  $t^* \leq 0$ , let the wall enthalpy be  $H_w$  (constant), and at time  $t^* > 0$ , there is a sudden change  $\Delta_1$  in the wall enthalpy and it is then maintained

for subsequent time (i.e., for  $t^* > 0$ ,  $H_w^* = H_w(1 + \Delta_1)$ ), whereas free stream velocity in  $x$ -direction  $u_e$  and the angular velocity of rotation  $\Omega$  remain the same for all time. In such a case, the boundary conditions in non-dimensional form reduce to:

$$(3.2) \quad \begin{aligned} &\text{for } t^* > 0, \\ &f = f_w, \quad F = 0, \quad s = 1, \\ &g = g_w + \Delta, \quad (\Delta = \Delta_1 g_w) \quad \text{at } \eta = 0, \\ &F = 1, \quad s = 0, \\ &g = 1 \quad \text{as } \eta \rightarrow \infty, \\ &\text{and at } t^* = 0, \\ &\Delta = 0. \end{aligned}$$

CASE 2. In this case, instead of changing the wall enthalpy, a sudden change ( $\Omega^* = \Omega(1 + \Delta)$ ,  $\Delta = 0$  for  $t^* \leq 0$  and  $\Delta = \text{const}$  for  $t^* > 0$ ) in the angular velocity of rotation is considered, so that the boundary conditions in non-dimensional form become:

$$(3.3) \quad \begin{aligned} &\text{for } t^* > 0, \\ &f = f_w, \quad F = 0, \\ &s = 1 + \Delta, \quad g = g_w \quad \text{at } \eta = 0, \\ &F = 1, \quad s = 0, \\ &g = 1 \quad \text{as } \eta \rightarrow \infty, \\ &\text{and at } t^* = 0, \\ &\Delta = 0. \end{aligned}$$

CASE 3. An impulsive change in the free-stream velocity in meridional direction is considered in this case. For time  $t^* \leq 0$ , let the velocity be  $u_e$  and at time  $t^* = 0$ , an impulsive change  $u_e^* = u_e(1 + \Delta)$  to the free stream velocity is given and kept steady thereafter. So the boundary conditions in non-dimensional form reduce to:

$$(3.4) \quad \begin{aligned} &\text{for } t^* > 0, \\ &f = f_w, \quad F = 0, \\ &s = 1, \quad g = g_w \quad \text{at } \eta = 0, \\ &F = 1 + \Delta, \quad s = 0, \\ &g = 1 \quad \text{as } \eta \rightarrow \infty, \\ &\text{and at } t^* = 0, \\ &\Delta = 0, \end{aligned}$$

where

$$f = \int_0^\eta F d\eta + f_w \quad \text{and} \quad f_w = -(\rho w)_w (\text{Re } x/2)^{1/2} / \rho_e u_e$$

is constant under the assumption that  $(\rho w)_w$  is constant. The parameter  $f_w$  is called the mass transfer parameter and it corresponds to suction or injection, according to whether  $f_w > 0$  or  $f_w < 0$  and  $\text{Re}_x = u_e x / \nu_e$  is the local Reynolds number.

#### 4. Results and discussions

The time-dependent boundary layer Eqs. (3.1) subject to the boundary conditions (3.2) or (3.3) or (3.4) which correspond to the different types of flow situations considered and the initial conditions have been solved numerically using Newton's linearization method and an implicit finite difference scheme of the Crank-Nicolson type. The grid sizes that we have used are as follows:  $\delta t^* = 0.00025$  for  $t^* \leq 0.05$ ,  $\delta t^* = 0.001$  for  $0.05 < t^* \leq 0.1$ ,  $\delta t^* = 0.005$  for  $0.1 < t^* \leq 0.5$ ,  $\delta t^* = 0.01$  for  $t^* > 0.5$ , and  $\delta \eta = 0.01$  is kept fixed throughout the computation. The choice of grid lengths has been found to be optimum since further reduction does not affect the results at least up to the fourth decimal place. The selection of  $\delta \eta$  is made such that it does not affect the results, even when  $\eta = O((t^*)^{1/2})$  and  $t^*$  is small. The solutions were iterated until the convergence criterion based on the wall shear and the heat transfer parameters  $F'_w$ ,  $s'_w$ ,  $g'_w$  is satisfied, that is

$$\text{Maximum} \left[ |(F'_w)^{n+1} - (F'_w)^n|, |(s'_w)^{n+1} - (s'_w)^n|, |(g'_w)^{n+1} - (g'_w)^n| \right] < \delta_1,$$

where  $\delta_1$  is a tolerance parameter which was set equal to  $10^{-4}$  in the calculations.

The quantities of physical interest are the skin friction and heat transfer coefficients, displacement and enthalpy thicknesses. Based on  $u$ -velocity, the equation defining the skin friction coefficient is

$$C_{f_x} = \frac{2 \left( \mu \frac{\partial u}{\partial z} \right)_{\eta=0}}{\rho_e (u_e^2)_{t^*=0}} = 2^{3/2} \text{Re}_x^{-1/2} N_w F'_w = 2^{3/2} \text{Re}_x^{-1/2} \bar{C}_{f_x},$$

where  $\bar{C}_{f_x} = N_w F'_w$ .

Displacement and enthalpy thicknesses based on  $u$ -velocity are defined as [11]

$$\delta_x^* = \int_0^\infty [1 - \rho u / \rho_e u_e] dz = x (2\text{Re}_x)^{-1/2} \int_0^\infty (g - F) d\eta = x (2\text{Re}_x)^{-1/2} \bar{\delta}_x^*,$$

$$\bar{\delta}_x^* = \delta_x^* (2\text{Re}_x)^{1/2} / x;$$

$$\delta_{H_x} = \int_0^\infty \frac{\rho u}{\rho_e \mu_e} \left[ \frac{h}{h_e} - 1 \right] dz = x (2\text{Re}_x)^{-1/2} \int_0^\infty F(g-1) d\eta = x (2\text{Re}_x)^{-1/2} \bar{\delta}_{H_x},$$

$$\bar{\delta}_{H_x} = \delta_{H_x} (2\text{Re}_x)^{1/2} / x.$$

Analogously, we define the quantities based on  $v$ -profiles;

$$C_{fy} = \frac{2 \left( \mu \frac{\partial v}{\partial z} \right)_{\eta=0}}{\rho_e (u_e^2)_{t^*=0}} = 2^{3/2} \text{Re}_x^{-1/2} \lambda N_w s'_w = 2^{3/2} \text{Re}_x^{-1/2} \bar{C}_{fy},$$

where  $\bar{C}_{fy} = \lambda N_w s'_w$ ,

$$\delta_y^* = \int_0^\infty \frac{\rho v}{\rho_w v_w} dz = x(2\text{Re}_x)^{-1/2} \int_0^\infty g_w s d\eta,$$

$$\delta_{Hy} = \int_0^\infty \frac{\rho v}{\rho_w v_w} \left[ \frac{h}{h_e} - 1 \right] dz = x(2\text{Re}_x)^{-1/2} \int_0^\infty s g_w (g - 1) d\eta.$$

However, in the present study only  $\delta_x^*$  and  $\delta_{Hx}$  will be presented.

The heat transfer coefficient in terms of the Stanton number is

$$\text{St} = \frac{\left( \frac{\mu}{\text{Pr}} \frac{\partial H}{\partial z} \right)_{\eta=0}}{(H_e - H_w) \rho_e (u_e)_{t^*=0}} = \text{Pr}^{-1} (\text{Re}_x/2)^{-1/2} N_w g'_w / (1 - g_w) = (\text{Re}_x/2)^{-1/2} \bar{\text{St}},$$

where

$$\bar{\text{St}} = \text{Pr}^{-1} N_w g'_w / (1 - g_w).$$

$F'_w$  and  $s'_w$  are called skin friction parameters in the respective directions and  $g'_w$  is the heat transfer parameter.

**Table 1. Comparison of skin friction and heat transfer parameters ( $F'_w, g'_w$ ) with BADE [13] for  $\text{Pr} = 2/3, f_w = 0.0, \lambda = 0$  and  $M = 0$ .**

$\omega$	$g_w$	$F'_w$		$g'_w$	
		Present study	BADE [13]	Present study	BADE [13]
1.0	0.2	0.6304	0.6303	0.3437	0.3438
1.0	0.8	0.8565	0.8566	0.0910	0.0909
0.7	0.4	0.5838	0.5837	0.2125	0.2125
0.7	0.8	0.8203	0.8202	0.0866	0.0865
0.5	0.2	0.3445	0.3447	0.1797	0.1796
0.5	0.4	0.5139	0.5137	0.1846	0.1845

Computations have been carried out on a CYBER-992 computer for various values of  $f_w$  ( $-0.5 \leq f_w \leq 0.5$ ),  $\lambda$  ( $2 \leq \lambda \leq 10$ ),  $M$  ( $5 \leq M \leq 10$ ),  $\omega$  ( $0.5 \leq \omega \leq 1.0$ ) and  $g_w$  ( $0.6 \leq g_w \leq 2.2$ ). For all the results which we present here we have assumed the Prandtl number  $\text{Pr} = 0.72$  and  $n = 1.5$ . In order to

accommodate the rapid thickening of boundary layer as the impulsive motion has started, we have taken the far field conditions at  $\eta = \eta_\infty = 20$ . At this point we should mention that our steady equations for a stationary sphere and without magnetic field coincides with those of VIMALA and NATH [10], when we replace  $a$  by  $a/2$  in the definition of  $\eta$ . A table of comparison (Table 1) and Fig. 2 show encouraging agreement with previous theories [10, 13] for some special cases. Moreover, our steady results for uniform rotation show excellent agreement with Ref. [9], but the comparison is not shown here for the sake of brevity.

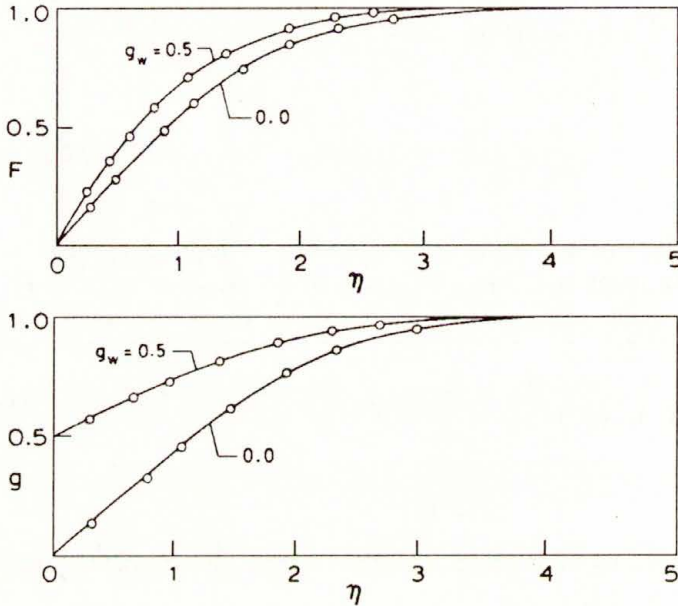


FIG. 2. Comparison of velocity ( $F$ ) and enthalpy ( $g$ ) profiles with the results of VIMALA and NATH [10] for  $t^* = 0$ ,  $Pr = 0.72$ ,  $\omega = 1$ ,  $f_w = 0$ ,  $\lambda = 0$ ,  $M = 0$ ;  $\circ$  results due to Ref. [10]; — present study.

### CASE 1. Unsteadiness caused by sudden change in wall enthalpy

The sphere is assumed to be rotating with constant angular velocity in a uniform stream of conducting fluid. A forced convection thermal boundary layer is then produced by impulsive changing of the wall temperature (enthalpy) of the sphere which was initially kept at a temperature (enthalpy) higher than the surrounding fluid temperature (enthalpy).

Figure 3 shows the effects of rotation ( $\lambda$ ) and magnetic parameter ( $M$ ) on the skin friction and heat transfer coefficients ( $\overline{C}_{f_x}$ ,  $-\overline{C}_{f_y}$ ,  $\overline{St}$ ) and their variation with time when the wall enthalpy is changed impulsively. The results show that both meridional skin friction and heat transfer [ $\overline{C}_{f_x}$ ,  $\overline{St}$ ] increase (decrease) suddenly to a maximum (minimum) value from their initial steady state (depending on the impulsive increase or decrease in the wall enthalpy), as the impulse is given at time  $t^* > 0$ . And then the quantities steadily decrease (increase) with time, finally

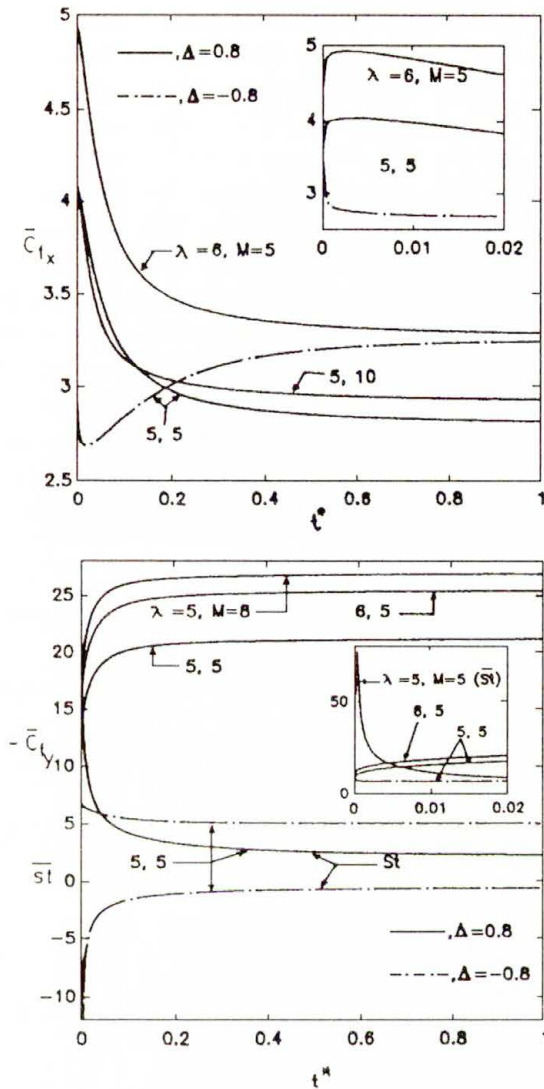


FIG. 3. Effects of rotation ( $\lambda$ ), and magnetic parameter ( $M$ ) on skin frictions and heat transfer ( $\overline{C}_{f_x}, -\overline{C}_{f_y}, \overline{St}$ ) for  $f_w = 0, \omega = 0.5$  and  $g_w = 1.4$ ; (unsteadiness due to impulsive change in wall enthalpy).

asymptotically approaching a clearly defined new steady state. From the inset of Fig. 3 (showing the behaviour of the physical quantities at time  $t^* = 0+$ ) we see that mostly heat transfer suffers sudden change immediately after the impulse, whereas azimuthal skin friction  $[-\overline{C}_{f_y}]$  shows its smooth transition. Moreover, it is observed that the skin frictions reach their steady state faster than the heat transfer. This is due to the fact that we have considered the case of impulsive wall heating (cooling), which also causes a rapid change in the heat transfer at

the wall near  $t^* = 0$ . As rotation ( $\lambda$ ) increases, both skin friction and heat transfer increase (however, its effect on the heat transfer is not shown here for the sake of compactness), and the effect is more pronounced on the azimuthal skin friction  $[\overline{C}_{f_y}]$ . This is because the shear force between the sphere and the adjacent fluid layer increases for higher rotation and its component in the azimuthal direction dominates for the simple reason that the direction of rotation of the sphere coincides with the azimuthal direction. But the basic trend of the flow behaviour immediately after the impulse remains the same for higher rotation. Figure 3 also shows that an increase in magnetic field strength ( $M$ ) causes skin frictions to increase, whereas its effect is observed to be negligible on the heat transfer. Another phenomenon may be observed that an impulsive increase and an impulsive decrease of wall enthalpy by the same amount does not reflect its effect on the physical quantities as mirror images. It can be seen more clearly in the subsequent figures that the impulsive decreasing processes take more time to reach a new steady state compared to the impulsive increasing processes.

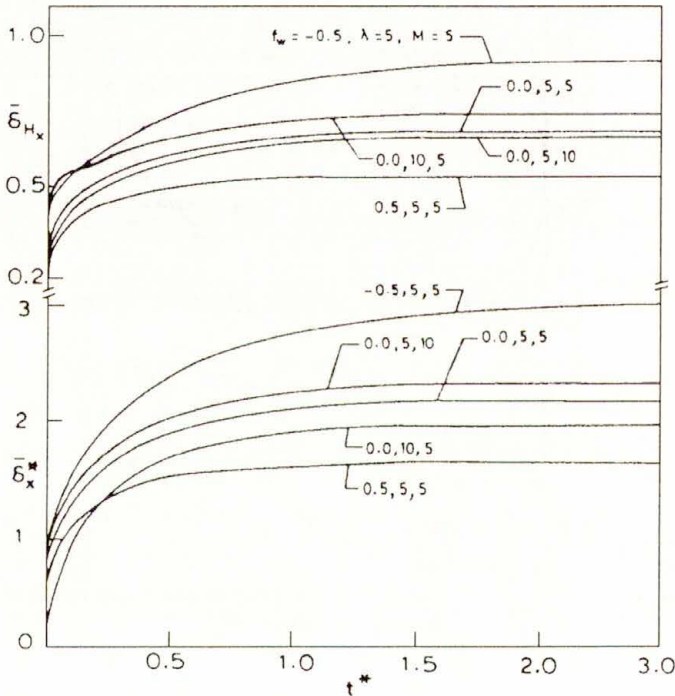


FIG. 4. Effects of mass transfer ( $f_w$ ), rotation ( $\lambda$ ), and magnetic parameter ( $M$ ) on displacement and enthalpy thickness  $[\delta_x^*, \delta_{H_x}]$  for  $\Delta = 0.8$ ,  $\omega = 0.5$  and  $g_w = 1.4$ ; (unsteadiness due to impulsive increase in wall enthalpy).

Figure 4 shows the effects of mass transfer ( $f_w$ ), rotation ( $\lambda$ ) and the magnetic parameter ( $M$ ) on displacement thickness ( $\delta_x^*$ ) and enthalpy thickness ( $\delta_{H_x}$ ) when

an impulsive increase in the wall enthalpy is considered. Both the displacement and enthalpy thickness are found to increase with time and they reach a steady state value for  $t^* \geq 3$ , and do not show any singular behaviour. With injection ( $f_w < 0$ ), both displacement and enthalpy thickness are found to increase but they show reverse effect with suction ( $f_w > 0$ ). This is due to the fact that the injected coolant pushes the boundary layer away from the surface and establishes a heat insulating layer, whereas suction works in the reverse way. As rotation ( $\lambda$ ) increases, the displacement thickness ( $\bar{\delta}_x^*$ ) decreases but the enthalpy thickness ( $\bar{\delta}_{H_x}$ ) increases. The reason behind this is that when we increase rotation of the sphere, the flow in the meridional direction gets reduced considerably in the boundary layer whereas it helps to increase the azimuthal flow. On the other hand, due to increase in rotation, the flow interaction in the boundary layer increases which helps in enhancing the enthalpy thickness ( $\bar{\delta}_{H_x}$ ). An increase in the magnetic field strength ( $M$ ) causes reduction in enthalpy thickness whereas it increases the displacement thickness. The boundary layer displacement thickness ( $\bar{\delta}_x^*$ ) becomes negative for cases of favourable pressure gradient with very low wall enthalpy (temperature). This occurs because the surface cooling produces an increase in density near the wall, so that there is more mass flow per unit flow area within the boundary layer than in the external flow [14]. However, such results are not shown here.

Figure 5 shows the effect of rotation ( $\lambda$ ) and time ( $t^*$ ) on the growth of velocity and enthalpy distribution ( $F, s, g$ ). The cause of unsteadiness is the same as that described in Fig. 3. It is observed that the meridional velocity ( $F$ ) shows overshoot for high rotation ( $\lambda = 10$ ) and with time, when an impulsive decrease in the wall enthalpy is considered, whereas impulsively increasing wall enthalpy process does not show any overshoot for  $t^* > 0.1$ , but it shows oscillatory nature in the new steady state ( $t^* = 2$ ). The meridional velocity is especially affected by compressibility. When the wall is heated, the density within certain layers of the boundary layer is reduced significantly, in spite of viscous retardation, the local flow is accelerated more than the external flow. Then velocity ( $F$ ) in some portion of the boundary layer reaches a maximum value greater than 1.0 before returning to its final value 1.0. The phenomenon can occur even when the wall temperature is less than the recovery temperature [14]. Here an increase in rotation has the effect of increasing the excess of the local velocities over the external velocity. Another interesting observation from Fig. 5 is that both meridional and azimuthal velocity ( $F$  &  $s$ ) overshoot temporarily the eventual steady state value when an impulsive increase in the wall enthalpy is considered, whereas in the impulsive decreasing process they increase with time and finally reach a new steady state. The enthalpy profiles ( $g$ ) show that at each point inside the boundary layer, enthalpy increases or decreases with time while approaching a new steady state, depending on the situation whether an impulsive increase or decrease of wall enthalpy is considered. It may also be observed that the enthalpy thickness increases when an impulsive increase in wall enthalpy is considered.

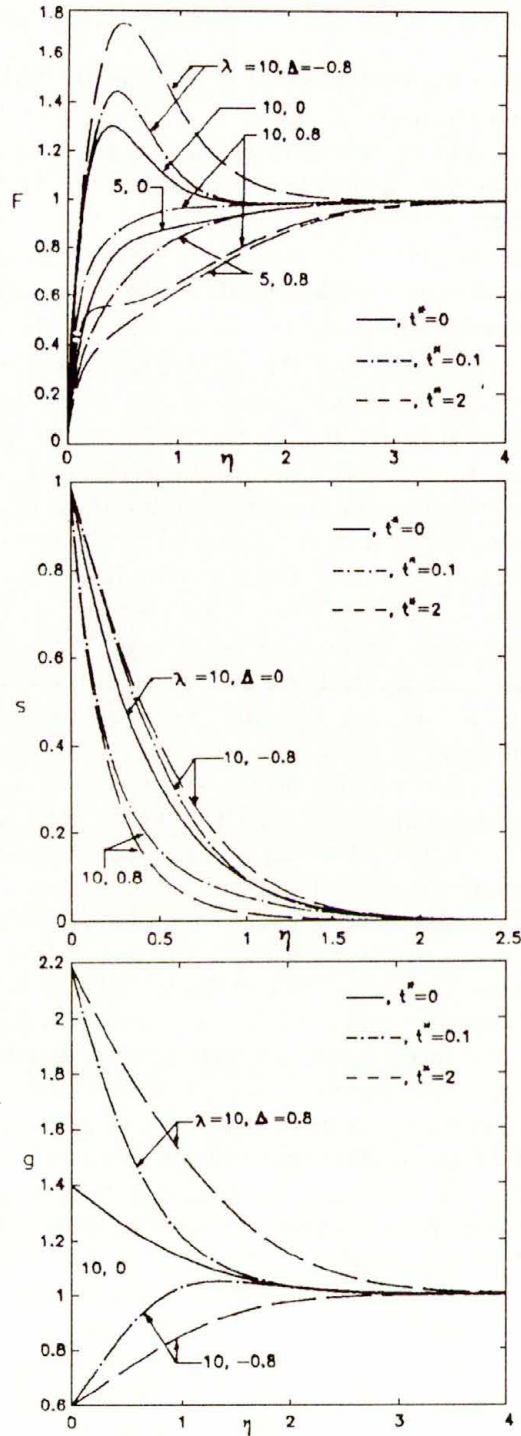


FIG. 5. Effects of rotation ( $\lambda$ ) and time ( $t^*$ ) on the velocity and enthalpy ( $F, s, g$ ) profiles for  $M = 5$ ,  $f_w = 0.0$ ,  $g_w = 1.4$  and  $\omega = 0.5$ ; (unsteadiness due to impulsive change in wall enthalpy).

CASE 2. In this case unsteadiness is caused by a sudden change in rotation of the sphere

Here we describe the transient motion when an impulsive change is given to the angular rotation of the sphere placed in a uniform axial stream of electrically conducting fluid.

Figure 6 shows the variation of skin friction and heat transfer  $[\overline{C}_{f_x}, -\overline{C}_{f_y}, \overline{St}]$  with time, and the effects of wall enthalpy ( $g_w$ ) and the viscosity index ( $\omega$ ) on the above mentioned quantities when the angular rotation of the sphere is suddenly changed to a new constant value. As it can be observed from the inset of Fig. 6, showing the effect of impulse immediately after it is imparted, the azimuthal skin friction  $[-\overline{C}_{f_y}]$  suffers much change in the beginning ( $t^* = 0+$ ). It increases or decreases to a maximum or minimum value from the initial ( $t^* = 0$ ) steady state and then decreases or increases with time (depending on whether impulsive increase or decrease in rotation is considered) while approaching a new steady state in an asymptotic way. This is due to the fact that the rotation is considered along the azimuthal direction and an impulsive change in the rotation of the sphere causes an instantaneous steep change in the azimuthal shear at the surface of the sphere. The transition for meridional skin friction and heat transfer ( $\overline{C}_{f_x}$  &  $\overline{St}$ ) is observed to be smooth. It may also be observed that it is the azimuthal skin friction  $[-\overline{C}_{f_y}]$  which reaches the new steady state faster, whereas the heat transfer takes more time to settle down. Moreover, once again it is observed that the transition time for impulsive decay process is longer than the impulsive increasing process as observed in Case 1. Figure 6 also shows that as wall enthalpy ( $g_w$ ) increases, both meridional skin friction and heat transfer ( $\overline{C}_{f_x}$ ,  $\overline{St}$ ) decrease, whereas the azimuthal skin friction  $[-\overline{C}_{f_y}]$  shows the opposite effect. The effect of variation of the density-viscosity product across the boundary layer is characterized by the parameter  $\omega$ . Both skin friction and heat transfer are found to increase significantly as the viscosity-index  $\omega$  increases, however results are shown only for meridional skin friction for the sake of brevity.

Figure 7 shows the distribution of velocity field  $[F, s]$  with time and the effect of magnetic parameter  $M$  on them. The meridional velocity ( $F$ ) shows overshoot when an impulsive increase in rotation is considered. An interesting observation is that the meridional velocity oscillates within the boundary layer (for impulsive increase in rotation), but does not show any overshoot, when magnetic field strength ( $M$ ) is increased, whereas the rest of the profiles approach their free stream value in a monotonic fashion. It may also be observed that the azimuthal velocity ( $s$ ) reaches its new steady state faster ( $t^* = 0.1$ ) when the impulsive increase in rotation is considered, whereas it takes longer time to settle down when the rotation of the sphere is reduced impulsively. In the case of impulsive decrease in rotation, both the velocities ( $F$  &  $s$ ) overshoot temporarily the eventual or new steady state value.

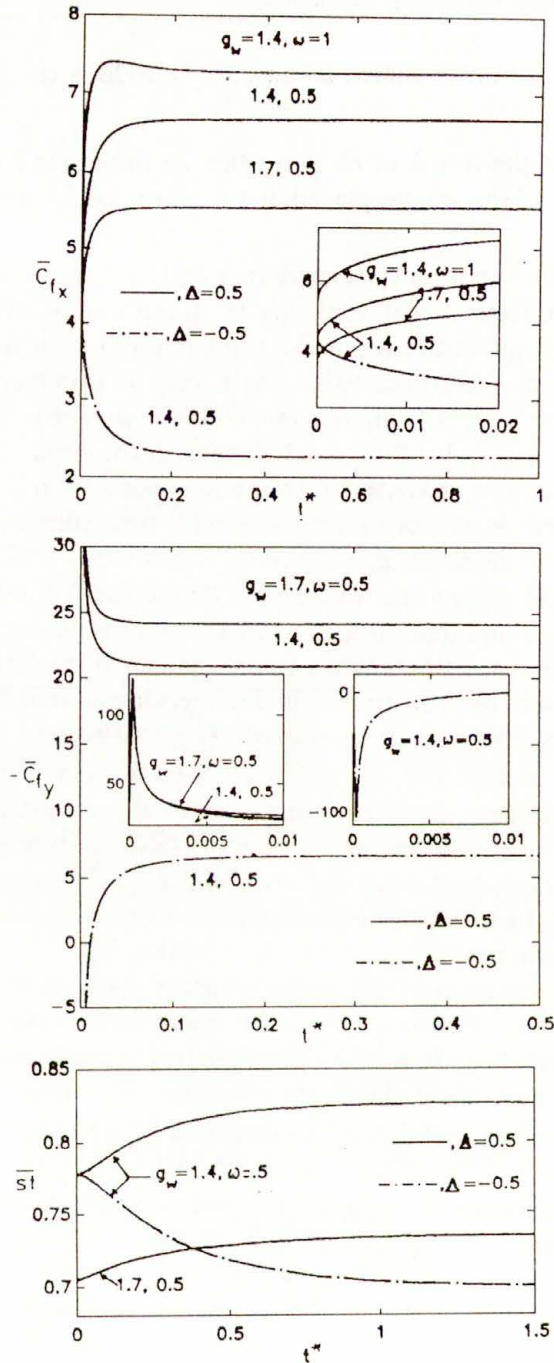


FIG. 6. Effects of wall enthalpy ( $g_w$ ) and viscosity-index ( $\omega$ ) on skin frictions and heat transfer ( $\bar{C}_{f_x}$ ,  $-\bar{C}_{f_y}$ ,  $\bar{St}$ ) for  $f_w = 0$ ,  $M = 5$  and  $\lambda = 6$ ; (unsteadiness due to impulsive change in rotation).

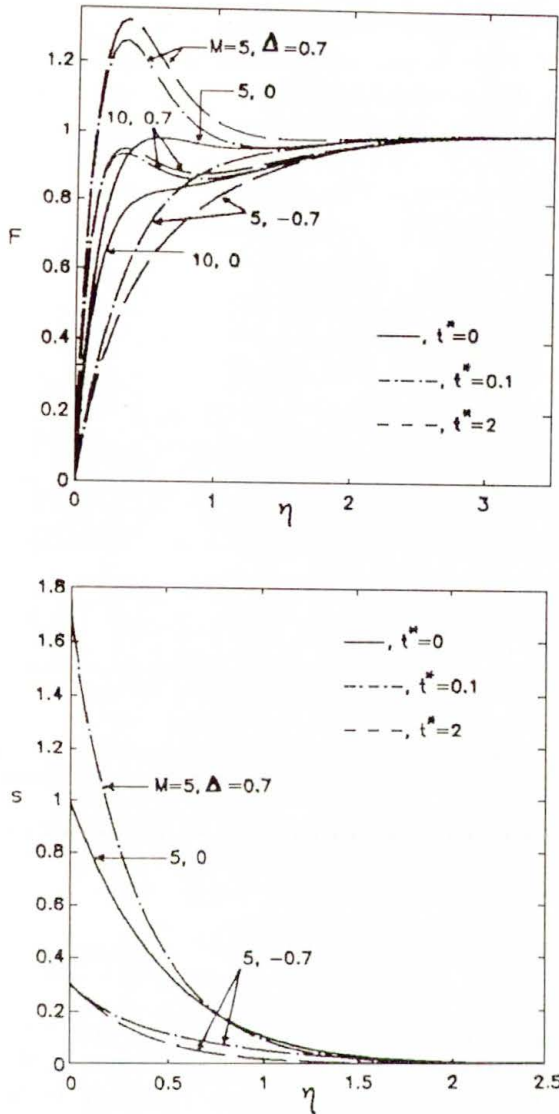


FIG. 7. Effects of magnetic parameter ( $M$ ) and time ( $t^*$ ) on the velocity ( $F, s$ ) profiles for  $f_w = 0, g_w = 1.4, \lambda = 7$  and  $\omega = 0.5$ ; (unsteadiness due to impulsive change in rotation).

CASE 3. Unsteadiness caused by sudden change in the meridional free-stream velocity

Figure 8 shows the distribution of meridional velocity ( $F$ ) when its free stream value is changed impulsively. The velocities overshoot inside the boundary layer before approaching their free stream value. The new steady ( $t^* = 2$ ) profile shows its oscillatory nature when the impulsive decrease in the free stream is considered. Moreover, it has been observed that at time  $t^* = 0.1$  its ( $F$ ) value

at any point inside the boundary layer is higher than the profile in its new steady state ( $t^* = 2$ ). The situation is just reverse when an impulsive increase in the free stream is considered. The unsteady profiles ( $t^* > 0$ ) show its monotonic nature at the edge of the boundary layer; this is probably because the impulse is given at the free stream.

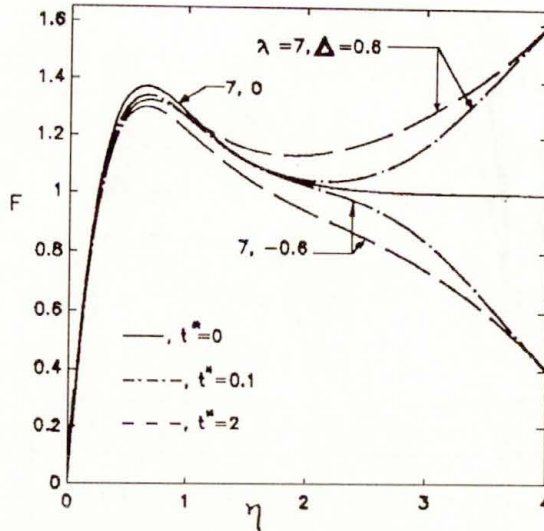


FIG. 8. The velocity ( $F$ ) profiles for  $f_w = 0$ ,  $M = 5$ ,  $g_w = 1.4$ ,  $\lambda = 7$  and  $\omega = 0.5$ ; (unsteadiness due to impulsive change in the meridional free stream velocity).

## 5. Conclusions

The transient behaviour of flow and heat transfer over a rotating sphere has been investigated numerically due to impulsive changes in the flow physics. A large change in the flow is observed at the early stage of transient motion. The rotation increases friction, heat transfer at the surface and the enthalpy thickness. The meridional velocity ( $F$ ) shows overshoot for high rotation and for the impulsive reduction of the wall enthalpy. It oscillates inside the boundary layer for higher magnetic field strength when an impulsive increase in rotation is considered. The transition time is longer for impulsive reduction processes, compared to impulsive increasing processes. Heat transfer takes longer time to settle down than skin frictions. For both impulsive increase in wall enthalpy and impulsive decrease in rotation of the sphere, the velocities overshoot temporarily before getting settled to the eventual steady state value, whereas, for the impulsive decrease in wall enthalpy or for the impulsive increase in rotation, the velocities increase with time while approaching a new steady state.

## References

1. E. BOLTZE, *Grenzschichten und Rotationskörpern in Flüssigkeiten mit kleiner Reibung*. Thesis, Göttingen 1908.
2. S.C.R. DENNIS and J.D.A. WALKER, *The initial flow past an impulsively started sphere at high Reynolds number*, J. Engng. Math., **5**, 263–278, 1971.
3. S.C.R. DENNIS and J.D.A. WALKER, *Numerical solution for time-dependent flow past an impulsively started sphere*, Phys. Fluids, **15**, 517–525, 1972.
4. W.H.H. BANKS and M.B. ZATUSKA, *The collision of unsteady laminar boundary layers*, J. Engng. Math., **13**, 193–212, 1979.
5. T. CEBECI, K. STEWARTSON and S.M. SCHIMKE, *Unsteady boundary layers close to the stagnation region of slender bodies*, J. Fluid Mech., **147**, 315–332, 1984.
6. S.C.R. DENNIS and P.W. DUCK, *Unsteady flow due to an impulsively started rotating sphere*, Computers Fluids, **16**, 291–310, 1988.
7. P.W. DUCK, *The unsteady laminar boundary layer on an axisymmetric body subject to small amplitude fluctuation in the free stream velocity*, J. Fluid Mech., **232**, 415–438, 1991.
8. M.C. ECE, *The initial boundary layer flow past a translating and spinning rotational symmetric body*, J. Engng. Math., **26**, 415–428, 1992.
9. M. KUMARI and G. NATH, *Heat and mass transfer in unsteady compressible axisymmetric stagnation point boundary layer flow over a rotating body*, Int. J. Heat Mass Transfer, **25**, 290–293, 1982.
10. C.S. VIMALA and G. NATH, *Unsteady laminar boundary layers in a compressible stagnation flow*, J. Fluid Mech., **70**, 561–572, 1975.
11. H. SCHLICHTING, *Boundary layer theory*, McGraw-Hill, New York 1979.
12. K.R. CRAMER and S.I. PAI, *Magneto-fluid dynamics for engineers and applied physics*, McGraw-Hill, New York 1973.
13. W.L. BADE, *Stagnation point heat transfer in a high temperature inert gas*, Phys. Fluids, **5**, 150–154, 1962.
14. C.B. COHEN and E. RESHOTKO, *Similar solutions for the compressible laminar boundary layer with heat transfer and pressure gradient*, NACA TN, 1293, 1956.

DEPARTMENT OF MATHEMATICS  
INDIAN INSTITUTE OF SCIENCE, BANGALORE, INDIA.

Received July 30, 1996.

# Boundary element method to the study of a Stokes flow past an obstacle in a channel

M. KOHR (CLUJ-NAPOCA)

IN THIS PAPER the author gives an integral representation for the stream function and for the vorticity, corresponding to the problem of the Stokes flow past an obstacle in a channel. Using the Green's functions of the biharmonic equation and of the Laplace equation for the infinite horizontal strip, the above problem is reduced to a set of integral equations on the boundary of the obstacle. The boundary element method is used to solve these integral equations. The numerical results are given for the case of a circular obstacle.

## 1. Introduction

IN THIS PAPER we describe a semi-direct boundary integral method which is used to the study of a two-dimensional Stokes flow in a wind tunnel past a rigid obstacle. To derive the set of boundary integral equations for the stream function and the flow vorticity, we construct the Green function of the biharmonic equation in an arbitrary simply connected domain. As a consequence, we obtain the Green function of the strip or of the half-plane.

The derived integral equations, which are valid in any point of the flow domain, are applied at the boundary of the domain resulting in a system of two scalar Fredholm integral equations on the boundary obstacle only for the stream function and vorticity. In fact, these equations represent the boundary integral formulation of our problem.

It should be noted that G. BEZINE and D. BONNEAU [1] presented an alternative boundary integral representation for the stream function in terms of boundary distributions of the velocity, shear stress, and the normal derivative of the vorticity, corresponding to a two-dimensional Stokes flow. Also, C.J. COLEMAN [3] has developed a semi-direct boundary integral representation in complex variables, using the stream function and the Airy stress function for the study of a plane creeping viscous flow.

Let us remark that a direct boundary-integral method for the solution of Stokes equations in an arbitrary two-dimensional domain was given by J.J.L. HIGDON [7]. He used the fundamental solution of the Stokes equation and he obtained a representation of the flow in terms of the velocity, the pressure and the stress tensor, respectively.

A nice direct method of integral equations was recently proposed by L. DRAGOŞ and A. DINU [4] for the study of a subsonic flow with circulation past thin airfoils

in a wind tunnel. A semi-direct boundary element method in the study of an incompressible flow in a channel was also applied by A. CARABINEANU and A. DINU [2]. They used the stream function.

## 2. Mathematical formulation

A fluid flow of velocity  $\mathbf{U}_\infty = (Uy(l-y), 0)$ , is placed between two walls being parallel to the  $Ox$ -axis. It is perturbed by the presence of an obstacle  $\Omega_i$ , with the boundary  $\Gamma$ . We determine the perturbation produced and the hydrodynamic forces acting on the obstacle. We suppose that the walls, denoted by  $L_1$  and  $L_2$ , have the equations:

$$\begin{aligned} L_1 &= \{(x, y) \mid x \in \mathbb{R}, \quad y = 0\}, \\ L_2 &= \{(x, y) \mid x \in \mathbb{R}, \quad y = l\}, \end{aligned}$$

where  $l > 0$ , and  $xOy$  is a Cartesian system of coordinates.

Also, the Reynolds number of the flow, denoted by  $Re$ , is supposed to be very small and hence the motion equations can be reduced to the creep equations and continuity equations, respectively (i.e. the Stokes equations):

$$(2.1) \quad \begin{aligned} \operatorname{div} \mathbf{v}(x) &= 0, & x \in D, \\ \operatorname{grad} P(x) - \mu \Delta \mathbf{v}(x) &= 0, & x \in D, \end{aligned}$$

where  $\mathbf{v}(u, v)$  is the global fluid velocity,  $P$  the global pressure and  $\mu$  the dynamic viscosity of the fluid. By  $D$  we denote the domain of the flow (Fig. 1).

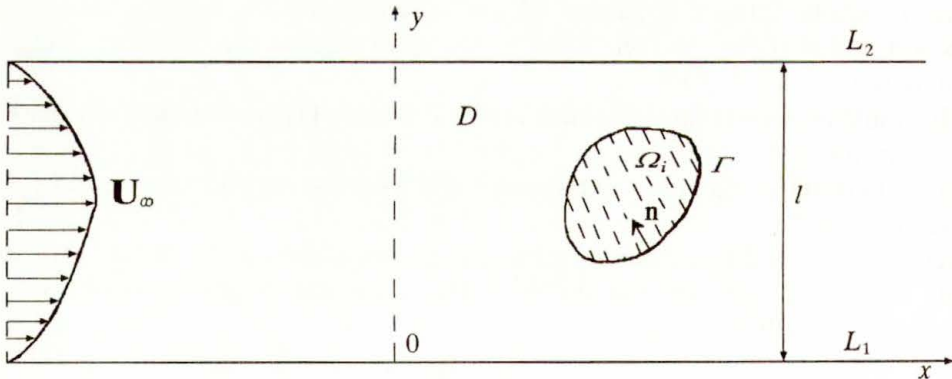


FIG. 1.

Using the stream function  $\psi$ , the above equations are reduced to the biharmonic equation

$$(2.2) \quad \Delta^2 \psi = 0$$

with the following boundary conditions:

$$(2.3) \quad \psi|_{L_1} = 0, \quad \psi|_{L_2} = C, \quad \psi|_{\Gamma} = b,$$

where  $C$  and  $b$  are unknown constants.

We have the following asymptotic conditions at infinity:

$$(2.4) \quad \lim_{|x| \rightarrow \infty} \left( \psi(x, y) - Uy^2 \left( \frac{l}{2} - \frac{y}{3} \right) \right) = 0, \quad \frac{\partial \psi}{\partial x} = 0,$$

$$\frac{\partial \psi}{\partial y} = Uy(l - y), \quad \text{as } |x| \rightarrow \infty.$$

After a simple analysis, we deduce that the rate of the flow in the channel, denoted by  $Q$ , is given by

$$(2.5) \quad Q = C.$$

On the other hand, from the boundary condition (2.3)<sub>2</sub>, we obtain

$$(2.6) \quad C = Q = \frac{Ul^3}{6}.$$

Let us now denote by  $\phi$  the stream function of the perturbation flow. Using the form of the stream function at infinity, we obtain that the global stream function can be written as:

$$(2.7) \quad \psi(x, y) = Uy^2 \left( \frac{l}{2} - \frac{y}{3} \right) + \phi(x, y).$$

The perturbation will be evaluated from the biharmonic equation

$$(2.8) \quad \Delta^2 \phi(x, y) = 0 \quad \text{in } \Omega,$$

with the boundary conditions:

$$(2.9) \quad \phi|_{L_1} = \phi|_{L_2} = 0,$$

$$\phi|_{\Gamma} = b - Uy^2 \left( \frac{l}{2} - \frac{y}{3} \right) \Big|_{\Gamma}$$

and the asymptotic conditions at infinity

$$(2.10) \quad \lim_{|x| \rightarrow \infty} \phi(x, y) = \lim_{|x| \rightarrow \infty} \text{grad } \phi(x, y) = 0.$$

### 3. The Green function of the biharmonic equation in an arbitrary simply connected domain

Let  $D$  be a simply connected domain in the  $(z)$  plane,  $z = x + iy$ , with the boundary  $C$ , and let  $w = f(z_0, z)$  be the conformal mapping of the domain  $D$  onto the domain  $|w| < 1$ , in the  $w$  plane, such that the fixed point  $z_0 \in D$  is mapped in  $w = 0$ .

We determine the function  $G(M_0, M)$ , where the points  $M_0$  and  $M$  correspond to  $z_0$  and  $z$ , with the following conditions:

- a)  $\Delta_M^2 G(M_0, M) = 0$ , for  $M \neq M_0$ ,
- b) in the neighbourhood of the point  $M_0$ ,  $G$  has the representation

$$G(M_0, M) = \frac{1}{8\pi} |M_0 M|^2 [\ln |M_0 M| - 1] + g(M_0, M),$$

where the function  $g(M_0, M)$  is a biharmonic function with respect to the point  $M$ , throughout the domain  $D$ ; and

- c)  $G(M_0, M) = 0$ .

The following theorem determines the function  $G$ .

**THEOREM.** *The function  $G$  is given by*

$$(3.1) \quad G(M_0, M) = \frac{1}{8\pi} |z - z_0|^2 \ln |f(z_0, z)|.$$

**P r o o f.** We prove that the function defined by (3.1) satisfies the conditions a), b), c). Because the function  $w = f(z_0, z)$  defines a conformal mapping between  $D$  and the unit disc, then it is an analytic function, with  $f(z, z_0) \neq 0$  for  $z \neq z_0$ .

Also the function  $\log f(z_0, z) = \ln |f(z_0, z)| + i \arg f(z_0, z)$  is analytic in the domain  $D$ , with the exception of the point  $z_0$ . The function  $\ln |f(z_0, z)| = \operatorname{Re} \log f(z_0, z)$  is a harmonic function and hence  $G$  given by (3.1), satisfy the condition a). Since  $f'(z, z_0) \neq 0$  in the domain  $D$  including the point  $z = z_0$  and  $f(z_0, z_0) = 0$ , the point  $z_0$  is a first order zero of the function  $f$ . Then, in a neighbourhood of this point we have:

$$(3.2) \quad f(z, z_0) = (z - z_0)\varphi(z, z_0),$$

where  $\varphi(z, z_0)$  is an analytic function in the respective neighbourhood of  $z_0$ , and  $\varphi(z, z_0) \neq 0$ . So

$$G(M_0, M) = \frac{1}{8\pi} |z - z_0|^2 [\ln |z - z_0| - 1] + \frac{1}{8\pi} |z - z_0|^2 \ln e|\varphi(z, z_0)|,$$

and the last function is denoted by  $g(M_0, M)$ . The condition b) is also satisfied.

Since  $f(z, z_0)|_C = 1$ , from (3.1) follows the condition c).

COROLLARY. The Green function of the biharmonic equation in the domain  $\Omega = \{(x, y) \mid x \in \mathbb{R}, 0 < y < l\}$  is given by

$$(3.3) \quad G(M_0, M) = \frac{1}{16\pi} [(x - x_0)^2 + (y - y_0)^2] \ln \frac{\operatorname{ch} \frac{\pi}{l}(x - x_0) - \cos \frac{\pi}{l}(y - y_0)}{\operatorname{ch} \frac{\pi}{l}(x - x_0) - \cos \frac{\pi}{l}(y + y_0)},$$

where  $M_0(x_0, y_0)$  and  $M(x, y)$  belong to  $\overline{\Omega}$ .

P r o o f. The conformal mapping of the domain  $\Omega$  onto the interior of the circle  $|w| < 1$ , has the form

$$f(z_0, z) = \frac{\exp\left(\frac{\pi}{l}z\right) - \exp\left(\frac{\pi}{l}z_0\right)}{\exp\left(\frac{\pi}{l}z\right) - \exp\left(\frac{\pi}{l}\bar{z}_0\right)}.$$

Performing elementary computations and applying the above theorem, we obtain Eq.(3.3).

#### 4. The integral representation of solution

We remark that the biharmonic equation  $\Delta^2\phi = 0$  is equivalent to the following system:

$$(4.1) \quad \begin{aligned} \Delta\phi &= \omega, \\ \Delta\omega &= 0, \end{aligned}$$

where  $\omega$  represents the vorticity of the perturbation flow.

In the preceding section we have determined the Green function  $G$  for the biharmonic operator in the infinite strip  $\Omega = \{(x, y) \mid x \in \mathbb{R}, 0 < y < l\}$ .

This function satisfies the following equation:

$$(4.2) \quad \Delta_q^2 G(p, q) = \delta(|p - q|), \quad \text{for } 0 < \eta < l,$$

where  $\delta$  is the Dirac distribution,  $p(x, y)$  is a variable point in  $\Omega$  where the solution is sought, and  $q(\xi, \eta)$  is a general point located on the boundary or in the domain  $\Omega$ . From (3.3) we have

$$(4.3) \quad G(x, y; \xi, \eta) = \frac{1}{16\pi} [(x - \xi)^2 + (y - \eta)^2] \ln \frac{\operatorname{ch} \frac{\pi}{l}(x - \xi) - \cos \frac{\pi}{l}(y - \eta)}{\operatorname{ch} \frac{\pi}{l}(x - \xi) - \cos \frac{\pi}{l}(y + \eta)},$$

$$G(x, y; \xi, \eta) = \frac{1}{8\pi} [(x - \xi)^2 + (y - \eta)^2] \ln \sqrt{\frac{\operatorname{sh}^2 \frac{\pi}{2l}(x - \xi) + \sin^2 \frac{\pi}{2l}(y - \eta)}{\operatorname{sh}^2 \frac{\pi}{2l}(x - \xi) + \sin^2 \frac{\pi}{2l}(y + \eta)}}.$$

The Green function  $F$  of the Laplace operator in the strip  $\Omega$  satisfies the following equation:

$$(4.4) \quad \Delta_q F(p, q) = \delta(|p - q|), \quad \text{for } 0 < \eta < l$$

and is given by (see [2]):

$$(4.5) \quad F(x, y; \xi, \eta) = \frac{1}{4\pi} \ln \frac{\operatorname{ch} \frac{\pi}{l}(x - \xi) - \cos \frac{\pi}{l}(y - \eta)}{\operatorname{ch} \frac{\pi}{l}(x - \xi) - \cos \frac{\pi}{l}(y + \eta)},$$

$$F(x, y; \xi, \eta) = \frac{1}{2\pi} \ln \sqrt{\frac{\operatorname{sh}^2 \frac{\pi}{2l}(x - \xi) + \sin^2 \frac{\pi}{2l}(y - \eta)}{\operatorname{sh}^2 \frac{\pi}{2l}(x - \xi) + \sin^2 \frac{\pi}{2l}(y + \eta)}}.$$

Using Green's identity for the functions  $\phi$  and  $\Delta_q G$ ,  $\omega$  and  $G$ , and for the functions  $\omega$  and  $F$ , we obtain the following integral representations:

$$(4.6) \quad \phi(p) = \int_{\partial D} \left[ \phi(q) \frac{\partial(\Delta_q G)}{\partial n_q}(p, q) - \Delta_q G(p, q) \frac{\partial \phi}{\partial n_q}(q) \right] ds_q$$

$$+ \int_{\partial D} \left[ \omega(q) \frac{\partial G(p, q)}{\partial n_q} - G(p, q) \frac{\partial \omega(q)}{\partial n_q} \right] ds_q, \quad p \in D,$$

$$\omega(p) = \int_{\partial D} \left[ \omega(q) \frac{\partial F}{\partial n_q} - F \frac{\partial \omega}{\partial n_q} \right] ds_q, \quad p \in D,$$

where  $D$  is the domain of the flow, exterior to the obstacle  $\Omega_i$  and enclosed by the walls  $L_0, L_1$ .

By  $\partial/\partial n_q$  we denote the differentiation with respect to the outward normal of  $D$ , in a point  $q$  of the boundary, denoted by  $\partial D$ .

We have satisfied the following properties:

$$(4.7) \quad F(x, 0; \xi, \eta) = F(x, l; \xi, \eta) = 0, \quad G(x, 0; \xi, \eta) = G(x, l; \xi, \eta) = 0,$$

$$(4.8) \quad \left. \frac{\partial F}{\partial n_q} \right|_{\partial \Omega} (x, 0; \xi, \eta) = \left. \frac{\partial F}{\partial n_q} \right|_{\partial \Omega} (x, l; \xi, \eta) = \left. \frac{\partial G}{\partial n_q} \right|_{\partial \Omega} (x, 0; \xi, \eta)$$

$$= \left. \frac{\partial G}{\partial n_q} \right|_{\partial \Omega} (x, l; \xi, \eta) = 0$$

and

$$(4.9) \quad \Delta_q G(x, 0; \xi, \eta) = \Delta_q G(x, l; \xi, \eta) = 0.$$

Also, we have

$$(4.9') \quad \frac{\partial \phi}{\partial n_q}(q) = 0 \quad \text{for } \eta = 0 \quad \text{or} \quad \eta = l.$$

Using the above properties and the asymptotic conditions at infinity (2.10), we derive the integral representation of solution, valid in any point of the flow domain:

$$(4.10) \quad \begin{aligned} \phi(p) = & \int_{\Gamma} \left[ \omega(q) \frac{\partial G(p, q)}{\partial n_q} - G(p, q) \frac{\partial \omega(q)}{\partial n_q} \right] ds_q \\ & + \int_{\Gamma} \left[ \phi(q) \frac{\partial}{\partial n_q} (\Delta_q G) - \Delta_q G(p, q) \frac{\partial \phi(q)}{\partial n_q} \right] ds_q \\ & + \int_{L_1 \cup L_2} \omega(q) \frac{\partial G}{\partial n_q}(p, q), \quad p \in D, \\ \omega(p) = & \int_{\Gamma} \left[ \omega(q) \frac{\partial F(p, q)}{\partial n_q} - F(p, q) \frac{\partial \omega}{\partial n_q} \right] ds_q \\ & + \int_{L_1 \cup L_2} \omega(q) \frac{\partial F}{\partial n_q}(p, q), \quad p \in D, \end{aligned}$$

where

$$(4.11) \quad \begin{aligned} \frac{\partial F(p, q)}{\partial n_q} = & \frac{1}{4l} \left[ \frac{\operatorname{sh} \frac{\pi}{l}(x-\xi)n_1 - \sin \frac{\pi}{l}(y+\eta)n_2}{\operatorname{ch} \frac{\pi}{l}(x-\xi) - \cos \frac{\pi}{l}(y+\eta)} \right. \\ & \left. - \frac{\operatorname{sh} \frac{\pi}{l}(x-\xi)n_1 + \sin \frac{\pi}{l}(y-\eta)n_2}{\operatorname{ch} \frac{\pi}{l}(x-\xi) - \cos \frac{\pi}{l}(y-\eta)} \right], \\ \frac{\partial G(p, q)}{\partial n_q} = & -\frac{1}{8\pi} [(x-\xi)n_1 + (y-\eta)n_2] \ln \frac{\operatorname{ch} \frac{\pi}{l}(x-\xi) - \cos \frac{\pi}{l}(y-\eta)}{\operatorname{ch} \frac{\pi}{l}(x-\xi) - \cos \frac{\pi}{l}(y+\eta)} \\ & - \frac{1}{16l} [(x-\xi)^2 + (y-\eta)^2] \left[ \frac{\operatorname{sh} \frac{\pi}{l}(x-\xi)n_1 - \sin \frac{\pi}{l}(y+\eta)n_2}{\operatorname{ch} \frac{\pi}{l}(x-\xi) - \cos \frac{\pi}{l}(y+\eta)} \right. \\ & \left. - \frac{\operatorname{sh} \frac{\pi}{l}(x-\xi)n_1 + \sin \frac{\pi}{l}(y-\eta)n_2}{\operatorname{ch} \frac{\pi}{l}(x-\xi) - \cos \frac{\pi}{l}(y-\eta)} \right]. \end{aligned}$$

Now, we suppose that the rigid obstacle denoted by  $\Omega_i$  with  $\partial\Omega_i = \Gamma$ , is fixed. The physical implication of vanishing of the fluid velocity on the boundary  $\Gamma$  provides that there is no tangential velocity on  $\Gamma$ , hence

$$(4.12) \quad \left. \frac{\partial \psi}{\partial n} \right|_{\Gamma} = 0,$$

and so

$$\left. \frac{\partial \phi}{\partial n} \right|_{\Gamma} = -Uy(l-y) \left. \frac{\partial y}{\partial n} \right|_{\Gamma}.$$

If we use the Green's identity in the domain  $\Omega_i$ , we obtain that the second integral term in (4.10)<sub>1</sub> is given by

$$\begin{aligned} \int_{\Gamma} \left[ \left( b - U\eta^2 \left( \frac{l}{2} - \frac{\eta}{3} \right) \right) \frac{\partial(\Delta G)}{\partial n_q} + U\Delta G \frac{\partial \eta}{\partial n_q} \right] ds_q \\ = -U \int_{\Gamma} \left[ (2\eta - l) \frac{\partial G}{\partial n_q}(p, q) - G(p, q) \frac{\partial}{\partial n_q} (2\eta - l) \right] ds_q. \end{aligned}$$

We remark that we must satisfy the boundary conditions (2.9). Using the properties (4.7)–(4.9), it is easy to show that for  $p \in D \rightarrow p_0 \in L_1$  or  $L_2$ , we obtain the equality with zero on the two sides of (4.10)<sub>1</sub>. Using the Plemelj's formula (see [6]) and the equation (4.10)<sub>2</sub>, we deduce the equality:  $\omega(p_0) = \omega(p_0)$ , for all  $p_0 \in L_1$  or  $L_2$ . For  $p \rightarrow p_0 \in \Gamma$ , from (4.10), we obtain a set of two equations with four unknowns:  $\omega$  and  $(\partial\omega/\partial n_q)$  on  $\Gamma$ , and  $\omega$  on  $L_1 \cup L_2$ . Then we impose the following arbitrary condition on the walls:

$$(4.13) \quad \omega(x, 0) = \omega(x, l) = 0, \quad \forall x \in \mathbb{R}.$$

From (4.10)–(4.13), we obtain the following integral representation on the boundary  $\Gamma$  only:

$$\begin{aligned} \phi(p) &= \int_{\Gamma} \left[ \omega(q) \frac{\partial G(p, q)}{\partial n_q} - G(p, q) \frac{\partial \omega(q)}{\partial n_q} \right] ds_q \\ (4.14) \quad &- U \int_{\Gamma} \left[ (2\eta - l) \frac{\partial G}{\partial n_q}(p, q) - G(p, q) \frac{\partial}{\partial n_q} (2\eta - l) \right] ds_q, \quad p \in \Gamma, \\ \omega(p) &= \int_{\Gamma} \left[ \omega(q) \frac{\partial F(p, q)}{\partial n_q} - F(p, q) \frac{\partial \omega(q)}{\partial n_q} \right] ds_q, \quad p \in \Gamma. \end{aligned}$$

The integrals which appear at the right-hand side of Eqs.(4.14) can be understood as a principal value in Cauchy' sense.

Because the fluid pressure  $P$  must be  $2\pi$ -periodic around the obstacle  $\Omega$ , we require  $\int_{\Gamma} \frac{\partial p}{\partial t} ds = 0$ , where  $\partial/\partial t$  represents the differentiation with respect to the unit tangent vector of  $\Gamma$ . If we use the property that the functions  $\omega$  and  $p$  are harmonically conjugate (see [6]), then we obtain the equation

$$(4.15) \quad \int_{\Gamma} \frac{\partial \omega}{\partial n} ds = 0.$$

### 5. Discretization of the integral equations

If  $p \in \Gamma$ , from Eqs. (4.14) and (4.15) we obtain the following Fredholm integral system:

$$(5.1) \quad \begin{aligned} b - Uy^2 \left( \frac{l}{2} - \frac{y}{3} \right) &= \int'_{\Gamma} \left[ \omega(q) \frac{\partial G(p, q)}{\partial n_q} - G(p, q) \frac{\partial \omega(q)}{\partial n_q} \right] ds_q \\ &\quad - U \int'_{\Gamma} \left[ (2\eta - l) \frac{\partial G}{\partial n_q}(p, q) - G(p, q) \frac{\partial}{\partial n_q} (2\eta - l) \right] ds_q, \\ \frac{1}{2} \omega(p) &= \int'_{\Gamma} \left[ \omega(q) \frac{\partial F(p, q)}{\partial n_q} - F(p, q) \frac{\partial \omega(q)}{\partial n_q} \right] ds_q, \\ \int_{\Gamma} \frac{\partial \omega(q)}{\partial n_q} ds_q &= 0, \end{aligned}$$

where the symbol  $'$  means the principal value in Cauchy's sense of the integral. For simplicity, this symbol will be omitted.

Our unknowns are the functions  $\omega$ ,  $\partial\omega/\partial n$  on  $\Gamma$  and the constant  $b$ .

In order to reduce the integral system (5.1) to an algebraic system, we use the collocation method. The contour  $\Gamma$  is approximated by a polygonal line determined by the segments  $\Gamma_j$  ( $j = \overline{1, N}$ ), and it is supposed that the midpoints  $M_j(x_j^*, y_j^*)$  of these segments are representative. Assuming the discretization equations (5.1) to be satisfied for  $(x, y) = (x_i^*, y_i^*)$ ,  $i = \overline{1, N}$ , we obtain the following linear system:

$$(5.2) \quad \begin{aligned} b - Uy_i^* \left( \frac{l}{2} - \frac{y_i^*}{3} \right) &= \sum_{j=1}^N \omega_j A_{ij} + \sum_{j=1}^N \left( \frac{\partial \omega}{\partial n} \right)_j B_{ij} \\ &\quad - U \sum_{j=1}^N (2y_j^* - l) A_{ij} + 2U \sum_{j=1}^N n_{2j} B_{ij}, \end{aligned}$$

$$(5.2) \quad \sum_{j=1}^N \left( \frac{\partial \omega}{\partial n} \right)_j \int_{\Gamma_j} ds_q = 0,$$

[cont.]

$$\frac{1}{2} \omega_i = \sum_{j=1}^N \omega_j C_{ij} + \sum_{j=1}^N \left( \frac{\partial \omega}{\partial n} \right)_j D_{ij}, \quad i = \overline{1, N},$$

where  $\omega_i = \omega(x_i^*, y_i^*)$ ,  $\left( \frac{\partial \omega}{\partial n} \right)_i = \frac{\partial \omega}{\partial n}(x_i^*, y_i^*)$ , and  $\mathbf{n}_2(x_i^*, y_i^*) = (n_1^i, n_2^i)$  is the normal unit vector to the segment  $\Gamma_i$ .

The coefficients of the above system are given by:

$$(5.3) \quad \begin{aligned} A_{ij} &= \frac{1}{8\pi} \int_{\Gamma_j} \left[ (x_i^* - \xi)n_1^j + (y_i^* - \eta)n_2^j \right] \ln \frac{\operatorname{ch} \frac{\pi}{l}(x_i^* - \xi) - \cos \frac{\pi}{l}(y_i^* - \eta)}{\operatorname{ch} \frac{\pi}{l}(x_i^* - \xi) - \cos \frac{\pi}{l}(y_i^* + \eta)} ds_q \\ &\quad - \frac{1}{16l} \int_{\Gamma_j} \left[ (x_i^* - \xi)^2 + (y_i^* - \eta)^2 \right] \left[ \frac{\operatorname{sh} \frac{\pi}{l}(x_i^* - \xi)n_1^j - \sin \frac{\pi}{l}(y_i^* + \eta)n_2^j}{\operatorname{ch} \frac{\pi}{l}(x_i^* - \xi) - \cos \frac{\pi}{l}(y_i^* + \eta)} \right. \\ &\quad \left. - \frac{\operatorname{sh} \frac{\pi}{l}(x_i^* - \xi)n_1^j - \sin \frac{\pi}{l}(y_i^* - \eta)n_2^j}{\operatorname{ch} \frac{\pi}{l}(x_i^* - \xi) - \cos \frac{\pi}{l}(y_i^* - \eta)} \right] ds_q, \\ B_{ij} &= -\frac{1}{16\pi} \int_{\Gamma_j} \left[ (x_i^* - \xi)^2 + (y_i^* - \eta)^2 \right] \ln \frac{\operatorname{ch} \frac{\pi}{l}(x_i^* - \xi) - \cos \frac{\pi}{l}(y_i^* - \eta)}{\operatorname{ch} \frac{\pi}{l}(x_i^* - \xi) - \cos \frac{\pi}{l}(y_i^* + \eta)} ds_q, \\ C_{ij} &= \frac{1}{4l} \int_{\Gamma_j} \left[ \frac{\operatorname{sh} \frac{\pi}{l}(x_i^* - \xi)n_1^j - \sin \frac{\pi}{l}(y_i^* + \eta)n_2^j}{\operatorname{ch} \frac{\pi}{l}(x_i^* - \xi) - \cos \frac{\pi}{l}(y_i^* + \eta)} \right. \\ &\quad \left. - \frac{\operatorname{sh} \frac{\pi}{l}(x_i^* - \xi)n_1^j - \sin \frac{\pi}{l}(y_i^* - \eta)n_2^j}{\operatorname{ch} \frac{\pi}{l}(x_i^* - \xi) - \cos \frac{\pi}{l}(y_i^* - \eta)} \right] ds_q, \\ D_{ij} &= -\frac{1}{4\pi} \int_{\Gamma_j} \ln \frac{\operatorname{ch} \frac{\pi}{l}(x_i^* - \xi) - \cos \frac{\pi}{l}(y_i^* + \eta)}{\operatorname{ch} \frac{\pi}{l}(x_i^* - \xi) - \cos \frac{\pi}{l}(y_i^* - \eta)} ds_q, \quad i, j = \overline{1, N}. \end{aligned}$$

To evaluate the above integrals, we denote by  $(x_1^j, y_1^j)$  and  $(x_2^j, y_2^j)$  the coordinates of the ends of segment  $\Gamma_j$ , in the order leaving the inside of the obstacle to the right. Then  $\Gamma_j$  will be parametrized by taking (see for example, [5]):

$$(5.4) \quad x = x_j^* + \frac{x_2^j - x_1^j}{2}t, \quad y = y_j^* + \frac{y_2^j - y_1^j}{2}t, \quad t \in [-1, 1],$$

where  $x_j^* = (x_1^j + x_2^j)/2$ ,  $y_j^* = (y_1^j + y_2^j)/2$  are the coordinates of the midpoints of the segment  $\Gamma_j$ ,  $j = \overline{1, N}$ .

From Eqs.(5.4), it follows that  $ds = (L/2)dt$ , where  $L$  is the length of the segment  $\Gamma_j$ , given by

$$(5.5) \quad L = \sqrt{(x_2^j - x_1^j)^2 + (y_2^j - y_1^j)^2}.$$

The coordinates of the unit vector  $\mathbf{n}^j$  will be calculated as follows:

$$(5.5') \quad \mathbf{n}^j = \left( \frac{y_2^j - y_1^j}{L}, -\frac{x_2^j - x_1^j}{L} \right).$$

For  $i = j$  we obtain:

$$(5.6) \quad \begin{aligned} A_{ii} &= \frac{1}{8\pi} \int_{\Gamma_i} [(x_i^* - \xi)n_1^i + (y_i^* - \eta)n_2^i] \ln \left[ \operatorname{ch} \frac{\pi}{l}(x_i^* - \xi) - \cos \frac{\pi}{l}(y_i^* + \eta) \right] ds_q \\ &+ \frac{1}{16l} \int_{\Gamma_i} \left[ \frac{\operatorname{sh} \frac{\pi}{2l}(x_i^* - \xi) \operatorname{ch} \frac{\pi}{2l}(x_i^* - \xi)n_1^i - \sin \frac{\pi}{2l}(y_i^* + \eta) \cos \frac{\pi}{2l}(y_i^* + \eta)n_2^i}{\operatorname{sh}^2 \frac{\pi}{2l}(x_i^* - \xi) + \sin^2 \frac{\pi}{2l}(y_i^* + \eta)(y_i^* + \eta)} \right] \\ &\quad \cdot [(x_i^* - \xi)^2 + (y_i^* - \eta)^2] ds_q, \\ B_{ii} &= \frac{1}{16\pi} \int_{\Gamma_i} [(x_i^* - \xi)^2 + (y_i^* - \eta)^2] \ln \left[ \operatorname{ch} \frac{\pi}{l}(x_i^* - \xi) - \cos \frac{\pi}{l}(y_i^* + \eta) \right] ds_q \\ &\quad - \frac{1}{32\pi} \int_{-1}^1 t^2 \ln \left[ \operatorname{ch} \frac{\pi}{2l}(x_1^i - x_2^i)t - \cos \frac{\pi}{2l}(y_1^i - y_2^i)t \right] dt, \\ C_{ii} &= -\frac{1}{4l} \int_{\Gamma_i} \left[ \frac{-n_1^i \operatorname{sh} \frac{\pi}{2l}(x_i^* - \xi) \operatorname{ch} \frac{\pi}{2l}(x_i^* - \xi)n_1}{\operatorname{sh}^2 \frac{\pi}{2l}(x_i^* - \xi) + \sin^2 \frac{\pi}{2l}(y_i^* + \eta)} \right. \\ &\quad \left. + \frac{n_2^i \sin \frac{\pi}{2l}(y_i^* + \eta) \cos \frac{\pi}{2l}(y_i^* + \eta)}{\operatorname{sh}^2 \frac{\pi}{2l}(x_i^* - \xi) + \sin^2 \frac{\pi}{2l}(y_i^* + \eta)} \right] ds_q, \\ D_{ii} &= -\frac{1}{2\pi} \int_{\Gamma_i} \ln \sqrt{\operatorname{sh}^2 \frac{\pi}{2l}(x_i^* - \xi) + \sin^2 \frac{\pi}{2l}(y_i^* + \eta)} ds_q \\ &\quad + \frac{1}{2\pi} L \ln \frac{\pi}{2l} - \frac{L}{2\pi} + \frac{L \ln \frac{L}{2}}{2\pi}. \end{aligned}$$

The coefficients (5.6) may be computed numerically, using the same technique as for the coefficients (5.2)–(5.3).

## 6. Numerical results

From (4.10), we can obtain the discretization form of the total stream function  $\psi$  in any point of the domain  $D$ :

$$(6.1) \quad \psi(p) = Uy^2 \left( \frac{l}{2} - \frac{y}{3} \right) + \sum_{j=1}^N \omega_j \int_{\Gamma_j} \frac{\partial G(p, q)}{\partial n_q} ds_q \\ - \sum_{j=1}^N \left( \frac{\partial \omega}{\partial n} \right)_j \int_{\Gamma_j} G(p, q) ds_q - U \sum_{j=1}^N (2y_j^* - l) \int_{\Gamma_j} \frac{\partial G}{\partial n_q}(p, q) ds_q \\ + U \sum_{j=1}^N n_{2j} \int_{\Gamma_j} G(p, q) ds_q, \quad p \in D.$$

Numerical computations of the method were performed for a fixed circular obstacle. It was considered that the circle had the center  $(X_0, Y_0)$ ,  $0 < Y_0 < l$  and the radius  $a$ . The maximum value chosen for  $N$  was 60. Also, we supposed that the segments  $\Gamma_j$  were of the same length.

The test of the method is given for the drag coefficient  $C_D$ , defined by:

$$(6.2) \quad C_D = \frac{1}{\frac{1}{2} \rho a^2 U^2 l^4} \int_{\Gamma} \{ \sigma_{nn}(q) \cos \theta(q) - \sigma_{tn}(q) \sin \theta(q) \} ds_q,$$

where  $\theta(q)$  is the angle between the unit normal vector  $\mathbf{n}(q)$  to the boundary  $\Gamma$ , and the positive  $Ox$ -axis. Symbols

$$(6.3) \quad \sigma_{nn} = -P - 2 \frac{\partial^2 \psi}{\partial t \partial n}, \quad \sigma_{tn} = -\frac{\partial^2 \psi}{\partial n^2} - \frac{\partial^2 \psi}{\partial t^2}, \quad \sigma_{tt} = -P + \frac{\partial^2 \psi}{\partial t \partial n}$$

denote the components of the stress tensor referred to the  $(\mathbf{t}, \mathbf{n})$  axes.

From (2.1)<sub>1</sub> and using the following property (see [8]):

$$(6.4) \quad \frac{\partial^2 \psi}{\partial t^2} = \frac{\partial^2 \psi}{\partial s^2} - \frac{1}{a} \frac{\partial \psi}{\partial n},$$

we obtain the drag coefficient  $C_D$  in the form:

$$(6.5) \quad C_D = \frac{2}{\rho a^2 U^2 l^4} \int_{\Gamma} \eta \left( \frac{\partial \omega}{\partial n}(q) - \frac{1}{a} \omega(q) \right) ds_q - \frac{2Y_0}{\rho a^3 U^2} \int_{\Gamma} \omega(q) ds_q.$$

If we assume  $\rho = 0.8$ ,  $a = 1$ ,  $l = 4$ ,  $U = 1$ ,  $X_0 = 0$ ,  $Y_0 = 2$ , then for  $47 \leq N \leq 60$ , we obtain the same value for the drag coefficient:  $C_D = 7.8537$ . Also, if we choose  $\rho = 0.8$ ,  $a = 1$ ,  $l = 4$ ,  $U = 2$ ,  $X_0 = 0$ ,  $Y_0 = 2$ , and

$47 \leq N \leq 60$ , it follows that  $C_D = 3.92699$ . These remarks show the extremely rapid convergence of the results when the number  $N$  of discretization elements increases. In the first case the constant  $b$  is equal to 0.5, for all  $N \geq 47$ , and in the last case  $b$  is equal to 0.3.

The Table 1 gives the values of the drag coefficients as the function of the velocity  $U$ , when  $a = 1, l = 4, X_0 = 0, Y_0 = 2$ . We observe that if the Reynolds number ( $Re = (\rho a U l^2) / \mu$ ,  $\rho, \mu$  are supposed to be fixed) increases, then the drag coefficient  $C_D$  decreases.

Table 1.

$U$	$N$	Drag coefficient $C_D$
1	60	7.8537861
1.5	60	5.2352625
2	60	3.9269824
4	60	0.4908738

Table 2.

$\rho$	$N$	Drag coefficient $C_D$
0.8	60	7.8537861
0.6	60	10.4717147
0.5	60	12.5660577

For  $U = 1, a = 1, l = 4, X_0 = 0$  and  $Y_0 = 2$ , respectively, the Table 2 gives the values of the coefficient  $C_D$  for some values of the density  $\rho$ . Finally, Figs. 2 and 3 represent the spectrum of the flow in the case  $a = 1, l = 4, X_0 = 0, Y_0 = 2$  and  $Y_0 = 2.5$ , respectively.

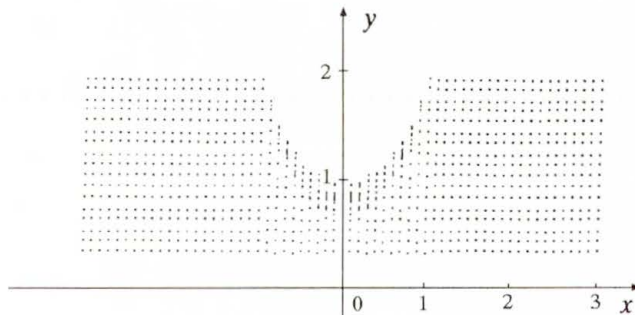


FIG. 2.

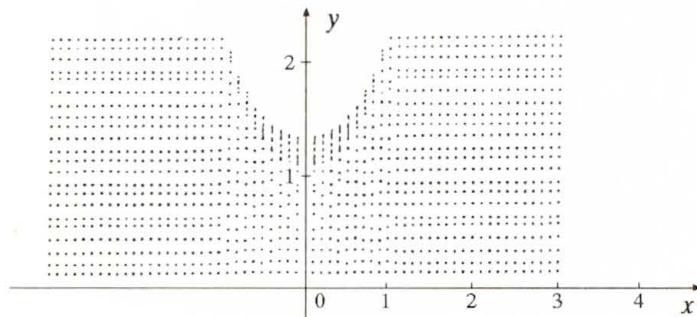


FIG. 3.

## References

1. G. BEZINE and D. BONNEAU, *Integral equation method for the study of two-dimensional Stokes flow*, Acta Mech., **41**, 197–209, 1981.
2. A. CARABINEANU and A. DINU, *The study of the incompressible flow past a smooth obstacle in a channel by the boundary element method*, Rev. Roum. Sci. Techn.-Mec. Appl., **38**, 6, 601–616, 1983.
3. C.J. COLEMAN, *A contour integral formulation of plane creeping Newtonian flow*, Quart. J. Mech. Appl. Math., **34**, 453–464, 1980.
4. L. DRAGOȘ and A. DINU, *The application of the boundary integral equations method to subsonic flow with circulation past thin airfoils in a wind tunnel*, Acta Mech., **103**, 17–30, 1994.
5. L. DRAGOȘ and A. DINU, *Application of the boundary element method to the thin airfoil theory*, AIAA J., **28**, 1822–1824, 1990.
6. L. DRAGOȘ, *The principles of continuous mechanics media* [in Romanian], Ed. Tehnică, București 1983.
7. J.J.L. HIGDON, *Stokes flow in arbitrary two-dimensional domain: shear flow over ridges and cavities*, J. Fluid Mech., **159**, 195–226, 1985.
8. M.A. KELMANSON, *A direct boundary integral equation formulation for the Oseen flow past a two-dimensional cylinder of arbitrary cross-section*, Acta Mech., **68**, 99–119, 1987.

“BABES-BOLYAI” UNIVERSITY  
FACULTY OF MATHEMATICS,

1. M. Kogalniceanu str., 3400 CLUJ-NAPOCA, ROMANIA.

Received August 19, 1996.

# Stability of micro-periodic materials under finite deformations

E. WIERZBICKI (WARSZAWA), C. WOŹNIAK (CZĘSTOCHOWA)  
and M. WOŹNIAK (ŁÓDŹ)

A NEW APPROACH to the stability analysis for highly-elastic micro-periodic composite materials subjected to finite deformations is proposed. The analysis is based on the refined macrodynamics of periodic structures which describes the effect of the microstructure size on the dynamic body behaviour. It is shown that the loss of stability can take place both on the macro- and micro-level and that the internal dynamic instability depends on the microstructure size. The obtained results are illustrated by a simple example.

## 1. Introduction

STABILITY OF HOMOGENEOUS elastic materials under finite deformations was investigated in the series of papers [1–9, 11–15, 18]; the main results can be found in the monograph [10]. The aim of this contribution is to outline a new approach to the problem of stability for composite bodies made of perfectly bonded elastic constituents subjected to large strains. It is assumed that in the natural configuration the material structure of the body is micro-periodic. The analysis is based on the refined macro-dynamics of composite materials, introduced in the framework of linear elasticity in [19] and extended to finite elastic deformations in [16, 17]. The effect of the unit cell length dimensions on the dynamic stability of a micro-periodic body and the existence of new kinds of material stability, related to the microstructure of a composite, are most important features of the proposed approach.

### Notations

Indices  $\alpha, \beta, \dots$  and  $i, j, \dots$  run over 1, 2, 3 and are related to the material and spatial coordinate systems, respectively. Capital Latin indices  $A, B, \dots$  run over 1,  $\dots, N$ ;  $N \geq 1$ . Summation convention holds for all aforementioned indices if not otherwise stated. By  $V_R$  we denote the region  $(-l_1/2, l_1/2) \times (-l_2/2, l_2/2) \times (-l_3/2, l_3/2)$  in a three-space of points  $\mathbf{X} = (X^\alpha)$ . An averaged value of any integrable  $V_R$ -periodic function  $f(\cdot)$  of  $\mathbf{X}$  will be denoted by

$$\langle f(\mathbf{X}) \rangle := \frac{1}{l_1 l_2 l_3} \int_{V_R} f(\mathbf{X}) dX^1 dX^2 dX^3.$$

Here and in the sequel the subscript  $R$  is related to the known reference configuration of the body under investigation.

## 2. Foundations

Let the highly-elastic composite body in the natural (reference) configuration occupy a region  $\Omega_R$  in a physical three-space and have in this configuration the  $V_R$ -periodic structure. The microstructure length parameter defined by  $l := \sqrt{(l_1)^2 + (l_2)^2 + (l_3)^2}$  is assumed to be sufficiently small compared to the smallest characteristic length dimension of  $\Omega_R$ . The position of an arbitrary point  $\mathbf{X}$ ,  $\mathbf{X} \in \Omega_R$ , of the body at an instant  $t$ ,  $t \geq 0$ , will be denoted by  $\mathbf{x} = \mathbf{p}(\mathbf{X}, t)$ ,  $\mathbf{X} = (X^\alpha) \in \Omega_R$ . Hence  $\mathbf{u}(\mathbf{X}, t) := \mathbf{p}(\mathbf{X}, t) - \mathbf{X}$  is a displacement vector from the natural configuration. The properties of the composite under consideration are determined by a mass density  $\varrho_R(\cdot)$  and a strain energy density function  $\varepsilon_R(\cdot, \nabla \mathbf{p})$ , which are  $V_R$ -periodic functions defined almost everywhere on  $\Omega_R$  and related, as densities, to the reference configuration.

The idea of the refined macrodynamics, explained in [19] and applied in a series of related papers, is based on the heuristic constraint assumption that the displacements  $u_i(\mathbf{X}, t)$  in a periodic composite can be represented by certain averaged displacements  $U_i(\cdot, t)$  on which highly-oscillating disturbances are superimposed, caused by the micro-inhomogeneity of a medium. To describe this situation, the concept of a regular macro-function was introduced in [19]; roughly speaking, a function  $F: \Omega_R \rightarrow \mathbf{R}$  is called a macro-function (for the known microstructure length parameter  $l$  and a certain accuracy  $\varepsilon_F$  assigned to numerical calculations of the values of  $F$ ) if for every  $\mathbf{X}, \mathbf{Z} \in \Omega_R$  such that  $\|\mathbf{X} - \mathbf{Z}\| < l$  condition  $|F(\mathbf{X}) - F(\mathbf{Z})| < \varepsilon_F$  holds. If similar conditions also hold for all derivatives of  $F$  then  $F$  is said to be a regular macro-function. The aforementioned constraint assumption specifies a class of motions given by

$$(2.1) \quad u_i(\mathbf{X}, t) = U_i(\mathbf{X}, t) + h^A(\mathbf{X})Q_i^A(\mathbf{X}, t), \quad \mathbf{X} \in \Omega_R, \quad t \geq 0,$$

where  $U_i(\cdot, t)$ ,  $Q_i^A(\cdot, t)$  are certain arbitrary regular macro-functions, and  $h^A(\cdot)$  are the postulated *a priori*  $V_R$ -periodic functions (hence depending on  $l$ ), satisfying for every  $\mathbf{X}$  the conditions  $h^A(\mathbf{X}) \in O(l)$ ,  $h^A_{,\alpha}(\mathbf{X}) \in O(1)$  as well as the condition  $\langle h^A \rangle = 0$ . Functions  $h^A(\cdot)$  are called micro-shape functions and from the qualitative viewpoint, they determine the investigated class of disturbances in displacements caused by the  $V_R$ -periodic structure of the composite. Functions  $U_i(\cdot)$ ,  $Q_i^A(\cdot)$  are the basic dynamic variables of the refined macrodynamics being referred to as macro-displacements and macro-internal variables, respectively. By virtue of Eq. (2.1), macro-internal variables  $Q_i^A$  describe the aforementioned disturbances in displacements from a quantitative viewpoint. Define by  $\mathbf{F}$  a field with components

$$F^i_{\alpha} := \delta^i_{\alpha} + U^i_{,\alpha}$$

which will be called the macro-deformation gradient. Hence every  $F^i_{\alpha}(\cdot, t)$ ,  $t \geq 0$ , is a certain regular macro-function. In the framework of the refined macrodynamics the deformation gradient  $\nabla \mathbf{p}$  is approximated by  $\mathbf{F} + \nabla h^A \mathbf{Q}^A$ , [19]. It

follows that the function  $\pi_R$  defined by

$$\pi_R = \pi_R(\mathbf{F}, \mathbf{Q}) := \langle \varepsilon_R(\mathbf{X}, \mathbf{F} + \nabla h^A(\mathbf{X})\mathbf{Q}^A) \rangle, \quad \mathbf{Q} := (\mathbf{Q}^1, \dots, \mathbf{Q}^N)$$

represents an averaged strain energy. Macro-deformation gradients  $\mathbf{F}$  and macro-internal variables  $\mathbf{Q}^A$  are restricted by the condition

$$\det(\mathbf{F} + \nabla h^A \mathbf{Q}^A) > 0.$$

Let us define  $g^A := l^{-1}h^A$ ; obviously, values of functions  $g^A$  satisfy conditions  $g^A(\mathbf{X}) \in O(1)$ . The field equations for  $U_i(\cdot), Q_i^A(\cdot)$  which were obtained in [17], after neglecting the body forces, can be written down in the form

$$(2.2) \quad S_R^{i\alpha}{}_{,\alpha} - \langle \rho_R \rangle \ddot{U}^i = 0, \quad H_R^{Ai} + l^2 \langle \rho_R g^A g^B \rangle \ddot{Q}^{Bi} = 0,$$

where

$$(2.3) \quad S_R^{i\alpha} = \frac{\partial \pi_R}{\partial F_{i\alpha}}, \quad H_R^{Ai} = \frac{\partial \pi_R}{\partial Q_i^A}.$$

Fields  $S_R^{i\alpha}$  and  $H_R^{Ai}$  are called the Piola – Kirchhoff macro-stresses and the micro-dynamic forces (related to  $\Omega_R$ ), respectively. In the natural configuration, i.e. for  $\mathbf{F} = \mathbf{1}$  and  $\mathbf{Q} = \mathbf{0}$ , the macro-stresses  $S_R^{i\alpha}$  and micro-dynamic forces  $H_R^{Ai}$  have to be equal to zero. If this condition is not satisfied by the derivatives of  $\langle \varepsilon_R \rangle$  with respect to  $\mathbf{F}$  and  $\mathbf{Q}$  then the strain energy function  $\pi_R$  in Eqs.(2.3) has to be assumed in the form

$$(2.4) \quad \pi_R = \pi_R(\mathbf{F}, \mathbf{Q}) := \langle \varepsilon_R(\mathbf{X}, \mathbf{F} + \nabla h^A(\mathbf{X})\mathbf{Q}^A) \rangle - \lambda_R^{i\alpha} (F_{i\alpha} - \delta_{i\alpha}) - \mu_R^{Ai} Q_i^A,$$

where

$$(2.5) \quad \lambda_R^{i\alpha} := \left. \frac{\partial \langle \varepsilon_R \rangle}{\partial F_{i\alpha}} \right|_{\mathbf{F}=\mathbf{1}, \mathbf{Q}=\mathbf{0}}, \quad \mu_R^{Ai} := \left. \frac{\partial \langle \varepsilon_R \rangle}{\partial Q_i^A} \right|_{\mathbf{F}=\mathbf{1}, \mathbf{Q}=\mathbf{0}}.$$

Formula (2.4) defines the macro-strain energy function related to the natural configuration of the body.

Let  $\Gamma_R$  be a part of  $\partial\Omega_R$  on which surface tractions  $s_R^i$  (averaged over the surface area) are known. The related boundary conditions are given by

$$(2.6) \quad S_R^{i\alpha} n_{R\alpha} = s_R^i \quad \text{on } \Gamma_R$$

with  $\mathbf{n}_R$  as a unit outward normal to  $\partial\Omega_R$ . It will be also assumed that on  $\partial\Omega_R \setminus \Gamma_R$ , values  $U_i^0$  of macro-displacements are prescribed:

$$(2.7) \quad U_i = U_i^0 \quad \text{on } \partial\Omega_R \setminus \Gamma_R.$$

Equations (2.2), (2.3) and boundary conditions (2.6), (2.7) hold for every  $t > 0$  and together with initial conditions for  $U_i, \dot{U}_i, Q_i^A, \dot{Q}_i^A$ , describe a certain boundary-value problem formulated in the framework of the refined macro-dynamics of a highly-elastic micro-periodic body and for a class of motions given by (2.1). The main feature of the refined macrodynamics is that the above problem takes into account the effect of the microstructure length-parameter  $l$  on the dynamic behaviour of the composite. It has to be emphasized that a solution to this problem has a physical sense only if  $U_i(\cdot, t), Q_i^A(\cdot, t)$  are regular macro-functions for every  $t \geq 0$ . For more detailed information the reader is referred to the references given in Introduction.

### 3. Analysis

Let us assume that a certain static deformation of the composite described by Eq.(2.1) is known, where the fields  $U_i = U_i(\mathbf{X}), Q_i^A = Q_i^A(\mathbf{X}), \mathbf{X} \in \Omega_R$  are constant in time and hence satisfy in  $\Omega_R$  the field equations

$$(3.1) \quad \left( \frac{\partial \pi_R(\mathbf{F}(\mathbf{X}), \mathbf{Q}(\mathbf{X}))}{\partial F_{i\alpha}} \right)_{,\alpha} = 0, \quad \frac{\partial \pi_R(\mathbf{F}(\mathbf{X}), \mathbf{Q}(\mathbf{X}))}{\partial Q_i^A} = 0, \quad \mathbf{X} \in \Omega_R,$$

and fulfil on  $\partial\Omega_R$  the time-independent boundary conditions of the form (2.6), (2.7); in (3.1)  $\mathbf{F}(\mathbf{X}) = \mathbf{1} + \nabla \mathbf{U}(\mathbf{X})$ . Every static deformation of the composite, defined by a pair  $\mathbf{E} = (\mathbf{U}(\cdot), \mathbf{Q}(\cdot))$  satisfying Eqs. (3.1), will be referred to as the equilibrium state. In order to investigate the stability of the above equilibrium state, the line of approach described in [10] will be applied. To this end let us assume that on the static deformation represented by a displacement field  $u_i(\mathbf{X}) = U_i(\mathbf{X}) + h^A(\mathbf{X})Q_i^A(\mathbf{X}), \mathbf{X} \in \Omega_R$ , a small deformation is superimposed, given by  $\varepsilon u_i(\mathbf{X}, t) = \varepsilon [U_i(\mathbf{X}, t) + h^A(\mathbf{X}) Q_i^A(\mathbf{X}, t)], t \geq 0$ , where  $\varepsilon$  is a small parameter, the squares and higher powers of which will be neglected as compared to  $\varepsilon$ , and where  $'U_i(\cdot, t), 'Q_i^A(\cdot, t)$  are arbitrary regular macro-functions. Using Eqs.(2.2), (2.3), (2.6), (2.7) and denoting

$$(3.2) \quad \begin{aligned} A_R^{i\alpha j\beta} &:= \frac{\partial^2 \pi_R(\mathbf{F}(\mathbf{X}), \mathbf{Q}(\mathbf{X}))}{\partial F_{i\alpha} \partial F_{j\beta}}, & B_R^{Aji\alpha} &:= \frac{\partial^2 \pi_R(\mathbf{F}(\mathbf{X}), \mathbf{Q}(\mathbf{X}))}{\partial F_{i\alpha} \partial Q_j^A}, \\ C_R^{ABij} &:= \frac{\partial^2 \pi_R(\mathbf{F}(\mathbf{X}), \mathbf{Q}(\mathbf{X}))}{\partial Q_i^A \partial Q_j^B}, & \mathbf{X} \in \Omega_R, \end{aligned}$$

after simple manipulations we obtain the linearized homogeneous field equations for  $'U_i, 'Q_i^A$ , which have to be satisfied in  $\Omega_R \times (0, \infty)$ :

$$(3.3) \quad \begin{aligned} & \left( A_R^{i\alpha j\beta} 'U_{j,\beta} + B_R^{Bji\alpha} 'Q_j^B \right)_{,\alpha} - \langle \varrho_R \rangle ' \ddot{U}^i = 0, \\ & l^2 \langle \varrho_R g^A g^B \rangle ' \ddot{Q}_i^B + C_R^{ABij} 'Q_j^B + B_R^{Aij\alpha} 'U_{j,\alpha} = 0, \end{aligned}$$

together with the homogeneous boundary conditions:

$$(3.4) \quad \begin{aligned} (A_R^{i\alpha j\beta} {}'U_{j,\beta} + B_R^{Bji\alpha} {}'Q_j^B) n_{R\alpha} &= 0 & \text{on } \Gamma_R \times (0, \infty), \\ {}'U_i &= 0 & \text{on } \partial\Omega_R \setminus \Gamma_R \times (0, \infty). \end{aligned}$$

From the definitions (3.2) and since  $\mathbf{F} = \mathbf{1} + \nabla \mathbf{U}$ , it follows that solutions  $'U_i, {}'Q_i^A$  to the boundary-value problems described by Eqs. (3.3), (3.4) depend on the known static deformation represented by the equilibrium state  $\mathbf{E} = (\mathbf{U}(\cdot), \mathbf{Q}(\cdot))$ . At the same time, every pair  $(\mathbf{F}, \mathbf{Q})$  satisfying the last of Eqs. (3.1) will be referred to as the local equilibrium state. Obviously, if a composite is in the equilibrium state  $(\mathbf{U}(\cdot), \mathbf{Q}(\cdot))$  then every  $(\mathbf{F}(\mathbf{X}), \mathbf{Q}(\mathbf{X}))$ ,  $\mathbf{X} \in \Omega_R$ , represents a certain local equilibrium state (but not conversely).

Now we shall pass to the analysis of some special cases.

First, let us assume that the superimposed deformations are time-independent, i.e.:

$$'U_i = {}'U_i(\mathbf{X}), \quad {}'Q_i^A = {}'Q_i^A(\mathbf{X}), \quad \mathbf{X} \in \Omega_R.$$

Under this assumption two special cases of instability can take place.

CASE 1.1. Let for every  $\mathbf{X} \in \Omega_R$  the linear transformation  $\mathbf{R}^{3N} \rightarrow \mathbf{R}^{3N}$  given by  $C_R^{ABij}$  be invertible for the known equilibrium state  $\mathbf{E} = (\mathbf{U}(\cdot), \mathbf{Q}(\cdot))$ . In this case the macro-internal variables  $'Q_i^A$  can be eliminated from Eqs. (3.3), (3.4) and we arrive at

$$(3.5) \quad \begin{aligned} (N_R^{i\alpha j\beta} {}'U_{j,\beta})_{,\alpha} &= 0 & \text{in } \Omega_R, \\ N_R^{i\alpha j\beta} {}'U_{j,\beta} n_{R\alpha} &= 0 & \text{on } \Gamma_R, \\ {}'U_i &= 0 & \text{on } \partial\Omega_R \setminus \Gamma_R, \end{aligned}$$

where we have denoted

$$N_R^{i\alpha j\beta} := A_R^{i\alpha j\beta} - B_R^{Aki\alpha} D_R^{ABkl} B_R^{Blj\beta}$$

and where  $D_R^{ABkl}$  determines the linear transformation  $\mathbf{R}^{3N} \rightarrow \mathbf{R}^{3N}$  inverse to that given by  $C_R^{ABkl}$ . If there exist non-trivial solutions to Eqs. (3.5) then the body in the equilibrium state  $\mathbf{E} = (\mathbf{U}(\cdot), \mathbf{Q}(\cdot))$  is assumed to have a hidden macro-instability, [10], and we deal with a *bifurcation of the equilibrium state E*. Moreover, if  $\Gamma_R = \emptyset$  then we arrive at the problem of the *internal macro-instability* investigated by BIOT [1, 2] as the internal buckling.

CASE 1.2. Now assume that under the known equilibrium state, a linear transformation  $\mathbf{R}^{3N} \rightarrow \mathbf{R}^{3N}$  determined by  $C_R^{ABkl}$  is singular for some local equilibrium state  $(\mathbf{F}(\mathbf{X}), \mathbf{Q}(\mathbf{X}))$ . In this case the body at the point  $\mathbf{X}$  is said to be in the state of a hidden micro-instability and we deal with a *bifurcation of the local equilibrium state (F(X), Q(X))*. Moreover if  $\mathbf{F} = \text{const}$ ,  $\mathbf{Q} = \text{const}$  in  $\Omega_R$  and  $\Gamma_R = \emptyset$ ,

then Eqs.(3.3) are satisfied by  $'U_i = 0, 'Q_i^A = \text{const}$  in  $\Omega_R$  and we deal with what can be called *the internal micro-instability*.

Second, let us assume that the superimposed motion is given by

$$'U_i(\mathbf{X}, t) = \bar{U}_i(\mathbf{X})e^{i\omega t}, \quad 'Q_i^A(\mathbf{X}, t) = \bar{Q}_i^A(\mathbf{X})e^{i\omega t},$$

where  $\omega$  is a certain complex number. Substituting the right-hand sides of the above formulae into Eqs. (3.3), (3.4) we obtain for  $\bar{U}_i, \bar{Q}_i^A$  the following system of equations

$$(3.6) \quad \begin{aligned} & \left( A_R^{i\alpha j\beta} \bar{U}_{j,\beta} + B_R^{Aj i\alpha} \bar{Q}_j^A \right)_{,\alpha} - \langle \varrho_R \rangle \omega^2 \bar{U}^i = 0, \\ & \left( C_R^{ABij} - l^2 \langle \varrho_R g^A g^B \rangle \delta^{ij} \omega^2 \right) \bar{Q}_j^B + B_R^{Aij\alpha} \bar{U}_{j,\alpha} = 0, \quad \text{in } \Omega_R, \end{aligned}$$

together with the boundary conditions

$$(3.7) \quad \begin{aligned} & \left( A_R^{i\alpha j\beta} \bar{U}_{j,\beta} + B_R^{Aj i\alpha} \bar{Q}_j^A \right) n_{R\alpha} = 0 \quad \text{on } \Gamma_R, \\ & \bar{U}_i = 0 \quad \text{on } \partial\Omega_R \setminus \Gamma_R. \end{aligned}$$

It has to be remembered that the eigenvalues  $\omega^2$  in Eqs.(3.6) depend on the known equilibrium state  $\mathbf{E} = (\mathbf{U}(\cdot), \mathbf{Q}(\cdot))$  since the coefficients in Eqs. (3.6), (3.7) are functions of  $\mathbf{F}(\mathbf{X}) = \mathbf{1} + \nabla \mathbf{U}(\mathbf{X})$  and  $\mathbf{Q}(\mathbf{X})$ , cf. formulae (3.2). The analysis of Eqs.(3.6), (3.7) leads to the so-called dynamic instability, [10]. Two special cases will be considered below.

CASE 2.1. Let us assume that for the known equilibrium state  $\mathbf{E} = (\mathbf{U}(\cdot), \mathbf{Q}(\cdot))$  and for every  $\mathbf{X} \in \Omega_R$  the linear transformation  $\mathbf{R}^{3N} \rightarrow \mathbf{R}^{3N}$  given by  $C_R^{ABij} - l^2 \langle \varrho_R g^A g^B \rangle \delta^{ij} \omega^2$  is invertible. Then every inverse transformation can be represented in the form of the asymptotic expansion

$$D_R^{ABkl} + l^2 \omega^2 D_R^{ADik} \langle \varrho_R g^D g^E \rangle D_R^{EBil} + o(l^2).$$

Neglecting terms  $o(l^2)$  we can eliminate  $\bar{Q}_j^B$  from Eqs. (3.6), (3.7). Defining

$$M_R^{i\alpha j\beta} := B_R^{Aik\alpha} D_R^{ADkl} \langle \varrho_R g^D g^E \rangle D_R^{EBlm} B_R^{Bjm\beta} \langle \varrho_R \rangle^{-1},$$

after some manipulations we arrive at the following system of equations for  $\bar{U}_i$ , which have to be satisfied in  $\Omega_R \times (0, \infty)$ :

$$(3.8) \quad \left( N_R^{i\alpha j\beta} \bar{U}_{j,\beta} \right)_{j,\alpha} + \langle \varrho_R \rangle \left[ \bar{U}^i - l^2 \left( M_R^{i\alpha j\beta} \bar{U}_{j,\beta} \right)_{,\alpha} \right] \omega^2 = 0$$

together with the boundary conditions

$$(3.9) \quad \begin{aligned} & \left( N_R^{i\alpha j\beta} - \langle \varrho_R \rangle l^2 \omega^2 M_R^{i\alpha j\beta} \right) \bar{U}_{j,\beta} n_{R\alpha} = 0 \quad \text{on } \Gamma_R \times (0, \infty), \\ & \bar{U}_j = 0 \quad \text{on } [\partial\Omega_R \setminus \Gamma_R] \times (0, \infty). \end{aligned}$$

Following [10] we shall assume that if  $\text{Im } \omega \geq 0$  then the equilibrium state  $\mathbf{E} = (\mathbf{U}(\cdot), \mathbf{Q}(\cdot))$  is stable. If in the vicinity of  $\mathbf{E}$  there exists a passage from  $\text{Im } \omega \geq 0$  to  $\text{Im } \omega < 0$ , then we deal with the loss of the *macro-vibrational stability* (provided that  $\text{Re } \omega \neq 0$ ) or the loss of the *macro-static stability* (if  $\text{Re } \omega = 0$ ) in this state. Moreover, if  $\Gamma_R = \emptyset$  then it is the loss of the *internal macro-vibrational* or *macro-static stability*, respectively.

CASE 2.2. Assume that for the known equilibrium state values  $\omega^2$  are the generalized eigenvalues given by  $(C_R^{ABij} - l^2 \omega^2 \langle \varrho_R g^A g^B \rangle \delta^{ij}) \bar{Q}_j^B = 0$  for some local equilibrium state  $(\mathbf{F}(\mathbf{X}), \mathbf{Q}(\mathbf{X}))$ . If  $\text{Im } \omega$  attains a negative value in this local equilibrium state then we shall deal with the loss of the *micro-vibrational stability* (for  $\text{Re } \omega \neq 0$ ) or the *micro-static stability* (for  $\text{Re } \omega = 0$ ). Moreover if  $\mathbf{F} = \text{const}$ ,  $\mathbf{Q} = \text{const}$ , in  $\Omega_R$  and  $\Gamma_R = \emptyset$  then Eqs. (3.6) are satisfied by  $'U_i = 0$ ,  $'Q_i^A = \text{const}$  in  $\Omega_R$  and we arrive at the problem of the loss of *internal micro-vibrational* or *micro-static stability*, respectively.

All the aforementioned cases of instability can be referred to as the local loss of stability. However, for micro-periodic highly-elastic materials we can also deal with the special case of a non-local instability described below.

CASE 3. Let us assume that for a certain  $\mathbf{X} \in \Omega_R$  there exists the macro-deformation gradient  $\mathbf{F}(\mathbf{X})$  for which the last of Eqs. (3.1) has more than one solution  $\mathbf{Q}$  satisfying together with  $\mathbf{F}$  condition  $\det(\mathbf{F} + \nabla h^A(\mathbf{Z})\mathbf{Q}^A) > 0$  for every  $\mathbf{Z} \in V_R + \mathbf{X}$ . In this case we deal with the non-local micro-instability. This kind of instability can be also referred to as the material instability strictly related to the micro-periodic heterogeneous structure of the composite body.

Summing up, the stability analysis for highly-elastic micro-periodic composites leads to the following three types of stability:

1. *Local macro-stability* described by Cases 1.1 and 2.1, which can be investigated similarly to the instability of homogeneous body.

2. *Local micro-stability* described by Cases 1.2 and 2.2 related to the investigations of the linear transformation given by  $C_R^{i\alpha j\beta}(\mathbf{F}, \mathbf{Q})$ .

3. *Non-local micro-stability* described by Case 3, related to the analysis of the last of Eqs. (3.1).

The problem of the non-local macro-stability is not investigated in this contribution. It has to be emphasized that the concept of the micro-stability is characteristic for composite micro-periodic bodies subjected to finite deformations.

#### 4. Analysis: incompressible bodies

The refined macrodynamics of micro-periodic composites made of highly-elastic incompressible constituents will take as a starting point the averaged incompressibility condition

$$(4.1) \quad \langle \det(\mathbf{F} + \nabla h^A(\mathbf{X})\mathbf{Q}^A) \rangle - 1 = 0.$$

It has to be emphasized that in the framework of the proposed macro-model, the exact incompressibility condition  $\det(\mathbf{F} + \nabla h^A(\mathbf{X})\mathbf{Q}^A) - 1 = 0$  may not be satisfied at every point  $\mathbf{X}$  of  $\Omega_R$ . Equation (4.1) can be also written in the explicit form

$$(4.2) \quad \det \mathbf{F} + \frac{1}{6} \varepsilon^{ijk} \varepsilon^{\alpha\beta\gamma} \left( 3 \langle h^A_{,\alpha} h^B_{,\beta} \rangle Q^A_i Q^B_j F_{k\gamma} + \langle h^A_{,\alpha} h^B_{,\beta} h^C_{,\gamma} \rangle Q^A_i Q^B_j Q^C_k \right) - 1 = 0,$$

where  $\varepsilon^{ijk}$ ,  $\varepsilon^{\alpha\beta\gamma}$  are the Ricci symbols.

In many special problems the analysis can be confined to a class of motions (2.1) in which all micro-shape functions satisfy the conditions:

$$(4.3) \quad \begin{aligned} \langle h^A_{,\alpha} h^B_{,\beta} \rangle &= 0 & \text{if } \alpha \neq \beta, \\ \langle h^A_{,\alpha} h^B_{,\beta} h^C_{,\gamma} \rangle &= 0 & \text{if } \alpha \neq \beta \neq \gamma \neq \alpha. \end{aligned}$$

This situation is typical for many disturbances investigated in dynamics of composite materials. In the simplest case relations (4.3) hold if every micro-shape function  $h^A(\cdot)$  depends exclusively on one arbitrary material coordinate  $X^\alpha$ . Under (4.3) the averaged incompressibility condition (4.2) reduces to the following one

$$(4.4) \quad \det \mathbf{F} - 1 = 0$$

being independent of macro-internal variables  $Q_i^A$ . The above condition represents the internal constraints imposed on the class of motions determined by Eqs.(2.1). Introducing the concept of a macro-pressure  $p_R = p_R(\mathbf{X})$  as a Lagrange multiplier related to Eq.(4.4), bearing in mind definitions (2.5) and modifying Eq.(2.4) to the form

$$(4.5) \quad \pi_R = \pi_R(\mathbf{F}, \mathbf{Q}) := \langle \varepsilon_R(\mathbf{X}, \mathbf{F} + \nabla h^A(\mathbf{X})\mathbf{Q}^A) \rangle - \lambda_R^{i\alpha} (F_{i\alpha} - \delta_{i\alpha}) - \mu_R^{A\alpha} Q_i^A + p_R(\det \mathbf{F} - 1),$$

we shall assume that the equilibrium equations (3.1) holds also for incompressible bodies (in the averaged sense explained above).

Summing up, under definitions (4.5), (2.5) and bearing in mind that  $\mathbf{F} = \mathbf{1} + \nabla \mathbf{U}$ , the equilibrium equations of the form (3.1) together with Eq.(4.4) lead to a system of equations for macro-displacements  $\mathbf{U}$ , macro-internal variables  $\mathbf{Q}^A$  and a macro-pressure  $p_R$ . This result holds true under conditions (4.3). If the above conditions do not hold then the averaged incompressibility condition has to be taken in its general form (4.2), and in Eq.(4.5) the term  $\det \mathbf{F} - 1$  has to be replaced by the left-hand side of Eq.(4.2).

The stability analysis for incompressible bodies has to be carried out similarly to that of the compressible bodies described in Sec.3. Apart from the superimposed small motions  $\varepsilon(U_i + h^A Q_i^A)$ , also a small excess of a macro-pressure

$\varepsilon' p_R$  has to be superimposed on  $p_R$ . Hence in the incremental equations, which for compressible bodies were given by Eqs. (3.3)–(3.9), we deal with terms involving  $'p_R$  and with the incremental form of Eq. (4.4). Under notation  $L_R := F^{-1}$  this equation is given by

$$L_R^{i\alpha} 'U_{i,\alpha} = 0.$$

The general line of approach to the stability analysis for incompressible composites, outlined in this section, will be illustrated by a simple example in the subsequent section of the paper.

**5. Example**

The general results obtained in this contribution will be now illustrated by the micro-stability analysis for a laminated body made of two perfectly bonded incompressible isotropic rubber-like materials. The scheme of the laminate is shown in the left-hand side of Fig. 1. Moreover, every lamina is assumed to be

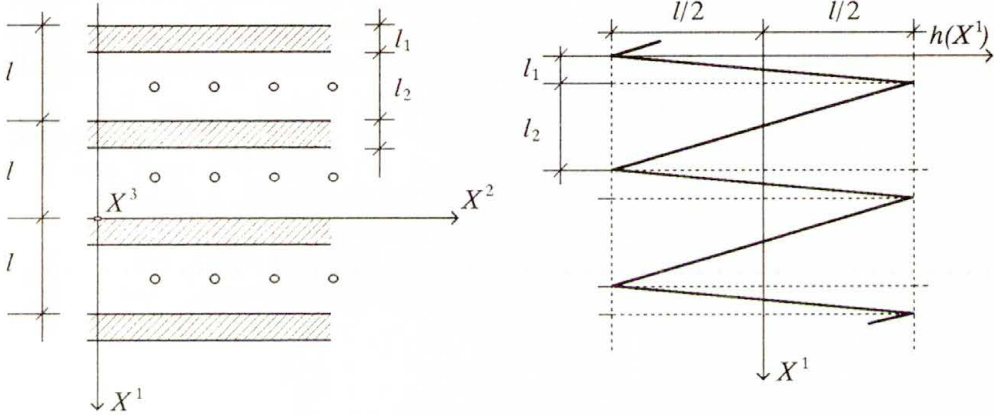


FIG. 1.

reinforced by a system of periodically distributed inextensible fibres parallel to the  $X^3$ -axis. Let the body be subjected to finite deformations caused by the uniform axial macro-strains along the coordinate axes. Using (3.1), the class of displacement fields under consideration will be expected in the form

$$(5.1) \quad \begin{aligned} u_1 &= U_1(X^1) + h^1(X^1)Q_1^1 + h^3(X^2)Q_1^3, \\ u_2 &= U_2(X^2) + h^2(X^1)Q_2^2, \\ u_3 &= 0, \end{aligned}$$

where

$$U_1(X^1) = (F_{11} - 1)X^1, \quad U_2(X^2) = (F_{22} - 1)X^2,$$

and (for the time being)  $F_{11}$ ,  $F_{22}$ ,  $Q_1^1$ ,  $Q_1^3$ ,  $Q_2^2$  are constants constituting the system of basic unknowns. We have tacitly assumed that the effect of periodic

inhomogeneity along  $X^2$ -axis on the displacement field is small and can be neglected. That is why a term  $h^4(X^2)Q_2^4$  in the second equation of (5.1) was not taken into account; the analysis involving this term is more complicated and will be given separately. The diagram of the micro-shape function  $h^1(\cdot)$  is shown on the right-hand side in Fig. 1; we also assume  $h^2(X^1) = l \cos(2\pi X^1/l)$  and  $h^3(X^2) = l_2 \sin(2\pi X^2/l_2)$ , where  $l_2$  is the period of the reinforcement along  $X^2$ -axis. In the problem under consideration  $V_R = (-l/2, l/2) \times (-l_2/2, l_2/2)$  and it is assumed that  $X^1 = 0$  is the plane of symmetry of the material structure of  $V_R$ .

Let us denote the basic unknown variables by means of

$$F_1 := F_{11}, \quad F_2 := F_{22}, \quad Q := Q_1^1, \quad Q_1 = Q_1^3, \quad Q_2 = Q_2^2.$$

It can be shown that the averaged incompressibility condition (4.1) yields

$$(5.2) \quad F_1 F_2 - 1 = 0.$$

Under Eq. (5.2) every quintuplet  $(F_1, F_2, Q, Q_1, Q_2)$  represents a certain micro-equilibrium state (now constant throughout the whole body) provided that the last of the equilibrium equations (3.1) holds; the first of these equations is identically satisfied since  $S_R^{i\alpha}$  are constant.

As we have stated in Sec. 2, in the framework of the refined macrodynamics the deformation gradient is approximated by  $\mathbf{F} + \nabla h^A(\mathbf{X})\mathbf{Q}^A$ , where now  $\mathbf{X} = (X^1, X^2)$ . In the problem under consideration, under extra notations

$$\begin{aligned} d &= d(X^1) := h^1_{,1}(X^1), \\ d_1 &= d_1(X^1) := h^2_{,1}(X^1), \\ d_2 &= d_2(X^2) := h^2_{,2}(X^2), \end{aligned}$$

the deformation gradient matrix is given by

$$\begin{bmatrix} F_1 + dQ & d_2 Q_1 & 0 \\ d_1 Q_2 & F_2 & 0 \\ 0 & 0 & 1 \end{bmatrix}$$

and for every  $\mathbf{X} \in \bar{V}_R := [-l/2, l/2] \times [-l_2/2, l_2/2]$  has to satisfy conditions

$$(5.3) \quad \begin{aligned} F_1 + d(\mathbf{X})Q &> 0, & F_2 &> 0, \\ F_1 F_2 + d(\mathbf{X})F_2 Q - d_1(\mathbf{X})d_2(\mathbf{X})Q_1 Q_2 &> 0. \end{aligned}$$

The components  $c_{\alpha\beta}$  of the deformed body metric tensor are given by the matrix

$$\begin{bmatrix} (F_1 + dQ)^2 + (d_1 Q_2)^2 & d_2(F_1 + dQ)Q_1 + d_1 F_2 Q_2 & 0 \\ d_2(F_1 + dQ)Q_1 + d_1 F_2 Q_2 & F_2^2 + (d_2 Q_1)^2 & 0 \\ 0 & 0 & 1 \end{bmatrix}$$

and the strain invariants  $I_1, I_2, I_3$  are equal to

$$\begin{aligned} I_1 &= \delta^{\alpha\beta} c_{\alpha\beta} = 1 + F_1^2 + F_2^2 + 2dF_1Q + (dQ)^2 + (d_1Q_1)^2 + (d_2Q_2)^2, \\ I_2 &= I_3 \delta_{\alpha\beta} c^{\alpha\beta} = 1 + F_1^2 + F_2^2 + 2d(F_1 + F_2)Q + (dQ)^2(1 + F_2^2) + (d_2Q_1)^2 \\ &\quad + (d_1Q_2)^2 + (d_1d_2Q_1Q_2)^2 - 2d_1d_2Q_1Q_2 - 2dd_1d_2F_2Q_1Q_2, \\ I_3 &= \det c_{\alpha\beta} = [(F_1 + dQ)F_2 - d_1d_2Q_1Q_2]^2. \end{aligned}$$

It has to be emphasized that in the applied approach, the local incompressibility condition  $\sqrt{I_3} - 1 = 0$  does not hold and we deal exclusively with the averaged form of this condition, given by Eq. (4.1) which now reduces to Eq. (5.2).

The strain energy function for rubber-like materials will be assumed in the known form

$$\varepsilon_R = C(I_1 - 3) + D(I_2 - 3),$$

where the material moduli  $C, D$  are now  $l$ -periodic functions of  $X^1$ , attaining different values in the adjacent laminae. Due to the presence of a reinforcement we shall also treat  $C, D$  as  $l_2$ -periodic functions of  $X^2$ . Hence  $C$  and  $D$  as well as the invariants  $I_1, I_2$  are  $V_R$ -periodic functions of  $\mathbf{X} = (X^1, X^2)$ . The formula (4.5) for the macro-strain energy function of an incompressible isotropic material is given by

$$\pi_R = \langle \varepsilon_R(\mathbf{X}, I_1(\mathbf{X}), I_2(\mathbf{X})) \rangle - \lambda_R^{i\alpha} (F_{i\alpha} - \delta_{i\alpha}) - \mu_R^{Ai} Q_i^A + p_R(\det \mathbf{F} - 1),$$

where the averaging operation has to be carried out with respect to  $\mathbf{X}$ , and  $\lambda_R^{i\alpha}, \mu_R^{Ai}$  are defined by Eqs. (2.5). After some calculations we obtain

$$\begin{aligned} \pi_R &= \langle C + D \rangle (F_1^2 + F_2^2 - 2) + 2[\langle (C + D)d \rangle F_1 + \langle Dd \rangle F_2] Q \\ &\quad + [\langle (C + D)d^2 \rangle + \langle Dd^2 \rangle F_2^2] Q^2 + \langle (C + D)d_2^2 \rangle Q_1^2 \\ &\quad + \langle (C + D)d_1^2 \rangle Q_2^2 + \langle D(d_1d_2)^2 \rangle (Q_1Q_2)^2 \\ &\quad - 2[\langle Dd_1d_2 \rangle + \langle Ddd_1d_2 \rangle F_2Q] Q_1Q_2 - \langle C + D \rangle (F_1 + F_2 - 2) \\ &\quad - 2[\langle (C + D)d \rangle + \langle Dd \rangle] Q + p_R(F_1F_2 - 1). \end{aligned}$$

Under notations

$$\begin{aligned} \alpha &:= \langle (C + D)d^2 \rangle, & \alpha_1 &:= \langle (C + D)d_1^2 \rangle, & \alpha_2 &:= \langle (C + D)d_2^2 \rangle, \\ \beta &:= \langle D(d_1d_2)^2 \rangle, & \gamma &:= \langle Dd^2 \rangle, & \phi &:= \langle Ddd_1d_2 \rangle, \\ \mu &:= \langle (C + D)d \rangle, & \nu &:= \langle Dd \rangle, & \chi &:= \langle Dd_1d_2 \rangle \end{aligned}$$

and setting

$$F := F_2 = (F_1)^{-1},$$

the second of the equilibrium equations (3.1) takes the form

$$(5.4) \quad \begin{aligned} (\alpha + \gamma F^2)FQ - \phi F^2 Q_1 Q_2 + (1 - F)(\mu - \nu F) &= 0, \\ (\alpha_1 Q_2 + \beta)Q_2 Q_1^2 - (\chi + \phi FQ)Q_1 &= 0, \\ (\alpha_2 Q_1 + \beta)Q_1 Q_2^2 - (\chi + \phi FQ)Q_2 &= 0. \end{aligned}$$

At the beginning let us consider two special cases.

First, assume that the laminae are not reinforced. In this case  $C(\cdot)$  and  $D(\cdot)$  are independent of  $X^2$  and

$$\begin{aligned} \phi &:= \langle Ddd_1 d_2 \rangle = \langle Ddd_1 \rangle \langle d_2 \rangle = 0, \\ \chi &:= \langle Dd_1 d_2 \rangle = \langle Dd_1 \rangle \langle d_2 \rangle = 0, \end{aligned}$$

because of  $\langle d_2 \rangle = 0$ . In this case there exists the unique solution to Eqs. (5.4) given by

$$(5.5) \quad Q = \frac{(F - 1)(\mu - \nu F)}{(\alpha + \gamma F^2)F}, \quad Q_1 = Q_2 = 0.$$

Second, let the body be homogeneous. Then, apart from conditions  $\phi = \chi = 0$ , we also obtain  $\mu = 0$  and  $\nu = 0$ . In this case  $Q = Q_1 = Q_2 = 0$  and by means of Eqs. (5.1), an arbitrary uniform biaxial strain, given by  $F_1 = F^{-1}$ ,  $F_2 = F$ , holds for every  $F > 0$ .

Now we shall pass to the general case of the micro-periodic body under consideration. In order to investigate the bifurcation of a micro-equilibrium state  $(F_1, F_2, Q, 0, 0)$  let us assume that  $Q_1 = \varepsilon' Q_1$ ,  $Q_2 = \varepsilon' Q_2$ , where  $\varepsilon \rightarrow 0$ . Let us also denote

$$\delta := \chi - \sqrt{\alpha_1 \alpha_2}, \quad \bar{\delta} := \chi + \sqrt{\alpha_1 \alpha_2}$$

and assume that  $\delta \bar{\delta} \neq 0$ . If  $\phi \neq 0$  then the non-zero solutions  $Q_1, Q_2$  to the second and third of Eqs. (5.4) exist either if

$$(5.6) \quad Q = -\frac{\delta}{\phi F}$$

or if

$$(5.7) \quad Q = -\frac{\bar{\delta}}{\phi F}.$$

The two aforementioned conditions will be treated separately.

Substituting the right-hand side of Eq. (5.6) into the first of Eqs. (5.4) (where now  $Q_1 Q_2 = \varepsilon^2 {}'Q_1 {}'Q_2 \rightarrow 0$ ) we arrive at

$$(5.8) \quad (\nu \phi - \gamma \delta)F^2 - \phi(\mu + \nu)F + \mu \phi - \alpha \delta = 0.$$

The above equation together with the condition  $F > 0$  represent the solution in which the bifurcation of a micro-equilibrium state  $(F^{-1}, F, Q, 0, 0)$ , where  $Q = -\delta(\phi F)^{-1}$ , takes place. Now assume

$$(5.9) \quad \nu\phi - \gamma\delta \neq 0$$

and define

$$(5.10) \quad b := \frac{\phi(\mu + \nu)}{\gamma\delta - \nu\phi}, \quad c := \frac{\alpha\delta - \mu\phi}{\gamma\delta - \nu\phi}.$$

It can be shown that the bifurcation can take place in the following cases:

(i) If  $c < 0$  and  $1 + b + c < 0$  then there exists one positive root  $F = F_E$  of Eq. (5.8) such that  $F_E > 1$ . In this case the bifurcation occurs under extension of the body along  $X^2$ -axis.

(ii) If  $c < 0$  and  $1 + b + c < 0$  then there exists one positive root  $F = F_C$  of Eq. (5.8) satisfying condition  $0 < F_C < 1$  and the bifurcation occurs under compression of the body along  $X^2$ -axis.

(iii) If  $c > 0$  and  $1 + b + c < 0$  then there exist two positive roots  $F = F_C$ ,  $F = F_E$  of Eq. (5.8) related to the compression and extension of the body along  $X^2$ -axis, respectively, i.e.,  $0 < F_C < 1$  and  $F_E > 1$ .

(iv) If  $\nu\phi - \gamma\delta = 0$  and

$$F = \frac{\mu\phi - \alpha\delta}{\gamma\delta + \mu\phi},$$

then we obtain  $F = F_E > 1$  if  $(\delta/\phi)(\mu + \nu) > 0$  or  $F = F_C$ ,  $0 < F_C < 1$ , if  $(\delta/\phi)(\mu + \nu) < \min\{0, (\mu/\alpha)(\mu + \nu)\}$ .

Let us also observe that since  $\delta \neq 0$ ,  $\alpha > 0$  and  $\gamma > 0$ , then the bifurcation cannot take place in the natural state in which  $F = 1$ .

If one from the above conditions takes place, then the value of  $Q$  for which the bifurcation occurs is determined by Eq. (5.6). The analysis similar to that given above can be carried out if the constant  $\delta$  will be replaced by the constant  $\bar{\delta}$ . In this case the value of  $Q$  related to the bifurcation state will be determined by Eq. (5.7) and instead of parameters  $b, c$ , under condition

$$\nu\phi - \gamma\bar{\delta} \neq 0,$$

we shall introduce the parameters

$$\bar{b} := \frac{\phi(\mu + \nu)}{\gamma\bar{\delta} - \nu\phi}, \quad \bar{c} := \frac{\alpha\bar{\delta} - \mu\phi}{\gamma\bar{\delta} - \nu\phi}.$$

Hence the discussion of cases (i)–(iii) remains unchanged if moduli  $b, c$  will be replaced by moduli  $\bar{b}, \bar{c}$ , respectively. Similarly, in the case (iv)  $\delta$  has to be

replaced by  $\bar{\delta}$ . It means that apart from values  $F_C, F_E$  of a macro-deformation gradients for which the bifurcation can take place, we also obtain two other values  $\bar{F}_C, \bar{F}_E$  related to the constants  $\bar{\delta}, \bar{b}$  and  $\bar{c}$ , where  $\bar{F}_C \in (0, 1)$ , and  $\bar{F}_E > 1$ .

Now let us investigate the problem of the nonlocal (postbifurcation) microstability. To simplify the calculations let us assume  $\alpha_1 = \alpha_2$  and denote  $\alpha_0 = \alpha_1 = \alpha_2$ . Using this assumption from Eqs. (5.4) we obtain either

$$(5.11) \quad \begin{aligned} (\alpha + \gamma F^2)FQ - \phi(FQ_1)^2 + (1 - F)(\mu - \nu F) &= 0, \\ \alpha_0 Q_1 + \beta Q_1^3 - (\chi + \phi FQ)Q_1 &= 0, \\ Q_2 &= Q_1, \end{aligned}$$

or

$$(5.12) \quad \begin{aligned} (\alpha + \gamma F^2)FQ + \phi(FQ_1)^2 + (1 - F)(\mu - \nu F) &= 0, \\ \alpha_0 Q_1 + \beta Q_1^3 + (\chi + \phi FQ)Q_1 &= 0, \\ Q_2 &= -Q_1. \end{aligned}$$

The two above cases have to be treated separately.

CASE 1. From Eqs. (5.11), apart from the solution

$$(5.13) \quad Q = \frac{(F - 1)(\mu - \nu F)}{(\alpha + \gamma F^2)F}, \quad Q_1 = Q_2 = 0,$$

which holds for every  $F > 0$  (and coincides with that given by Eqs. (5.5)), we also obtain two other solutions

$$(5.14) \quad \begin{aligned} Q &= -\frac{(\beta\nu + \alpha_0\phi - \chi\phi)F^2 - \beta(\mu + \nu)F + \beta\mu}{[\alpha\beta + (\beta\gamma - \phi^2)F^2]F}, \\ Q_1^2 &= -\beta\frac{(\nu\phi - \gamma\delta)F^2 - \phi(\mu + \nu)F - \mu\phi + \alpha\delta}{\alpha\beta + (\beta\gamma - \phi^2)F^2}, \quad Q_2 = Q_1, \end{aligned}$$

where we have denoted  $\delta := \chi - \alpha_0$ .

CASE 2. From Eqs. (5.12), apart from the solution (5.13) which holds for every  $F > 0$  we obtain two other solutions

$$(5.15) \quad \begin{aligned} Q &= -\frac{(\beta\nu - \alpha_0\phi - \chi\phi)F^2 - \beta(\mu + \nu)F + \beta\mu}{[\alpha\beta + (\beta\gamma - \phi^2)F^2]F}, \\ Q_1^2 &= \beta\frac{(\nu\phi - \gamma\bar{\delta})F^2 - \phi(\mu + \nu)F - \mu\phi - \alpha\bar{\delta}}{\alpha\beta + (\beta\gamma - \phi^2)F^2}, \quad Q_2 = -Q_1, \end{aligned}$$

where  $\bar{\delta} := \chi + \alpha_0$ .

Under assumption  $\beta\gamma > \phi^2$  and using notations introduced above solutions (5.14) hold, for  $F \in (0, F_C]$  and  $F \geq F_E$ , where  $F_C < 1 < F_E$ . If  $F \in (F_C, F_E)$  then there exists solution given by Eqs. (5.13). At the same time solutions (5.15) hold for  $F \in (0, \bar{F}_C]$  and  $F \geq \bar{F}_E$ , where  $\bar{F}_C < 1 < \bar{F}_E$ . If  $F \in (\bar{F}_C, \bar{F}_E)$  the solution is given by Eqs. (5.13). It means that there can exist two kinds of bifurcations; in the first case after the bifurcation we obtain  $Q_1 = Q_2$  and in the second  $Q_1 = -Q_2$ .

It has to be remembered that all the obtained results have the physical sense if and only if conditions (5.3) hold for every  $\mathbf{X} \in \bar{V}_R$ .

The micro-bifurcation cannot take place in materials for which either conditions  $b^2 < 4c$  and  $\bar{b}^2 < 4\bar{c}$  or conditions  $b \leq 0$ ,  $c \geq 0$  and  $\bar{b} \leq 0$ ,  $\bar{c} \geq 0$  hold. In this case there exist one micro-equilibrium path  $(F_1, F_2, Q, Q_1, Q_2)$  in which  $F_2 = F$ ,  $F_1 = F^{-1}$  and Eqs. (5.5) hold for every  $F > 0$ .

To make the above example more clear from the physical viewpoint we have stated at the beginning of this section that the variables  $F_1$ ,  $F_2$  as well as  $Q_1$ ,  $Q_2$ ,  $Q_3$  are constant throughout the body. However, all investigations given above also hold true if the aforementioned variables are arbitrary regular macro-functions of  $\mathbf{X} \in \Omega_R$ . In this case we can also take into account the first of Eqs. (3.1) and after that pass to the analysis of the macro-stability of a body.

## 6. Conclusions

The obtained general relations concerning stability of highly-elastic periodic composites under finite deformations yield the analytical basis for calculations of different special problems. Following the general comments given at the end of Sec.3 we can mention here the problems of macro-stability and those of the local and non-local micro-stability. It can be seen that in the problems of macro-stability, after neglecting the effect of the microstructure length dimension on the dynamic behaviour of the body, the obtained formulae are similar to those of the nonlinear elasticity of homogeneous bodies. Under this approximation terms involving  $l^2$  drop out from Eqs.(3.8), (3.9). Hence the first new result is the investigation of the effect of the microstructure length parameter  $l$  on the dynamic macro-stability of the body. The second new result is the existence of the local and non-local micro-stability in highly-elastic composites. This phenomenon is due to the micro-periodic material structure of the body and was illustrated in Sec.5. More general applications of the obtained results are under consideration and will be presented in a separate paper.

## Acknowledgment

This research was supported by KBN, Warsaw, under grant 7T07A01711.

## References

1. M.A. BIOT, *Internal buckling under initial stress in finite elasticity*, Proc. Roy. Soc., A **273**, 1963.
2. M.A. BIOT, *Further development of the theory of internal buckling of multilayers*, Bull. Geol. Soc. Am., **75**, 1965.
3. M.A. BIOT, *Interfacial instability in finite elasticity under initial stress*, Proc. Roy. Soc., A **273**, 1963.
4. M.A. BIOT, *Surface instability in finite anisotropic elasticity under initial stress*, J. Math. Mech., **6**, 12, 1963.
5. M.A. BIOT, *Theory of stability of multilayered continua in finite anisotropic elasticity*, J. Franklin Inst., **276**, 1963.
6. A.E. GREEN and A.J.M. SPENCER, *The stability of a circular cylinder under finite extension and torsion*, J. Math. Phys., **37**, 4, 1959.
7. GUO ZHONG-HENG, *The problem of stability and vibration of a circular plate subject to finite initial deformation*, Arch. Mech. Stos., **14**, 1, 1962.
8. GUO ZHONG-HENG and W. URBANOWSKI, *Stability of non-conservative systems in the theory of elasticity of finite deformations*, Arch. Mech. Stos., **15**, 2, 1963.
9. Z. WESOŁOWSKI, *Experimental investigation of hollow spheres loaded by external hydrostatic pressure* [in Polish], Rozpr. Inż., **11**, 4, 1963.
10. Z. WESOŁOWSKI, *Dynamical problems of nonlinear elasticity* [in Polish], PWN, Warszawa 1974.
11. Z. WESOŁOWSKI, *Stability in some cases of tension in the light of the theory of finite strain*, Arch. Mech. Stos., **14**, 6, 1962.
12. Z. WESOŁOWSKI, *Stability of a full elastic sphere uniformly loaded on a surface*, Arch. Mech. Stos., **16**, 5, 1964.
13. Z. WESOŁOWSKI, *Stability of an elastic orthotropic parallelepiped subject to finite elongation*, Bull. Acad. Polon. Sci., Série Sci. Tech., **12**, 3, 1964.
14. Z. WESOŁOWSKI, *Stability of an elastic thick-walled spherical shell loaded by an external pressure*, Arch. Mech. Stos., **19**, 1, 1967.
15. Z. WESOŁOWSKI, *The axially symmetric problem of stability loss of an elastic bar subject to tension*, Arch. Mech. Stos., **15**, 3, 1963.
16. E. WIERZBICKI, *Nonlinear macro-micro dynamics of laminated structures*, J. Theor. Appl. Mech., **33**, 2, 1995.
17. E. WIERZBICKI, C. WOŹNIAK and M. WOŹNIAK, *Finite rotations in the refined macrodynamics of composite materials*, J. Theor. Appl. Mech., **33**, 1, 1995.
18. E.W. WILKES, *On the stability of a circular tube under end thrust*, Q.J. Mech. Appl. Math., **8**, 1, 1955.
19. C. WOŹNIAK, *Refined macrodynamics of periodic structures*, Arch. Mech., **45**, 3, 1993.

WARSAW UNIVERSITY

FACULTY OF MATHEMATICS, COMPUTER SCIENCES AND MECHANICS

e-mail: ewar@mimuw.edu.pl

CZEŹSTOCHOWA UNIVERSITY OF TECHNOLOGY

INSTITUTE OF MATHEMATICS AND COMPUTER SCIENCE

ul. Dąbrowskiego 69, 42-200 CZEŹSTOCHOWA

and

ŁÓDŹ UNIVERSITY OF TECHNOLOGY

DEPARTMENT OF GEOTECHNICS AND STRUCTURE ENGINEERING, ŁÓDŹ.

Al. Politechniki 2, 90-924 ŁÓDŹ 40, POLSKA.

Received August 22, 1996.

# Plasma double layer system leading to chaos, intermittency and flicker noise

A.J. TURSKI and B. ATAMANIUK (WARSZAWA)

ELECTROSTATIC DOUBLE LAYERS appear in plasma and semiconductor systems with flow of electric current. The systems display bifurcations, chaos, intermittency and power-law of spectral power density that is  $1/f$ -noise also called flicker noise. Fractal analysis of experimental data recorded in time (time-series analysis) indicates that the plasma dynamic systems are of low dimension. Colored and fractal noise influence on measured data may disqualify that conclusion. A piecewise linear dynamical system is considered to clarify this problem. Bifurcation tree, intermittent chaos and  $1/f$ -noise are revealed by the dynamic system.

## 1. Introduction

THE STUDY OF PLASMA systems may be performed by analyzing experimental data recorded as a series of measurements in time of pertinent and easily accessible state variables of the system, e.g. electric current, voltage, densities and velocities. In most cases, such variables describe a global or averaged properties of the system. Although there already exists a vast literature describing experimental results concerning bifurcation, intermittency and chaos in plasma discharge and turbulent systems, a complete and coherent discussion and theory derived from plasma equations are still lacking. Plasma discharges produced by electric current flow and revealing self-oscillations (Hopf bifurcation), saddle-node and period-doubling bifurcations, intermittency and chaos are of our interest. We assume that the cause of the occurring phenomena is charge separation leading to double layers (DL), which are localized in space. The wave length of the wave phenomena is much greater than the physical size of the system and we can consider DL as a lumped element. The assumption allow us to construct a simplified model. It is based on piecewise linear voltage-charge characteristic of a capacitor simulating DL. The model can be realized in the form of nonlinear electrical circuit and the measured variables are to be compared with those analytically computed. By virtue of the circuit equation analysis [1], Poincaré map is derived. Calculation of bifurcation trees and strange attractors for different parameter sets are displayed and intermittency, saddle-node and period-doubling bifurcations are revealed.

Plasma experimental data recorded as a series of measurements in time are analyzed by use of fractal dimension and the average dimension, most often correlation dimension, is low and that implies the low-dimensional dynamical system [2, 3]. This conclusion was very recently criticized for the two reasons. One stems from the fact that the apparent correlation dimension may result from the class of

stochastic noises with a power-law of spectral power density,  $f^{-\alpha}$ , the so-called colored noise, which leads to a low finite value for the correlation dimension, see [4]. The second reason is related to intermittency which leads to the same power-law spectra and low fractal dimension. The low correlation dimension of such noise means that the trajectories in the state space exhibit fractal behaviour along the trajectories, while the fractality of a strange attractor associated with a chaotic system is perpendicular to the motion such that each trajectory returns at time close to the starting points. The methods which have been used in the studies of the correlation dimension [3, 4] do not distinguish between these two kinds of fractalities. The situation around this topic has remained unclear and we offer some nonlinear circuit analogue models, which show promising results. We introduce two notions – one is a colored stochastic noise and its power-law spectra for low frequencies, and the other one is intermittent chaos leading to  $f^{-\alpha}$  noise. It deserves notice that the  $f^{-\alpha}$  noises are ubiquitous phenomena concerning elements of electronics, acoustics, mechanics, traffics, etc., see [5, 6, 7]. Consideration of dynamical system with piecewise linear nonlinearity may contribute to understanding of the problem.

## 2. Colored noise

Colored stochastic noise  $\eta(t)$  is based on an extension of the space of variables so that  $\eta(t)$  itself becomes a variable driven by white noise  $\zeta(t)$ . In particular, if  $\eta(t)$  is exponentially correlated Gaussian noise then one can write the set of stochastic differential equations

$$(2.1) \quad \dot{x}(t) = G(x) + g(x)\eta(t),$$

$$(2.2) \quad \dot{\eta}(t) = -\frac{1}{\tau_c}\eta(t) + \zeta(t),$$

where  $G(x)$  is the deterministic “force” and  $\zeta(t)$  is Gaussian white noise with correlation function

$$(2.3) \quad \langle \zeta(t)\zeta(\tau) \rangle = 2D \delta(t - \tau).$$

Then it can be easily seen that (2.2) leads to the exponential correlation function

$$(2.4) \quad \langle \eta(t)\eta(\tau) \rangle = \frac{D}{\tau_c} e^{-\frac{|t-\tau|}{\tau_c}}.$$

The probability density  $P(x, \eta; (t/x_0), \eta_0)$  obeys a Fokker–Planck equation. Bicolored stochastic noise assumes two additional variables  $\eta_1(t)$  and  $\eta_2(t)$  with constants  $\tau_{c1}$  and  $\tau_{c2}$ , see Eq.(2.2), driven by white noises with  $D_1$  and  $D_2$ , respectively.

We note that colored noise had a low correlation dimension as determined from the Grassberger – Procaccia (GP) algorithm [4]. The stochastic process generated by one or two colors can be expressed as discrete Fourier series [4]

$$(2.5) \quad X(i) = \sum_{k=1}^{N/2} C_k \cos(2\pi i k/N - \phi_k),$$

where  $\phi_k$  are random phases in the range  $[0, 2\pi]$  for each wave number  $k$ ,  $f = k/N$  is a frequency, and the coefficients  $C_k$  are related to the power spectrum  $P(k) = Q k^{-\alpha}$ , that is

$$(2.6) \quad C_k = \left[ P(k) \frac{2\pi}{N} \right]^{1/2}$$

for bicolored noise, we have two powers  $\alpha_1, \alpha_2$ , and  $\alpha_1$  is valid for the range  $k < k_c$  and  $\alpha_2$  is valid for  $k > k_c$ . Critical value  $k_c$  is such that it relates to a frequency at which there is a break in the power spectrum of the measured variable. The condition of continuity is fulfilled if  $Q_1 k^{-\alpha_1} = Q_2 k^{-\alpha_2}$ .

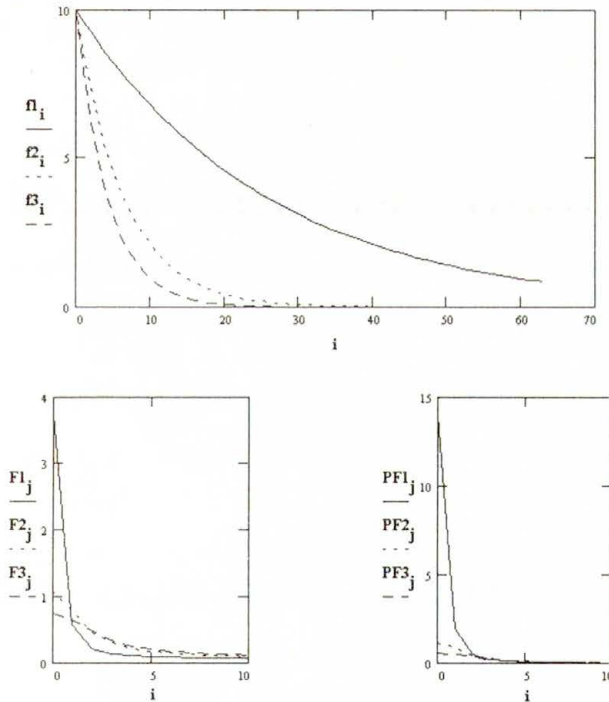


FIG. 1. Exponential correlation functions –  $f1_i, f2_i, f3_i$  versus  $i$ , related Fourier transforms  $F1_j, F2_j, F3_j$  and power Fourier transforms  $PF1_j, PF2_j, PF3_j$  versus  $j$ .

Computer calculated and plotted Fig. 1 refers to the correlation functions (2.4) and exhibits  $f_{l,i} = A \exp(-k_l t_i)$ , where  $l = 1, 2, 3; k_1 = 0.25, k_2 = 1, k_3 = 1.5$

and  $t_i = 0 \div 63$ . Also Fourier transforms  $F_{1,j} = FFT(f_1)$ ,  $F_{2,j}$ ,  $F_{3,j}$  are shown as well as power spectra  $PF_{1,j} = (|F_{1,j}|)^2$ ,  $PF_{2,j}$ , and  $PF_{3,j}$  are depicted.

The Fourier transform

$$(2.7) \quad F_{l,j} = \frac{A_l}{\pi} \frac{1}{\omega_j^2 + k_l^2}, \quad l = 1, 2, 3$$

is the well known Lorentzian spectral density revealing flicker noise. This approach is to be used in cases of more complex correlation functions.

### 3. Intermittency and flicker noises

The phenomena of flicker noise have long posed some enigmatic questions. First and foremost is the question of how is it possible that in systems of minute physical size there occur processes on the time scale so long as to allow for divergences in their spectra? The appearance of broadband spectra and, at the same time, the rising of the low-frequency end have long been associated with the onset of chaotic behaviour. Chaotic signals as well as stochastic ones are assumed to have stationary statistic and the correlation function

$$(3.1) \quad \langle x(t) x(\tau) \rangle \equiv C_x(\tau).$$

Since noise waves have infinite energy but finite power, we must define a power spectral density.

The autocorrelation function for a noise wave  $x(t)$  is defined as the time average

$$(3.2) \quad C_x(\tau) \equiv \lim_{T \rightarrow \infty} \frac{1}{2T} \int_{-T}^T x(t + \tau) x(t) dt$$

and then

$$C_x(\tau) = C_x(-\tau).$$

The spectral density of the noise wave  $x(t)$  is defined as the Fourier transform

$$(3.3) \quad S_x(f) = \int_{-\infty}^{\infty} C(\tau) e^{-2\pi i \tau f} d\tau,$$

where  $S_x(f)$  must be real and positive and if  $x(t)$  is real, we have

$$S_x(f) = S_x(-f).$$

Bifurcation and chaotic features of dynamical systems of finite number of freedom-degrees are investigated by use of Poincaré maps, which are discrete processes. In case of one-dimensional map

$$(3.4) \quad x_{n+1} = g(x_n),$$

the discrete autocorrelation function  $C_x(m)$  of  $x_n$  is

$$(3.5) \quad C_x(m) = \lim_{N \rightarrow \infty} \frac{1}{2N + 1} \sum_{n=-N}^N x_{n+m} x_n,$$

and spectral density

$$(3.6) \quad S_x(f) = \sum_{m=-\infty}^{\infty} C_x(m) e^{-2\pi m i f}.$$

By virtue of symmetry, we have

$$(3.7) \quad S_f = \sum_{m=0}^{\infty} C(m) \cos(2\pi m f),$$

where

$$(3.8) \quad C_x(m) = \lim_{N \rightarrow \infty} \frac{1}{N} \sum_{n=0}^N x_{n+m} x_n.$$

Let us consider a logistic map

$$(3.9) \quad x_{n+1} = R x_n(1 + x_n) \equiv g(x_n)$$

where  $0 < R < 4$ .

Just below period 3, there is a saddle-node bifurcation for  $R_c = 1 + (8)^{1/2}$  and then at  $R = R_c - \varepsilon$ , an intermittent signal appears. For any  $\varepsilon > 0$ , correlation functions  $C_x(m)$  decay exponentially with a decay time  $\tau \sim \varepsilon^{-1/2}$ , see [5]. By plotting the power spectrum of the third iterate  $g^3(x)$  we can thus get an apparent  $1/f^2$  divergence, with a cut-off that can again be pushed down to arbitrarily small frequencies by lowering  $\varepsilon$ . There are three types of intermittenencies. The first one is connected with transition from saddle-node bifurcation to chaos, second with Hopf bifurcation and the third one with period doubling bifurcation. Figure 2 demonstrates the computed results of the intermittent signal  $x_n$  versus  $n$  for  $R = 3.74474 < R_c$ , its correlation function

$$(3.10) \quad C_s = \frac{1}{N + 2 - s} \left( \sum_{k=0}^{N+1-s} x_{k+s} x_s \right)$$

and Fourier transform  $K C_s := FFT(C_s)$  as well as power spectral density, that is  $P K C_s := (|K C_s|)^2$ . Spectral densities reveal  $1/f$  divergence in vicinity of  $f = 0$ , ( $s = 0$ ). This approach is to be used in cases of more complex Poincaré maps.

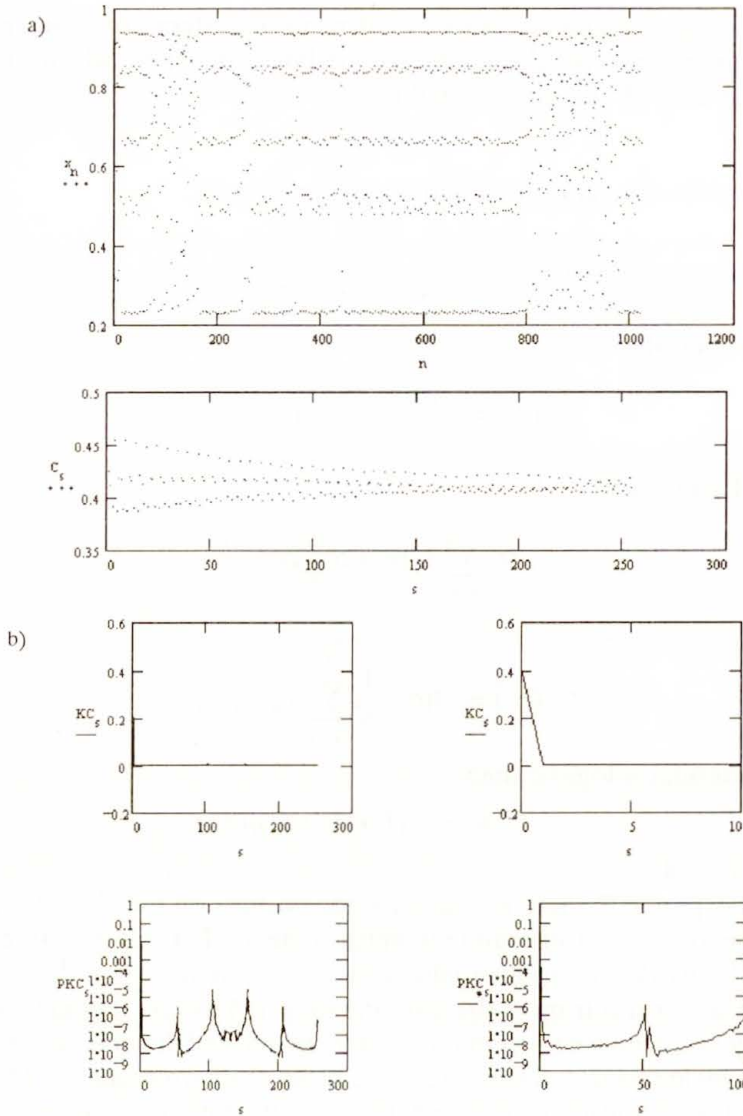


FIG. 2. a) Intermittent signal  $x_n$  versus  $n$  for logistic map  $x_{n+1} = Rx_n(1 - x_n)$  where  $R = 3.74474$  and its correlation function  $C_s$ . b) Fourier transform  $KC_s$ , and  $PKC_s$  versus  $s$ . The right-hand side drawings of  $KC_s$  and  $PKC_s$  are enlarged in vicinity of  $s = 0$  and demonstrate  $1/f$  - noise behaviour.

#### 4. Charge separation and double layer simulations

Charge separation in plasmas takes place due to electric current flow. Formation of DL starts when electron and ion convection velocities of the flow satisfy Bohm conditions, e.g. see Galeev and Sagdeev, Ch. 1 in the monograph [8]. The

negative anomalous resistivity of plasma discharges leads to self-oscillation [9] and then nonlinear voltage-charge characteristic is responsible for bifurcation, intermittency and chaos. The characteristic is similar, if not identical, to that of junction capacitance of semiconductor diode, which is based on charge separation. Self-oscillations of plasma discharges are revealed by use of electrical circuit with nonlinear resistance, e.g. see [10]. The problem is classical in plasma discharges. The next step is a simulation of plasma discharge system by a driven R–L–Diode circuit, see [1, 9]. The circuit ordinary differential equations are reduced to the following 2-D Poincaré map [1, 9]:

$$(4.1) \quad \begin{aligned} x_{n+1} &= y_n - 1 + \begin{cases} a_1 x_n & \text{for } x_n \geq 0, \\ -a_2 x_n & \text{for } x_n < 0, \end{cases} \\ y_{n+1} &= b x_n, \end{aligned}$$

where  $x_n$  and  $y_n$  are responsible for charge and current in the circuit, and

$$(4.2) \quad \begin{aligned} a_1 &= e^{\lambda_1} + e^{\lambda_2}, \\ b &= -e^{\lambda_1 + \lambda_2} = -e^{-R/2Lf}, \\ \lambda_{1,2} &= -\frac{R}{2Lf} \pm \frac{1}{2f} \left[ \left( \frac{R}{L} \right)^2 - \frac{4}{LC_{1,2}} \right]^{1/2}. \end{aligned}$$

$R, L, C_1, C_2$  are circuit elements and  $f$  is the frequency of the driving voltage. Characteristic values  $\lambda_{1,2}$  are real or complex conjugate, hence  $a_1$  and  $b$  are always real positive and real negative numbers, respectively. A piecewise linear characteristic ( $C_1, C_2$ ) is a satisfactory substitute for the nonlinear voltage-charge characteristic, see [1, 9]. The coefficient  $a_2$  depends on amplitude and frequency of the driving voltage and can be numerically determined. The graphs of  $a_2$  versus driving voltage for a given number of frequencies  $f$  are given in [1]. We note, that the following equation

$$(4.3) \quad \frac{d^2u}{dt^2} + k \frac{du}{dt} + f(u) + E_0 = E(t),$$

where

$$f(u) = \begin{cases} \alpha u & \text{for } u \geq 0, \\ \beta u & \text{for } u < 0 \end{cases}$$

is a piecewise linear function and

$$E(t) = E^0 \sin(\omega t) \simeq \text{sgn}(\sin(\omega t)),$$

possesses the Poincaré map given by Eq.(4.1).

From extensive laboratory measurements and digital computer simulations, S. TANAKA *et al.* [1], have found that in order to reproduce the same qualitative

behaviour of the dynamical system, a piecewise linear voltage-charge characteristic is satisfactory. Furthermore, it was observed that the sinusoidal voltage source can be replaced by square wave voltage of the source period  $T = 1/f$  without altering the bifurcation structures. Therefore, we analyze Eq. (4.1) as a structure representing dynamics of the system with a nonlinear element responsible for charge separation. We believe, that intermittent chaos and flicker noise have not yet been revealed for the system. We exhibit our numerical calculation results. Figure 3 shows the “bifurcation tree” that is  $x_{l,m}$  versus  $a_2$  where  $l = 650, 651, \dots, 750$  represents the iteration number, see Eq. (4.1) where  $n = l$ , whereas  $m$  is responsible for  $a_2(m)$ , which changes from 0 to 10 as  $m$  changes from 0 to  $M$ , e.g.  $M = 200$ . The second variable  $y_{l,m}$  is similar since  $y_{l+1,m} = bx_{l,m}$ . It reflects the physical situation that each point in this bifurcation tree diagram represents a 1-D Poincaré section of electric current trajectory taken at each fundamental period  $T = 1/f$  of the sinusoidal voltage source. Iteration results for  $l = 0, 1, 2, \dots, 649$  are not depicted here. They concern mainly transition points to periodic and chaotic states. The following striking features are seen in this diagram.

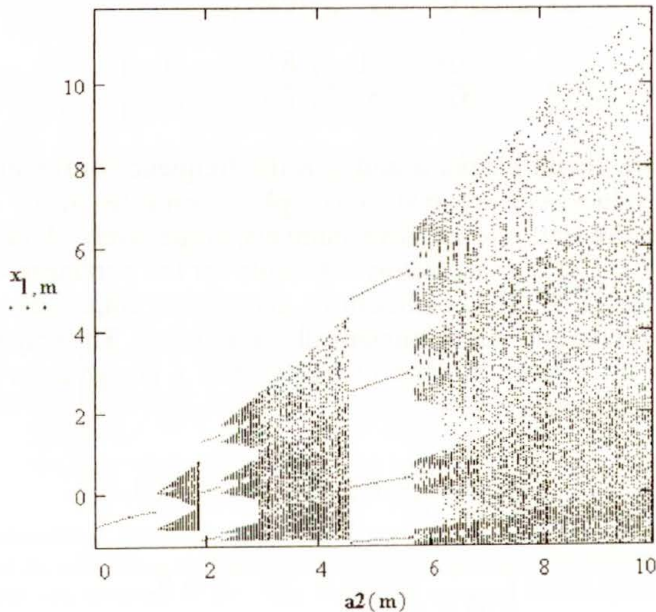


FIG. 3. Bifurcation tree of Eq. (4.1),  $l = 650, \dots, 750$ ,  $l$  is iteration number  $n \leftrightarrow l$  and  $m$  is responsible for  $a_2(m)$  changes along horizontal axis.

(i) A succession of large periodic windows whose periods increase exactly by one as we move from one window to the next at its right side (saddle-node bifurcation). On the left side of each chaotic band we observe transition to chaos via period-doubling bifurcation.

(ii) Going along trajectories we can expect a 1st-type intermittency at the right-hand side of boundary of each band of chaos and a 3rd-type one at the left side of the boundary of chaotic bands.

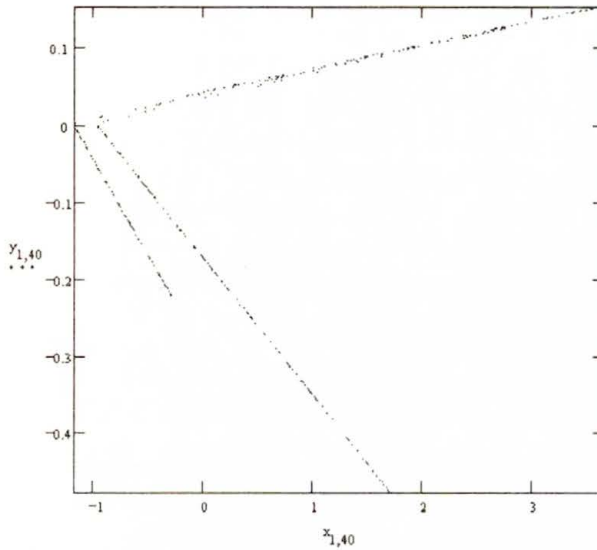


FIG. 4. Strange attractor for  $a_2 = 4$ .

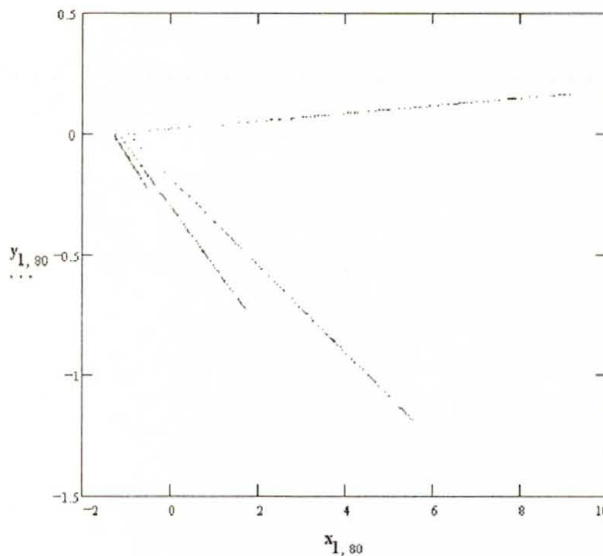


FIG. 5. Strange attractor for  $a_2 = 8$ .

Figures 4 and 5 show a 2-D Poincaré sections taken for  $a_2 = 4$  and  $a_2 = 8$ , that is the second and third chaotic bands, see Fig. 3. They are strange attractors associated with a chaotic motion perpendicular to the trajectories. The attractors

are composed of a number of branches and the number increases as we move from left to the right bands.

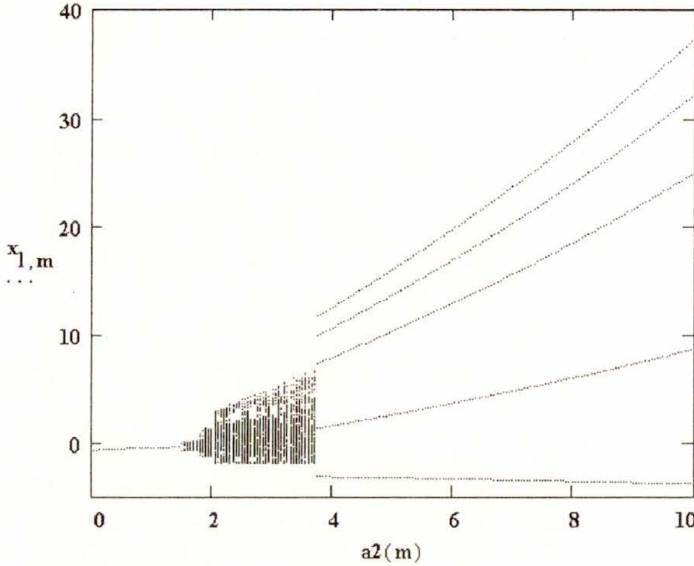


FIG. 6. Bifurcation tree for Eq. (4.1),  $x_{l,m}$  versus  $a_2(m) \Rightarrow m$ , where  $l$  is iteration number and  $a_1 = 1.13$ ,  $b = -0.5$ .

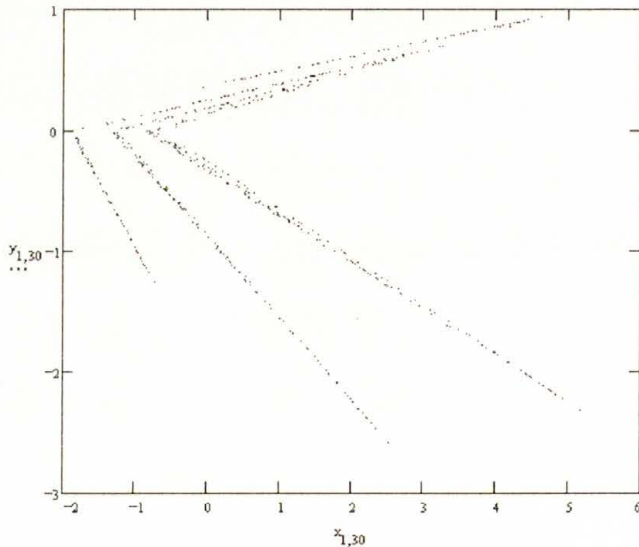


FIG. 7. Strange attractor for  $a_2 = 3$ .

Figures 6, 7 and 8 show the bifurcation tree and strange attractors for selected parameters  $a_1 = 1.13$  and  $b = -0.5$ . There is only one chaotic band and two large periodic windows. The strange attractors are composed of 5 branches for  $a_2 = 3$

and 3.5. The number of periods jumps from 1 to 5 as we move from left to the right-hand periodic windows. One can expect  $1/f$  fluctuations along trajectories due to the 1-st and 3-rd- type of intermittency.

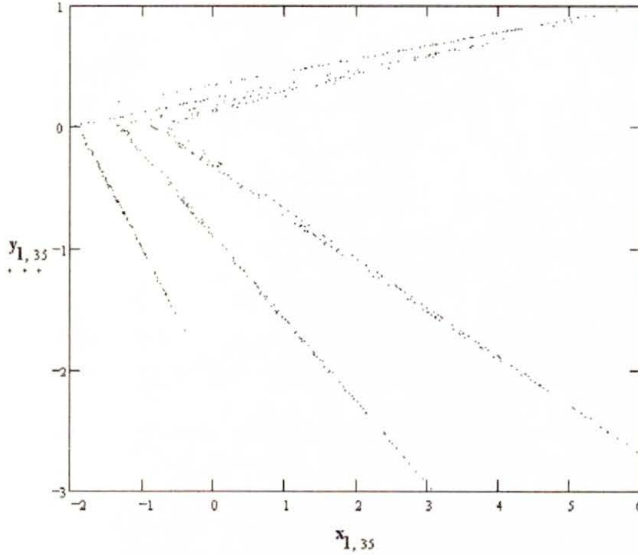


FIG. 8. Strange attractor for  $a_2 = 3.5$ .

Figure 9 exhibits computed Lyapunov exponents- $\lambda_x$  determining variation of  $x_n$  versus  $a_2$  for the bifurcation tree depicted above. We note that the calculated negative values of  $\lambda_x$  and stable periodic windows of the bifurcation tree as well as positive values of  $\lambda_x$  and chaotic band are related, respectively.

To demonstrate intermittency of our system given by Eq. (4.1) we determined a number of values of  $a_2$  for which intermittent chaos occurs. We may expect such values of  $a_2$  at the transition of periodic windows and chaotic bands. It is worth noting that, in some cases, very high precision of calculation of  $a_2$  is necessary.

Figure 10 shows intermittent state variable (signal)  $x_n$  versus  $n$ , strange attractor  $y_n$  versus  $x_n$ , power spectrum  $PX_n$  that is a fast Fourier transform (FFT) of  $x_n^2$ , correlation function  $C_s$  computed according to Eq. (3.10) and its power spectrum density for a selected value  $a_2 = 1.94610199282$ . This figure shows intermittency of saddle-node type, which is located at the boundary of the first chaos band and 3-period window, see Fig. 3. The intermittent signal consists of chaotic part and inclusions of 2, 3 and 4-periodic parts. Also, the strange attractor reveals periodic parts in the form of isolated points. Power spectrum density -  $PX_n$  displays  $1/f$  fluctuations (flicker noise) in the vicinity of  $n = 0$ . The correlation function diagram and the power spectrum of the function confirm this property.

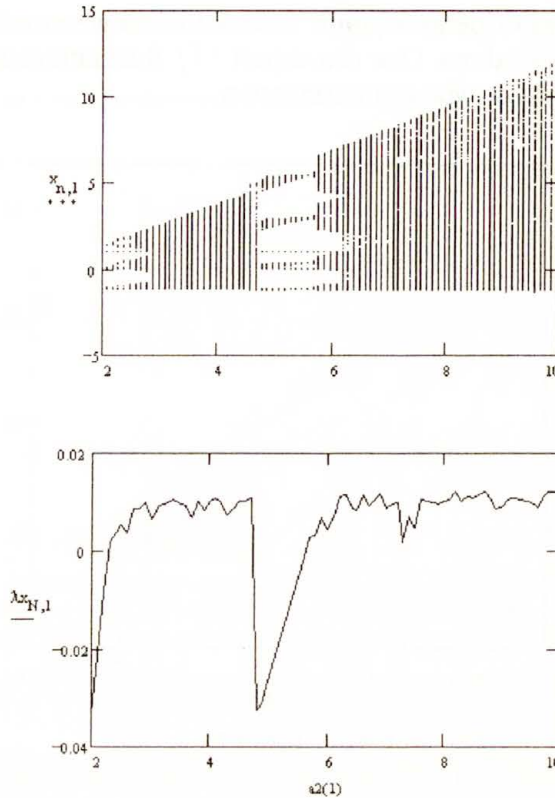


FIG. 9. Lyapunov exponent  $\lambda_x$  versus  $a_2$  in relation to bifurcation tree of Eq. (4.1)  $a_1 = 0.7$ ,  $b = -0.13$ , and  $a_2 = 0 \div 10$ .

Figures 11 and 12 show two intermittently chaotic regimes. They concern transition from the chaotic band to the 4-periodic window (Fig. 3). For a given value of  $a_2$ , see Fig. 11, we have predominantly chaotic  $x_n$  but if we add only  $10^{-14}$  to  $a_2$  then  $x_n$  changes drastically (4-periodicity prevails). The shape of strange attractors is nearly the same but that one responsible for the more chaotic case seems to be more “dense”. Also here, the power spectrum has no sharp peaks, in contrast to the less chaotic case. Correlation functions are distinctly different. One is similar to the purely chaotic correlation and the other one to the periodic case. Flicker noise components are more significant for the case of less chaotic variable.

The last figure, Fig. 13, shows the state variable  $x_n$  versus  $n$  for the bifurcation tree presented in Fig. 6. We found the value of  $a_2 = 3.7241$ , which is characteristic for a transition from chaotic band to 5-periodic window. The selected value of  $a_2$  is such that nearly a half of the variable  $x_n$  is chaotic and a half is 5-periodic. Power spectrum correlation function and flicker noise contributions are characteristic for intermittency.

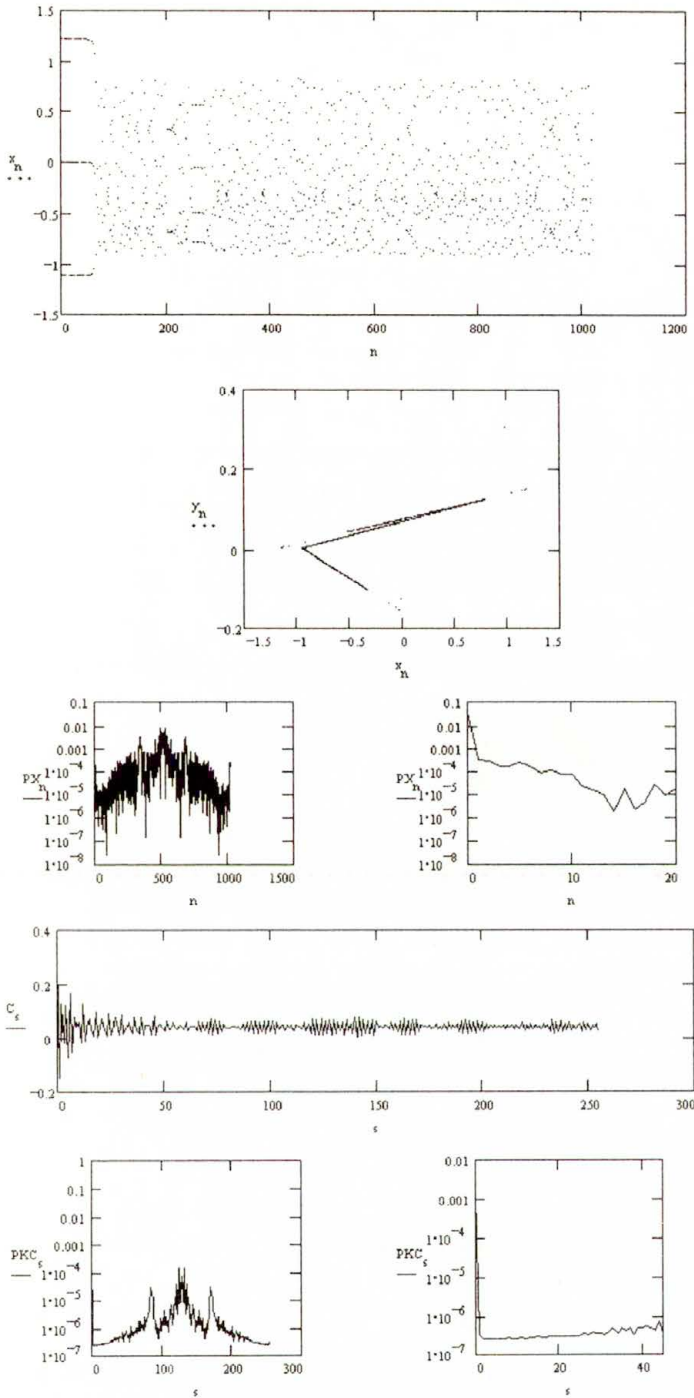


FIG. 10. Intermittent state variable  $x_n$  versus  $n$  (here time), strange attractor  $y_n$  versus  $x_n$ , power spectrum  $PX_n = FFT(x_n^2)$  versus  $n$  (here frequency), the correlation function  $C_s$  versus  $s$  (here time) computed according to Eq. (3.10) and its power spectrum  $PKC_s = FFT(C_s^2)$  versus  $s$  (here frequency). Parameter of Eq. (4.1);  $a_1 = 0.7$ ,  $b = -0.13$  and  $a_1 = 1.94610199282$ .

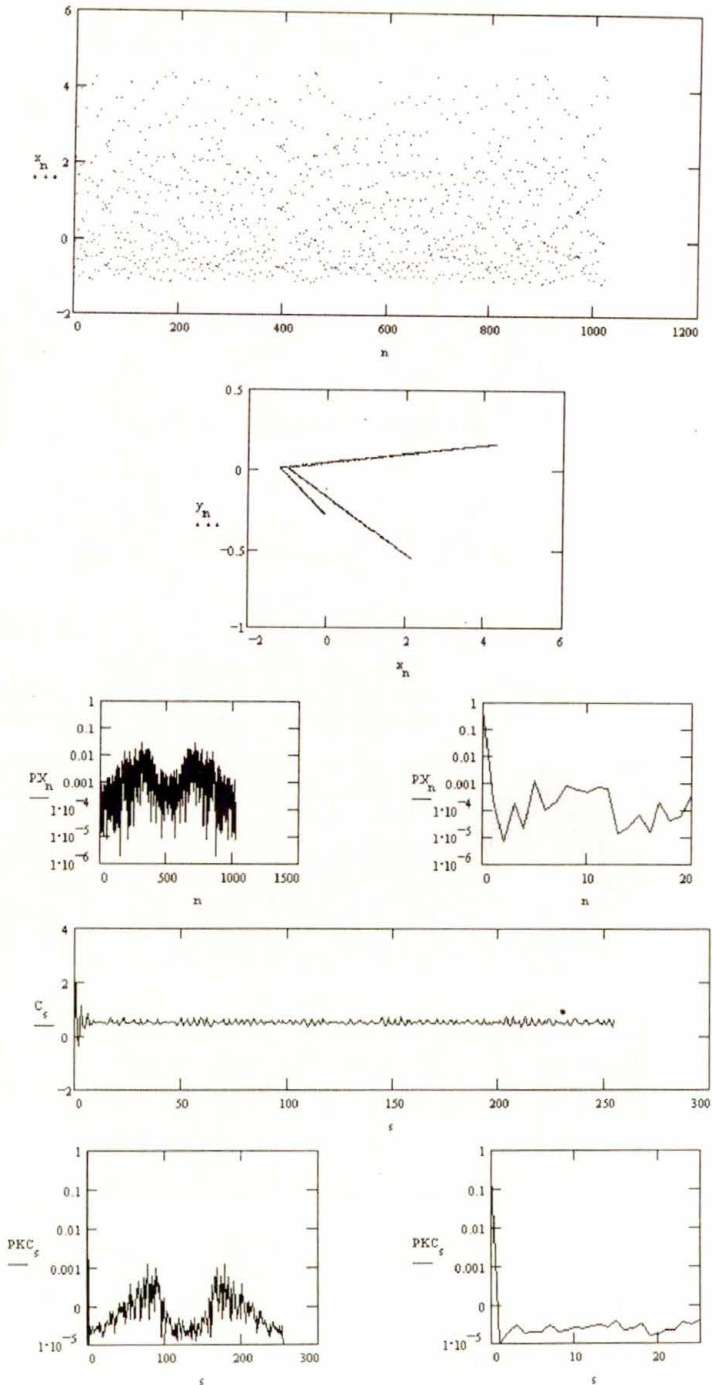


FIG. 11. Intermittent state variable  $x_n$  versus  $n$  (here time), strange attractor  $y_n$  versus  $x_n$ , power spectrum  $PX_n = FFT(x_n^2)$  versus  $n$  (here frequency), the correlation function  $C_s$  versus  $s$  (here time) computed according to Eq. (3.10) and its power spectrum  $PKC_s = FFT(C_s^2)$  versus  $s$  (here frequency). Parameter of Eq. (4.1);  $a_1 = 0.7$ ,  $b = -0.13$  and  $a_2 = 4.57988001000011$ .

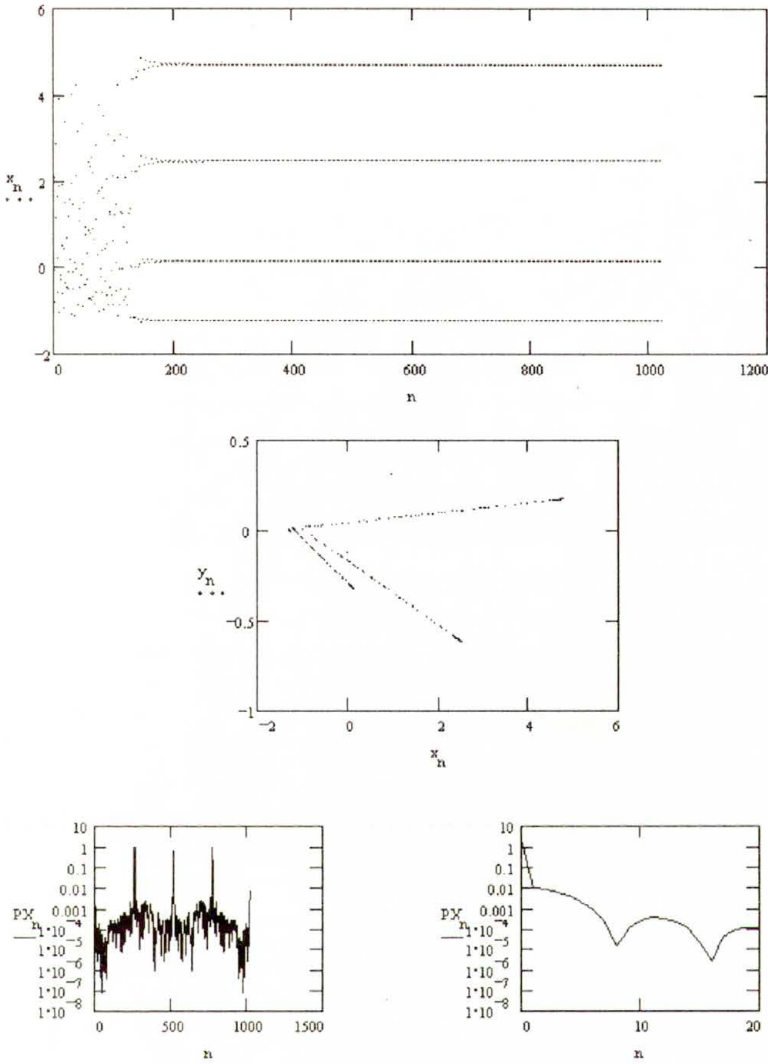


FIG. 12. Intermittent state variable  $x_n$  versus  $n$  (here time), strange attractor  $y_n$  versus  $x_n$ , power spectrum  $PX_n = FFT(x_n^2)$  versus  $n$  (here frequency). Parameter of Eq. (4.1);  $a_1 = 0.7$ ,  $b = -0.13$  and  $a_2 = 4.57988001000012$ .

The intermittent signals presented here were selected from a great number of computed examples of chaotic regimes. We note that the state variable  $y_n$  can be easily obtained in virtue of the following relation:  $y_{n+1} = bx_n$ , see Eq. (4.1). We see that the chaotic bands are self-similar and therefore, intermittent variables  $x_n$  can be found inside of each chaotic band. For instance, the central chaotic band of Fig. 3 is composed of three self-similar sections, which appear as we divide the band by two horizontal lines and each section is similar to the entity. The same property shows all chaotic bands of Fig. 3.

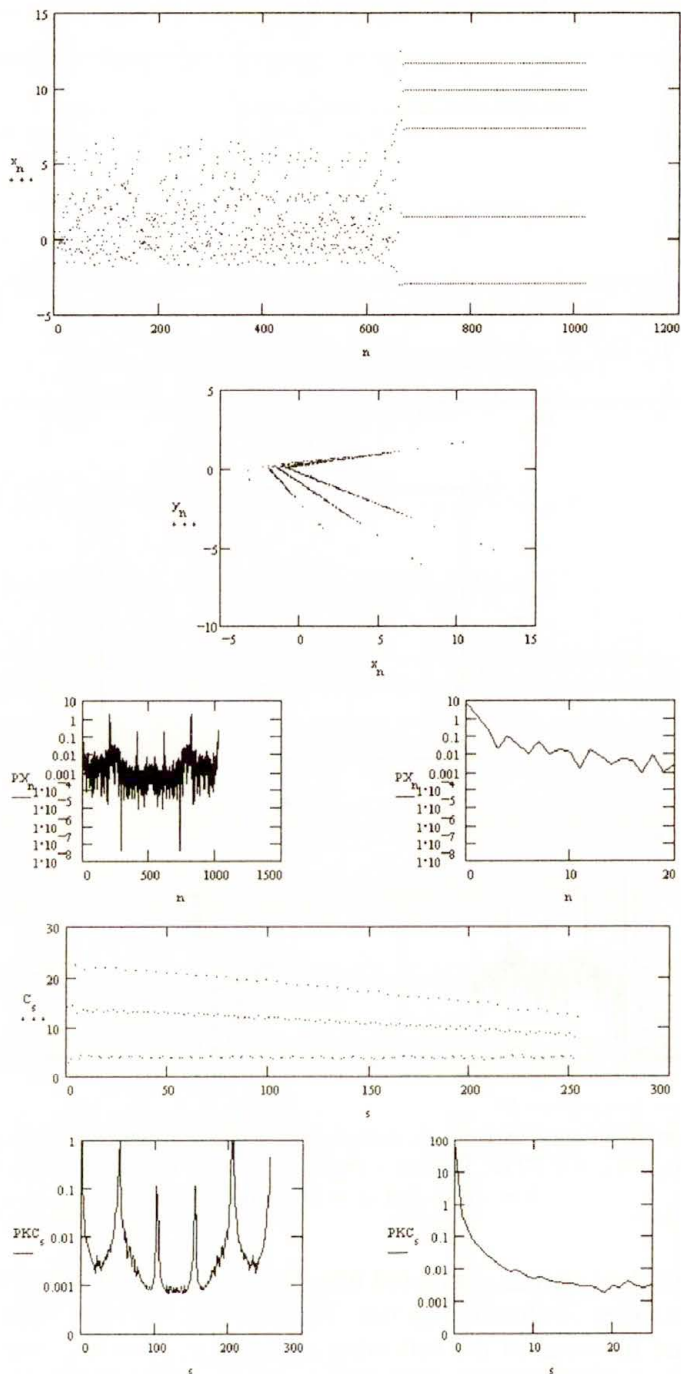


FIG. 13. Intermittent state variable  $x_n$  versus  $n$  (here time), strange attractor  $y_n$  versus  $x_n$ , power spectrum  $PX_n = FFT(x_n^2)$  versus  $n$  (here frequency), the correlation function  $C_s$  versus  $s$  (here time) computed according to Eq. (3.10) and its power spectrum  $PKC_s = FFT(C_s^2)$  versus  $s$  (here frequency). Parameter of Eq. (4.1);  $a_1 = 1.13$ ,  $b = -0.5$  and  $a_2 = 3.7241$ .

## 5. Conclusions

The dynamical system considered here is advantageous as it may be easily measured and computed. There are three parameters  $a_1$ ,  $b$  and  $a_2$  which allow for applications and simulations of different dynamical processes. Three fundamental features deserve attention. The assumed piecewise linear approximations of nonlinear characteristics allow to expose the most complex properties of nonlinear systems, e.g. important types of bifurcations, self-similarity, chaos, intermittency, fractality and flicker noise. A number of papers are devoted to the theory of piecewise linear maps, we refer to the following [5, 11, 12] and [13].

The next features concern flicker noise or  $1/f$  fluctuations of intermittently chaotic variables. In principle, we are not able to distinguish colored noise, coming from outside to the system, from the intermittent signal of the system, which generates the noise. In the case of colored noise, however, the trajectory produces a fractal curve that wanders erratically; the correlation dimension is a measure of the fractal dimension of this curve and is unrelated to the existence of an attractor. In addition, the correlation dimension is related to the power law spectral index  $\alpha(f^{-\alpha})$  by  $D_{cr} = 2/(\alpha - 1)$ , see [4]. Fractal dimension of strange attractors is the last feature of our comments. Varying the parameter  $a_2$  we may select intermittently chaotic variable of higher or lower contents of chaos. In this way, we may change fractal dimensions of an attractor as well as the power law spectral index  $\alpha$ . According to our computer calculations, lowering content of chaos in intermittent signal causes higher content of  $f^{-\alpha}$  fluctuations but lowers fractal dimension of strange attractors. This conclusion concerns only the ranges of parameters  $a_1$ ,  $b$  and  $a_2$  considered here.

## Acknowledgments

The paper was partly supported by the State Committee for Scientific Research (KBN) through the grant No. 2P03C01210.

## References

1. S. TANAKA, T. MATSUMOTO and CHUA, *Bifurcation scenario in a driven R-L-diode circuit*, *Physica*, **28D**, 317–344, 1987.
2. D. WELXING, H. WEI, W. XIAODONG and C.X. YU, *Quasiperiodic transition to chaos in a plasma*, *Phys. Rev. Lett.*, **70**, 170–173, 1993.
3. T. KLINGER and A. PIEL, *Investigations of attractors arising from the interaction of drift waves and potential relaxation instabilities*, *Phys. Fluids*, **B4**, 12, 3990, 1992.
4. A.S. OSBORN and A. PROVANZALE, *Finite correlation dimension for stochastic system with power-law spectra*, *Physica*, **D35**, 357, 1989.
5. H.G. SCHUSTER, *Deterministic chaos. An introduction*, Second revised Ed., VCH Verlagsgesellschaft, Weinheim, Germany 1988.
6. E. INFELD and G. ROWLANDS, *Nonlinear waves, solitons and chaos*, Cambridge University Press, Cambridge 1992.

7. J. HIRSH, B. HUBERMAN and D. SCALPINO, *Theory of intermittency*, Phys. Rev., A **25**, 1, 519–532, 1982.
8. R.Z. SAGDEEV and M.N. ROZENBLUTH, *Foundation of plasma physics* [in Russian], Vol. 2, Supple., Energo Atomizdat, Moskva 1984.
9. A.J. TURSKI, *Modelling of aurora double layers leading to oscillations and chaos*, Part 1 [in Polish], IFTR Report, 38, 1989; and Part 2, IFTR Reports, 20, 1990.
10. N. MINORSKY, *Nonlinear oscillations*, D. Van Nostrand Co., Toronto-New York-London 1962.
11. T. TÉL, *Invariant curves, attractors, and phase diagram of piecewise linear map with chaos*, J. Stat. Phys., **33**, 1, 195–221, 1983.
12. T. TÉL, *Fractal dimension of the strange attractor in piecewise linear two-dimensional map*, Phys. Lett., **971**, 6, 219–223, 1983.
13. V. MAISTRENKO and I. SUSHKO, *Period adding phenomenon in piecewise linear endomorphism arising from electronic systems*, Proc. of the Workshop NDES–94, Kraków, Poland, 39–44, 1994.

POLISH ACADEMY OF SCIENCES  
INSTITUTE OF FUNDAMENTAL TECHNOLOGICAL RESEARCH

e-mail: aturski@ippt.gov.pl

e-mail: bataman@ippt.gov.pl

Received August 28, 1996.

# Slow viscous flow about a permeable circular cylinder

SUJIT KUMAR KHAN and D. PALANIAPPAN (SANDUR)

SLOW STEADY two-dimensional motion of a viscous incompressible fluid about a porous circular cylinder is considered, using Darcy law for the flow in the porous region and Jones conditions on the contour of the cylinder. The problem is formulated in terms of Stokes stream function and velocity, and pressure fields of the modified flow in the presence of porous cylindrical boundary are obtained explicitly. It is observed that the Stokes paradox exists even in this case. Several other illustrative examples are presented to justify the usefulness of the method. It is found that the potential (point) singularities in the presence of a cylinder produce uniform flow at large distances, its strength being independent of porosity. However, the Stokes singularities (such as Stokeslet etc.) produce uniform flow at infinity, and its strength depends on the porosity as well as on the location of those singularities in the presence of the cylinder. The known results in two-dimensional Stokes flow are deduced as special cases from our result.

## 1. Introduction

THERE EXISTS an extensive literature on two-dimensional creeping flow (Stokes flow) problems, in which the inertial effects are negligible in comparison with the viscous effects in a viscous incompressible fluid. The problem, in general, can be reduced to finding solution of biharmonic equation that represents two-dimensional slow viscous flow past a finite body. It is quite well-known that there is no solution of the biharmonic equation for the streaming flow past a finite body, what is widely known as Stokes paradox. However, the slow streaming flow at large distances from a finite body may be obtained from the solution of the biharmonic equation for locally generated two-dimensional flows in an unbounded fluid. JEFFERY [1] has shown that two rigid circular cylinders of equal radius, rotating with equal but opposite angular velocities, produce a uniform stream at large distances. DORREPAAL *et al.* [2] have also explained such phenomenon by considering a rotlet or a Stokeslet in front of a rigid circular cylinder which lead to a uniform flow at infinity. SMITH [3] considered the simplest situation of a single sink positioned in front of a circular cylinder, and concluded that there was a uniform stream in this case also. The solution due to SMITH [3] was also obtained earlier by AVUDAINAYAGAM and JOTHIRAM [4] by an approach similar to that of DORREPAAL *et al.* [2].

The purpose of the present paper is to discuss the solution of biharmonic equation representing the two-dimensional Stokes flow in the presence of a porous circular cylinder. The corresponding three-dimensional problem with spherical and plane boundaries have been investigated by several authors in different contexts [5–12]. In this paper, we consider a general Stokes flow past a stationary infinite circular porous cylinder (using Darcy model) in a viscous, incompressible

fluid. The velocity and pressure fields in the Stokes region are obtained explicitly from the stream function which satisfies the biharmonic equation. The Darcy region velocity is derived by using the fact that the Darcy pressure satisfies the Laplace equation. The solutions of the two regions are matched at the contour of the cylinder using the boundary conditions due to JONES [13]. It is shown that the Stokes paradox continues to exist with these conditions at the contour of the cylinder. Several illustrative examples are worked out to justify the usefulness of the present method. It is noted that the point singularities located in front of the cylinder produce a uniform stream at infinity, and its speed

- 1) depends on their location alone in the case of potential singularities;
- 2) depends on their location as well as porosity in the case of Stokes singularities.

This fact may be due to the validity of the Darcy equations which are restricted to low porosity of the region. The above observation would have to be checked by using Brinkman model equations which are valid for high porosity.

## 2. Mathematical formulation

Consider the slow steady flow (creeping flow or Stokes flow) of a viscous incompressible fluid past an infinite circular permeable (porous) cylinder (Darcy region) of radius  $a$ . For the flow outside the cylinder, the governing equations are the linearised Navier–Stokes equations or simply the Stokes equations

$$(2.1) \quad \mu \nabla^2 \mathbf{q} = \nabla p,$$

$$(2.2) \quad \nabla \cdot \mathbf{q} = 0.$$

Here  $\mathbf{q}$  is the velocity vector with components  $(q_r, q_\theta, 0)$  in the radial and transverse directions  $(r, \theta)$  respectively,  $p$  the pressure and  $\mu$  the coefficient of viscosity of the fluid.

The flow inside the porous infinite cylinder ( $0 \leq r \leq a$ ) is governed by Darcy's law

$$(2.3) \quad \mathbf{Q} = -\frac{k}{\mu} \nabla P,$$

$$\nabla \cdot \mathbf{Q} = 0,$$

where  $\mathbf{Q}$  is the volume rate per unit cross-sectional area,  $P$  the Darcy pressure and  $k > 0$  is the permeability coefficient.

The appropriate boundary conditions on  $r = a$  are as follows:

- (i) the pressure is continuous across the boundary of the cylinder

$$(2.4) \quad p(a, \theta) = P(a, \theta);$$

(ii) the radial velocity is continuous at the boundary of the cylinder

$$(2.5) \quad q_r(a, \theta) = Q_r(a, \theta);$$

(iii) JONES condition [13] for tangential velocity on the cylinder is that the tangential stress is proportional to the difference in the tangential velocities of the two regions, i.e

$$(2.6) \quad T_{r\theta}|_{r=a} = \mu \left[ \frac{1}{r} \frac{\partial q_r}{\partial \theta} + r \frac{\partial}{\partial r} \left( \frac{q_\theta}{r} \right) \right]_{r=a} = \frac{\alpha}{\sqrt{k}} [q_\theta - Q_\theta]_{r=a},$$

where  $T_{r\theta}$  is the tangential stress component and  $\alpha$  is a parameter which completely depends on the porous medium.

### 3. Method of solution

It is well-known that the Stokes equations (2.1) and (2.2) in two dimensions, when expressed in terms of stream function, reduce to

$$(3.1) \quad \nabla^4 \psi = 0,$$

where

$$\nabla^2 \equiv \frac{\partial^2}{\partial r^2} + \frac{1}{r} \frac{\partial}{\partial r} + \frac{1}{r^2} \frac{\partial^2}{\partial \theta^2}$$

and

$$(3.2) \quad q_r = -\frac{1}{r} \frac{\partial \psi}{\partial \theta},$$

$$(3.3) \quad q_\theta = \frac{\partial \psi}{\partial r};$$

$q_r$ ,  $q_\theta$  are the components of velocity along  $r$  and  $\theta$  directions, respectively. The general solution of (3.1) in polar coordinates is given by

$$(3.4) \quad \psi = \sum_{n=0}^{\infty} \left[ A_n r^n + B_n r^{n+2} + \frac{C_n}{r^n} + \frac{D_n}{r^{n-2}} \right] (\cos n\theta + \sin n\theta),$$

where we have excluded the terms which give nonzero vorticity at infinity. The constants  $A_n$  and  $B_n$  are assumed to be known and will be determined from the given flow field. For convenience we proceed further with the terms involving  $\sin n\theta$  in the Fourier expansion (3.4) only, since the calculation for the other part

involving  $\cos n\theta$  is similar. Now the components of velocity and pressure in the Stokes region obtained from (3.2), (3.3) and (2.1) are

$$(3.5) \quad \begin{aligned} q_r &= - \sum_{n=1}^{\infty} \left[ A_n r^{n-1} + B_n r^{n+1} + \frac{C_n}{r^{n+1}} + \frac{D_n}{r^{n-1}} \right] n \cos n\theta, \\ q_\theta &= \sum_{n=1}^{\infty} \left[ n A_n r^{n-1} + (n+2) B_n r^{n+1} - \frac{n C_n}{r^{n+1}} - (n-2) \frac{D_n}{r^{n-1}} \right] \sin n\theta, \\ p &= p_0 - \mu \sum_{n=1}^{\infty} \left[ 4(n+1) B_n r^n + 4(n-1) \frac{D_n}{r^n} \right] \cos n\theta. \end{aligned}$$

In the porous region (i.e.  $r < a$ ) the Darcy pressure satisfies the Laplace equation  $\nabla^2 P = 0$ . Therefore,

$$(3.6) \quad P = P_0 + \sum_{n=1}^{\infty} E_n r^n \cos n\theta.$$

The components of velocity inside the porous cylinder in  $r$  and  $\theta$  directions now become

$$(3.7) \quad \begin{aligned} Q_r &= -\frac{k}{\mu} \frac{\partial P}{\partial r} = -\frac{k}{\mu} \sum_{n=1}^{\infty} n E_n r^{n-1} \cos n\theta, \\ Q_\theta &= -\frac{k}{\mu} \frac{\partial P}{r \partial \theta} = \frac{k}{\mu} \sum_{n=1}^{\infty} n E_n r^{n-1} \sin n\theta. \end{aligned}$$

The stream function for the Darcy region may also be defined and given by

$$(3.8) \quad \psi^+ = \frac{k}{\mu} \sum_{n=1}^{\infty} E_n r^n \sin n\theta,$$

where  $\nabla^2 \psi^+ = 0$ . It should be noted here that in (3.6) we have omitted the terms which do not produce finite velocities at the origin.

The general expressions for the pressure and velocity fields in both the regions will now be solved for the constants  $C_n$ ,  $D_n$ ,  $E_n$  expressed in terms of  $A_n$  and  $B_n$  using the boundary conditions (2.4)–(2.6).

Application of the boundary conditions (2.4)–(2.6) in the general solutions yields

$$(3.9) \quad \begin{aligned} \frac{C_n}{a^{2n}} &= \frac{\left( (n-1) \frac{\alpha a}{\sqrt{k}} - \frac{4k}{a^2} n(n-1)^2 \right) A_n}{M_n} \\ &+ \frac{\left( -2n + \frac{\alpha a}{\sqrt{k}} n + 4 \frac{a\sqrt{k}}{a} (n-1)(n+2) \right) a^2 B_n}{M_n}, \end{aligned}$$

$$(3.9) \quad \frac{D_n}{a^{2n-2}} = - \frac{\left(2 + \frac{\alpha a}{\sqrt{k}}\right) n A_n}{M_n} + \frac{\left(\frac{\alpha a}{\sqrt{k}} + \frac{4\alpha\sqrt{k}}{a} n + \frac{4k}{a^2} n(n+1)\right) (n+1) a^2 B_n}{M_n},$$

$$E_n = - \frac{4\mu}{a^2} \left[ \frac{- \left(2 + \frac{\alpha a}{\sqrt{k}}\right) n(n-1) A_n}{M_n} + \frac{\left(2n - \frac{\alpha a}{\sqrt{k}}(n-2)\right) (n+1) a^2 B_n}{M_n} \right],$$

where

$$M_n = 2n + \frac{\alpha a}{\sqrt{k}} + 4\alpha \frac{\sqrt{k}}{a} n(n-1) + \frac{4k}{a^2} n(n+1)(n-1).$$

## 4. Examples

### 4.1. Uniform flow along $OX$

For the uniform flow with a speed  $U$  along  $OX$ , we have

$$q_r = -U \cos \theta, \quad q_\theta = U \sin \theta$$

and

$$(4.1) \quad \psi_0 = Ur \sin \theta.$$

Therefore we have  $A_1 = U$ ,  $A_n = 0$  for all  $n \geq 2$  and  $B_n = 0$  for all  $n$ . The coefficients  $C_n$ ,  $D_n$  and  $E_n$  as calculated from (3.9)–(3.11) are

$$(4.2) \quad C_1 = 0, \quad D_1 = -U, \quad E_1 = 0.$$

This implies  $\psi = 0$ . Thus a uniform flow about a porous cylinder is not possible, which is the usual Stokes paradox known in the literature.

### 4.2. Quadratic potential flow

In this case

$$(4.3) \quad \psi_0(r, \theta) = -\frac{U}{3} r^3 \sin 3\theta$$

( $U/3$  is a shear velocity) and  $A_1 = A_2 = 0$ ,  $A_3 = -U/3$ ,  $A_n = 0$  for all  $n \geq 4$  and  $B_n = 0$  for all  $n$ . The coefficients  $C_3$  and  $D_3$  are found from (3.9) and are given by

$$(4.4) \quad \begin{aligned} C_3 &= \frac{\left(2\frac{\alpha a}{\sqrt{k}} - 48\frac{k}{a^2}\right) \left(-\frac{U}{3}\right) a^6}{\left(6 + \frac{\alpha a}{\sqrt{k}} + 24\frac{\alpha\sqrt{k}}{a} + 96\frac{k}{a^2}\right)}, \\ D_3 &= \frac{\left(2 + \frac{\alpha a}{\sqrt{k}}\right) U a^4}{\left[6 + \frac{\alpha a}{\sqrt{k}} + 24\frac{\alpha\sqrt{k}}{a} + 96\frac{k}{a^2}\right]}, \\ E_3 &= -\frac{4\mu}{a^2} U \left[ \frac{2\left(2 + \frac{\alpha a}{\sqrt{k}}\right)}{\left(6 + \frac{\alpha a}{\sqrt{k}} + 24\frac{\alpha\sqrt{k}}{a} + 96\frac{k}{a^2}\right)} \right]. \end{aligned}$$

Now the complete stream function for the two flow fields are given by

$$(4.5) \quad \begin{aligned} \psi &= \frac{U}{3} \left[ -r^3 - \frac{\left(\frac{2\alpha a}{\sqrt{k}} - \frac{48k}{a^2}\right) \frac{a^6}{r^3}}{\left(6 + \frac{\alpha a}{\sqrt{k}} + 24\frac{\alpha\sqrt{k}}{a} + 96\frac{k}{a^2}\right)} \right. \\ &\quad \left. + 3 \frac{\left(2 + \frac{\alpha a}{\sqrt{k}}\right) \frac{a^4}{r}}{\left(6 + \frac{\alpha a}{\sqrt{k}} + 24\frac{\alpha\sqrt{k}}{a} + 96\frac{k}{a^2}\right)} \right] \sin 3\theta, \\ \psi^+ &= \frac{8k}{a^2} U \left[ \frac{\left(2 + \frac{\alpha a}{\sqrt{k}}\right)}{\left(6 + \frac{\alpha a}{\sqrt{k}} + 24\frac{\alpha\sqrt{k}}{a} + 96\frac{k}{a^2}\right)} \right] r^3 \sin 3\theta. \end{aligned}$$

Stream lines in Stokes' region are plotted for different values of porosity in Fig. 1. We observe that in the limit  $(\alpha/\sqrt{k}) \rightarrow \infty$ ,  $k = 0$ , we recover in (4.5)<sub>1</sub> the stream function for the quadratic potential flow past a circular cylinder [14]. When  $(\alpha/\sqrt{k}) = 0$ ,  $k = 0$ , we obtain the quadratic potential flow past a shear-free cylinder [15].

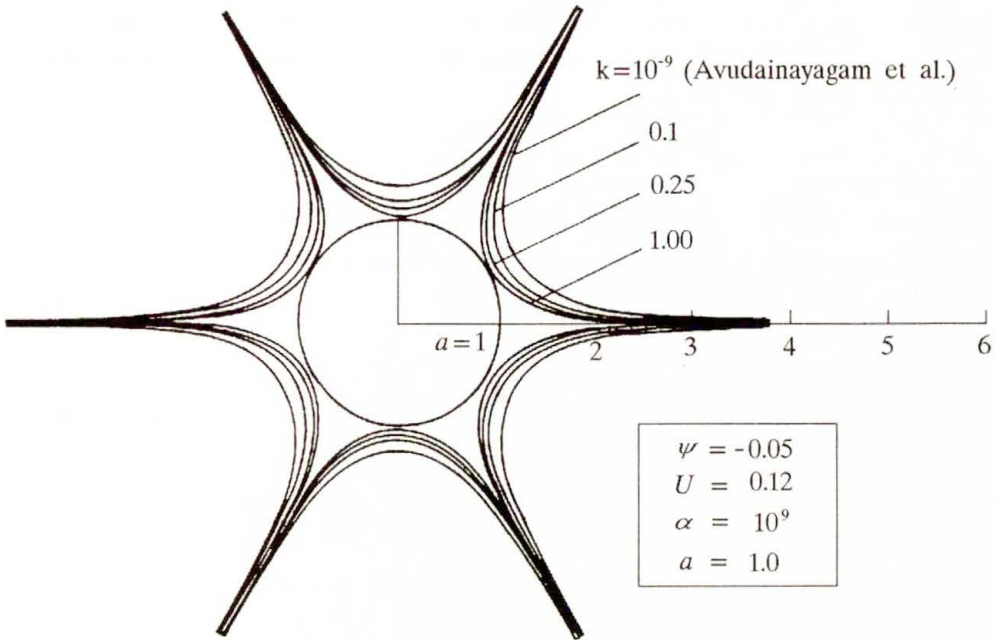


FIG. 1. Stream function  $\psi(r, \theta)$  in Stokes region.

Another interesting special case may be deduced from Eq.(4.5)<sub>1</sub>. If we let  $(\alpha/\sqrt{k}) - (1/\lambda\mu) = 0$ , then (4.5)<sub>1</sub> reduces to

$$(4.6) \quad \psi = \frac{U}{3} \left[ -r^3 - \frac{2(1-\beta)}{(\beta+2)} \frac{a^6}{r^3} + \frac{3\beta}{(\beta+2)} \frac{a^4}{r} \right] \sin 3\theta,$$

where  $\beta = 1 + (\alpha/2\lambda\mu)$ . This solution corresponds to the quadratic flow past a circular cylinder with mixed slip-stick conditions [16]. In the present case the boundary condition (2.6) becomes  $q_\theta = \lambda T_{r\theta}$  on  $r = a$  where  $\lambda$  is here the slip parameter. Thus our solution includes all the possible quadratic flows past a cylinder indicating that the boundary conditions (2.4)–(2.6) are assumed in a more general form.

### 4.3. Source outside a circular cylinder

Consider a source of unit strength located at  $(c, 0)$ ,  $c > a$ . The stream function corresponding to a source in an unbounded flow is

$$(4.7) \quad \psi_0(r, \theta) = \tan^{-1} \frac{r \sin \theta}{c - r \cos \theta}.$$

Equation (4.7) may be expanded into a Fourier series as

$$(4.8) \quad \psi_0 = \sum_{n=1}^{\infty} \frac{r^n}{nc^n} \sin n\theta.$$

Therefore  $A_n = 1/nc^n$  and  $B_n = 0$  for all  $n$ . The coefficients  $C_n$  and  $D_n$  can be calculated from (3.9) and the modified stream function in the presence of a porous cylinder is:

for  $r > a$ ,

$$(4.9) \quad \psi(r, \theta) = \sum_{n=1}^{\infty} \left[ r^n + \frac{\left( (n-1) \frac{\alpha a}{\sqrt{k}} - \frac{4k}{a^2} n(n-1)^2 \right) a^{2n}}{M_n} \frac{a^{2n}}{r^n} - \frac{\left( 2 + \frac{\alpha a}{\sqrt{k}} \right) n a^{2n-2}}{M_n r^{n-2}} \right] \frac{1}{nc^n} \sin n\theta;$$

for  $r < a$

$$(4.10) \quad \psi^+ = \frac{4k}{a^2} \sum_{n=1}^{\infty} \frac{\left( 2 + \frac{\alpha a}{\sqrt{k}} \right) (n-1) r^n}{M_n c^n} \sin n\theta.$$

It will be of some interest to study the asymptotic behaviour of (4.9) as  $r$  approaches infinity. In the limit as  $r \rightarrow \infty$ , Eq.(4.9) becomes

$$(4.11) \quad \psi = -\frac{1}{c} r \sin \theta.$$

This is a uniform flow along the negative  $x$ -direction at large distance from the porous cylinder.

This conclusion has already been drawn by SMITH [3] in the case of a source acting outside a rigid cylinder. We remark that the porosity has no effect on the speed of the uniform stream at large distance. Perhaps, this may be due to the fact that the porosity is small in Darcy flow.

#### 4.4. Stokeslet outside a circular cylinder

Now let us consider a Stokeslet of strength  $F$  located at  $(0, c)$ ,  $c > a$ . The stream function corresponding to the Stokeslet in an unbounded region is

$$(4.12) \quad \psi_0 = F(r \cos \theta - c) \log R_1,$$

where  $R_1^2 = r^2 + c^2 - 2cr \cos \theta$ . The constants  $A_n$ ,  $B_n$ ,  $C_n$ ,  $D_n$  and  $E_n$  can be obtained in the similar way as that explained in the above example. The stream-functions for the two flow fields in the presence of a Stokeslet in front of a

porous circular cylinder may be constructed with these constants. The asymptotic form of the perturbed external flow field as  $r \rightarrow \infty$  is given by

$$(4.13) \quad \psi(r, \theta) = \frac{F \left[ - \left( 2 + \frac{\alpha a}{\sqrt{k}} \right) \frac{1}{2} + \left( \frac{\alpha a}{\sqrt{k}} + 4 \frac{\alpha \sqrt{k}}{a} + \frac{8k}{a^2} \right) \frac{a^2}{2c^2} \right]}{\left[ 2 + \frac{\alpha a}{\sqrt{k}} \right]} r \cos \theta.$$

Hence, at large distances, the Stokeslet produces a uniform flow whose strength depends on the location of the singularity and on the porosity. The variation of the speed for different values of  $\alpha/\sqrt{k}$  are shown graphically (see Fig. 2). The

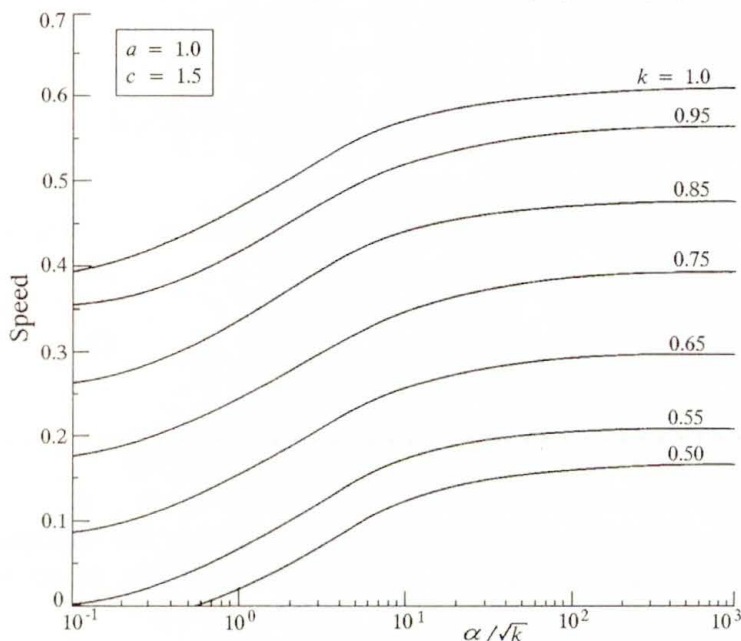


FIG. 2. Stokeslet-cylinder combination-effect of permeability on the speed at large distances.

effect of porosity on the stream function at large distances is shown in Fig. 3. In the limit when  $k = 0$  and  $(\alpha a/\sqrt{k}) \rightarrow \infty$ , we recover the result obtained by DORREPAAL *et al.* [2] for a rigid circular cylinder. In the limit of  $(\alpha/\sqrt{k}) = 0$  and  $k = 0$  we get

$$(4.14) \quad \psi(r, \theta) = -\frac{F}{2} r \cos \theta.$$

Therefore a Stokeslet in the presence of a shear-free circular cylinder produces a uniform flow at large distances, its strength being independent of the location and porosity. If we let  $\frac{\alpha}{\sqrt{k}} = \frac{1}{\lambda\mu} = \frac{2(\beta - 1)}{a}$ , where  $\beta = 1 + (a/2\lambda\mu)$  as in example

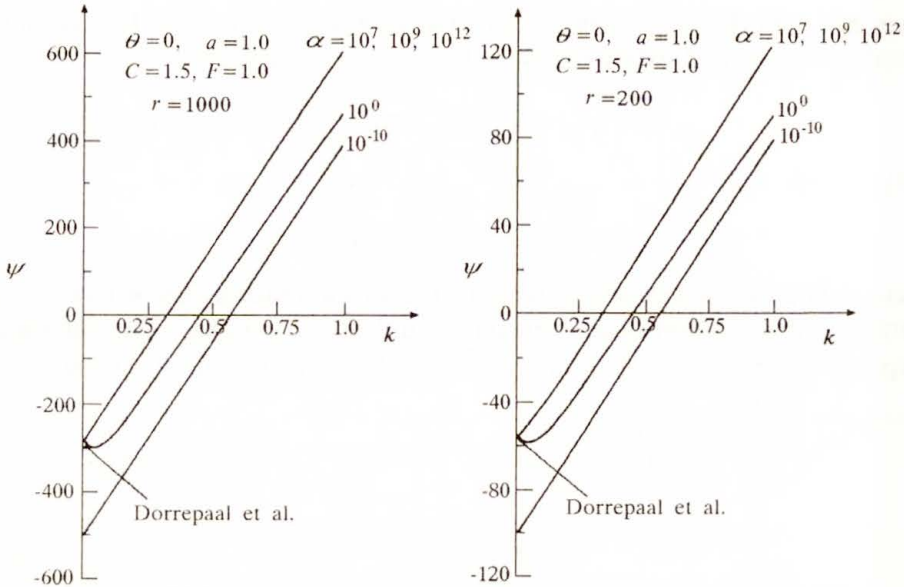


FIG. 3. Stokeslet-cylinder combination-effect of porosity on the stream function at large distance.

(4.2), Eq. (4.13) reduces to

$$(4.15) \quad \psi = F \left[ \frac{-\beta + (\beta - 1) \frac{a^2}{c^2}}{2\beta} \right] r \cos \theta.$$

This solution corresponds to the asymptotic behaviour of the Stokeslet in front of the cylinder when mixed slip-stick conditions are applied at the contour of the cylinder.

### Acknowledgments

The authors are grateful to Prof. N. RUDRAIAH, Vice-chancellor Gulbarga University for having given constant encouragement in carrying out this research work. They also wish to thank K. ARCHANA for careful verification of the calculations.

### References

1. G.B. JEFFERY, *The rotation of two circular cylinders in a viscous fluid*, Proc. R.Soc. London, Ser. A., **101**, 169–174, 1922.
2. J.M. DORREPAAL, M.E. O'NEIL and K.B. RANGER, *Two-dimensional Stokes flows with cylinders and line singularities*, Mathematika, **31**, 65–75, 1984.

3. S.H. SMITH, *Some limitations of two-dimensional unbounded Stokes flow*, Phys. Fluids, A 2, 10, 1724–1730, 1990.
4. A. AVUDAINAYAGAM and B. JOTHIRAM, *No-slip images of certain line singularities in a circular cylinder*, Int. J. Engng. Sci., 25, 9, 1193–1205, 1987.
5. D.D. JOSEPH and L.N. TAO, *The effect of permeability on the slow motion of a porous sphere in a viscous liquid*, ZAMM, 44, 361–364, 1964.
6. D.D. JOSEPH and L.N. TAO, *Lubrication of a porous bearing*, J. Appl. Mech., Trans. ASME, Series E, 33, 753–760, 1966.
7. D.D. JOSEPH and C.L. SHIR, *Lubrication of a porous bearing – Stokes solution*, J. Appl. Mech., Trans. ASME, Series E, 33, 761–767, 1966.
8. G.S. BEAVERS and D.D. JOSEPH, *Boundary conditions at a naturally permeable wall*, J. Fluid Mech., 30, 1, 197–207, 1967.
9. G.S. BEAVERS, E.M. SPARROW and R.A.J. MAGNUSON, *Experiments on coupled parallel flows in a channel and a bounding porous medium*, Trans. ASME. J. Basic Engng., 92, 843–848, 1970.
10. D. PALANIAPPAN, *Arbitrary Stokes flow past a porous sphere*, Mechanics Research Communications, 20, 4, 309–317, 1993.
11. B.S. PADMAVATHI, T. AMARANATH and D. PALANIAPPAN, *Stokes flow about a porous spherical particle*, Arch. Mech., 46, 1–2, 191–199, 1994.
12. P.G. SAFFMANN, *On the boundary condition at the surface of a porous medium*, Studies in Appl. Math., 50, 93–101, 1971.
13. I.P. JONES, *Low Reynolds number flow past a porous spherical shell*, Proc. Camb. Phil. Soc., 73, 231–238, 1973.
14. A. AVUDAINAYAGAM, B. JOTHIRAM and J. RAMAKRISHNA, *A necessary condition for the existence of a class of plane Stokes flows*, Quart. J. Mech. Appl. Math., 39, 3, 425–434, 1986.
15. R. USHA and K. HEMALATHA, *A note on plane Stokes flow past a shear free impermeable cylinder*, ZAMP, 44, 1, 73–84, 1993.
16. B.S. PADMAVATHI and T. AMARANATH, *Circle theorem for Stokes flow with mixed slip-stick boundary conditions*, Mech. Research Communications, 20, 6, 439–446, 1993.

DEPARTMENT OF MATHEMATICS  
GULBARA UNIVERSITY, P.G. CENTRE, KDR NAGAR,  
Sandur-583119, Bellary District, Karnataka, INDIA.

Received September 13, 1996.

## Second sound speed in a crystal of NaF at low temperature

W. KOSIŃSKI (WARSZAWA),  
K. SAXTON and R. SAXTON (NEW ORLEANS)

WE DERIVE a physically justifiable model of heat conduction for rigid heat conductors based on a recent approach involving the gradient generalization of an internal state variable. The model accounts for observable phenomena in solid dielectric crystals, related to wave-like conduction of heat in certain ranges of low temperatures and a rapid decay of the speed of thermal waves close to a temperature value  $\vartheta_\lambda$ , at which the conductivity of the material reaches a peak.

### 1. Introduction

FINITE SPEED thermal waves, known collectively as second sound, distinguishing them from generally faster propagating mechanical waves, were first detected in  $^3\text{He}$ , ([1]), and then in high purity dielectric crystals of sodium fluoride, NaF, ([8]), and bismuth, Bi, ([16]). It has been observed that there exists a (material-dependent) temperature value below which second sound begins to be observed. The temperature values of this type have been measured to be close to those at which the conductivity of the material reaches a peak, a useful discussion of which can be found in the review papers [6, 10, 11].

In order to match regimes of different material behaviour, we will adapt the gradient generalization of the internal state variable theory in [14] to qualitative experimental results from the literature, so as to specify admissible forms of constitutive equations and material functions. In particular, our derivation is based on two experimentally observed phenomena not included in existing thermodynamic theories of second sound. The first is related to the propagation of heat pulses in solid specimens. It has been observed, ([8]), that in some range of temperature at which experiments have been performed, the time of arrival of heat pulses sent through a specimen is an approximately linear function of the reference temperature. However near the upper limit of measured temperature values, the time, measured by the leading edge of heat pulses, rises rapidly with increasing temperature. The latter corresponds to a very fast decay (with respect to temperature) of the second sound speed. The second phenomenon concerns the heat conductivity, in that close to a particular temperature the conductivity of the material reaches a peak, ([9]). In our model, motivated by the experimental data, we make the hypothesis that the temperature of maximum heat conductivity coincides with that below which second sound appears. Above this temperature value the heat conduction becomes purely diffusive, obeying a general nonlinear Fourier law. We call this *critical* temperature  $\vartheta_\lambda$ . Furthermore,

our approach allows us to relate  $\vartheta_\lambda$ , the temperature at which heat conductivity reaches a maximum, to  $\vartheta_m$ , a temperature separating two distinct families of discontinuity waves.

## 2. General framework

In [12], the material gradient of an internal, scalar, state variable was introduced as a fundamental state variable in the response functions of thermoelastic materials. In the course of obtaining consequences for the laws of thermodynamics, a modified Fourier-type law was found leading to finite speeds of propagation of thermal and thermomechanical waves. This model differed from an earlier one, ([13]), in the form of the evolution and constitutive equations, however essentially the same model as earlier has been used in the investigation of second sound phenomena ([3, 4]).

In the present paper we will begin with the generalized semi-empirical model, developed recently in [14]. The principal assertion is that the thermodynamic temperature  $\vartheta$  is not by itself sufficient in describing some highly nonequilibrium phenomena, including the observed occurrence of low temperature heat pulses. Thus, besides the temperature and its gradient, a further internal variable,  $\beta$ , and *its* gradient are introduced into the constitutive equations. The variable  $\beta$  is in a certain sense a nonequilibrium temperature, related to the thermodynamic temperature through an initial value problem, and represents a history of the temperature field.

A rather general dependence of the free energy  $\psi$  was allowed in [14] on the various variables. However to avoid constraints between  $\vartheta$  and  $\beta$ , this framework reduces to the following set of constitutive relations,

$$(2.1) \quad \psi = \psi(\vartheta, \beta, \nabla\beta), \quad \eta = -\partial_\vartheta\psi(\vartheta, \beta, \nabla\beta),$$

$$(2.2) \quad \mathbf{q} = \mathbf{q}(\vartheta, \nabla\vartheta, \beta, \nabla\beta), \quad \dot{\beta} = f(\vartheta, \beta),$$

in which the symbol  $\nabla$  denotes the gradient operator. Here  $\mathbf{q}$  is the heat flux vector,  $\eta$  the entropy density,  $\vartheta$  the thermodynamic temperature measured on the absolute scale, and  $\psi$  the free energy per unit volume related to  $\varepsilon$ , the internal energy per unit volume, by

$$(2.3) \quad \psi = \varepsilon - \eta\vartheta.$$

Balance of energy and the second law of thermodynamics imply

$$(2.4) \quad \varepsilon_t + \operatorname{div}\mathbf{q} = r,$$

$$(2.5) \quad \eta_t + \operatorname{div}(\mathbf{q}/\vartheta) \geq r/\vartheta,$$

where  $r$  is the body heat supply per unit volume. In this case the second law will take the form of the residual inequality

$$(2.6) \quad -\partial_{\nabla\beta}\psi \cdot \partial_{\beta}f\nabla\beta - \partial_{\beta}\psi f - (\partial_{\nabla\beta}\psi\partial_{\vartheta}f + \vartheta^{-1}\mathbf{q}) \cdot \nabla\vartheta \geq 0.$$

In the isotropic case, the dependence of  $\mathbf{q}$  on the gradients  $\nabla\vartheta$  and  $\nabla\beta$  can take the form

$$(2.7) \quad \mathbf{q} = -k\nabla\vartheta - \alpha\nabla\beta,$$

where the coefficients  $k$  and  $\alpha$  may depend on the scalar quantities  $\vartheta$ ,  $\beta$ ,  $|\nabla\vartheta|$ ,  $|\nabla\beta|$  and  $\nabla\vartheta \cdot \nabla\beta$ .

However, as discussed in [2], it becomes reasonable to make the following assumptions while remaining consistent with classical thermostatics, at the same time making it straightforward to use experimental results to identify the material functions needed:

- the free energy is independent of  $\beta$  and quadratic in  $|\nabla\beta|$ ,
- the coefficients  $k$  and  $\alpha$  depend only on  $\vartheta$ .

Then we have the following representation for the free energy (cf. [2])

$$(2.8) \quad \psi = \psi_1(\vartheta) + \frac{1}{2}\psi_2(\vartheta)|\nabla\beta|^2$$

and the residual inequality simplifies to the form

$$(2.9) \quad -\psi_2\partial_{\beta}f|\nabla\beta|^2 + (\vartheta^{-1}\alpha - \psi_2\partial_{\vartheta}f)\nabla\vartheta \cdot \nabla\beta + \vartheta^{-1}k|\nabla\vartheta|^2 \geq 0.$$

We note that the form (2.8) is one of consequences of the second law of thermodynamics in the original semi-empirical theory (i.e. when  $k = 0$ ) under the hypothesis that  $\alpha$  depends only on  $\vartheta$ , as we have assumed above.

It is not hard to show that the last inequality will be satisfied for any choice of  $\nabla\vartheta$  and  $\nabla\beta$  if and only if

$$(2.10) \quad \partial_{\beta}f(\vartheta, \beta)\psi_2(\vartheta) \leq 0, \quad k(\vartheta) \geq 0$$

and

$$(2.11) \quad \left(\partial_{\vartheta}f(\vartheta, \beta)\psi_2(\vartheta) - \vartheta^{-1}\alpha(\vartheta)\right)^2 \leq -4\partial_{\beta}f(\vartheta, \beta)\psi_2(\vartheta)\vartheta^{-1}k(\vartheta).$$

The latter inequality should hold for any choice of  $k(\vartheta) \geq 0$ , in particular for  $k(\vartheta) = 0$ . This gives the compatibility condition

$$(2.12) \quad \alpha(\vartheta) = \vartheta\psi_2(\vartheta)\partial_{\vartheta}f(\vartheta, \beta)$$

(cf. [2]). From (2.12), we obtain the consequence  $\partial_\beta \partial_\vartheta f(\vartheta, \beta) = 0$ , which leads to the existence of two single-variable functions  $f_1, f_2$ , and to the splitting

$$(2.13) \quad f(\vartheta, \beta) = f_1(\vartheta) + f_2(\beta).$$

In this way we have the same set of compatibility conditions as in the previous setup, however, now the heat flux vector can satisfy the more general constitutive equation (2.7).

### 3. The NaF model

We now specialize to one space dimension and make some refinements in the behaviour of constitutive terms, particularly in the light of experimental evidence concerning NaF, ([9]). In the absence of a body heat supply, the balance of energy, Eq. (2.4), reduces to

$$(3.1) \quad \varepsilon_t + q_x = 0,$$

and, using (2.2) and (2.13), the evolution of  $\beta$  is described by

$$(3.2) \quad \beta_t = f_1(\vartheta) + f_2(\beta).$$

The heat flux, (2.7), is given by

$$(3.3) \quad q = -k(\vartheta)\vartheta_x - \alpha(\vartheta)\beta_x,$$

while the second law implies

$$(3.4) \quad \alpha(\vartheta) = \psi_{20}\vartheta^2 f_1'(\vartheta),$$

by (2.12) and the following particular choice

$$(3.5) \quad \psi = \psi_1(\vartheta) + \frac{1}{2}\psi_{20}\vartheta\beta_x^2$$

for  $\psi$ , where  $\psi_2(\vartheta) = \psi_{20}\vartheta$ , and  $\psi_{20}$  is a constant (see (2.8)). In this case  $\varepsilon$  reduces to a function of  $\vartheta$  alone, by (2.1) and (2.3).

Finally, we define the specific heat  $c_v$  by

$$(3.6) \quad c_v(\vartheta) = \varepsilon'(\vartheta) = c_0\vartheta^3,$$

where  $c_0$  denotes Debye's constant.

Combining Eqs. (3.1), (3.3) and (3.6) provides an equation describing the evolution of  $\vartheta$ , which can be used in conjunction with (3.2) to give a third order system in the pair  $(\vartheta, \beta)$ ,

$$(3.7) \quad c_v(\vartheta)\vartheta_t - (k(\vartheta)\vartheta_x + \alpha(\vartheta)\beta_x)_x = 0.$$

As concrete examples, let us define two  $C^1$ -homeomorphisms

$$f_1 : \mathbb{R} \rightarrow (-\infty, 0], \quad \text{and} \quad f_2 : \mathbb{R} \rightarrow \mathbb{R}.$$

For the first, we set

$$(3.8) \quad f_1(z) = a(|z|^{p-1}z)_-, \quad 1 < p < 2,$$

where  $a$  is a positive constant, and the subscript  $-$  means that when  $z \geq 0$ ,  $f_1$  is taken to be zero. For the second, put

$$(3.9) \quad f_2(z) = -b|z|^{h-1}z, \quad h \geq \frac{p}{2-p},$$

where  $b$  is another positive constant. In both cases,  $z$  represents  $\vartheta - \vartheta_\lambda$  where  $\vartheta_\lambda$  denotes the *critical* temperature at which the heat conductivity of the material reaches a peak.

The basic form of  $f_1$  becomes evident when the characteristic velocity, as a function of temperature, is compared with empirical data (cf. Fig. 1). The form of  $f_2$ , however, is taken in order to describe qualitatively the observed phenomenon of the heat conductivity peak; further experimental data for heat conduction obtained under quasi-static conditions would be useful to refine this.

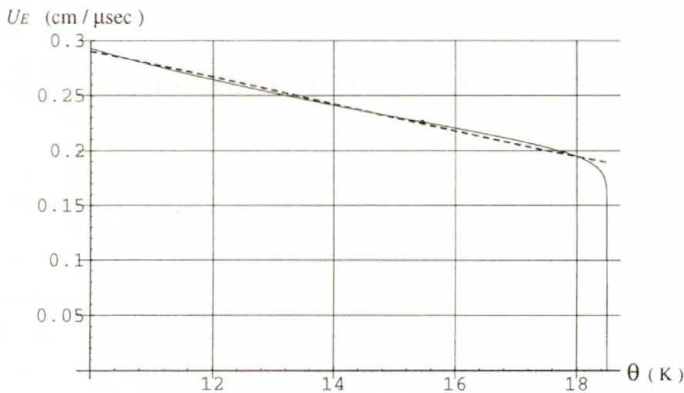


FIG. 1. Characteristic velocity (solid curve),  $U_E = 0.85(18.5 - \vartheta)^{0.04} / \vartheta^{0.5}$ , ahead of wave for  $p = 1.04$ ,  $\vartheta_\lambda = 18.5$ , together with empirical data (dotted curve),  $U_E = (9.09 + 0.00222\vartheta^{3.1})^{-0.5}$ , (COLEMAN and NEWMAN, [4]).

It can be shown that in the *quasi-static* case, for which  $f_1(\vartheta) + f_2(\beta) = 0$ , (i.e.  $\beta$  is a function of  $\vartheta$ ), the heat flux (3.3) now reduces to

$$(3.10) \quad q = -(k(\vartheta) + c\psi_{20}\vartheta^2)|(\vartheta - \vartheta_\lambda)_-|^{p(1+1/h)-2}\vartheta_x,$$

where  $c$  depends on  $a, b, p$  and  $h$ .

Moreover, an expression for the second sound speed,  $U_E$ , (the speed of small amplitude waves for the case  $k(\vartheta) = 0$ ) is given by

$$(3.11) \quad U_E^2 = \frac{\psi_{20}}{c_0 \vartheta} a^2 p^2 (\vartheta - \vartheta_\lambda)_-^{2(p-1)}.$$

We note that (3.10) predicts a peak in heat conductivity as  $\vartheta$  tends to  $\vartheta_\lambda$  from below, followed by a sharp drop. At the same time, in particular if  $p$  is close to 1, (3.11) delivers a sudden drop to zero of the wave speed  $U_E$ . Both phenomena are to be expected on leaving the second sound regime and entering one of purely diffusive heat conductivity.

Raw data for  $U_E(\vartheta)$  has been given for crystals of NaF of varying purity in [8], with an empirical relation,  $U_E = (9.09 + 0.00222\vartheta^{3.1})^{-0.5}$  cm/ $\mu$ sec provided in [4]. The dependence of conductivity on temperature and purity is also described in [9], temperature of peak conductivity increasing with purity. The purest sample had a peak in conductivity at around 18.5 K which we take here to be  $\vartheta_\lambda$ , below which second sound waves began to appear. In the figure above, we observe qualitatively and quantitatively similar behaviour (over the region of data availability) to the empirical form of  $U_E(\vartheta)$  in [4, 7]. In the present approach we have obtained this behaviour using the example for  $f_1$  above, when  $p = 26/25$ . The rapid drop at 18.5 K reflects our assumption that  $U_E$  vanishes at  $\vartheta_\lambda$ . On reaching this temperature the pulse disappears into the diffusive signal.

The choices we have made for  $f_1$  and  $f_2$  in this special case lead to a finite conductivity peak as  $\vartheta \rightarrow 18.5$  K if  $h = 13/12$ , and to infinite conductivity in the same limit if  $h > 13/12$ . The definition of  $f_1(\vartheta - \vartheta_\lambda)$ , (3.8), then makes the conductivity drop to  $k(\vartheta)$  for  $\vartheta > \vartheta_\lambda$ .

It is possible to investigate the behaviour of shock waves for the system (3.1) and (3.2), for which the temperature  $\vartheta$  has a discontinuity when  $k(\vartheta) = 0$ . These shocks, propagating to the right into an unperturbed state  $\vartheta^+$ , satisfy Lax's admissibility condition, ([5]), if  $s_r \leq \sigma \leq s_l$ , where  $\sigma = \sigma(\vartheta^+, \vartheta^-)$  is the shock speed, and  $s_l = s_l(\vartheta^+, \vartheta^-)$ ,  $s_r = s_r(\vartheta^+)$  denote the characteristic speeds, respectively in front of and behind the shock. Note that  $s_r = U_E$ , evaluated at  $\vartheta^+$ . The choice of the functions  $f_1, f_2$ , predicts a temperature state  $\vartheta^+ = \vartheta_m < \vartheta_\lambda$  into which shocks do not propagate. This temperature is found to be related to  $\vartheta_\lambda$  according to

$$(3.12) \quad \vartheta_m = \frac{1}{3p-2} \vartheta_\lambda.$$

If  $\vartheta^+ < \vartheta_m$ , then for admissible shocks, the temperature,  $\vartheta^-$ , behind the wave lies between  $\vartheta^+$  and  $\vartheta_{**}$  ( $\vartheta_{**} < \vartheta_m$  is a temperature depending on  $\vartheta^+$ ) and is greater than  $\vartheta^+$ . If  $\vartheta^+ > \vartheta_m$ , the temperature behind the wave lies between  $\vartheta^+$  and  $\vartheta_{**}$  (now  $\vartheta_{**} > \vartheta_m$ ), which is here less than  $\vartheta^+$ . These two cases correspond to "hot" and "cold" shocks, respectively. A similar result was

obtained in [17], however the current model manages to connect the observed transition to diffusive behaviour at  $\vartheta_\lambda$  with the change in wave propagation at  $\vartheta_m$ .

This model appears to have some additional flexibility as compared to other theories where second sound persists to certain degrees at all temperatures, ([8, 15]). The presence of two regimes, hyperbolic and parabolic, provides the possibility of describing further phenomena related to ballistic phonons and second sound as discussed in [6], including broadening of smooth heat pulses, ([8, 9]), and diffusive heat conduction related to the parabolic regime.

## Acknowledgment

Part of this research has been conducted during a one month stay of one of the authors (W. K.) at the Department of Mathematics and Computer Science of Loyola University, New Orleans, in the summer of 1995. His stay and research were supported by NSF Grant GER-9450202 at Loyola University.

## References

1. C.C. ACKERMAN, B. BERTMAN, H.A. FAIRBANK and R.A. GUYER, *Second sound in solid helium*, Phys. Rev. Letters, **16**, 789–791, 1966.
2. V.A. CIMMELLI, W. KOSIŃSKI and K. SAXTON, *Modified Fourier law – comparison of two approaches*, Arch. Mech., **44**, 4, 409–415, 1992.
3. B.D. COLEMAN, M. FABRIZIO and R. OWEN, *On the thermodynamics of second sound in dielectric crystals*, Arch. Rational Mech. Anal., **80**, 2, 135–158, 1982.
4. B.D. COLEMAN and D. C. NEWMAN, *Implication of a nonlinearity in the theory of second sound in solids*, Phys. Rev. B, **32**, 1492–1498, 1988.
5. C.M. DAFERMOS, *Hyperbolic systems of conservation laws*, [in:] Systems of Nonlinear Partial Differential Equations, J.M. BALL [Ed.], NATO ASI series (C), vol. 111, D. Reidel Publishing Company, pp. 25–70, 1983.
6. W. DREYER and H. STRUCHTRUP, *Heat pulse experiments revisited*, Continuum Mech. Thermodyn., **5**, 3–50, 1993.
7. K. FRISCHMUTH and V.A. CIMMELLI, *Hyperbolic heat conduction with variable relaxation time*, J. Theor. Appl. Mech., **34**, 1, 67–76, 1996.
8. H.E. JACKSON, C.T. WALKER and T.F. MCNELLY, *Second sound in NaF*, Phys. Rev. Letters, **25**, 1, 26–28, 1970.
9. H.E. JACKSON and C.T. WALKER, *Thermal conductivity, second sound, and phonon-phonon interactions in NaF*, Physical Review B, **3**, 4, 1428–1439, 1971.
10. D.D. JOSEPH and L. PREZIOSI, *Heat waves*, Rev. Mod. Phys., **61**, 41, 1–62, 1989.
11. D.D. JOSEPH and L. PREZIOSI, *Addendum to the paper “Heat Waves”*, (Rev. Mod. Phys., **61**, 41, 1989), Rev. Mod. Phys., **62**, 2, 375–392, 1990.
12. W. KOSIŃSKI, *Elastic waves in the presence of a new temperature scale*, [in:] Elastic Wave Propagation, M.F. MCCARTHY and M. HAYES [Eds.], Elsevier Science (North Holland), pp. 629–634, 1989.
13. W. KOSIŃSKI and P. PERZYNA, *Analysis of acceleration waves in materials with internal parameters*, Arch. Mech., **24**, 4, 629–643, 1972.
14. W. KOSIŃSKI and W. WOJNO, *Gradient generalization to internal state variable approach*, Arch. Mech., **47**, 3, 523–536, 1995.
15. T.F. MCNELLY, S.J. ROGERS, D.J. CHAMIN, R.J. ROLLEFSON, W.M. GOUBAU, G.E. SCHMIDT, J.A. KRUMHANSI and R.O. POHL, *Heat pulses in NaF: onset of second sound*, Phys. Rev. Letters, **24**, 3, 100–102, 1970.

16. V. NARAYANAMURTI and R.C. DYNES, *Observation of second sound in bismuth*, Phys. Rev. Letters, **28**, 22, 1461–1465, 1972.
17. T. RUGGERI, A. MURACCHINI and L. SECCIA, *Continuum approach to phonon gas and shape changes of second sound via shock waves theory*, Il Nuovo Cimento, **16**, D 1, 15–44, 1994.

POLISH ACADEMY OF SCIENCES  
INSTITUTE OF FUNDAMENTAL TECHNOLOGICAL RESEARCH  
e-mail: wkos@ippt.gov.pl;

DEPARTMENT OF MATHEMATICS AND COMPUTER SCIENCE  
LOYOLA UNIVERSITY, NEW ORLEANS, USA  
e-mail: saxton@beta.loyno.edu

and

DEPARTMENT OF MATHEMATICS  
UNIVERSITY OF NEW ORLEANS, NEW ORLEANS, USA  
e-mail: rsaxton@math.uno.edu

*Received September 20, 1996.*

# An integrity basis for plane elasticity tensors

M. VIANELLO (MILANO)

AN ISOTROPIC functional basis of 5 polynomials is shown to be also an integrity basis for the space of plane elasticity tensors. A decomposition of each element in this space into a direct sum of “harmonic” tensors is used to compute or estimate the distance between an arbitrary elasticity tensor and the three non-trivial symmetry classes, to allow for the determination of the material symmetry when the elastic coefficients are known only to within a given approximation.

## 1. Introduction

LET  $\mathbb{E}la$  BE THE SPACE of two-dimensional elasticity tensors, which describe the constitutive equations for plane linearly elastic bodies, and let  $O(2)$  be the group of orthogonal transformations on the two-dimensional Euclidean space. A function  $\psi$  defined on  $\mathbb{E}la$  is isotropic, or, equivalently, an  $O(2)$ -invariant, if  $\psi(\mathbb{C}) = \psi(\mathbf{Q} * \mathbb{C})$  for all  $\mathbb{C} \in \mathbb{E}la$  and  $\mathbf{Q} \in O(2)$ , where, as we shall see more precisely later on, the asterisk denotes an action of  $O(2)$  on  $\mathbb{E}la$ . A finite collection  $B$  of such invariants is a *functional basis* if each other invariant is a function of the elements of  $B$ . If these elements are polynomials, and *all* isotropic polynomials are also expressible as *polynomial* functions of them, this collection is an *integrity basis* (or *Hilbert basis*) for the action of  $O(2)$ . A similar set of definitions covers the case in which the action of the group of proper rotations  $SO(2)$  is considered, and the corresponding invariants are said to be *hemitropic*.

It is a classical result that every integrity basis is also a functional basis. The proof, which is far from trivial, is based on a lemma which shows that “polynomials separate the orbits”. More explicitly, this statement means that whenever two elements do not lie on the same orbit, there is at least one invariant polynomial which takes different values on them. For a modern proof of this important result we refer to the paper by WINEMAN and PIPKIN [17, Sec. 6]. On the other hand, it is not difficult to provide counterexamples showing that, in general, a functional basis is *not* an integrity basis.

In Sec. 4 we construct a functional basis of 5 polynomials  $I_n$  for the isotropic invariants on  $\mathbb{E}la$ . Similar results were recently obtained by ZHENG [18] and by BLINOWSKI, OSTROWSKA-MACIEJEWSKA and RYCHLEWSKI [3]. Indeed, the technique used in the present paper is very similar to the discussion contained there, and the basis found is essentially equivalent. However, in addition, here it is shown that the set  $\{I_n\}$  is also an *integrity basis* for the action of  $O(2)$  on  $\mathbb{E}la$ , which is the main goal of this paper.

For the sake of clarity and self-completeness we choose to offer a detailed presentation of some mathematical preliminaries, even if this can be seen as an alternative derivation of similar results contained in [3].

The key mathematical step is the decomposition of an elasticity tensor into a quadruplet formed by: two scalars  $\lambda$  and  $\mu$ , a second-order tensor  $\mathbf{H}$  and a fourth-order tensor  $\mathbb{K}$ , both symmetric and traceless. A description of this technique, when applied for other goals to the three-dimensional case, is contained in some papers by BACKUS [1], BAERHEIM [2], COWIN [6], FORTE and VIANELLO [8] and, moreover, in a classical treatise by SCHOUTEN [15]. However, except for reference [3], we are not aware of any other presentation of a similar decomposition for plane elasticity.

The insight coming from this approach is used to represent the action of  $O(2)$  on  $\mathbb{E}^2$  through a pair of orthogonal transformations on the two-dimensional spaces to which  $\mathbf{H}$  and  $\mathbb{K}$  belong. This point of view allows for a natural construction of a functional basis, thus providing a confirmation, with a slightly different approach, of a similar conclusion reached in [3]. Moreover, the proof that the set  $\{I_n\}$  is an integrity basis is strongly dependent on the isomorphism between the action of  $O(2)$  on  $\mathbb{E}^2$  and the action of the same group on products of complex planes, which can be easily deduced only in view of the previous considerations.

Constitutive equations for two-dimensional linearly elastic bodies are divided into *four* symmetry classes by a relation stating that two elasticity tensors are equivalent when their symmetry groups are conjugate in  $O(2)$ . Once a functional basis has been established, it is not difficult, through its geometric interpretation, to obtain a complete characterization of the symmetry classes as *zero-sets* of appropriate collections of invariant polynomials. As noticed in [3], this is a useful result in itself, since it allows for an easy determination of the symmetry class of an elasticity tensor. Moreover, it shows clearly that the collection of tensors with non-minimal symmetry group is a set of *measure zero*.

An interesting problem originates from the experimental errors contained in the numerical data describing elasticity tensors, as it was recently noted also by FRANÇOIS, BERTHAUD and GEYMONAT [5]. In view of the above considerations, the question of symmetry class has, with “probability one”, the same answer: The material has no special symmetry. What is really important is a comparison between the precision of our experimental apparatus and the distance between  $\mathbb{C}$  and the closest tensor of a given symmetry. If this distance is smaller than a certain value, we may reasonably say that, within the approximation allowed, the material described by  $\mathbb{C}$  does belong to that symmetry class. In view of our geometric approach, we propose some formulas, ready for applications, which allow for a quick evaluation of the relevant distances. We believe some of the results to be new.

## 2. Symmetry groups and symmetry classes

We use small (resp., capital) boldface letters for vectors (resp., second-order tensors) of  $\mathcal{V}$ , the translation space of a *two*-dimensional Euclidean space  $\mathcal{E}$ .

Scalars are denoted by Greek letters and fourth-order tensors are written with a blackboard bold font, such as  $\mathbb{C}$ . A superscript  $T$  is used for the transpose and the space of symmetric tensors is called  $\text{Sym}$ . We use subscripts for the components of vectors or tensors with respect to a fixed orthonormal basis  $\mathbf{e}_i$  ( $i = 1, 2$ ). Thus, for instance,  $\mathbf{v} = v_i \mathbf{e}_i$  and  $\mathbf{T} = T_{ij} \mathbf{e}_i \otimes \mathbf{e}_j$ , where the sum over repeated indexes is understood and the symbol  $\otimes$  stands for the tensor product. The subspace of  $\text{Sym}$  formed by all traceless tensors (such that  $A_{ii} = 0$ ) is  $\text{Dev}$ , while the space of all fourth-order tensors  $\mathbb{H}$  which are symmetric and traceless is  $\mathbb{D}\text{ev}$ . More precisely,  $\mathbb{H} \in \mathbb{D}\text{ev}$  if  $H_{ijkl}$  is unchanged by any permutation of the indexes and, moreover,  $H_{iikl} = 0$ . The group of orthogonal transformations of  $\mathcal{V}$  is  $O(2)$ , where the unit element is denoted by  $\mathbf{I}$ , and the subgroup of *rotations*, formed by all  $\mathbf{Q} \in O(2)$  with determinant equal to one, is  $SO(2)$ . We write  $\mathbf{Q}(\theta)$  for the rotation such that

$$(2.1) \quad \mathbf{Q} \mathbf{e}_1 = \cos \theta \mathbf{e}_1 + \sin \theta \mathbf{e}_2, \quad \mathbf{Q} \mathbf{e}_2 = -\sin \theta \mathbf{e}_1 + \cos \theta \mathbf{e}_2,$$

and we denote by  $\tilde{\mathbf{Q}}$  the reflection with respect to the  $\mathbf{e}_1$  direction:  $\tilde{\mathbf{Q}} \mathbf{e}_1 = \mathbf{e}_1$ ,  $\tilde{\mathbf{Q}} \mathbf{e}_2 = -\mathbf{e}_2$ . Obviously,  $O(2)$  is generated by  $SO(2)$  and  $\tilde{\mathbf{Q}}$ .

For an extensive introduction to linear elasticity we refer to classical conventions (see, e.g., GURTIN [10]). Here, we simply recall that an *elasticity tensor*  $\mathbb{C}$  is a symmetric linear map of  $\text{Sym}$ , which gives the stress tensor  $\mathbf{T}$  as a function of the infinitesimal strain  $\mathbf{E}$ :  $\mathbf{T} = \mathbb{C}[\mathbf{E}]$ . Thus, the components of  $\mathbb{C}$  satisfy the following index symmetries:

$$C_{ijkl} = C_{jikl} = C_{ijlk} = C_{klij}.$$

The *symmetry group*  $g(\mathbb{C})$  is the collection of all orthogonal transformations  $\mathbf{Q}$  such that

$$\mathbb{C}[\mathbf{Q} \mathbf{E} \mathbf{Q}^T] = \mathbf{Q} \mathbb{C}[\mathbf{E}] \mathbf{Q}^T, \quad \forall \mathbf{E} \in \text{Sym}.$$

It is convenient to define an *action* of  $O(2)$  on  $\mathbb{E}la$ , the 6-dimensional space of (plane) elasticity tensors. For each  $\mathbf{Q} \in O(2)$  and each  $\mathbb{C} \in \mathbb{E}la$ , let  $\mathbf{Q} * \mathbb{C}$  be defined by

$$(\mathbf{Q} * \mathbb{C})_{pqrs} := Q_{pi} Q_{qj} Q_{rk} Q_{sl} C_{ijkl}.$$

Thus, the symmetry group is

$$g(\mathbb{C}) := \{\mathbf{Q} \in O(2) \mid \mathbf{Q} * \mathbb{C} = \mathbb{C}\}.$$

A straightforward consequence of this definition is that  $g(\mathbf{Q} * \mathbb{C}) = \mathbf{Q} g(\mathbb{C}) \mathbf{Q}^T$ . Moreover, by continuity,  $g(\mathbb{C})$  is *closed*. Hence, as a consequence of classical results (see, e.g., the book by GOLUBITSKY, STEWART and SCHAEFFER [9, Ch. XIII, Th. 6.1]), we know that  $g(\mathbb{C})$  is *conjugate* to exactly one of the elements in the following collection:

$$\Sigma := \{\mathbf{I}, Z_n, D_n, SO(2), O(2)\} \quad (n \geq 2),$$

where  $Z_n$  and  $D_n$  denote, respectively, the *cyclic* and *dihedral* groups of order  $n$  (for an extensive coverage of this topic see also MILLER'S book [11]).

The space  $\mathbb{E}la$  is divided into *symmetry classes* by a relation defining  $\mathbb{C}_1$  and  $\mathbb{C}_2$  as equivalent when  $g(\mathbb{C}_1)$  is conjugate to  $g(\mathbb{C}_2)$  in  $O(2)$ . Let  $\mathbb{E}la(G)$  be the collection of all elasticity tensors such that their symmetry groups are conjugate to  $G \in \Sigma$ . Then,  $\mathbb{C}_1$  and  $\mathbb{C}_2$  have conjugate symmetry groups if and only if they belong to the same  $\mathbb{E}la(G)$ , and the problem of finding the number and type of symmetry classes is equivalent to the problem of determining which  $\mathbb{E}la(G)$  are empty and which are not. The answer is known (see, e.g., RYCHLEWSKI [14, Sec. 8]), even if some contradictory statements can still be found in the literature (cf., e.g., ZHENG [19, Sec. 3.3], where the Author seems to suggest otherwise). However, the discussion of Sec. 3 has the following statement as a direct consequence: *There are exactly four non-empty sets  $\mathbb{E}la(G)$ , for  $G = Z_2, D_2, D_4, O(2)$ .*

We use the following terminology to classify the symmetries, depending on which element of  $\Sigma$  the group  $g(\mathbb{C})$  is conjugate to: *anisotropic* for  $Z_2$ , *orthotropic* for  $D_2$ , *tetragonal* for  $D_4$  and *isotropic* for  $O(2)$ . Notice that only  $\mathbb{E}la(O(2))$  is a linear subspace of  $\mathbb{E}la$ .

As mentioned before, it is almost impossible that an elasticity tensor obtained from experimental data might have any special symmetry at all. As we recall in Sec. 5, the set of tensors with symmetry  $D_2, D_4$  or  $O(2)$  has the structure of an *algebraic manifold* of measure zero, formed by the null-set of a finite number of polynomials. Thus, anisotropic elasticity tensors are *dense* in  $\mathbb{E}la$ . From this point of view, the question of interest becomes a different one: We would like to know *how close* a given  $\mathbb{C}$  is to classes of non-minimal symmetry.

The final section contains a computation of the distance between  $\mathbb{C}$  and  $\mathbb{E}la(G)$ , for  $G = D_2, D_4$  or  $O(2)$ , which is defined to be the infimum of the distance between  $\mathbb{C}$  and  $\mathbb{C}^*$ , as the latter varies over  $\mathbb{E}la(G)$  (an obvious Euclidean norm and a corresponding distance are defined in the space of elasticity tensors).

### 3. A decomposition for the space of elasticity tensors

A finite-dimensional vector space is decomposed into a direct sum of subspaces which are irreducible under the action of a compact group (see, e.g., [9] or [11]). In our particular context it is possible to show that the decomposition of  $\mathbb{E}la$  is described by an  $SO(2)$ -invariant isomorphism which maps  $\mathbb{C}$  into a quadruplet  $(\lambda, \mu, \mathbf{H}, \mathbb{K})$ , where  $\lambda$  and  $\mu$  are scalars, while  $\mathbf{H}$  and  $\mathbb{K}$  belong to  $\text{Dev}$  and  $\mathbb{D}ev$ , respectively. More explicitly, for a given  $\mathbb{C} \in \mathbb{E}la$ :

$$\lambda = (3C_{ppqq} - 2C_{pqpq})/8, \quad \mu = (2C_{pqpq} - C_{ppqq})/8,$$

$$H_{ik} = [2C_{ipkp} - C_{pqpq}\delta_{ik}]/12,$$

$$K_{ijkl} = C_{ijkl} - [\delta_{ij}C_{kplp} + \delta_{kl}C_{ipjp} + \delta_{ik}C_{lpjp} + \delta_{lj}C_{ipkp} + \delta_{il}C_{jpkp} + \delta_{jk}C_{iplp}]/6 \\ + [C_{ppqq}(5\delta_{ij}\delta_{kl} - \delta_{ik}\delta_{lj} - \delta_{il}\delta_{jk})]/12 - [C_{ppqq}(3\delta_{ij}\delta_{kl} - \delta_{ik}\delta_{lj} - \delta_{il}\delta_{jk})]/8,$$

( $\delta_{ij}$  is Kronecker's delta). *Vice versa*, the elasticity tensor  $\mathbb{C}$  corresponding to  $(\lambda, \mu, \mathbf{H}, \mathbb{K})$  is:

$$C_{ijkl} = K_{ijkl} + \delta_{ij}H_{kl} + H_{ij}\delta_{kl} + \delta_{ik}H_{lj} + H_{ik}\delta_{lj} + \delta_{il}H_{jk} + H_{il}\delta_{jk} \\ + \lambda\delta_{ij}\delta_{kl} + \mu(\delta_{ik}\delta_{lj} + \delta_{il}\delta_{jk}).$$

The validity of this decomposition can be directly checked through substitutions followed by lengthy computations. Moreover, it is not difficult to see that this is a variation, and an indirect confirmation, of a quite similar result presented by BLINOWSKI *et al.* [3]. However, it is perhaps useful to spend a few words on a short description of the rationale behind our derivation, for which we followed the scheme adopted by BAERHEIM [2] in three dimensions. The first step consists in writing  $C_{ijkl}$  as the sum of a completely symmetric part  $S_{ijkl}$  and an "asymmetric" part  $A_{ijkl}$ :

$$S_{ijkl} := (C_{ijkl} + C_{iklj} + C_{iljk})/3, \quad A_{ijkl} := (2C_{ijkl} - C_{iklj} - C_{iljk})/3.$$

This corresponds to a decomposition of  $\mathbb{E}la$  into a direct sum of two orthogonal subspaces. Since the dimension of  $\mathbb{E}la$  is 6 and the space of completely symmetric fourth-order tensors has dimension 5, it follows that  $A_{ijkl}$  is a scalar multiple of a fixed asymmetric tensor, say:

$$A_{ijkl} = \alpha(2\delta_{ij}\delta_{kl} - \delta_{ik}\delta_{lj} - \delta_{il}\delta_{jk}).$$

Next, we use the fact that for each  $S_{ijkl}$  there is a unique pair of tensors  $\mathbf{A} \in \text{Sym}$  and  $\mathbb{K} \in \text{Dev}$  such that

$$S_{ijkl} = K_{ijkl} + \delta_{(ij}A_{kl)},$$

where the parenthesis denotes full symmetrization with respect to the enclosed set of indexes or, more precisely,

$$\delta_{(ij}A_{kl)} = \delta_{ij}A_{kl} + A_{ij}\delta_{kl} + \delta_{ik}A_{lj} + A_{ik}\delta_{lj} + \delta_{il}A_{jk} + A_{il}\delta_{jk}.$$

This property is a reformulation of a well-known result on polynomials, which naturally correspond to symmetric tensors, as discussed in [9, Ch. XIII, Sec. 7, Prop. 7.1].

Finally, we use the decomposition of each element of  $\text{Sym}$  into the sum of a "spherical" part (i.e., a multiple of  $\mathbf{I}$ ) and an element  $\mathbf{H}$  of  $\text{Dev}$ , so that we may write

$$A_{ij} = H_{ij} + \beta\delta_{ij}/2.$$

Trivial substitutions followed by an appropriate change of names yield the decomposition, which, with obvious meaning, is written as

$$(3.1) \quad \mathbb{C} = (\lambda, \mu, \mathbf{H}, \mathbb{K}).$$

An action of  $O(2)$  on  $\text{Dev}$  is defined by

$$\mathbf{Q} * \mathbf{A} := \mathbf{Q}\mathbf{A}\mathbf{Q}^T, \quad \forall \mathbf{Q} \in O(2), \quad \forall \mathbf{A} \in \text{Dev}.$$

It is a matter of simple computations to check that

$$\mathbf{Q} * \mathbb{C} = (\lambda, \mu, \mathbf{Q} * \mathbf{H}, \mathbf{Q} * \mathbb{K}), \quad \forall \mathbf{Q} \in O(2),$$

and, consequently,  $g(\mathbb{C}) = g(\mathbf{H}) \cap g(\mathbb{K})$ , where  $g(\mathbf{H})$  is defined in the natural way. It is now clear why the action of  $O(2)$  on  $\text{Dev}$  and  $\mathbb{D}\text{ev}$  is of great interest, and the importance of the geometric description of this action which is obtained in the final part of this section.

It is convenient to define an appropriate *orthonormal* basis in each of these spaces. For  $\text{Dev}$  we use:

$$\mathbf{E}_1 := \frac{\sqrt{2}}{2}(\mathbf{e}_1 \otimes \mathbf{e}_1 - \mathbf{e}_2 \otimes \mathbf{e}_2), \quad \mathbf{E}_2 := \frac{\sqrt{2}}{2}(\mathbf{e}_1 \otimes \mathbf{e}_2 + \mathbf{e}_2 \otimes \mathbf{e}_1).$$

The basis for  $\mathbb{D}\text{ev}$  is more complex:

$$\begin{aligned} \mathbb{E}_1 &:= \frac{\sqrt{8}}{8}(\mathbf{e}_1 \otimes \mathbf{e}_1 \otimes \mathbf{e}_1 \otimes \mathbf{e}_1 + \mathbf{e}_2 \otimes \mathbf{e}_2 \otimes \mathbf{e}_2 \otimes \mathbf{e}_2 - \mathbf{e}_1 \otimes \mathbf{e}_1 \otimes \mathbf{e}_2 \otimes \mathbf{e}_2 - \mathbf{e}_1 \otimes \mathbf{e}_2 \otimes \mathbf{e}_1 \otimes \mathbf{e}_2 \\ &\quad - \mathbf{e}_2 \otimes \mathbf{e}_1 \otimes \mathbf{e}_1 \otimes \mathbf{e}_2 - \mathbf{e}_2 \otimes \mathbf{e}_1 \otimes \mathbf{e}_2 \otimes \mathbf{e}_1 - \mathbf{e}_1 \otimes \mathbf{e}_2 \otimes \mathbf{e}_2 \otimes \mathbf{e}_1 - \mathbf{e}_2 \otimes \mathbf{e}_2 \otimes \mathbf{e}_1 \otimes \mathbf{e}_1), \\ \mathbb{E}_2 &:= \frac{\sqrt{8}}{8}(\mathbf{e}_1 \otimes \mathbf{e}_1 \otimes \mathbf{e}_1 \otimes \mathbf{e}_2 + \mathbf{e}_1 \otimes \mathbf{e}_1 \otimes \mathbf{e}_2 \otimes \mathbf{e}_1 + \mathbf{e}_1 \otimes \mathbf{e}_2 \otimes \mathbf{e}_1 \otimes \mathbf{e}_1 + \mathbf{e}_2 \otimes \mathbf{e}_1 \otimes \mathbf{e}_1 \otimes \mathbf{e}_1 \\ &\quad - \mathbf{e}_2 \otimes \mathbf{e}_2 \otimes \mathbf{e}_2 \otimes \mathbf{e}_1 - \mathbf{e}_2 \otimes \mathbf{e}_2 \otimes \mathbf{e}_1 \otimes \mathbf{e}_2 - \mathbf{e}_2 \otimes \mathbf{e}_1 \otimes \mathbf{e}_2 \otimes \mathbf{e}_2 - \mathbf{e}_1 \otimes \mathbf{e}_2 \otimes \mathbf{e}_2 \otimes \mathbf{e}_2). \end{aligned}$$

In view of (2.1), through direct substitution it is not difficult to show that

$$\mathbf{Q}(\theta) * \mathbf{E}_1 = \cos(2\theta)\mathbf{E}_1 + \sin(2\theta)\mathbf{E}_2, \quad \mathbf{Q}(\theta) * \mathbf{E}_2 = -\sin(2\theta)\mathbf{E}_1 + \cos(2\theta)\mathbf{E}_2,$$

while more lengthy computations are needed to prove that

$$\mathbf{Q}(\theta) * \mathbb{E}_1 = \cos(4\theta)\mathbb{E}_1 + \sin(4\theta)\mathbb{E}_2, \quad \mathbf{Q}(\theta) * \mathbb{E}_2 = -\sin(4\theta)\mathbb{E}_1 + \cos(4\theta)\mathbb{E}_2.$$

Moreover, since  $\tilde{\mathbf{Q}}\mathbf{e}_1 = \mathbf{e}_1$  and  $\tilde{\mathbf{Q}}\mathbf{e}_2 = -\mathbf{e}_2$ ,

$$\tilde{\mathbf{Q}} * \mathbf{E}_1 = \mathbf{E}_1, \quad \tilde{\mathbf{Q}} * \mathbf{E}_2 = -\mathbf{E}_2, \quad \tilde{\mathbf{Q}} * \mathbb{E}_1 = \mathbb{E}_1, \quad \tilde{\mathbf{Q}} * \mathbb{E}_2 = -\mathbb{E}_2.$$

In conclusion, each  $\mathbf{Q}(\theta)$  acts on  $\text{Dev}$  as a rotation of  $2\theta$  and on  $\mathbb{D}\text{ev}$  as a rotation of  $4\theta$ , while  $\tilde{\mathbf{Q}}$  is simply a reflection with respect to the “horizontal” axes spanned by  $\mathbf{E}_1$  and  $\mathbb{E}_1$ . The geometric insight provided by this point of view makes easy a proof of the fact that there are only symmetry classes corresponding to groups  $Z_2$ ,  $D_2$ ,  $D_4$ , and  $O(2)$ .

#### 4. An integrity basis

The Euclidean structure of  $\text{Dev}$  and  $\mathbb{D}\text{ev}$  is obtained by introducing the inner products  $\mathbf{A} \cdot \mathbf{B} = A_{ij} B_{ij}$  and  $\mathbb{H} \cdot \mathbb{K} = H_{ijkl} K_{ijkl}$ . We use the symbol  $|\cdot|$  to denote the norm in both spaces. For a given  $\mathbb{C} = (\lambda, \mu, \mathbf{H}, \mathbb{K})$ , let  $\alpha$  be the angle between  $\mathbf{H}$  and  $\mathbf{E}_1$ , and let  $\beta$  be the angle between  $\mathbb{K}$  and  $\mathbf{E}_1$ . Furthermore, we need the following definitions:

$$(4.1) \quad \begin{aligned} H_1 &:= |\mathbf{H}| \cos \alpha = \mathbf{H} \cdot \mathbf{E}_1, & H_2 &:= |\mathbf{H}| \sin \alpha = \mathbf{H} \cdot \mathbf{E}_2, \\ K_1 &:= |\mathbb{K}| \cos \beta = \mathbb{K} \cdot \mathbf{E}_1, & K_2 &:= |\mathbb{K}| \sin \beta = \mathbb{K} \cdot \mathbf{E}_2. \end{aligned}$$

The geometric view of the action of  $O(2)$  on  $\text{Dev}$  and  $\mathbb{D}\text{ev}$  makes the choice of *four* independent polynomial invariants quite obvious:

$$I_1 = \lambda, \quad I_2 := \mu, \quad I_3 := |\mathbf{H}|^2, \quad I_4 := |\mathbb{K}|^2.$$

Thus, we only need to find a fifth invariant, and, to this end, we consider the angle  $\gamma := 2\alpha - \beta$ . Since the action of  $\mathbf{Q}(\theta)$  maps  $\alpha$  onto  $\alpha + 2\theta$  and  $\beta$  onto  $\beta + 4\theta$ , it follows that  $\gamma$  is left fixed. However, it is also straightforward to see that, under  $\tilde{\mathbf{Q}}$ ,  $\gamma$  is mapped onto  $-\gamma$ . Thus, the conclusion is that this angle is an  $SO(2)$ -invariant, but *not* an  $O(2)$ -invariant. A natural choice for the fifth isotropic invariant  $\mathcal{I}$  is the cosine of  $\gamma$ :

$$\mathcal{I} := \cos \gamma = \cos(2\alpha - \beta).$$

This function is not a polynomial and thus we expand it as

$$\mathcal{I} = (\cos^2 \alpha - \sin^2 \alpha) \cos \beta + 2 \sin \alpha \cos \alpha \sin \beta$$

and use definitions (4.1) to obtain the fifth polynomial isotropic invariant:

$$I_5 := |\mathbf{H}|^2 |\mathbb{K}| \mathcal{I} = (H_1^2 - H_2^2) K_1 + 2 H_1 H_2 K_2.$$

The steps followed for the construction of the collection  $\{I_n\}$  show that a necessary and sufficient condition for  $\mathbb{C}_1$  and  $\mathbb{C}_2$  to be on the same orbit is that  $I_n(\mathbb{C}_1) = I_n(\mathbb{C}_2)$  ( $1 \leq n \leq 5$ ). It is a well-known result that this condition is necessary and sufficient for  $\{I_n\}$  to be a *functional basis* (see, e.g., WEYL [16], WINEMAN and PIPKIN [17, Sec. 4, p.190]).

As an additional remark, we notice that if the  $SO(2)$ -invariant polynomial

$$I_6 := |\mathbf{H}|^2 |\mathbb{K}| \sin \gamma = 2 H_1 H_2 K_1 - (H_1^2 - H_2^2) K_2$$

is added to the previous list, we obtain a functional basis for  $SO(2)$ -invariant functions on  $\mathbb{E}1a$ . However, in this case, there is a *relation* (or *syzygy*) among the

elements of the collection  $\{I_m\}$  ( $1 \leq m \leq 6$ ):  $I_5^2 + I_6^2 = I_3^2 I_4$ . This is obviously due to the trigonometric identity between  $\sin \gamma$  and  $\cos \gamma$ .

Our aim is now to prove that the collection of invariants  $\{I_n\}$  is indeed an integrity basis, and not only a functional basis.

**THEOREM 1.** *For each  $O(2)$ -invariant real-valued polynomial  $p$  on  $\mathbb{E}1a$ , there is a polynomial  $\pi$  in 5 variables such that*

$$p(\mathbb{C}) = \pi(I_1(\mathbb{C}), I_2(\mathbb{C}), I_3(\mathbb{C}), I_4(\mathbb{C}), I_5(\mathbb{C})), \quad \forall \mathbb{C} \in \mathbb{E}1a.$$

A convenient technique of proof is based on the idea of looking at the action of  $O(2)$  on  $\text{Dev}$  and  $\mathbb{D}\text{ev}$  as an action on the complex plane  $\mathbb{C}$ , and then to apply straightforward considerations from the complex number theory. This method was applied by PIERCE [12] to a similar problem.

More precisely, the product between  $\text{Dev}$  and  $\mathbb{D}\text{ev}$  is seen as  $\mathbb{C}^2$ . Then, the action of a rotation  $\mathbf{Q}(\theta) \in SO(2)$  on this space is defined through the unit complex number  $\exp(i\theta)$  as

$$\mathbf{Q} * (z_1, z_2) := (\exp(i2\theta)z_1, \exp(i4\theta)z_2), \quad \forall (z_1, z_2) \in \mathbb{C}^2.$$

Moreover, the action of  $\tilde{\mathbf{Q}}$  (reflection with respect to the ‘‘horizontal’’ axes) corresponds to complex conjugation:  $\tilde{\mathbf{Q}} * (z_1, z_2) := (\bar{z}_1, \bar{z}_2)$ . According to this point of view, we rewrite three of the invariants as

$$(4.2) \quad I_3 = |z_1|^2, \quad I_4 = |z_2|^2, \quad I_5 = \Re(z_1^2 \bar{z}_2).$$

In view of the decomposition of  $\mathbb{E}1a$  described in Sec.3, we now choose to look at polynomial functions of elasticity tensors as being defined on  $\mathcal{R}^2 \times \mathbb{C}^2$ . Moreover, we notice that each polynomial in the real variables  $x$  and  $y$  can be written as a polynomial in the complex variables  $z$  and  $\bar{z}$ , where  $z = x + iy$ . For this reason, we have

$$(4.3) \quad p(\mathbb{C}) = \sum c_{lmrstu} \lambda^l \mu^m z_1^r \bar{z}_1^s z_2^t \bar{z}_2^u,$$

where the index range depends on the degree of  $p$ . However, since we are only interested in real-valued polynomials, the restriction  $c_{lmrstu} = \bar{c}_{lmrsut}$  must be satisfied. Moreover, invariance under the action of  $\tilde{\mathbf{Q}}$  is guaranteed by  $c_{lmrstu} = c_{lmrsut}$ , which combined with the previous condition, implies that all the coefficients are real.

The action of  $\mathbf{Q}(\theta) \in SO(2)$  yields

$$p(\mathbf{Q} * \mathbb{C}) = \sum c_{lmrstu} \lambda^l \mu^m z_1^r \bar{z}_1^s z_2^t \bar{z}_2^u \exp[i(2r - 2s + 4t - 4u)]$$

and, from  $p(\mathbb{C}) = p(\mathbf{Q} * \mathbb{C})$ , we deduce that invariance under the action  $SO(2)$  is guaranteed when the non-zero coefficients in (4.3) satisfy a relation which simplifies to

$$r - s = 2(u - t).$$

Thus, by inspection, we deduce that there are three types of non-zero terms in the sum defining  $p$ : (a) Those for which  $r = s$  and  $u = t$ ; (b) Those for which  $\tau := u - t$  and  $r - s = 2\tau$  are positive integers; (c) Those for which  $\tau := t - u$  and  $s - r = 2\tau$  are positive integers.

Case (a) is simple, because we rewrite each such addendum as

$$c_{lmrruu} \lambda^l \mu^m (z_1 \bar{z}_1)^r (z_2 \bar{z}_2)^u = c_{lmrruu} \lambda^l \mu^m |z_1|^{2r} |z_2|^{2u}, \quad (\text{no sum}),$$

and, in view of (4.2), this is a monomial in the invariants  $I_3$  and  $I_4$ . The symmetries of the coefficients  $c_{lmrstu}$  imply that the sum of the terms corresponding to cases (b) and (c) can be written as

$$\sum c_{lmrstu} \lambda^l \mu^m [z_1^r \bar{z}_1^s z_2^t \bar{z}_2^u + z_1^s \bar{z}_1^r z_2^u \bar{z}_2^t], \quad r < s, \quad t < u,$$

which is

$$2 \sum c_{lmrstu} \lambda^l \mu^m \Re[z_1^r \bar{z}_1^s z_2^t \bar{z}_2^u], \quad r < s, \quad t < u.$$

Since  $r = s + 2\tau$  and  $u = t + \tau$ , we conclude that this sum is

$$2 \sum c_{lmrstu} \lambda^l \mu^m |z_1|^{2s} |z_2|^{2t} \Re[(z_1^2 \bar{z}_2)^\tau], \quad r < s, \quad t < u.$$

Finally, in view of the binomial formula, the real part of  $z^\tau$  is always a polynomial in the variables  $x := \Re z$  and  $y^2 := (\Im z)^2 = |z|^2 - x^2$ . Thus, we deduce that  $\Re[(z_1^2 \bar{z}_2)^\tau]$  is a polynomial in  $I_3, I_4$  and  $I_5$ , and this concludes the proof that the collection  $\{I_n\}$  is an integrity basis. As a final remark, we wish to draw the reader's attention to the fact that, with a similar technique, it is possible to prove that this collection, plus the sixth invariant  $I_6$ , is also an integrity basis for the action of the group  $SO(2)$  on  $\mathbb{E}a$ .

### 5. Symmetry classes and invariants

A complete characterization of each one of the three non-trivial symmetry classes mentioned in Theorem 1 as the intersection of the zero-sets of isotropic polynomials is directly deducible from the geometric interpretation of the invariants introduced. This was also shown in [3], but, for the reader's convenience, we repeat here a formulation of this result, which can be easily proved using the concepts previously introduced.

PROPOSITION 1.

$$\begin{aligned} \mathbb{C} \in \mathbb{E}a(O(2)) &\Leftrightarrow I_3 = I_4 = 0, & \mathbb{C} \in \mathbb{E}a(D_4) &\Leftrightarrow I_3 = 0, \quad I_4 \neq 0, \\ \mathbb{C} \in \mathbb{E}a(D_2) &\Leftrightarrow \begin{cases} I_3 \neq 0, & I_4 = 0, \\ I_3 \neq 0, & I_4 \neq 0, \quad I_5^2 - I_3^2 I_4 = 0, \end{cases} \\ \mathbb{C} \in \mathbb{E}a(Z_2) &\Leftrightarrow I_3 \neq 0, \quad I_4 \neq 0, \quad I_5^2 - I_3^2 I_4 \neq 0. \end{aligned}$$

We are now left with the problem of determining the distance between an elasticity tensor obtained through experimental observations of a given material of unknown symmetry and the symmetry classes  $\mathbb{E}la(O(2))$ ,  $\mathbb{E}la(D_4)$  and  $\mathbb{E}la(D_2)$ . As we shall see, only the distance with the first two classes can be computed explicitly, while for the third one the problem is left in a more general setting.

Before completing this discussion, it is important to make clear a further point. In principle, we are not so much interested in the distance between a given  $\mathbb{C}$ , which here we shall assume to be *anisotropic*, and the other three symmetry classes, but, rather, in the distance between them and the *orbit* of  $\mathbb{C}$ . The reason is clear when we think that two different elasticity tensors  $\mathbb{C}_1$  and  $\mathbb{C}_2$  lying on the same orbit (i.e., such that there is an orthogonal  $\mathbf{Q}$  with the property that  $\mathbb{C}_1 = \mathbf{Q} * \mathbb{C}_2$ ) represent the *same* material differently rotated in space. Thus, properly speaking, physical meaning pertains to the orbits, rather than to the elasticity tensors themselves. This observation, which is also discussed by BOEHLER, KIRILLOV and ONAT [4], shows the importance of having at our disposal a functional basis of isotropic invariants, to separate the orbits and decide when two elasticity tensors correspond to the same material body. Incidentally, we note that a functional basis for three-dimensional elasticity is not yet known, even if a partial answer is provided in [4], and a complete solution was recently announced by ZHENG and BETTEN [20, Abstract] and is expected to be published in a forthcoming paper by the same Authors.

However, we now prove that all the elasticity tensors on the same orbit have equal distance from any given symmetry class. Direct substitution shows that the action of  $O(2)$  on  $\mathbb{E}la$  is distance-preserving:  $d(\mathbb{C}_1, \mathbb{C}_2) = d(\mathbf{Q} * \mathbb{C}_1, \mathbf{Q} * \mathbb{C}_2)$ , for all  $\mathbf{Q} \in O(2)$ . In other words, this action is a homomorphism of  $O(2)$  into the group of orthogonal transformations of  $\mathbb{E}la$ . For convenience of notation, we let  $\mathcal{S}$  be any one of the four symmetry classes of elasticity tensors. Then  $\mathbf{Q} * \mathcal{S} = \mathcal{S}$  for all orthogonal  $\mathbf{Q}$ . Thus,

$$\begin{aligned} d(\mathbf{Q} * \mathbb{C}, \mathcal{S}) &:= \inf_{\mathbb{C}^* \in \mathcal{S}} d(\mathbf{Q} * \mathbb{C}, \mathbb{C}^*) = \inf_{\mathbb{C}^* \in \mathcal{S}} d(\mathbf{Q} * \mathbb{C}, \mathbf{Q} * \mathbb{C}^*) \\ &= \inf_{\mathbb{C}^* \in \mathcal{S}} d(\mathbb{C}, \mathbb{C}^*) =: d(\mathbb{C}, \mathcal{S}). \end{aligned}$$

The interested reader will find a more complete discussion of many aspects of the geometry of the orbits of elasticity tensors under the action of the orthogonal group in a paper by RYCHLEWSKI [13].

Our goal is now to compute explicitly the square of the distance between a given tensor  $\mathbb{C} = (\lambda, \mu, \mathbf{H}, \mathbb{K})$ , which is assumed to be *isotropic*, and each one of the three remaining symmetry classes. We write this quantity as follows:

$$\Delta(\mathbb{C}, \mathcal{G}) := |d(\mathbb{C}, \mathbb{E}la(\mathcal{G}))|^2.$$

Let  $\mathcal{G} = O(2)$ . Then, for a generic isotropic  $\mathbb{C}^*$  we may write the decomposi-

tion (3.1) as  $\mathbb{C}^* = (\lambda^*, \mu^*, 0, 0)$ . Thus,

$$|d(\mathbb{C}, \mathbb{C}^*)|^2 = (\lambda - \lambda^*)^2 + (\mu - \mu^*)^2 + |\mathbf{H}|^2 + |\mathbb{K}|^2.$$

It is now obvious that minimization as  $\mathbb{C}^*$  varies over  $\text{Ela}(O(2))$  requires  $\mathbb{C}^* = (\lambda, \mu, 0, 0)$  and, consequently,

$$\Delta(\mathbb{C}, O(2)) = |\mathbf{H}|^2 + |\mathbb{K}|^2 = I_3 + I_4.$$

A geometric interpretation of this result is straightforward:  $\mathbb{C}^*$  is simply the orthogonal projection of  $\mathbb{C}$  onto the subspace of isotropic tensors, and  $\Delta(\mathbb{C}, O(2))$  is the square of the distance between the two. The problem of determining the isotropic elasticity tensor which is the closest to a given  $\mathbb{C}$  is classical and, for three-dimensional elasticity, this solution is discussed in many textbooks (see, e.g., FEDOROV [7, Ch. 5, Sec. 26, pp. 174–175]).

We now address the issue of determining  $\Delta(\mathbb{C}, D_4)$ . The decomposition of a generic tetragonal elasticity tensor is:  $\mathbb{C}^* = (\lambda^*, \mu^*, 0, \mathbb{K}^*)$ . Thus,

$$|d(\mathbb{C}, \mathbb{C}^*)|^2 = (\lambda - \lambda^*)^2 + (\mu - \mu^*)^2 + |\mathbf{H}|^2 + |\mathbb{K} - \mathbb{K}^*|^2,$$

and minimization implies that  $\mathbb{C}^* = (\lambda, \mu, 0, \mathbb{K})$ . In conclusion,

$$\Delta(\mathbb{C}, D_4) = |\mathbf{H}|^2 = I_3.$$

The computation of  $\Delta(\mathbb{C}, D_2)$  is more complex. In view of Proposition 1, the symmetry class  $\text{Ela}(D_2)$  can be seen as the union of two disjoint subsets  $S_1$  and  $S_2$ , formed, respectively, by elasticity tensors such that  $I_4 = 0$  and such that  $I_4 \neq 0$  with  $I_5^2 = I_3^2 I_4$ . Minimization of the distance between a given  $\mathbb{C}$  and  $S_1$  yields the inequality

$$\Delta(\mathbb{C}, D_2) \leq I_4,$$

which, in any case, is a useful estimate of  $\Delta(\mathbb{C}, D_2)$ . To complete our analysis we need a better description of the set  $S_2$ , which is characterized by the condition  $\cos \gamma = \pm 1$ . Let  $\psi$  and  $\phi$  be the angles that the two tensor components in the decomposition (3.1) of a generic element of  $S_2$  form, respectively, with  $\mathbf{E}_1$  and  $\mathbb{E}_1$ . Then,  $\psi = \phi/2 + k\pi/2$ , for some integer  $k$ . The element of  $S_2$  minimizing the distance from  $\mathbb{C} = (\lambda, \mu, \mathbf{H}, \mathbb{K})$  is obviously  $\mathbb{C}^* = (\lambda, \mu, \mathbf{H}^*, \mathbb{K}^*)$ , where  $\mathbf{H}^*$  and  $\mathbb{K}^*$  are chosen in such a way that the sum  $|\mathbf{H} - \mathbf{H}^*|^2 + |\mathbb{K} - \mathbb{K}^*|^2$  is an absolute minimum. We may now use elementary geometry considerations to show that

$$|\mathbf{H} - \mathbf{H}^*|^2 + |\mathbb{K} - \mathbb{K}^*|^2 = (K_1 \sin \phi - K_2 \cos \phi)^2 + (H_1 \sin(\phi/2) - H_2 \cos(\phi/2))^2.$$

Let  $\Delta^*$  be the minimum of this distance as  $\phi$  varies over  $[0, 2\pi)$ . In view of the definitions (4.1) we deduce that

$$\Delta^* = \min_{\phi \in [0, 2\pi)} \{ |\mathbb{K}|^2 \sin^2(\phi - \beta) + |\mathbf{H}|^2 \sin^2(\phi/2 - \alpha) \}.$$

Moreover, since this quantity is invariant under the action of  $O(2)$  on  $\mathbb{C}$  we may also assume that  $\alpha = 0$  and, as a consequence,  $\gamma = -\beta$ . Thus, in conclusion,

$$\Delta^* = \min_{\phi \in [0, 2\pi)} \{I_4 \sin^2(\phi + \gamma) + I_3 \sin^2(\phi/2)\},$$

and

$$\Delta(\mathbb{C}, D_2) = \min\{I_4, \Delta^*\}.$$

The research supported by GNFM of CNR (Italy).

## References

1. G. BACKUS, *A Geometrical picture of anisotropic elastic tensors*, Reviews of Geophysics and Space Physics, **8**, 3, 633–671, 1970.
2. R. BAERHEIM, *Harmonic decomposition of the anisotropic elasticity tensor*, Q. J. Mech. Appl. Math., **46**, 3, 391–419, 1993.
3. A. BLINOWSKI, J. OSTROWSKA-MACIEJEWSKA and J. RYCHLEWSKI, *Two-dimensional Hooke's tensors – isotropic decomposition, effective symmetry criteria*, Arch. Mech., **48**, 2, 325–345, 1996.
4. J.P. BOEHLER, A.A. KIRILLOV and E.T. ONAT, *On the polynomial invariants of the elasticity tensor*, J. Elasticity, **34**, 97–110, 1994.
5. M. FRANÇOIS, Y. BERTHAUD and G. GEYMONAT, *Une nouvelle analyse des symétries d'un matériau élastique anisotrope. Exemple d'utilisation à partir de mesures ultrasonores*, C. R. Acad. Sci. Paris, 322 (Série II b), 87–94, 1996.
6. S.C. COWIN, *Properties of the anisotropic elasticity tensor*, Q. J. Mech. Appl. Math., **42**, 2, 249–266, 1989.
7. F.I. FEDOROV, *Theory of elastic waves in crystals*, Plenum Press, New York 1968.
8. S. FORTE and M. VIANELLO, *Symmetry classes for elasticity tensors*, J. Elasticity, **43**, 2, 81–108, 1996.
9. M. GOLUBITSKY, I. STEWART and D.G. SCHAEFFER, *Singularities and groups in bifurcation theory*, vol. 2, Springer-Verlag, New York – Berlin 1985.
10. M.E. GURTIN, *The linear theory of elasticity*, [in:] Mechanics of Solids II, C. TRUESDELL [Ed.], volume VIa/2, Handbuch der Physik, pp. 1–295, Springer, Berlin 1972.
11. W. MILLER, *Symmetry groups and their applications*, Academic Press, New York – London 1972.
12. J.F. PIERCE, *Representations for transversely hemitropic and transversely isotropic stress-strain relations*, J. Elasticity, **37**, 243–280, 1995.
13. J. RYCHLEWSKI, *Zur Abschätzung der Anisotropie*, Z. Angew. Math. Mech. (ZAMM), **65**, 6, 256–258, 1985.
14. J. RYCHLEWSKI, *Unconventional approach to linear elasticity*, Arch. Mech., **47**, 2, 149–171, 1995.
15. J.A. SCHOUTEN, *Tensor analysis for physicists*, Oxford University Press, London 1951.
16. H. WEYL, *The classical groups, their invariants and representations*, Princeton University Press, Princeton 1946.
17. A.S. WINEMAN and A.C. PIPKIN, *Material symmetry restrictions on constitutive equations*, Arch. Rational Mech. Anal., **17**, 184–214, 1964.
18. Q.-S. ZHENG, *A note on representation for isotropic functions of 4th-order tensors in 2-dimensional space*, Z. Angew. Math. Mech. (ZAMM), **74**, 8, 357–359, 1994.
19. Q.-S. ZHENG, *Theory of representations for tensor functions – a unified invariant approach to constitutive equations*, AMR, Applied Mech. Reviews, **47**, 11, 545–587, 1994.
20. Q.-S. ZHENG and J. BETTEN, *On the tensor function representations of 2nd-order and 4th-order tensors. Part I*, Z. Angew. Math. Mech. (ZAMM), **75**, 4, 269–281, 1995.

DIPARTIMENTO DI MATEMATICA  
POLITECNICO DI MILANO, ITALY  
e-mail: mauvia@mate.polimi.it

Received September 23, 1996.

# The stochastic vortex method for viscous incompressible flows in a spatially periodic domain

J. SZUMBARSKI and A. STYCZEK (WARSZAWA)

THE RANDOM VORTEX METHOD for two-dimensional, nonstationary flows of a viscous liquid in a spatially periodic, infinite system of airfoils is considered. The main idea is to approximate the evolution of the vorticity by a large set of small “vortex particles” (vortex blobs), which are transported in the velocity field (convection) and perform random walks according to Wiener process with standard deviation depending on the viscosity (diffusion). The velocity field is due to the induction of vortex blobs and includes also certain potential components. Since the flow domain is not simply connected, additional constraints concerning the vorticity production on the boundaries are introduced. They are necessary to obtain a solution with physically correct, single-valued pressure field. The results of numerical calculations are also presented.

## 1. Introduction

DURING LAST TWO DECADES, large amount of research work has been devoted to the development of more sophisticated variants of vortex methods, to widening the range of their applications and improving their computational efficiency. Since 1973, when CHORIN published his fundamental paper [1], many authors have applied a stochastic approach to calculate flows with various geometrical configurations. However, a majority of available publications on external flows focus on flows around individual contours only, although, from the engineering point of view, multi-body systems are even more important.

The aim of this paper is to present the random vortex algorithm for flows which are periodic with respect to one spatial variable. The standard engineering example is a flow in a cascade of airfoils, which is used as a model of turbomachinery flows. The numerical method constructed here is a natural extension of the method proposed by STYCZEK [2] and its primary version was also the subject of the thesis of one of the authors (see [3]). The current version includes careful treatment of the pressure problem arising due to multiply connected geometry of the flow domain. More refined numerical results are also obtained.

We remind briefly the general idea of the stochastic approach to viscous liquid motion (more detailed discussion and examples of applications can be found in [2, 4, 5 and 6]). The equation of the vorticity transport (Helmholtz equation) in an incompressible, viscous and two-dimensional flow can be written in the following form:

$$(1.1) \quad \partial_t \omega + \partial_x(u\omega) + \partial_y(v\omega) = \nu \Delta \omega .$$

This equation is formally identical to the Fokker–Planck equation corresponding to a diffusive stochastic process with the convective vector equal to the velocity of

the flow  $\mathbf{V} = [u, v]$  and with the diagonal matrix of diffusion  $\text{Diag}[2\nu, 2\nu]$ . Thus the evolution of the vorticity field can be described on the “microscopic level” as a movement of a large (theoretically infinite) set of “vortex particles”, governed by the following Ito equations

$$(1.2) \quad \begin{aligned} dx(t) &= u(t, x(t), y(t)) dt + \sqrt{2\nu} dW_x, \\ dy(t) &= v(t, x(t), y(t)) dt + \sqrt{2\nu} dW_y. \end{aligned}$$

Here  $W_x$  and  $W_y$  are independent Wiener processes.

In a numerical simulation “vortex particles” can be constructed in many ways. Here the vortex blobs i.e. small circular vortices with uniform vorticity distribution are used. It should be emphasised that there is no natural, independent boundary condition for the vorticity field – there are only conditions for the velocity. It is known, however, that the vorticity is produced on the boundaries. In the vortex method new vortex blobs are created on the boundaries in each time step in order to satisfy the boundary condition for the velocity. Some of these blobs subsequently enter the flow domain, while the others move randomly across the boundary and are eliminated. This process gives rise to the diffusive flux of the vorticity through the contours of embedded bodies. All vortex blobs are convected in the velocity field which is partly due to the induction, and also has additional potential components necessary to fulfil boundary conditions and providing appropriate asymptotic behaviour of the velocity field (the condition at infinity).

In the case of a cascade flow the domain is not simply connected. Then there exist velocity and vorticity fields which satisfy the continuity and Helmholtz equations, but correspond to meaningless, multivalued pressure distributions. In order to avoid such “solutions”, additional constraints should be imposed on the velocity field (see, for instance, [6] or [7]). These constraints have the form of following integral equalities:

$$(1.3) \quad \frac{d}{dt} \oint_{C_k} U_g^t(s) ds + \int_{C_k} \left( U_g^n \omega - \nu \frac{d}{dn} \omega \right) (s) ds = 0,$$

where  $C_k$  denotes  $k$ -th component of the boundary of a multiply connected flow region and  $U_g$  is the boundary velocity distribution. If  $U_g$  is fixed in time then we have the condition

$$(1.4) \quad \int_{C_k} \left( U_g^n \omega - \nu \frac{d}{dn} \omega \right) (s) ds = 0$$

which means that the total flux (convective and diffusive) of the vorticity through the contour  $C_k$  should be zero. In particular, on an impermeable boundary we

have simply

$$(1.5) \quad \oint_{C_k} \frac{d}{dn} \omega ds = 0.$$

It is interesting that the stochastic vortex method developed by Styczek automatically ensures the equality (1.5) in the case of an external flow around a single contour. If the geometry is more complicated, the conditions (1.4) or (1.5) must be stated explicitly. However, direct implementation of the above equalities requires sufficient regularity of the vorticity field. In the considered method the vorticity is a piecewise constant function of space variables and its normal derivative on the boundary is not properly defined. We show that this difficulty can be overcome by writing explicitly the conditions for the balance between the vorticity production and vorticity flux across the boundaries during one time step.

## 2. Formulation of the problem

We consider the viscous liquid motion in the exterior of the spatially periodic system of airfoils. The period of the cascade geometry and of the flow field is assumed to be  $2\pi$ . The inlet line is identified with  $y$ -axis. The computational domain is a strip region shown in Fig. 1. Boundary conditions for the velocity field are prescribed on the inlet line segment  $\partial D_W$  and on the contour of the airfoil  $\partial D_P$ .

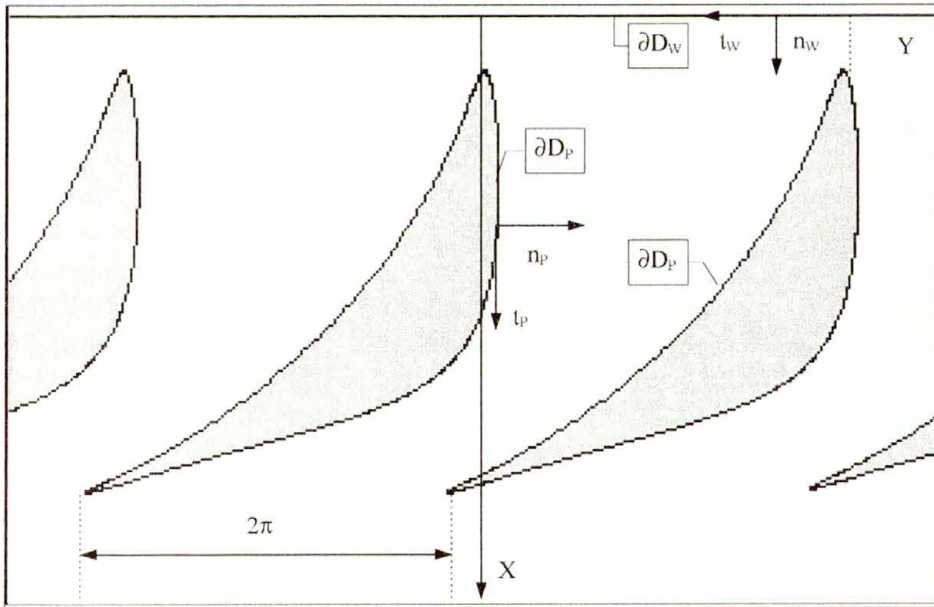


FIG. 1. The computational domain.

The mathematical formulation, which is adequate for the vortex method is following:

Determine the velocity  $\mathbf{V} = [u(t, x, y), v(t, x, y)]$  and the vorticity

$$\omega = \omega(t, x, y) = \partial_x v - \partial_y u$$

satisfying

1) Helmholtz and the continuity equation

$$\begin{aligned} \partial_t \omega + u \partial_x \omega + v \partial_y \omega &= v \delta \omega, \\ \partial_x u + \partial_y v &= 0; \end{aligned}$$

2) conditions of  $y$ -periodicity

$$\begin{aligned} u(t, x, y + 2\pi k) &= u(t, x, y), \\ v(t, x, y + 2\pi k) &= v(t, x, y), \\ \omega(t, x, y + 2\pi k) &= \omega(t, x, y), \quad k = \dots, -2, -1, 0, 1, 2, \dots; \end{aligned}$$

3) boundary conditions

$$\begin{aligned} u \Big|_{\partial D_P} &= 0, & v \Big|_{\partial D_P} &= 0, \\ u \Big|_{\partial D_W} &= u_W(y), & v \Big|_{\partial D_W} &= v_W(y). \end{aligned}$$

This formulation is purely kinematic – the pressure has been eliminated, but it can be recovered *a posteriori* from the velocity and vorticity fields. The results of such calculations are physically sensible provided that the velocity and vorticity were constructed taking pressure correctness conditions (1.4) into account.

### 3. Elements of the numerical method

#### 3.1. $Y$ -periodic vortex blob

The velocity field induced by the vortex blobs must be  $y$ -periodic. To satisfy this demand we use  $y$ -periodic vortex blobs (PVB) which are simply infinite,  $y$ -periodic systems of ordinary vortex blobs (with identical radii  $\varrho$  and charge of vorticity  $\Gamma$ ) uniformly spaced with the distance  $2\pi$  along straight lines parallel to the  $y$ -axis. The position of a PVB is a pair  $(x_0, y_0)$  of the coordinates of this vortex blob in the system which is located in the computational domain. The velocity induced by a PVB is given by the following expressions

$$(3.1) \quad V_{\text{ind}} = \begin{cases} \sum_{n=-\infty}^{\infty} \frac{\Gamma}{2\pi i} \frac{1}{z - (z_0 + 2\pi n)} = \frac{\Gamma}{4\pi i} \coth\left(\frac{z - z_0}{2}\right) \\ \frac{\Gamma}{4\pi i} \coth\left(\frac{z - z_0}{2}\right) - \frac{\Gamma}{2\pi i} \frac{1}{z - (z_0 + 2n\pi i)} + \frac{\Gamma}{2\pi i} \frac{\overline{z - (z_0 + 2\pi i)}}{\varrho^2}. \end{cases}$$

We apply here a convenient complex notation. The upper formula is used when the point  $z = x + iy$  is located outside the PVB's vortex cores and is nothing more than the well known formula for spatially periodic system of point vortices (see [9]). The lower formula is applied when the point  $z$  happens to drop inside the  $n$ -th vortex core of the PVB, the center of which is  $z_0 + 2n\pi i$ ,  $z_0 = x_0 + iy_0$ .

The velocity field induced by a PVB has an important asymptotic property, namely

$$(3.2) \quad \begin{aligned} \lim_{x \rightarrow \infty} V_{\text{ind}} &= \frac{\Gamma}{4\pi i} \Rightarrow u_{\text{ind}} \rightarrow 0, & v_{\text{ind}} &\rightarrow \frac{\Gamma}{4\pi}, \\ \lim_{x \rightarrow -\infty} V_{\text{ind}} &= -\frac{\Gamma}{4\pi i} \Rightarrow u_{\text{ind}} \rightarrow 0, & v_{\text{ind}} &\rightarrow -\frac{\Gamma}{4\pi}. \end{aligned}$$

Thus, if we consider the induction of a system of PVBs, then the behaviour of the velocity at infinity is determined by the total vorticity charge of this system – in particular the velocity vanishes at infinity only when the total charge of vorticity is zero. This is an important difference as compared with any finite system of vortex blobs, where the velocity at infinity tends to zero in any case.

### 3.2. $Y$ -periodic ideal fluid flow

We are going to construct the total velocity field as a sum of several components. Some of them carry vorticity, the other are potential. It is reasonable to consider separately an ideal liquid flow since it provides a natural way to satisfy a part of boundary conditions on the inlet line and to prescribe the velocity at infinity. Then the following mathematical problem is to be solved:

Determine the potential of the velocity  $\Phi_P$  such that:

- 1)  $\Phi_P$  is a harmonic function in the domain  $D$ ;
- 2) the velocity  $\mathbf{V}_P = \nabla\Phi_P$  is  $y$ -periodic i.e.

$$\mathbf{V}_P(t, x, y + 2k\pi) = \mathbf{V}_P(t, x, y), \quad k = 0, \pm 1, 2, \dots;$$

- 3) the Neumann boundary condition is satisfied:

$$\frac{d\Phi_P}{dn} = \begin{cases} 0 & \text{on } \partial D_P, \\ u_W(y) & \text{on } \partial D_W, \end{cases}$$

where  $u_W(y) = u_W(y + 2k\pi)$ ,  $k = 0, \pm 1, 2, \dots$ ;

- 4) the circulation of  $\mathbf{V}_P$  along the inlet  $\partial D_W$  is given

$$\Gamma|_{\partial D_W} = - \int_{\partial D_W} v_W(y) dy.$$

Vector  $[u_W, v_W]$  denotes the given velocity distribution on  $\partial D_W$ . It is convenient to seek  $\Phi_P$  in the form of

$$(3.3) \quad \Phi_P(x, y) = \bar{u}_\infty x + \bar{v}_\infty y + \frac{\Gamma_P}{4\pi} y + \Gamma_P \Phi_C + \Phi_1 + \Gamma_P \Phi_2$$

where meanings of the symbols are the following:

$$(3.4) \quad \bar{u}_\infty = \frac{1}{2\pi} \int_0^{2\pi} u_W(y) dy, \quad \bar{v}_\infty = \frac{1}{2\pi} \int_0^{2\pi} v_W(y) dy,$$

$\Gamma_P$  – the circulation of an airfoil-connected vortex,  $\Phi_C$  – the potential of the velocity field induced by a unitary airfoil-connected vortex, defined as

$$(3.5) \quad \Phi_C = \operatorname{Re} \left[ \frac{1}{2\pi i} \operatorname{Ln} \sinh \frac{z - z_C}{2} \right].$$

$\Phi_1, \Phi_2$  – additional  $y$ -periodic harmonic functions, their derivatives vanishing at infinity. The potential  $\Phi_P$  fulfils the imposed boundary conditions if

$$(3.6) \quad \text{and} \quad \frac{d}{dn} (\bar{u}_\infty x + \bar{v}_\infty y + \Phi_1) = \begin{cases} 0 & \text{on } \partial D_P, \\ u_W(y) & \text{on } \partial D_W, \end{cases}$$

$$\frac{d}{dn} \left( \frac{y}{4\pi} + \Phi_C + \Phi_2 \right) = 0 \quad \text{on } \partial D_P \cup \partial D_W.$$

Thus we obtain the following Neumann conditions for  $\Phi_1$  and  $\Phi_2$ :

$$(3.7) \quad \frac{d\Phi_1}{dn} = \begin{cases} -\bar{\mathbf{V}}_\infty \cdot \mathbf{n} & \text{on } \partial D_P, \\ u_W(y) - \bar{u}_\infty & \text{on } \partial D_W, \end{cases}$$

$$\frac{d\Phi_2}{dn} = -\frac{d\Phi_C}{dn} - \frac{n_y}{4\pi} \quad \text{on } \partial D_P \cup \partial D_W,$$

where  $\mathbf{n} = [n_x, n_y]$  is the internal normal vector on the boundary.

Assume that the functions  $\Phi_1$  and  $\Phi_2$  have been already determined. Then the differentiation of  $\Phi_P$  on the boundary yields

$$(3.8) \quad V_t(s) = \bar{\mathbf{V}}_\infty \cdot \mathbf{t} + \Gamma_P \left( \frac{t_y}{4\pi} + \frac{d\Phi_C}{ds} + \frac{d\Phi_2}{ds} \right),$$

where  $\mathbf{t} = [t_x, t_y]$  denotes the tangent vector on the boundary and  $s$  is the arc length coordinate. If we assume that the value  $s = 0$  corresponds to the

rear stagnation point then the condition  $V_t(0) = 0$  yields the circulation of the airfoil-connected vortex  $\Gamma_P$

$$(3.9) \quad \Gamma_P = \frac{\bar{\mathbf{V}}_\infty \cdot \mathbf{t} + \frac{d}{dt}\Phi_1}{\frac{1}{4\pi}t_y + \frac{d}{ds}(\Phi_C + \Phi_2)}.$$

Now we describe briefly the mathematical technique we apply to find the harmonic functions  $\Phi_1$  and  $\Phi_2$ . If we consider a  $y$ -periodic function  $\Phi$ , harmonic in the domain  $D$  and such that

$$\int_{\partial D} \frac{d\Phi(Q)}{dn_Q} ds_Q = 0 \quad \text{and} \quad \int_{\partial D} \frac{d\Phi(Q)}{ds_Q} ds_Q = 0$$

i.e. it is not a real or an imaginary part of any multivalued complex function, then the function  $\Phi$  is the only solution of the boundary integral equation (see [9] and [10])

$$(3.10) \quad \begin{aligned} \Phi(P) + \frac{1}{\pi} \int_{\partial D} \operatorname{Re} \left( \frac{1}{2} \coth \frac{z_Q - z_P}{2} \cdot n_Q \right) \Phi(Q) ds_Q \\ = \frac{1}{\pi} \int_{\partial D} \operatorname{Re} \left( \operatorname{Ln} \sinh \frac{z_Q - z_P}{2} \right) \frac{d\Phi(Q)}{dn_Q} ds_Q, \\ n_Q = (n_x + in_y)(s_Q). \end{aligned}$$

This is the Fredholm second kind integral equation. If the curvature of the boundary is finite, the kernel is bounded. This equation can be solved numerically using, for instance, the Boundary Element Method.

Having the boundary distribution of the function  $\Phi$ , we can calculate the vector field  $\mathbf{V} = \nabla\Phi$  using the following procedure. First we determine the boundary value of this field

$$V(s_P) = \left( \frac{d\Phi}{ds} - i \frac{d\Phi}{dn} \right) (s_P) \cdot t^*(s_P), \quad t^*(s_P) = (t_x - it_y)(s_P), \quad P \in \partial D.$$

Next we are able to calculate  $V(z)$  for any complex  $z = x + iy$  by means of the  $y$ -periodic Cauchy integral

$$(3.11) \quad V(z) = \frac{1}{4\pi i} \int_{\partial D} V(\zeta) \coth \frac{\zeta - z}{2} d\zeta.$$

It is important that the solution of the boundary integral equation defines the mapping

$$(3.12) \quad L : \frac{d\Phi}{dn} \rightarrow \frac{d\Phi}{ds}$$

i.e., in the hydrodynamic context, it transforms the normal velocity to the tangent one. This mapping is a unique, linear and continuous operator. We will use this operator in the next section while deriving an equation for the boundary vortex layer.

### 3.3. Construction of the complete velocity field

The full velocity of a viscous,  $y$ -periodic flow is expressed as

$$(3.13) \quad \mathbf{V} = \mathbf{V}_P + \mathbf{V}_O + \mathbf{V}_W + \mathbf{V}_A + \mathbf{V}_C + \mathbf{V}_V.$$

In (3.13) we denote

- $\mathbf{V}_P$  the velocity of the potential flow (previous section),
- $\mathbf{V}_O$  the velocity induced by old i.e. previously created PVBs,
- $\mathbf{V}_W$  the velocity induced by new, boundary PVBs,
- $\mathbf{V}_C$  the velocity induced by an additional, airfoil-connected vortex with the circulation  $\Gamma_C$ ,
- $\mathbf{V}_A$  an additional potential velocity field vanishing at infinity,
- $\mathbf{V}_V$  a uniform, vertical stream i.e.  $\mathbf{V}_V = [0, v_V]$ .

All the velocity components are  $y$ -periodic vector fields. In each time step the following unknowns should be calculated:

- 1) the circulations of new PVBs  $\{\gamma_1, \dots, \gamma_N\}$ ,
- 2) the circulation  $\Gamma_C$ ,
- 3) the vertical flow  $v_V$ ,
- 4) the potential velocity field  $V_A$ .

The role of all unknowns will be explained further on. In general, new PVBs and the velocity  $V_A$  are necessary to fulfil the boundary conditions for the velocity. Additional “free parameters”  $\Gamma_C$  and  $v_V$  are included in order to satisfy a condition at infinity and to ensure correctness of the pressure.

The velocity decomposition written in natural coordinates for boundary points on  $\partial D_W$  yields

$$(3.14) \quad \begin{aligned} V_P^t + V_A^t + V_C^t + V_O^t + V_W^t - v_V + v_{IN} &= 0, \\ V_A^n + V_O^n + V_W^n + V_C^t &= 0. \end{aligned}$$

We have taken into account that  $V_P^n = u_{IN}$ ,  $V_V^n = 0$  and  $V_V^t = -v_{IN}$ .

Analogously, for the points on the airfoil contour  $\partial D_P$  we obtain

$$(3.14') \quad \begin{aligned} V_P^t + V_A^t + V_O^t + V_W^t + V_C^t + V_V^t &= 0, \\ V_A^n + V_O^n + V_W^n + V_C^n + V_V^n &= 0. \end{aligned}$$

This time the equality  $V_P^n = 0$  has been used.

From (3.14), the normal velocity  $V_A^n$  can be expressed as

$$(3.15) \quad \begin{aligned} V_A^n &= -(V_O^n + V_W^n + V_C^n) && \text{on } \partial D_W, \\ V_A^n &= -(V_O^n + V_W^n + V_C^n + V_V^n) && \text{on } \partial D_P. \end{aligned}$$

The boundary operator  $L$  applied to  $V_A^n$  gives  $V_A^t$  expressed in terms of other velocity components. This results in the following equation

$$(3.16) \quad \begin{aligned} V_P^t + V_O^t + V_W^t + V_C^t - v_V + v_{IN} - L(V_O^n + V_W^n + V_C^n) &= 0 && \text{on } \partial D_W, \\ V_P^t + V_O^t + V_W^t - L(V_O^n + V_W^n + V_C^n + V_V^n) &= 0 && \text{on } \partial D_P. \end{aligned}$$

We call (3.16) *the equation of the boundary vortex layer* since the unknown here is the distribution of the vorticity (circulation) generated on the boundary. We approximate this vortex layer by a finite set of PVBs located on the boundary and inducing the velocity component  $V_W$ . The circulations  $\{\gamma_1, \dots, \gamma_N\}$  of these PVBs are to be determined. Since new PVBs are born always in the same positions, we can introduce two sets of functions  $\{T_i(s), i = 1, \dots, N\}, \{N_i(s), i = 1, \dots, N\}$ , which describe tangent and normal velocity distributions induced by the boundary PVBs with unitary circulations. Then the components of  $V_W$  can be written as follows

$$(3.17) \quad V_W^t = \sum_{i=1}^N \gamma_i T_i(s), \quad V_W^n = \sum_{i=1}^N \gamma_i N_i(s).$$

Equation (3.16) can be solved in the mean integral sense over a finite set of boundary segments. The division of the boundary lines into segments is quite natural – each boundary PVB overlaps a small part of the inlet line or the airfoil contour. In other words, the boundary is divided into  $N$  separate segments, each accompanied by an adjacent PVB. If we now substitute (3.17) to (3.16) and integrate the latter on each segment  $\sigma_j = [s_j, s_{j+1}]$  then the following system of linear equations will be obtained:

$$(3.18) \quad \begin{aligned} \sum_{i=1}^N \left[ \int_{\sigma_j} (T_i - LN_i)(s) ds \right] \cdot \gamma_i &= - \int_{\sigma_j} (V_P^t + V_O^t + V_C^t + v_{IN})(s) ds \\ &+ \int_{\sigma_j} L(V_O^n + V_C^n)(s) ds + v_V(s_{j+1} - s_j) && \text{for } \sigma_j \in \partial D_W, \\ \sum_{i=1}^N \left[ \int_{\sigma_j} (T_i - LN_i)(s) ds \right] \cdot \gamma_i &= - \int_{\sigma_j} (V_P^t + V_O^t + V_C^t + V_V^t)(s) ds \\ &+ \int_{\sigma_j} L(V_O^n + V_C^n + V_V^n)(s) ds && \text{for } \sigma_j \in \partial D_P. \end{aligned}$$

The system (3.18) consists of  $N = N_W + N_P$  equations. However, it is not closed since we have two additional unknowns  $\Gamma_C$  (hidden in  $\mathbf{V}_C$ ) and  $v_V$ . In order to obtain a solvable problem we have to formulate two equations more.

First we consider the behaviour of the velocity field at infinity. The following condition of asymptotic consistency of nonviscous (potential) flow  $\mathbf{V}_P$  and full, viscous flow  $\mathbf{V}$  is postulated

$$(3.19) \quad \lim_{x \rightarrow \infty} \mathbf{V} = \lim_{x \rightarrow \infty} \mathbf{V}_P \quad \Rightarrow \quad \lim_{x \rightarrow \infty} (\mathbf{V}_O + \mathbf{V}_W + \mathbf{W}_C + \mathbf{V}_V) = 0.$$

Taking into account the asymptotic formulas (3.2) the condition (3.19) implies that

$$(3.20) \quad \Gamma_O + \Gamma_W + \Gamma_C + 4\pi v_V = 0.$$

The velocity fields  $\mathbf{V}_P$  and  $\mathbf{V}$  are  $y$ -periodic, their circulations along the inlet line  $\partial D_W$  are equal and they are asymptotically consistent at infinity. Then, from the Stokes theorem, one concludes that the total charge of the vorticity in the flow is equal to  $\Gamma_P$ . This means, in particular, that the total amount of vorticity in the flow is fixed in time. This conclusion is important for further considerations concerning the pressure condition (1.4). It should be also noticed that total vorticity charge is not identical to total charge of the circulation of PVBs. The reason is that the vortex cores of PVBs have finite dimensions, and some of them protrude partly from the computational domain.

Now we focus on the problem of the pressure correctness. In order to obtain physically meaningful pressure field, the total vorticity production on each boundary line must be equal to zero. Since the total charge of the vorticity within the flow is fixed due to the asymptotic consistency condition (3.19), it suffices to consider the vorticity generation process only on one of the boundary lines – it is more convenient to choose  $\partial D_P$ .

The amount of the vorticity created on the airfoil contour in one time step is defined as the difference between the contribution of new PVBs located on this contour and the vorticity charge carried by these PVBs which have left the computational domain in the previous time step by penetrating the interior of the airfoil. More precisely, the flux of the vorticity through the airfoil contour emerges for two reasons:

A) some PVBs protruding from the computational domain into the airfoil interior move to different positions,

B) some PVBs (in particular those located closely to the airfoil contour) can jump randomly out of the computational domain – they are eliminated.

Both types of the events mentioned above give rise to the vorticity flux across  $\partial D_P$ . However, the direct calculation of this flux (especially due to events of A type) is a rather strenuous problem. Fortunately, we have a very convenient indicator of the vorticity flux – the circulation of the velocity on the airfoil contour. At the beginning of each time step (i.e. before the PVBs' movement), the

boundary conditions are satisfied and the velocity circulation on  $\partial D_P$  is exactly zero. As a result of PVBs' motion, the boundary distribution of the velocity is slightly perturbed – its circulation on  $\partial D_P$  is, in general, different from zero. This variation is related directly to the amount of vorticity which left the flow domain due to PVBs' motion. This amount should be balanced by the contribution of new PVBs generated on  $\partial D_P$  at the beginning of the next time step. The mathematical expression for this balance is the following

$$(3.21) \quad \Omega_W^{n+1}(\partial D_P) = \Gamma_P + \Gamma_C^n + \overline{\Omega}_O^n(D_P) + \Gamma_{\text{OUT}}^n(\partial D_P).$$

In (3.21) we have used the following notation:

$\Omega_W^{n+1}(\partial D_P)$  – the contribution of new PVBs (i.e. created at the beginning of the  $(n+1)$ -th time step) on  $\partial D_P$ ,

$\overline{\Omega}_O^n(D_P)$  – the amount of vorticity carried by old PVBs, which sticks out from the computational domain or, equivalently, is inside the airfoil  $D_P$ ,

$\Gamma_{\text{OUT}}^n(\partial D_P)$  – the sum of circulations of PVBs removed from the computational domain because they have penetrated into  $D_P$ .

Now, the following equality holds

$$(3.22) \quad \Omega_W^{n+1}(\partial D_P) = \Gamma_W^{n+1}(\partial D_P) - \overline{\Omega}_W^{n+1}(D_P),$$

where  $\Gamma_W^{n+1}$  denotes the sum of circulations of new PVBs on  $\partial D_P$ , while  $\overline{\Omega}_W^{n+1}(D_P)$  denotes the amount of vorticity carried by these PVBs, but sticking out from the flow domain into  $D_P$ .

From (3.21) and (3.22) we derive the equation

$$(3.23) \quad \Gamma_W^{n+1}(\partial D_P) = \Gamma_P + \Gamma_C^n + \Gamma_{\text{OUT}}^n(\partial D_P) + \overline{\Omega}_O^n(D_P) + \overline{\Omega}_W^{n+1}(D_P).$$

The velocity field  $\mathbf{V}$  fulfils the boundary conditions at the beginning of the  $(n+1)$ -th time step. Thus its circulation along  $\partial D_P$  is equal to zero, which implies that

$$(3.24) \quad \Gamma_P + \Gamma_C^{n+1} + \overline{\Omega}_O^n(D_P) + \overline{\Omega}_W^{n+1}(D_P) = 0.$$

The last equation allows for eliminating troublesome quantities  $\overline{\Omega}_W^{n+1}(D_P)$  and  $\overline{\Omega}_O^n(D_P)$ . Finally we obtain the equation involving only the circulations

$$(3.25) \quad \Gamma_W^{n+1}(\partial D_P) = \Gamma_{\text{OUT}}^n(\partial D_P) - (\Gamma_C^{n+1} - \Gamma_C^n).$$

Equations (3.20) and (3.25) supplement the system (3.18) giving together a solvable algebraic problem. However, it is interesting to show that Eq.(3.20) can be replaced by the other one, which is, in a certain sense, symmetric to Eq.(3.25).

If we subtract Eq. (3.20) written for the  $n$ -th time step from the same equation but written for the next,  $(n+1)$ -th step, then the result will be as follows:

$$(3.26) \quad \Gamma_O^{n+1} - \Gamma_O^n + \Gamma_W^{n+1} - \Gamma_W^n + \Gamma_C^{n+1} - \Gamma_C^n + 4\pi(v_V^{n+1} - v_V^n) = 0.$$

Now, from Eq. (3.25) we have

$$(3.27) \quad \Gamma_C^{n+1} - \Gamma_C^n = \Gamma_{\text{OUT}}^n(\partial D_P) - \Gamma_W^{n+1}(\partial D_P).$$

The substitution of (3.27) to (3.26) yields

$$(3.28) \quad \Gamma_O^{n+1} - \Gamma_O^n + \Gamma_W^{n+1} - \Gamma_W^n + \Gamma_{\text{OUT}}^n(\partial D_P) - \Gamma_W^{n+1}(\partial D_P) + 4\pi(v_V^{n+1} - v_V^n) = 0.$$

Writing the balance of the total charge of circulations of PVBs

$$(3.29) \quad \Gamma_O^{n+1} = \Gamma_O^n + \Gamma_W^n(\partial D_W) + \Gamma_W^n(\partial D_P) - \Gamma_{\text{OUT}}^n(\partial D_P) - \Gamma_{\text{OUT}}^n(\partial D_W)$$

we are able to eliminate  $\Gamma_O^{n+1}$  from (3.28). Moreover, the following equality holds

$$(3.30) \quad \Gamma_W^{n+1} = \Gamma_W^{n+1}(\partial D_P) + \Gamma_W^{n+1}(\partial D_W).$$

After substitution of (3.29) and (3.30) to (3.26) most of the terms cancel and we end up with the following, simple condition

$$(3.31) \quad \Gamma_W^{n+1}(\partial D_W) = \Gamma_{\text{OUT}}^n(\partial D_W) - 4\pi(v_V^{n+1} - v_V^n).$$

Summarising, the linear, algebraic system (3.18) can be completed by the pair of additional equations, which read

$$(3.32) \quad \begin{aligned} \sum_{i=1}^{N_P} \gamma_i^{n+1} &= \Gamma_{\text{OUT}}^n(\partial D_P) - (\Gamma_C^{n+1} - \Gamma_C^n), \\ \sum_{i=N_P+1}^{N_P+N_W} \gamma_i^{n+1} &= \Gamma_{\text{OUT}}^n(\partial D_W) - 4\pi(v_V^{n+1} - v_V^n). \end{aligned}$$

These equations are remarkably symmetrical. The first one describes the variation of the airfoil-connected vortex and involves the information concerning only the airfoil contour. The second equation describes the variation of the additional, vertical stream and involves the information concerning only the inlet line. The vortex and the vertical stream provide the mechanism for controlling the vorticity production on the airfoil and on the inlet line, respectively, which in turn ensures physical correctness of the pressure field.

### 3.4. Summary of the computational algorithm

We summarise briefly main steps of the numerical method. The calculation of each step of the flow evolution begins with the computation of the right-hand sides of the system (3.18). Then the linear equations (3.18) coupled with the pair of Eqs.(3.32) are solved. As a result, the circulations of new PVBs, the airfoil-connected circulation  $\Gamma_C$  and the vertical stream velocity  $v_V$  for the new time step are determined. Next the boundary distribution of  $V_A^n$  is evaluated from (3.15). The solution of the boundary integral equation yields the value of the harmonic potential  $\Phi_A$  and, after differentiation, the tangent velocity  $V_A^t$ . This way the complete velocity  $\mathbf{V}_A$  on the boundary is known and can be reconstructed in the flow domain (in particular in PVBs centres) via  $y$ -periodic Cauchy integral. Other components of the velocity field can be calculated directly from the induction formulas (1.4) ( $\mathbf{V}_O$ ,  $\mathbf{V}_W$  and  $\mathbf{V}_C$ ) or are determined in advance ( $\mathbf{V}_P$ ) and interpolated to PVB centres from nodes of an auxiliary grid.

The key problem is the computational efficiency. Actually direct application of the induction formulas for all PVBs leads to enormous computational cost excluding the possibility to perform computations on widely available, small computers. A natural way to overcome this difficulty is to calculate the induced velocity only in the grid points and then interpolate it. However, two problems appear immediately. First, the interpolation of velocity smooths out fine, local variations, which can remove important details of the flow pattern. Secondly, the velocity interpolation should be divergence-free. To avoid these problems we applied a hybrid approach – the interaction between close PVBs is calculated from exact formulas (3.1), while distant induction is determined via an interpolation. The interpolating algorithm is based on the fact that the velocity induced by a PVB is potential outside the vortex core. Thus we can calculate the complex potential function of this velocity in grid points and then interpolate it in grid cells by complex polynomials to obtain, after differentiation, a divergence-free approximation of the velocity. This method has an obvious disadvantage – the approximate velocity field is not continuous on the cell sides. In other words, the approximation of the velocity is divergence-free only in a weak sense. This difficulty can be partly cured by using more complicated, Hermitean interpolation algorithms.

Now the problem of initial condition will be considered shortly. While dealing with external flows we have generally two possibilities:

- 1) sudden “switching on” of the viscosity, or
- 2) continuous acceleration from the state of rest.

In the first case the viscosity suddenly appears in an ideal liquid flow, which causes first generation of the vortex particles to be created. In the second one, the flow is viscous from the very beginning and is progressively accelerated by changing the free stream velocity. Both methods have certain good and weak points. The first one is not physical and, which is much worse, the primary generated vortex particles are charged with relatively large circulations – they can induce locally a velocity comparable in magnitude with the free stream velocity. The sec-

ond method is more natural but during acceleration one has to deal with a more complicated version of the pressure problem. If the acceleration is performed by rescaling the “ideal-flow background”  $\mathbf{V}_P$ , then the total amount of the vorticity in the flow field changes in time and this fact must be taken into account while formulating the pressure correctness condition. Our choice is the first method supplemented by the concept of vortex particle splitting. The idea is to limit the permissible value of the velocity induced by a single PVB to small fraction of the free-stream velocity, say to several percent. This means that every PVB born on the boundary, which is too “strong”, is immediately split into a number of “weaker” PVBs moving separately (their trajectories diverge since they perform separate random walks). Although this procedure brings rapid increase of the number of PVBs, in the computations it has also significant advantages. It provides fast saturation of the computational domain with the vortex particles which is desirable when one is interested mainly in the final, quasi-stationary state, not a transient one.

Another important problem is associated with artificial or numerical viscosity. Although the vortex methods are, at least in principle, grid-free, the built-in vorticity discretization produces inevitably an effect of additional, nonphysical diffusion rate. This phenomenon is connected with two parameters of vortex particles, theoretically infinitesimal, but in practice always finite – a radius and a circulation charge. It is quite obvious that the radii of the PVBs vortex cores should be as small as possible – otherwise the method would be unable to resolve fine-scale details of the vorticity and velocity fields. Large PVBs mean that the flow is too organised spatially – relatively large portions of fluid are in regular (“laminar”) movement. In the language of modern dynamical system theory, the number of degrees of freedom of such flow is too small – the corresponding, effective “viscosity” is larger than that assumed in the random walk process. Similar effect is obtained when the vortex particles are too “strong”. Regions of weak vorticity cannot be reproduced properly, the vorticity gradients are exaggerated and strong, local variations of the induced velocity make PVBs to spread rapidly in all directions like in a diffusion process. It should be emphasised that the above description is only a simple heuristics – no systematic investigation of the artificial viscosity in vortex methods is known to the authors. The practical experience says that the limit of the induced velocity on the level of several percent is sufficient in a sense, that further splitting of PVBs does not make any visible effects on the velocity and vorticity field. Nevertheless, the “real” Reynolds number obtained in our simulations is surely lower than the “theoretical” one resulting from the assumed value of the viscosity.

#### 4. Results of numerical computations

The general data chosen in sample calculations are the following:

- The inlet line  $\partial D_W$  is divided uniformly into 120 segments while the airfoil

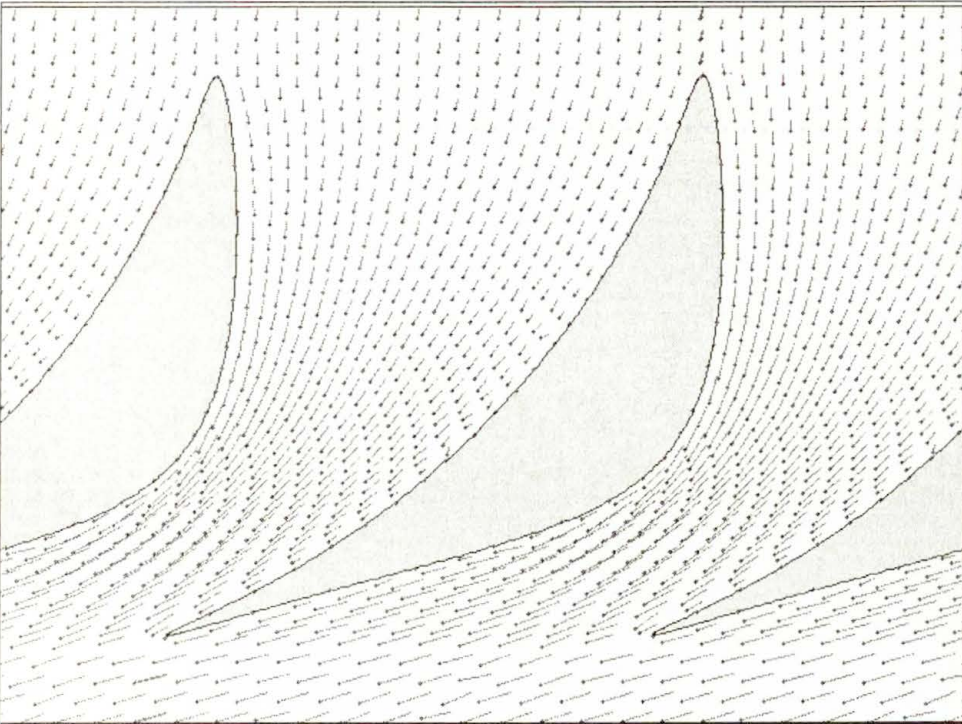
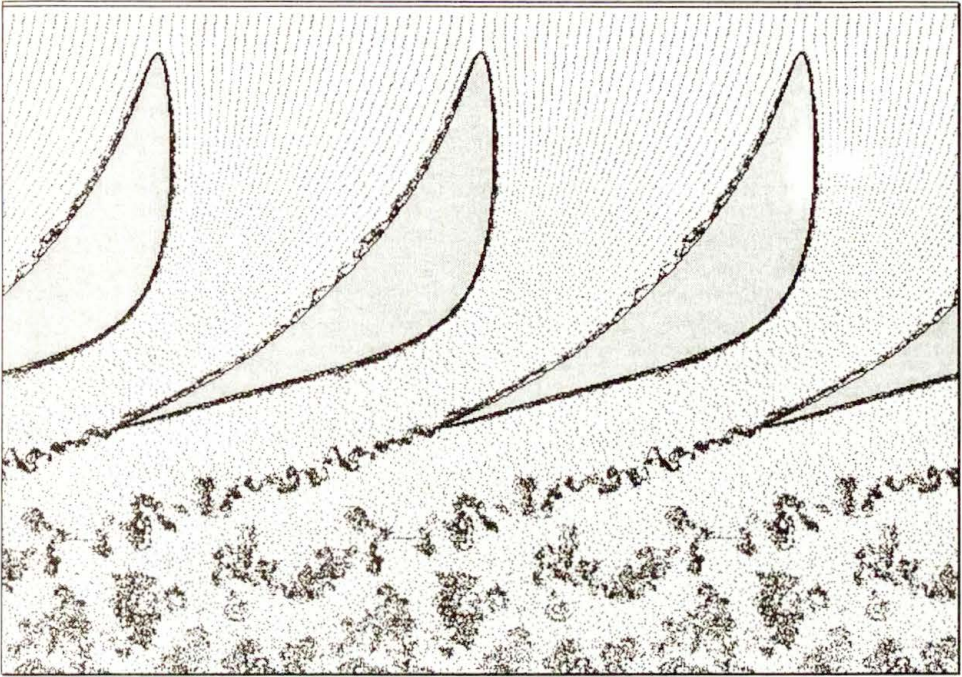


FIG. 2. The PVBs and instantaneous velocity field for  $t = 12.0$  (case I).

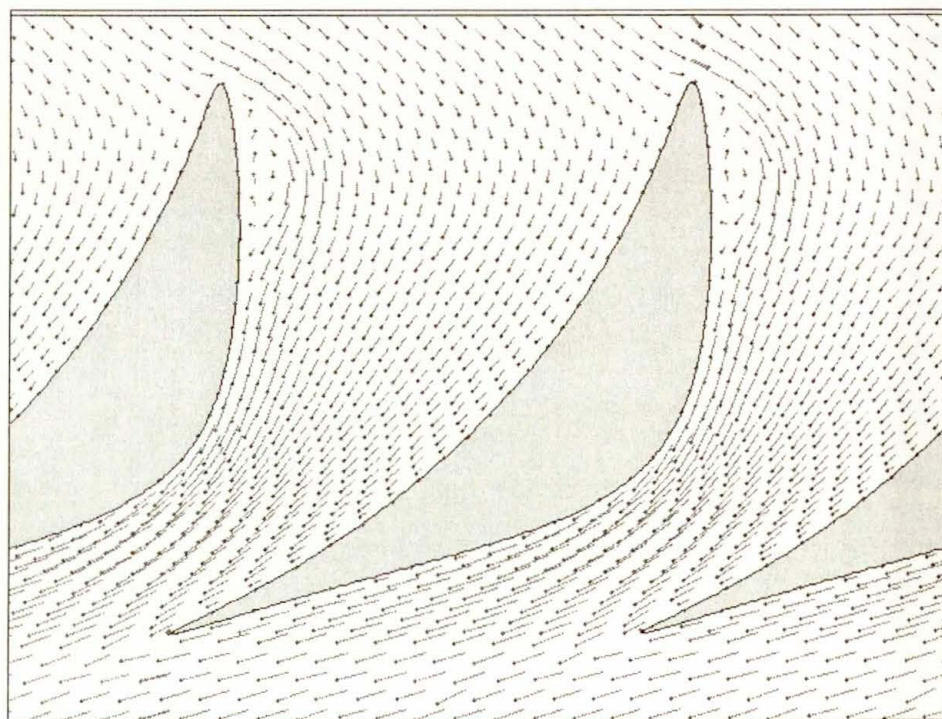
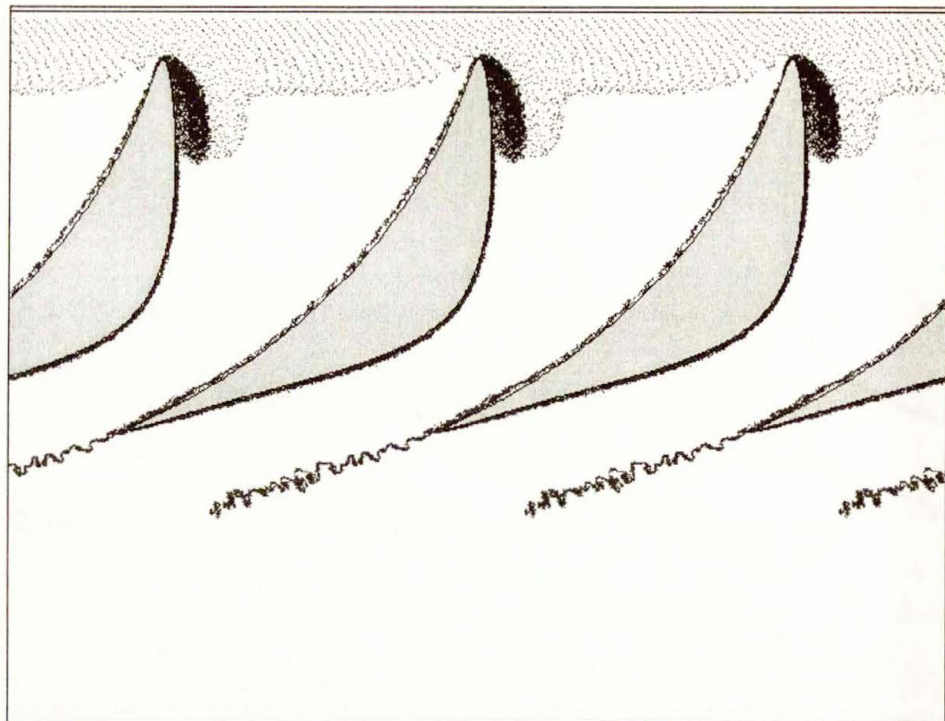


FIG. 3 a. The PVBs and instantaneous velocity field at  $t = 2.0$  (case II).

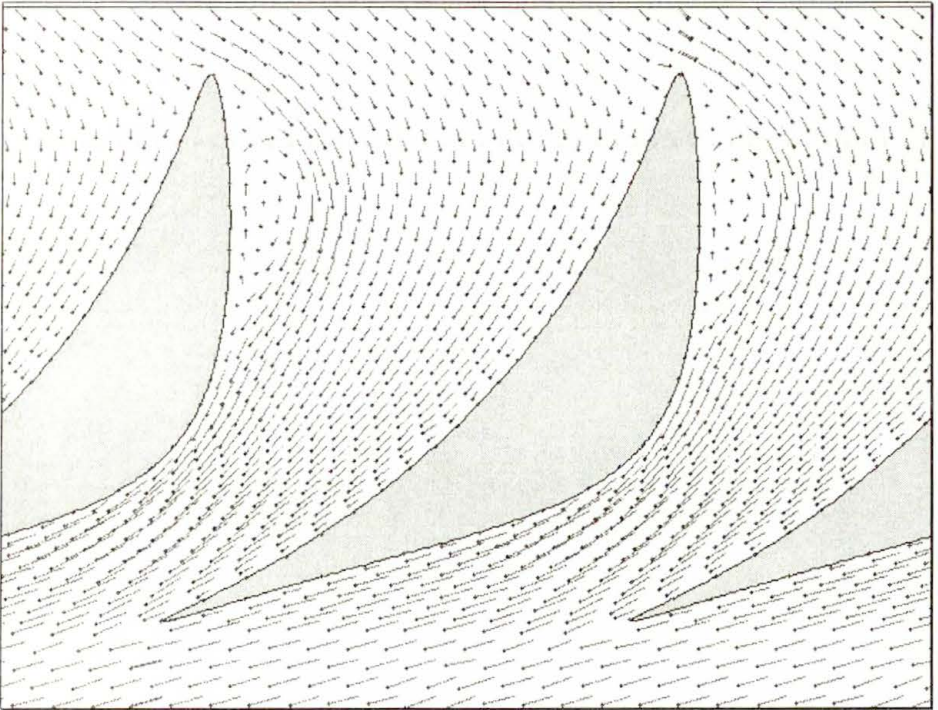
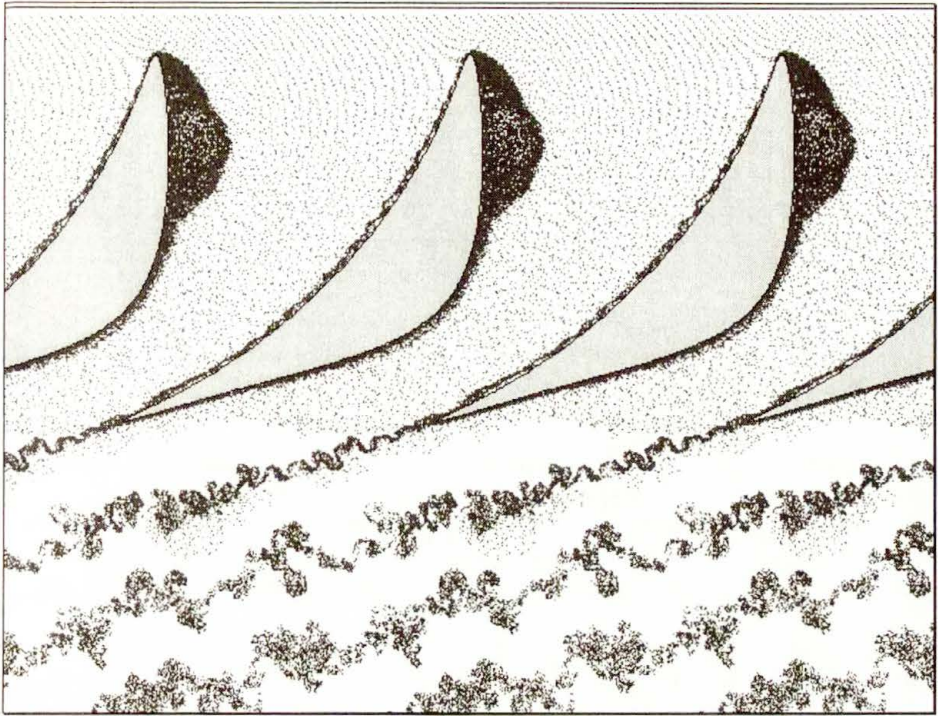


FIG. 3 b. The PVBs and instantaneous velocity field at  $t = 6.0$  (case II).

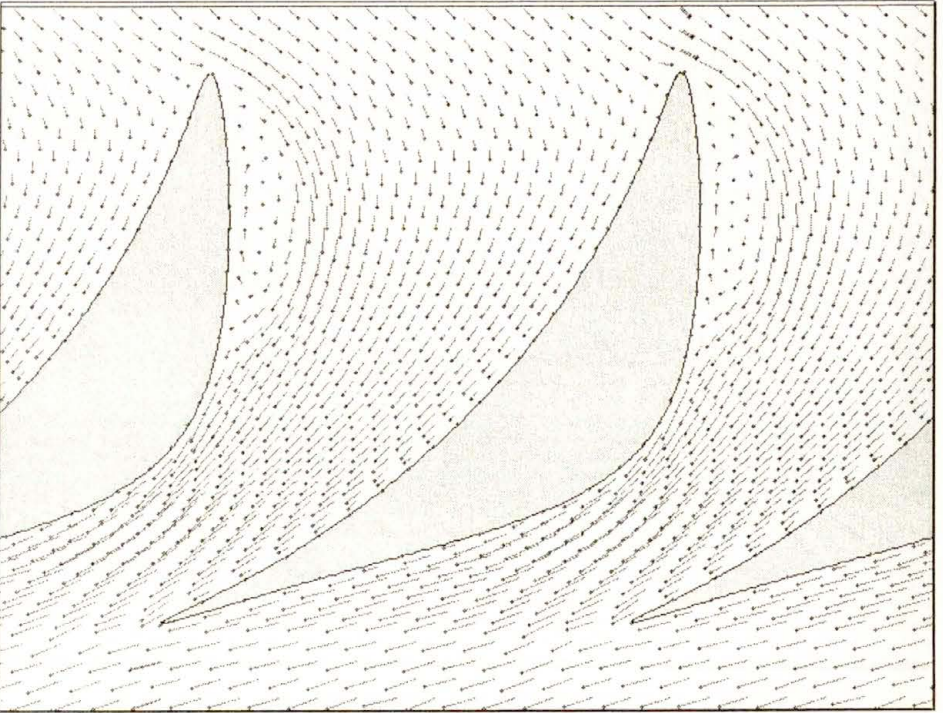


FIG. 3 c. The PVBs and instantaneous velocity field at  $t = 12.0$  (case II).

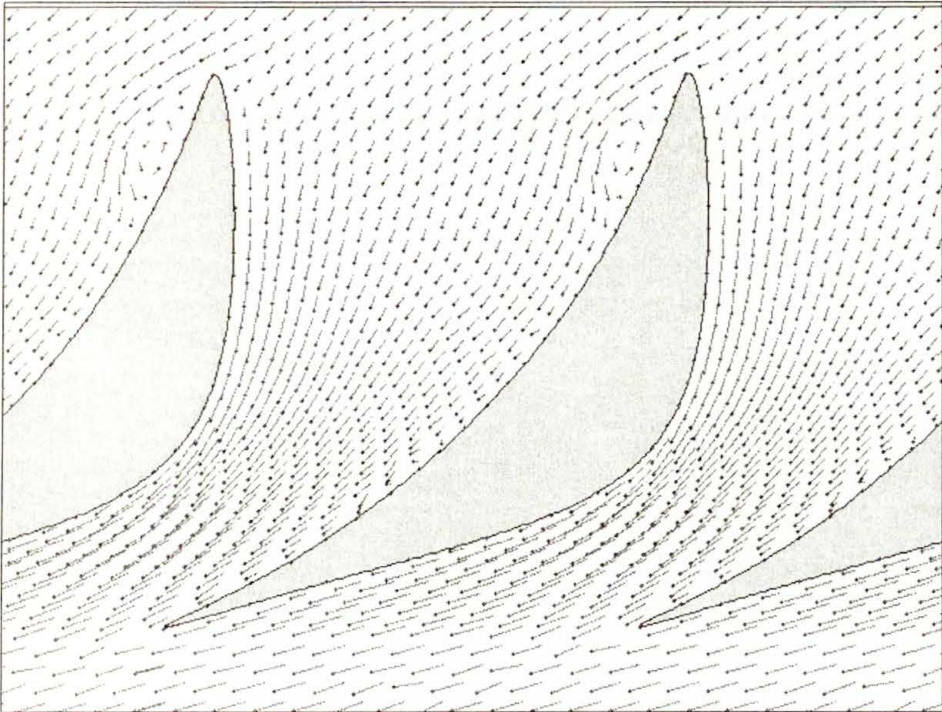
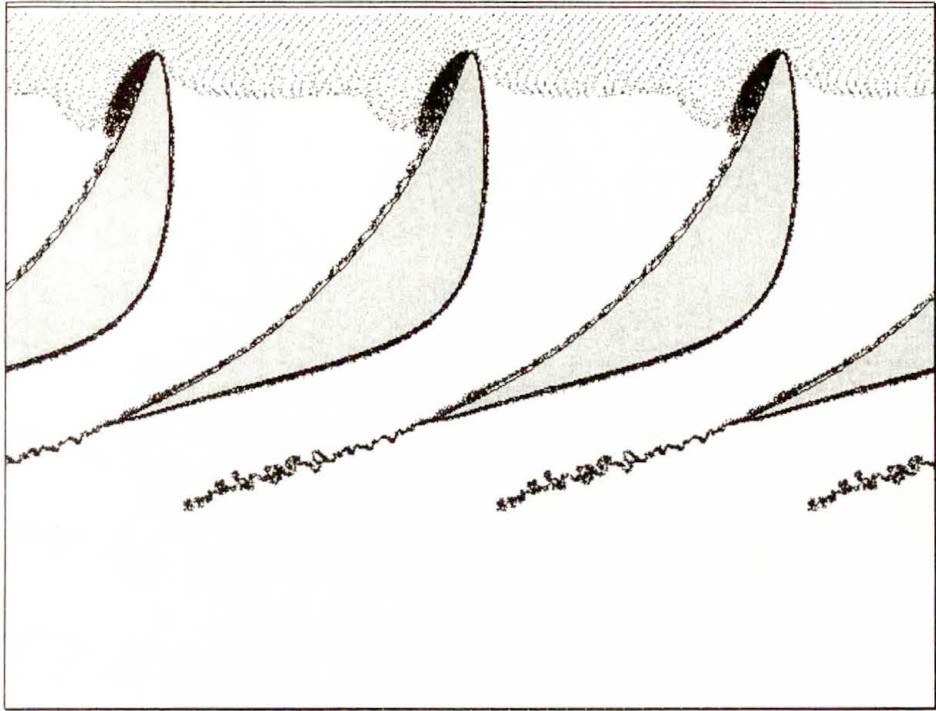


FIG. 4 a. The PVBs and instantaneous velocity field at  $t = 2.0$  (case III).

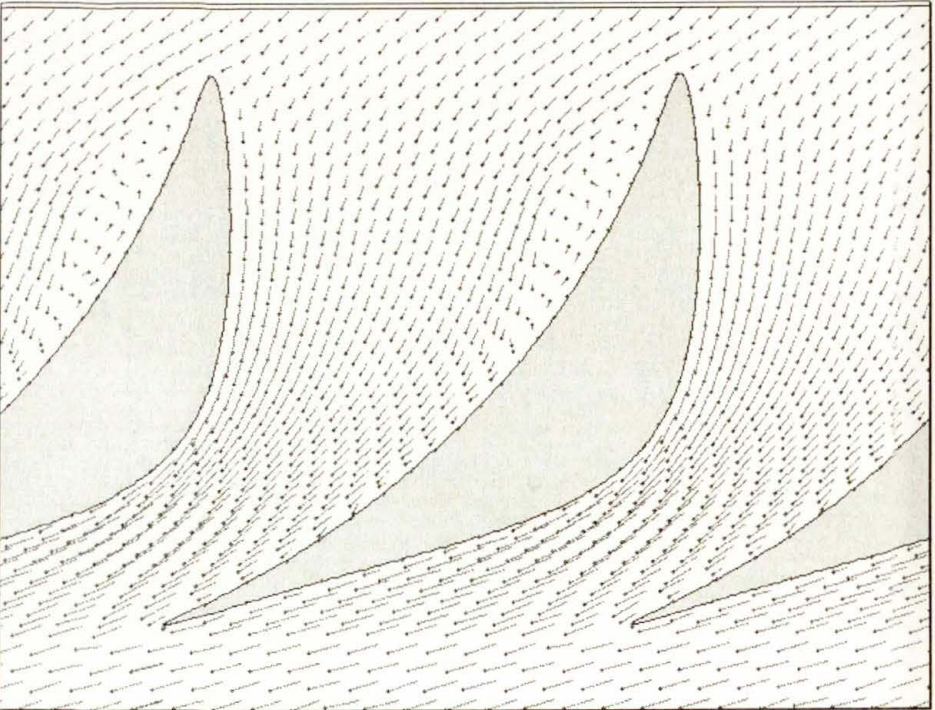
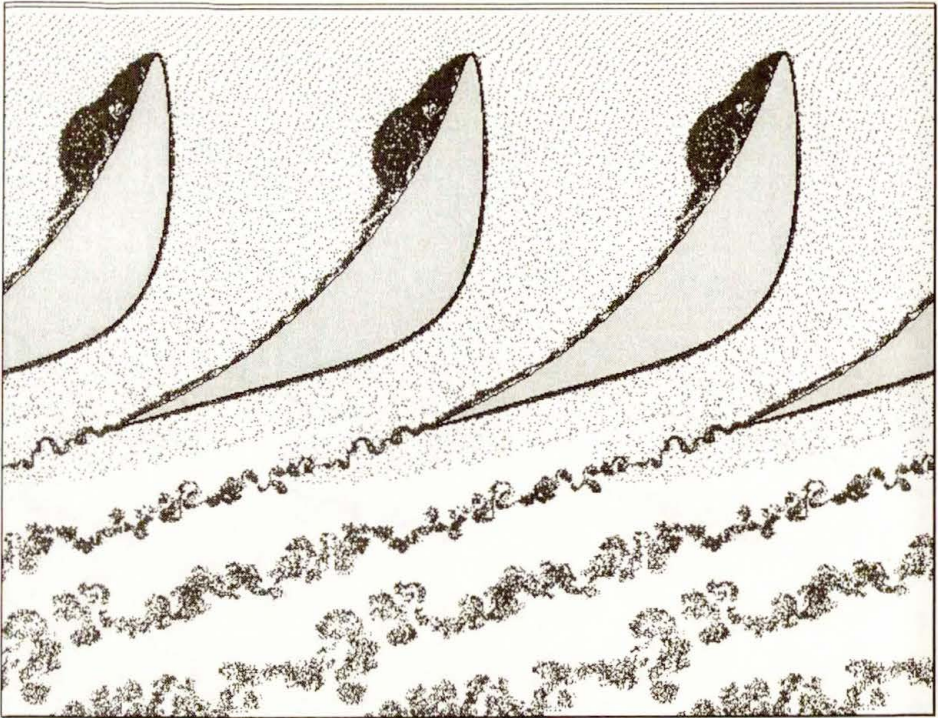


FIG. 4 b. The PVBs and instantaneous velocity field at  $t = 6.0$  (case I).

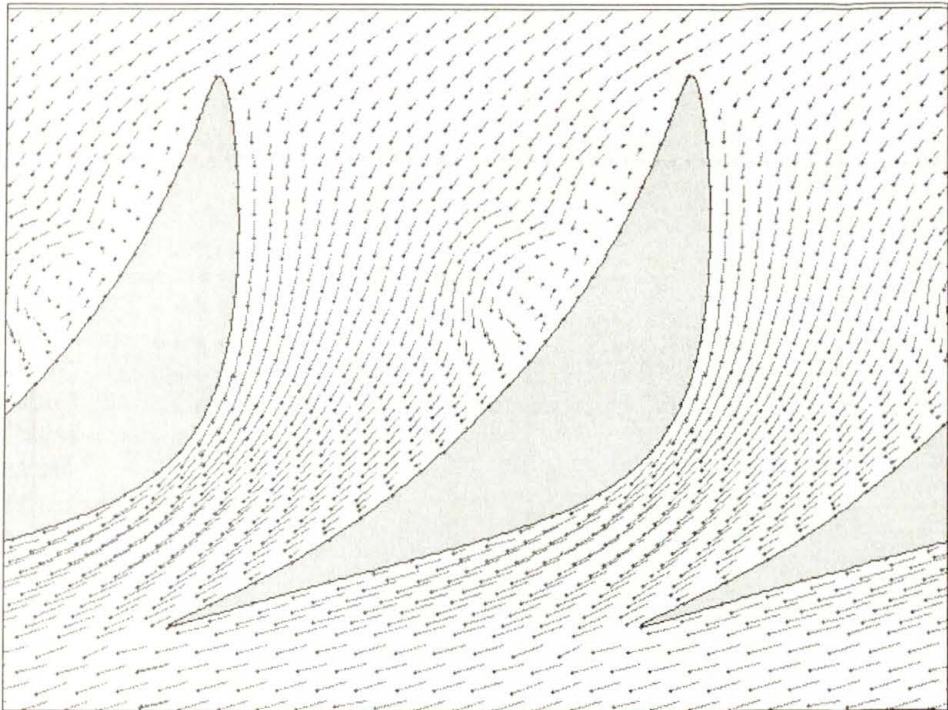
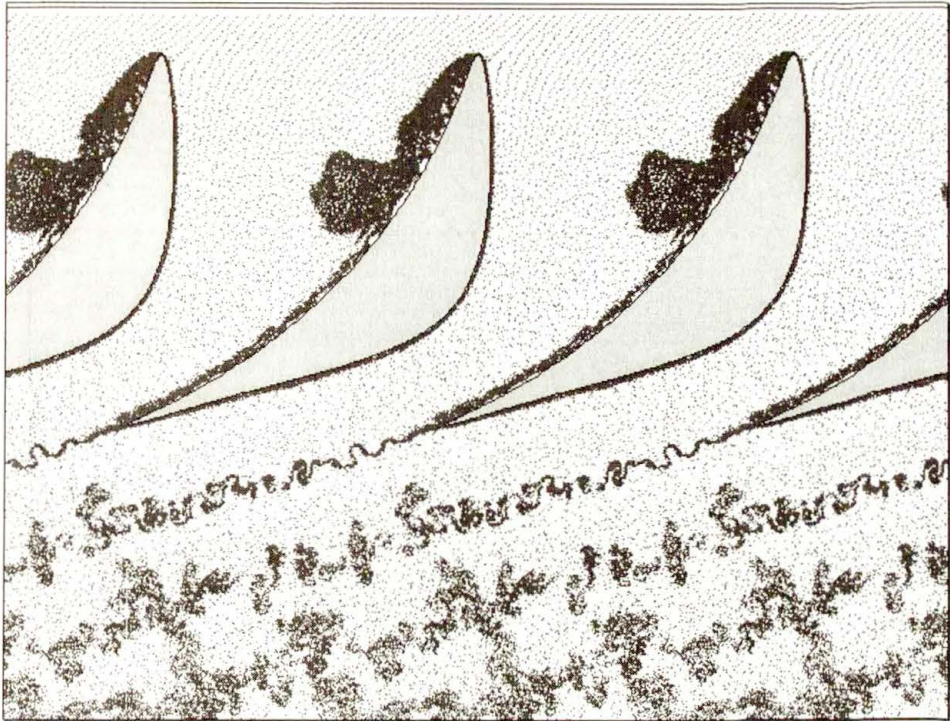
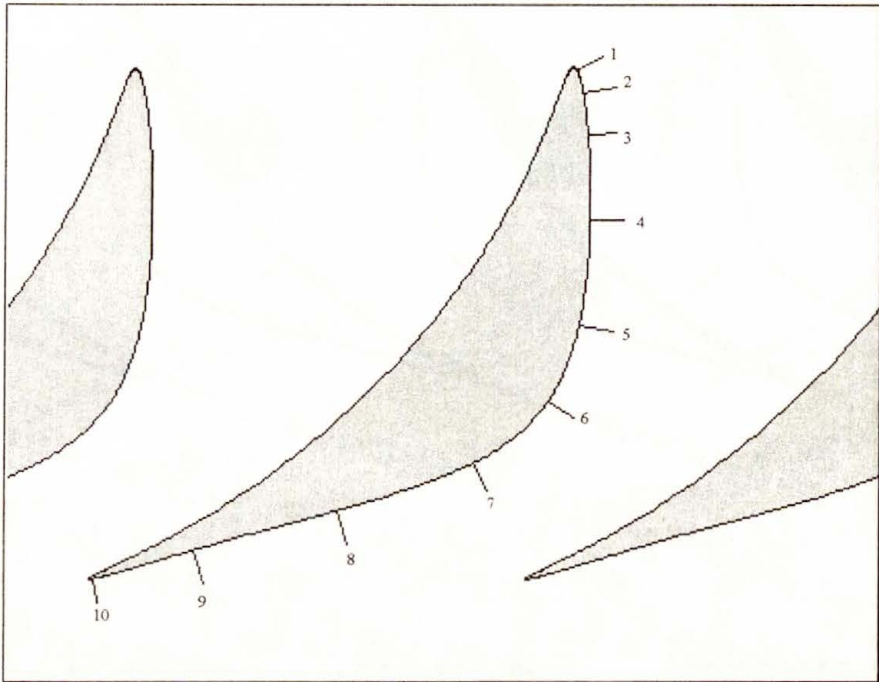


FIG. 4 c. The PVBs and instantaneous velocity field at  $t = 12.0$  (case III).

a)



b)

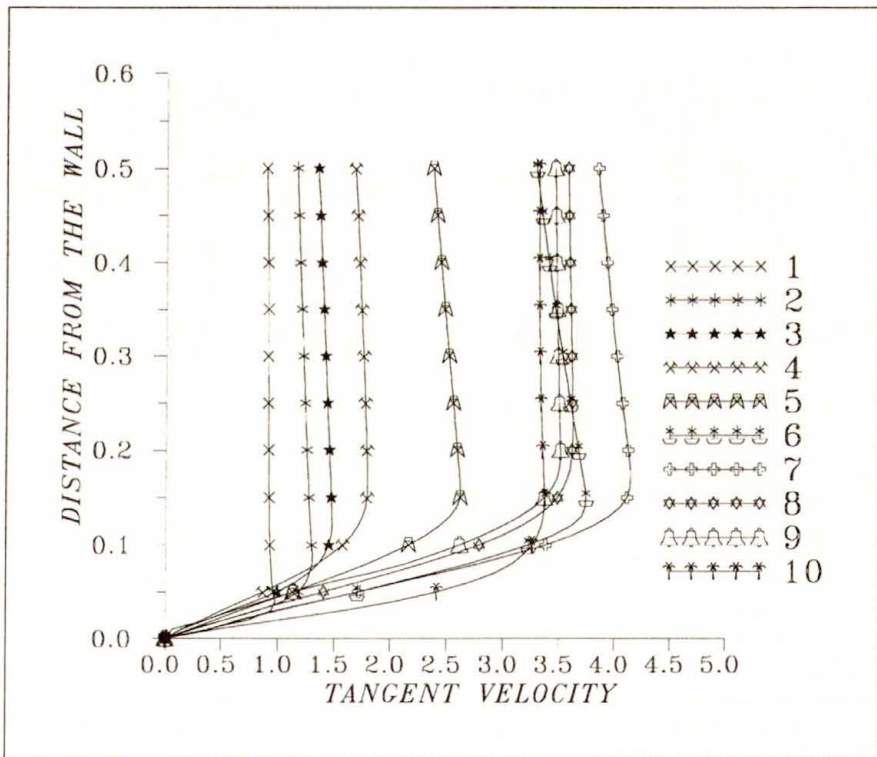


FIG. 5. The averaged boundary layer velocity field distribution calculated at indicated positions.

contour  $\partial D_P$  into 520 segments. The dimension of the algebraic system connected with the boundary integral equation is 640;

- Each PVB of next generation is adjacent to four subsequent segments, hence  $N_W = 30$  and  $N_P = 130$ ;
- The inlet line velocity distribution is uniform and fixed in time;
- Reynolds number calculated on the basis of a characteristic length (the chord of the airfoil), the assumed viscosity and the value of the inlet velocity is approximately  $10^5$ ;
- Time step is fixed ( $\Delta t = 0.05$ ) and the Ito equations are solved by the Euler integration scheme.

Three cases of flow with different inlet conditions are presented:

- 1) low angle of incidence flow  $u_W = 1.0, v_W = -0.2$ ,
- 2) high positive angle of incidence flow  $u_W = 1.0, v_W = 1.0$ ,
- 3) high negative angle of incidence flow  $u_W = 1.0, v_W = -1.0$ .

The instantaneous positions of PVBs and the velocity field calculated in the first case are presented in Fig. 2. Analogous results for the second case are shown in Fig. 3 and, for the third case, in Fig. 4. In all cases the growth of vortical structures in wakes is apparent. In the cases of a high angle of attack, the closed separation regions appear and evolve in time. Figure 5 a shows locations of the sections perpendicular to the airfoil contour, where the averaged velocity distributions of the boundary layer were calculated in the first case. The computed velocity profiles are shown in Fig. 5 b.

## 5. Concluding remarks

The stochastic vortex method proposed above seems to be capable of reproducing characteristic features of nonstationary viscous flows in spatially periodic domains. The effect of local separation has been captured and the velocity distribution in the boundary layer exhibits reasonable qualitative features. The boundary layer thickness is, however, much exaggerated. The reason is that the characteristic dimension of PVBs is of the same order (or even greater) as this thickness at the considered Reynolds number. Obviously, flow details of such a spatial scale cannot be properly resolved. It can be expected that significant improvement would be achieved if the number of PVBs were much greater and their vortex cores were much finer. Also some other types of vortex particles (like  $y$ -periodic vortex sheets) could be applied in the vicinity of the airfoil contours.

Although only stationary inlet velocity distributions are considered here, it is not difficult to generalise the method to nonstationary or even random inlet conditions. Such generalisation would allow us to perform approximate calculations of multi-stage cascade flows: the velocity behind a row of blades and relative movement of the rows would yield the nonstationary inlet conditions for the next row. Randomness of the inlet conditions can be applied to simulate turbulent fluctuations in an incoming stream.

## References

1. A.J. CHORIN, *Numerical study of slightly viscous flow*, J. Fluid Mech., **53**, p. 785, 1973.
2. A. STYCZEK, *The vortex-blobs method of simulating the viscous liquid motion*, Arch. Mech. Engng., **34**, p. 225–241, 1987.
3. J. SZUMBARSKI, *The application of the random vortex method for the nonstationary flow in the cascade of airfoils* [in Polish], Ph.D. Thesis, Warsaw University of Technology, 1993.
4. B. MODRZEWSKA-PONIZY and A. STYCZEK, *Modelling a plane jet via the vortex-blobs method*, Arch. Mech. Engng., **39**, 1991.
5. J. BLAZEWICZ and A. STYCZEK, *The stochastic simulation of a viscous flow past an airfoil*, J. Theor. Appl. Mech., **31**, part 1 in No. 1, part 2 in No. 4, 1993.
6. A. STYCZEK and P. WALD, *Fast and efficient vortex blobs simulation of the flow past the circular cylinder*, Arch. Mech. Engng., **42**, p. 281–298, 1995.
7. M.D. GUNZBURGER, J.S. PETERSON, *Finite-element method for the streamfunction-vorticity equations: boundary-condition treatment and multiply connected domains*, SIAM J. Sci. Stat. Comp., **9**, 4, p. 650–668, 1988.
8. V. GIRAULT and P. RAVIART, *Finite element methods for Navier–Stokes equations*, Springer Series in Computational Mathematics, Vol. 5, 1986.
9. T. CHMIELNIAK, *Foundations of the profiles and airfoil palisades* [in Polish], Ossolineum, Wrocław 1989.
10. J. SZUMBARSKI, *The method of the boundary integral equation for the potential flow inside the palisade of airfoils in a semi-infinite domain*, J. Theor. Appl. Mech., **31**, 2, 1993.

WARSAW UNIVERSITY OF TECHNOLOGY  
DEPARTMENT OF AERODYNAMICS  
e-mail: jasz@meil.pw.edu.pl

Received October 4, 1996.

## BRIEF NOTES

### Non-polynomial representations of orthotropic tensor functions in the three-dimensional case: an alternative approach

S. JEMIOŁO and J.J. TELEGA (WARSZAWA)

THE OBJECTIVE of this paper is to extend some of the results obtained in [1] to the three-dimensional case. Functional bases and generators for symmetric second-order orthotropic tensor functions are derived.

#### 1. Introduction

THE THEORY of representation of tensor functions has been developed for more than thirty years [2–5]. The results obtained within the framework of this theory yield general forms of isotropic [6–15] and anisotropic [16–22] tensor functions. Most complete results were obtained for scalar-valued, vector-valued, symmetric and skew-symmetric tensor-valued functions of the second order, dependent on vectors as well as symmetric and skew-symmetric tensors of the second order.

Theoretical foundations of the formulation of anisotropic constitutive relationships were laid, among others, in the books [23–26]. There the group theory and the theory of representation of tensor functions were exploited. Anisotropic materials constitute an important class of structural materials in many fields of engineering. Hence the need for further development of the constitutive theory, where the theory of representation of tensor functions plays an important role, cf. [3, 27–30].

The determination of a representation of a tensor function in the so-called canonical form reduces to finding irreducible sets of basic invariants and generators of this function. One distinguishes polynomial and non-polynomial representations of tensor functions [3, 23]. To find the polynomial representation of a tensor function it is sufficient to determine the relevant integrity basis. Once this basis is established, generators are obtained by a simple process of integration [23]. An integrity basis is said to be irreducible if none of its elements can be expressed as a polynomial in the remaining elements, cf. [23]. A set of invariants is said to constitute a functional basis, for given arguments and a symmetry group of the considered function, if any other invariant of the same arguments can be expressed as a scalar function of these invariants. A non-polynomial representation is irreducible if none of the generators can be expressed as a linear

combination of the remaining generators, with the coefficients being arbitrary functions of the functional basis. WANG [6–8], SMITH [9, 10] and BOEHLER [11] proved that in the general case a non-polynomial representation, if compared with the corresponding polynomial representation, contains less generators and invariants.

The aim of this note is the determination of the representation of a non-polynomial orthotropic scalar function as well as orthotropic, symmetric tensor-valued function of the second order. Our approach is alternative to that used by BOEHLER [18, 19]. Those functions depend on a finite number of symmetric, second order tensors. Thus we extend to the three-dimensional case the results presented in our earlier paper [1].

## 2. Formulation of the problem

Our aim is to determine the non-polynomial representations of the following functions

$$(1) \quad \begin{aligned} s &= f(\mathbf{A}_p; \mathbf{H}), & f: \underbrace{T_s \times \dots \times T_s}_{(P+1)\text{-times}} &\rightarrow R, \\ \mathbf{S} &= \mathbf{F}(\mathbf{A}_p; \mathbf{H}), & \mathbf{F}: \underbrace{T_s \times \dots \times T_s}_{(P+1)\text{-times}} &\rightarrow T_s, \end{aligned}$$

where  $\mathbf{A}_p$  are symmetric second order tensors,  $\mathbf{A}_p \in T_s$ ,  $T_s = \{\mathbf{A} \in T: \mathbf{A} = \mathbf{A}^T\}$ ,  $p = 1, \dots, p$  and  $T = E \otimes E$ ;  $\mathbf{A}^T$  stands for the transpose of a tensor  $\mathbf{A}$ . Here  $E$  is the three-dimensional Euclidean space and  $\mathbf{H}$  is a symmetric, positive-definite tensor of the second order. The tensor  $\mathbf{H}$  plays the role of a parametric tensor, i.e.  $\mathbf{H} = \text{const}$ . The function  $f$  is a scalar-valued function while  $\mathbf{F}$  is a symmetric, second order tensor function. Suppose that (1) are to be constitutive relationships. Then  $\mathbf{A}_p$  are causes,  $\mathbf{H}$  models the structure of a material while  $s$  and  $\mathbf{S}$  are responses or effects. Within the framework of the classical continuum mechanics, such relationships should be invariant with respect to the group of automorphisms of the space  $E$ , cf. [25]. In other words, they have to satisfy the so-called principle of isotropy of the physical space. Consequently, the functions appearing in (1) fulfil the following conditions:

$$(2) \quad \forall \mathbf{Q} \in O: \quad \begin{aligned} f(\mathbf{A}_p; \mathbf{H}) &= f(\mathbf{Q}\mathbf{A}_p\mathbf{Q}^T; \mathbf{Q}\mathbf{H}\mathbf{Q}^T), \\ \mathbf{Q}\mathbf{F}(\mathbf{A}_p; \mathbf{H})\mathbf{Q}^T &= \mathbf{F}(\mathbf{Q}\mathbf{A}_p\mathbf{Q}^T; \mathbf{Q}\mathbf{H}\mathbf{Q}^T), \end{aligned}$$

where  $O$  denotes the full orthogonal group, that is

$$(3) \quad O \equiv \{\mathbf{Q} \in T: \mathbf{Q}\mathbf{Q}^T = \mathbf{Q}^T\mathbf{Q} = \mathbf{I}\}.$$

Here  $\mathbf{I}$  stands for the identity tensor.

According to our assumption, the tensor  $\mathbf{H}$  has three distinct eigenvalues, say  $H_i$  ( $i = 1, 2, 3$ ). Thus we may write

$$(4) \quad \mathbf{H} = H_1 \mathbf{e}_1 \otimes \mathbf{e}_1 + H_2 \mathbf{e}_2 \otimes \mathbf{e}_2 + H_3 \mathbf{e}_3 \otimes \mathbf{e}_3, \quad H_1 \neq H_2 \neq H_3 \neq H_1,$$

where  $\mathbf{e}_i$  are unit eigenvectors of the tensor  $\mathbf{H}$ . We observe that the group of external symmetries of the tensor  $\mathbf{H}$ , given by

$$(5) \quad S \equiv \left\{ \mathbf{Q} \in O: \quad \mathbf{Q} \mathbf{H} \mathbf{Q}^T = \mathbf{H} \right\},$$

is the orthotropy group. Moreover, the eigenvectors of  $\mathbf{H}$  determine the so-called principal axes of orthotropy of a material. This statement becomes obvious if we compare (4) and (5) with the corresponding definitions given in the papers [3, 18–20, 25].

Let

$$(6) \quad \mathbf{M}_i = \mathbf{e}_i \otimes \mathbf{e}_i \quad (\text{no summation on } i = 1, 2, 3),$$

then we recover, by taking account of (4) and (6) in (1), provided that (2) is satisfied, the problem considered in the papers [18, 19].

From (2) and (5) it follows that

$$(7) \quad \begin{aligned} \forall \mathbf{Q} \in S: \quad & f(\mathbf{A}_p; \mathbf{H}) = f(\mathbf{Q} \mathbf{A}_p \mathbf{Q}^T; \mathbf{H}), \\ & \mathbf{Q} \mathbf{F}(\mathbf{A}_p; \mathbf{H}) \mathbf{Q}^T = \mathbf{F}(\mathbf{Q} \mathbf{A}_p \mathbf{Q}^T; \mathbf{H}). \end{aligned}$$

In other words, the functions  $f(\dots; \mathbf{H})$ ,  $\mathbf{F}(\dots; \mathbf{H})$  are orthotropic functions of the tensors  $\mathbf{A}_p$ .

### 3. Determination of the orthotropic functional basis

Since the tensor  $\mathbf{H}$  has three distinct eigenvalues, therefore in order to determine the functional basis for the scalar function (1)<sub>1</sub> we may exploit the results obtained by SMITH [10]. To this end it is sufficient to consider the case (2ii) studied by SMITH [10, pp.905–907]. The functional basis derived in this manner is presented in Table 1.

It can easily be proved that the representation of the scalar function (1)<sub>1</sub> depicted in Table 1 is equivalent to the results obtained by BOEHLER in [18, 19]. Boehler’s orthotropic functional basis is presented in Table 2.

Both functional bases are equivalent because:

$$(8) \quad \begin{aligned} \text{tr} \mathbf{A}_p &= \text{tr} \mathbf{M}_1 \mathbf{A}_p + \text{tr} \mathbf{M}_2 \mathbf{A}_p + \text{tr} \mathbf{M}_3 \mathbf{A}_p, \\ \text{tr} \mathbf{A}_p^2 &= \text{tr} \mathbf{M}_1 \mathbf{A}_p^2 + \text{tr} \mathbf{M}_2 \mathbf{A}_p^2 + \text{tr} \mathbf{M}_3 \mathbf{A}_p^2, \\ \text{tr} \mathbf{H}^a \mathbf{A}_p^b &= H_1^a \text{tr} \mathbf{M}_1 \mathbf{A}_p^b + H_2^a \text{tr} \mathbf{M}_2 \mathbf{A}_p^b + H_3^a \text{tr} \mathbf{M}_3 \mathbf{A}_p^b, \\ \text{tr} \mathbf{A}_p \mathbf{A}_q &= \text{tr} \mathbf{M}_1 \mathbf{A}_p \mathbf{A}_q + \text{tr} \mathbf{M}_2 \mathbf{A}_p \mathbf{A}_q + \text{tr} \mathbf{M}_3 \mathbf{A}_p \mathbf{A}_q, \\ \text{tr} \mathbf{H}^a \mathbf{A}_p \mathbf{A}_q &= H_1^a \text{tr} \mathbf{M}_1 \mathbf{A}_p \mathbf{A}_q + H_2^a \text{tr} \mathbf{M}_2 \mathbf{A}_p \mathbf{A}_q + H_3^a \text{tr} \mathbf{M}_3 \mathbf{A}_p \mathbf{A}_q, \quad a, b = 1, 2, \end{aligned}$$

where  $\text{tr}$  stands for the trace of a tensor; for instance  $\text{tr} \mathbf{A} \mathbf{B} = \text{tr}(\mathbf{A} \mathbf{B})$ , where  $\mathbf{A} \mathbf{B} = \text{tr}_{(2,3)} \mathbf{A} \otimes \mathbf{B}$ .

Table 1. Functional basis for the scalar function  $(1)_1$ .

Arguments	Basic invariants
$\mathbf{A}_p$	$\text{tr} \mathbf{A}_p, \text{tr} \mathbf{A}_p^2, \text{tr} \mathbf{A}_p^3, \text{tr} \mathbf{H} \mathbf{A}_p, \text{tr} \mathbf{H}^2 \mathbf{A}_p, \text{tr} \mathbf{H} \mathbf{A}_p^2, \text{tr} \mathbf{H}^2 \mathbf{A}_p^2$
$\mathbf{A}_p, \mathbf{A}_q$	$\text{tr} \mathbf{A}_p \mathbf{A}_q, \text{tr} \mathbf{A}_p^2 \mathbf{A}_q, \text{tr} \mathbf{A}_p \mathbf{A}_q^2, \text{tr} \mathbf{H} \mathbf{A}_p \mathbf{A}_q, \text{tr} \mathbf{H}^2 \mathbf{A}_p \mathbf{A}_q$
$\mathbf{A}_p, \mathbf{A}_q, \mathbf{A}_r$	$\text{tr} \mathbf{A}_p \mathbf{A}_q \mathbf{A}_r, \quad p, q, r = 1, \dots, P; \quad p < q < r$

Table 2. Orthotropic functional basis after BOEHLER [19].

Arguments	Basic invariants
$\mathbf{A}_p$	$\text{tr} \mathbf{M}_1 \mathbf{A}_p, \text{tr} \mathbf{M}_1 \mathbf{A}_p^2, \text{tr} \mathbf{A}_p^3, \text{tr} \mathbf{M}_2 \mathbf{A}_p, \text{tr} \mathbf{M}_2 \mathbf{A}_p^2, \text{tr} \mathbf{M}_3 \mathbf{A}_p, \text{tr} \mathbf{M}_3 \mathbf{A}_p^2$
$\mathbf{A}_p, \mathbf{A}_q$	$\text{tr} \mathbf{M}_1 \mathbf{A}_p \mathbf{A}_q, \text{tr} \mathbf{A}_p^2 \mathbf{A}_q, \text{tr} \mathbf{A}_p \mathbf{A}_q^2, \text{tr} \mathbf{M}_2 \mathbf{A}_p \mathbf{A}_q, \text{tr} \mathbf{M}_3 \mathbf{A}_p \mathbf{A}_q$
$\mathbf{A}_p, \mathbf{A}_q, \mathbf{A}_r$	$\text{tr} \mathbf{A}_p \mathbf{A}_q \mathbf{A}_r, \quad p, q, r = 1, \dots, P; \quad p < q < r$

#### 4. Determination of generators of an orthotropic tensor-valued function of the second order

In order to derive the representation of the function  $(1)_2$  under the condition  $(2)_2$ , we shall apply the method similar to that used in the papers [1, 13, 14, 31, 32]. This method is based on the idea primarily proposed in the paper by the second author [30]. First, we construct a scalar function, say  $g$ , defined by

$$(9) \quad g = \text{tr} \mathbf{F} \mathbf{C},$$

linear with respect to the second argument or  $\mathbf{C}$ . Here  $\mathbf{C}$  is a symmetric second order tensor while  $\mathbf{F}$  is the function  $(1)_2$ . The function  $g$  has the following form:

$$(10) \quad g(\mathbf{A}_p, \mathbf{C}; \mathbf{H}) = \tilde{g}(I_t, J_s) = \sum_{s=1}^S \phi(I_t) J_s,$$

where  $I_t$  are invariants listed in Table 1 whereas  $J_s$  are invariants linear in  $\mathbf{C}$ , see Table 3 below.

The canonical form of the tensor-valued function  $(1)_2$  is found from

$$(11) \quad \mathbf{F}(\mathbf{A}_p, \mathbf{H}) = \frac{1}{2} \left( \frac{\partial g}{\partial \mathbf{C}} + \frac{\partial g}{\partial \mathbf{C}^T} \right) = \frac{\partial g}{\partial \mathbf{C}} = \sum_{s=1}^S \phi_s(I_t) \frac{\partial J_s}{\partial \mathbf{C}} = \sum_{s=1}^S \bar{\phi}_s(I_t) \mathbf{G}_s.$$

The results of calculations are summarised in Table 4, where the generators  $\mathbf{G}_s$  are listed.

**Table 3. Invariants linear in C.**

Arguments	Invariants $J_s$
C	$\text{tr} C, \text{tr} H C, \text{tr} H^2 C$
C, $A_p$	$\text{tr} A_p C, \text{tr} A_p^2 C, \text{tr} H A_p C, \text{tr} H^2 A_p C$
C, $A_p, A_q$	$\text{tr} A_p A_q C, \quad p, q, r = 1, \dots, P; \quad p < q$

**Table 4. Generators of the function (1)<sub>2</sub>.**

Arguments	Generators
	$I, H, H^2$
$A_p$	$A_p, A_p^2, H A_p + A_p H, H^2 A_p + A_p H^2$
$A_p, A_q$	$A_p A_q + A_q A_p, \quad p, q = 1, \dots, P; \quad p < q$

The generators obtained in this way are equivalent to those derived by BOEHLER [19] and listed in Table 5. To corroborate this statement, it is sufficient to exploit the following identities:

$$\begin{aligned}
 (12) \quad I &= M_1 + M_2 + M_3, \\
 H^a &= H_1^a M_1 + H_2^a M_2 + H_3^a M_3, \quad a = 1, 2, \\
 2A_p &= M_1 A_p + M_1 A_p + M_2 A_p + M_2 A_p + M_3 A_p + M_3 A_p, \\
 H^a A_p + H^a A_p &= H_1^a (M_1 A_p + M_1 A_p) + H_2^a (M_2 A_p \\
 &\quad + M_2 A_p) + H_3^a (M_3 A_p + M_3 A_p).
 \end{aligned}$$

**Table 5. Boehler's [5] generators of the orthotropic tensor function.**

Arguments	Generators
	$M_1, M_2, M_3$
$A_p$	$M_1 A_p + M_1 A_p, M_2 A_p + M_2 A_p, M_3 A_p + M_3 A_p, A_p^2$
$A_p, A_q$	$A_p A_q + A_q A_p, \quad p, q = 1, \dots, P; \quad p < q$

## Acknowledgment

The authors were supported by the State Committee for Scientific Research (Poland) through the grant No. PB 0729/P4/94/06.

## References

1. S. JEMIOŁO and J.J. TELEGA, *An alternative approach to the representation of orthotropic tensor functions in the two-dimensional case*, Arch. Mech., **48**, 219–230, 1996.

2. J.J. TELEGA, *Theory of invariants: from Boole to the present. Tensor functions and concomitants* [in Polish], [in:] *Methods of Functional Analysis in Plasticity*, J.J. TELEGA [Ed.], Ossolineum, Wrocław 1981, 331–361.
3. J.P. BOEHLER [Ed.], *Applications of tensor functions in solid mechanics*, CISM Courses and Lectures No. 292, Springer-Verlag, Wien-New York 1987.
4. J. RYCHLEWSKI and J.M. ZHANG, *On representation of tensor functions: A review*, *Advances in Mech.*, **14**, 75–94, 1991.
5. S. JEMIOŁO and J.J. TELEGA, *Invariants and tensor functions: Fundamentals and some applications to solid and fluid mechanics*, 1st Conference on Application of Algebraic Invariants, Warszawa 26–27 XI 1994, Proc. Wyd. SGGW, 45–98, 1996.
6. C.C. WANG, *On representations for isotropic functions. Part I and II*, *Arch. Rat. Mech. Anal.*, **33**, 249–287, 1969.
7. C.C. WANG, *A new representation theorem for isotropic functions. Part I and II*, *Arch. Rat. Mech. Anal.*, **36**, 166–223, 1970.
8. C.C. WANG, *Corrigendum*, *Arch. Rat. Mech. Anal.*, **43**, 392–395, 1971.
9. G.F. SMITH, *On a fundamental error in two papers of C.C. Wang*, *Arch. Rat. Mech. Anal.*, **36**, 161–165, 1971.
10. G.F. SMITH, *On isotropic functions of symmetric tensors, skew-symmetric tensors and vectors*, *Int. J. Engng. Sci.*, **9**, 899–916, 1971.
11. J.P. BOEHLER, *On irreducible representations for isotropic scalar functions*, *ZAMM*, **57**, 323–327, 1977.
12. S. PENNISI and M. TROVATO, *On the irreducibility of Professor G.F. Smith's representations for isotropic functions*, *Int. J. Engng. Sci.*, **25**, 1059–1065, 1987.
13. J. KORSGAARD, *On the representation of two-dimensional isotropic functions*, *Int. J. Engng. Sci.*, **28**, 653–662, 1990.
14. J. KORSGAARD, *On the representation of symmetric tensor-valued isotropic functions*, *Int. J. Engng. Sci.*, **28**, 1331–1346, 1990.
15. Q.-S. ZHENG, *On the representations for isotropic vector-valued, symmetric tensor-valued and skew-symmetric tensor-valued functions*, *Int. J. Engng. Sci.*, **31**, 1013–1024, 1993.
16. J.E. ADKINS, *Symmetry relations for orthotropic and transversely isotropic materials*, *Arch. Rat. Mech. Anal.*, **4**, 193–213, 1960.
17. J.E. ADKINS, *Further symmetry relations for transversely isotropic materials*, *Arch. Rat. Mech. Anal.*, **5**, 263–274, 1960.
18. J.P. BOEHLER, *Lois de comportement anisotrope des milieux continus*, *J. Méc.*, **17**, 153–190, 1978.
19. J.P. BOEHLER, *A simple derivation of representations for non-polynomial constitutive equations in some cases of anisotropy*, *ZAMM*, **59**, 157–167, 1979.
20. I-SHIH LIU, *On representations of anisotropic invariants*, *Int. J. Engng. Sci.*, **20**, 1099–1109, 1982.
21. Q.-S. ZHENG, *On transversely isotropic, orthotropic and relative isotropic functions of symmetric tensors and vectors. Part I-V*, *Int. J. Engng. Sci.*, **31**, 1399–1453, 1993.
22. Q.-S. ZHENG, *Two-dimensional tensor function representation for all kinds of material symmetry*, *Proc. R. Soc. Lond.*, **A 443**, 127–138, 1993.
23. A.J.M. SPENCER, *Theory of invariants*, [in:] *Continuum Physics*, Vol. I, A.C. ERINGEN [Ed.], Academic Press, 1971.
24. E. KIRAL and A.C. ERINGEN, *Constitutive equations of nonlinear electromagnetic-elastic crystals*, Springer-Verlag, New York 1990.
25. J. RYCHLEWSKI, *Symmetry of causes and effects* [in Polish], PWN, Warszawa 1991.
26. G.F. SMITH, *Constitutive equations for anisotropic and isotropic materials*, North-Holland, Amsterdam, London, New York, Toronto 1994.
27. S.C. COWIN, *The relationship between the elasticity tensor and the fabric tensor*, *Mech. Materials*, **4**, 137–147, 1985.

28. S.C. COWIN, *Fabric dependence of an anisotropic strength criterion*, Mech. Materials, **5**, 251–260, 1986.
29. S.C. COWIN, *Wolff's law of trabecular architecture at remodeling equilibrium*, J. Biomechanical Engng., **108**, 83–88, 1986.
30. J.J. TELEGA, *Some aspects of invariant theory in plasticity, Part I. New results relative to representation of isotropic and anisotropic tensor functions*, Arch. Mech., **36**, 147–162, 1984.
31. S. JEMIOŁO, *Some comments on the representation of vector-valued isotropic function*, J. Theoret. App. Mech., **31**, 121–125, 1993.
32. S. JEMIOŁO and M. KWIECIŃSKI, *On irreducible number of invariants and generators in the constitutive relationships*, Engng. Trans., **39**, 241–253, 1990.

WARSAW UNIVERSITY OF TECHNOLOGY  
INSTITUTE OF STRUCTURAL MECHANICS

and

POLISH ACADEMY OF SCIENCES  
INSTITUTE OF FUNDAMENTAL TECHNOLOGICAL RESEARCH

e-mail: jtelega@ippt.gov.pl

Received July 5, 1996.